Compound drivers of hydroclimatic extremes in large river basins

Khanal, Sonu

2021

document version
Publisher's PDF, also known as Version of record

PhD Thesis

Compound drivers of hydroclimatic extremes in large river basins

Mapping future floods and water resources by modeling compound drivers at multiple spatial and temporal scales

Samengestelde oorzaken van overstromingen

In kaart brengen van toekomstige overstromingen en watervoorraden door samengestelde factoren te modelleren op meerdere ruimtelijke en temporele schalen

Sonu Khanal

Amsterdam 2021

Faculty of Science

Vrije University

Promotoren:
Prof.dr.ir. B.J.J.M. van den Hurk
Prof.dr. W.W. Immerzeel

Copromotor:
Dr. A.F. Lutz

Examination committee:

Prof.dr. J.C.J.H. Aerts
Vrije University, The Netherlands
Prof.dr. M.F.P. Bierkens
Utrecht Univerity, The Netherlands
Prof.dr. F. Ludwig
Wageningen University, The Netherlands
Dr. A.B. Shrestha
International Centre for Integrated Mountain Development, Nepal
Prof.dr. L.M. Tallaksen
University of Oslo, Norway

ISBN 978-94-6423-568-5
Published by Faculty of Science, Vrije University, the Netherlands
Printed by ProefschriftMaken || proefschriftmaken.nl

Correspondence to Sonu Khanal, s.khanal@futurewater.nl/sonu.khanal19@gmail.com

Typesetting: Rene Wijngaard, Sonu Khanal, Martijn de Klerk and proefschriftmaken.nl
Cover image painted by Kriti Shrestha

VRIJE UNIVERSITEIT

Compound drivers of hydroclimatic extremes in large river basins

Mapping future floods and water resources by modeling compound drivers at multiple spatial and temporal scales

ACADEMISCH PROEFSCHRIFT

ter verkrijging van de graad Doctor
aan de Vrije Universiteit Amsterdam,
op gezag van de rector magnificus
prof.dr. C.M. van Praag,
in het openbaar te verdedigen
ten overstaan van de promotiecommissie
van de Faculteit der Bètawetenschappen
op donderdag 25 november 2021 om 9.45 uur
in een bijeenkomst van de universiteit,
De Boelelaan 1105

door

Sonu Khanal

geboren te Syangja, Nepal

Promotoren:
Prof.dr.ir. B.J.J.M. van den Hurk
Prof.dr. W.W. Immerzeel

Copromotor:
Dr. A.F. Lutz

Examination committee:

Prof.dr. J.C.J.H. Aerts
Vrije University, The Netherlands
Prof.dr. M.F.P. Bierkens
Utrecht Univerity, The Netherlands
Prof.dr. F. Ludwig
Wageningen University, The Netherlands
Dr. A.B. Shrestha
International Centre for Integrated Mountain Development, Nepal
Prof.dr. L.M. Tallaksen
University of Oslo, Norway

Contents

Summary

Extremes are of prime importance to the society and the ecosystem as they tend to influence the overall environment more than a likely event. Among other disasters, hydro-climatic extremes such as floods and droughts, have a severe impact on the society as the damage is high due to their large spatial coverage and high cost of protection. These hydro-climatic extreme events often result from one extreme state or amplification due to many other contributing mild or extreme states, i.e., compound extremes. Compound events are multifaceted, complex and are often associated with regions and different spatio-temporal scales. For instance, co-occurrence of fluvial floods accompanied with high groundwater storage or a strong wind that enforces a storm surge along the coast are typical examples of compound events in coastal regions. Likewise, the co-occurrence of heavy precipitation accompanied with high temperatures that leads to heavy snow and ice melt runoff or saturated soil moisture conditions are typical examples of the compound events in mountain environments. The societal and economic losses due to compound extremes are manifold higher in magnitude compared to the impacts of those from individual extremes alone. An increase in frequency and magnitude of compound flood events at a regional and global scale has been witnessed over the past few decades. Climate change is expected to exacerbate the intensity, frequency, and duration of these compound flood events. Information on the probability of occurrence and prediction of time and location of compound events is necessary to assess the future risk. To understand the future impact of compound flood events at different spatio-temporal aggregation levels and climate zones, i.e., mountains, flood plains, and coasts, it is inevitable to examine the mechanisms of compound floods. To this end, novel modelling approaches have been developed to better understand the compound flood mechanisms and its impacts in climatically diverse regions around the world.

Mountain water originating from the melting of snow and ice reserves, and orographic rainfall is transported via river systems and is an important water resource to millions of people living in the lowlands. High Mountain Asia (HMA) serves as a major water source for large rivers in Asia and is pivotal in satisfying the downstream societal and environmental requirements. The climate of HMA has witnessed many changes in recent decades and has diverse effects on the region's water availability. The complex topography and harsh conditions impose difficulties in managing ground stations at high altitudes, thus the historical trends in climate are poorly understood. Often trends are calculated using a limited number of in-situ observations mainly observed in the valleys, which do not represent the climatic changes at high altitudes. Past studies are scattered around the basin, national and regional level, used different data, spatio-temporal resolution, and approaches. Variability in approaches, data, and methods makes it even more challenging to align and compare the changes around different regions. For this reason, the first study of this thesis uses state-of-the-art high-resolution reanalysis ERA5 data to detect similarities and contrasts in historical climate change over the entire HMA using one consistent methodology. Analysis reveals that while the temperature is consistently increasing at a higher rate than the global warming rate, precipitation changes are not uniform, with substantial temporal and spatial variation in particular for the higher altitudes of HMA. Winter warming and summer wetting are dominant for the interior basins (Plateau of Tibet interior and Tarim). In contrast, the western (the Indus, the Helmand, the Amu Darya, the Syr Darya, and the Balkash) and eastern basins (the Yellow, the Yangtze, the Salween, and the Mekong) are coherently drying. A coherent and significant increasing trend in heatwaves is observed across all regions in HMA. The results reveal that trends in heavy precipitation days show higher variability in the southern (the Ganges, the Brahmaputra, and the Irrawaddy) and eastern basins (the Yellow, the Yangtze, the Salween, and the Mekong) as compared to other regions in HMA. While precipitation and temperature-related indicators show varying tendencies, their compound occurrence is coherent in the monsoon-dominated basins. These changes in extreme climate indicators imply substantial increases in the future occurrence of hazards like floods, landslides and droughts, which in turn may impact economic production and infrastructure.

Summary

Via compensating and contrasting impacts of extreme precipitation and temperature on the discharge volume from the HMA headwaters, changes in climatic variables give rise to nonlinear, non-stationary, and non-uniform responses of cryospheric and hydrological variables such as snow, glaciers, soil moisture, and groundwater, at varying spatial and temporal scales. The systemic effect of the compound occurrence of extreme precipitation and temperature and their impacts on the seasonality and trends in total water availability for HMA is largely unresolved. To robustly assess the 21st century climate change impact on water resources in HMA at a wide range of temporal scales, a high-resolution cryospheric-hydrological model for HMA is used to quantify the compound effects of future changes in precipitation and temperature based on projections from coupled model intercomparison project 6 (CMIP6) ensembles. A novel large-scale snow sublimation parameterization is used to estimate an essential component of the water balance in mountainous regions, i.e., snow sublimation, for the second study of this thesis. To avoid the pitfalls of equifinality in model calibration, a three-step sequential calibration strategy is used to calibrate model parameters related to snow, glacier, and rainfall-runoff processes. Analysis reveals that the contrasting responses of HMA's rivers are primarily dictated by their hydrological regimes. At the seasonal scale, the earlier onset of melting causes a shift in the magnitude and peak of water availability, to earlier in the year. At the decade to century-scale, after an initial increase, the glacier melt declines by the mid (2036–2065) or end of the century (2071–2100). Despite a large variability in hydrological regimes across HMA's rivers, results indicate relatively consistent climate change responses across HMA in terms of total water availability at decadal time scales. Although total water availability increases for the headwaters, changes in seasonality and magnitude diverge widely between basins and need to be addressed while adapting to future changes in a region where food security, energy security as well as biodiversity, and the livelihoods of many depend on water from HMA.

Often hydrological systems are governed by processes with memory at different time scales. Hydrologic processes remember the past atmospheric anomalies and their effects are reflected in subsequent events or periods. Spatio-temporal variation of hydrological processes that have a strong lagged autocorrelation (memory), such as soil moisture, snow accumulation and the antecedent hydro-climatic conditions, significantly impact the peaks of flood waves. Ignoring these memory processes leads to biased estimates of floods and high river levels that are sensitive to the occurrence of these compounding hydro-meteorological processes. The third study of this thesis investigates the role of memory in hydrological and meteorological systems at different temporal scales for the Rhine basin. The hydrological regime of the Rhine river basin is simulated using a cryospheric-hydrological model forced with atmospheric conditions from an ensemble of runs generated by a high-resolution regional climate model. The findings show that meltwater from antecedent anomalous snowfall results in a time shift of the discharge peak. Soil moisture modulates the rainfall-runoff relationship and generates a strong runoff response at high soil moisture levels and buffers the generation of runoff peaks at low levels. Results show that meteorological autocorrelation (manifesting itself by the occurrence of clustered precipitation events) has a strong impact on the magnitude of peak discharge. Removing meteorological autocorrelation at time scales longer than five days reduces peak discharge by 80% relative to the reference climate. At time scales longer than 30 days this meteorological autocorrelation loses its significant role in generating high discharge levels. Finally, the study illustrates how hydrological memory from snow accumulation and soil moisture complements the generation of extreme discharges. These findings are relevant when exploring the effect of extreme discharge events that are caused by a compound occurrence of these drivers.

The coastal community is at higher risk of compound flooding compared to the upstream areas due to the additional risk from sea storms. Risk of river flooding, in low-lying countries like the Netherlands where flood defense infrastructure protects the densely populated hinterland, typically only occurs during the winter season when deep Atlantic low-pressure systems precipitate large amounts of water over the European Alps and Central Europe. The accompanying frontal systems lead to large rainfall amounts, which can result in river discharges exceeding critical thresholds. Often these deep low-pressure systems have the potential to induce significant storm surge levels along the coast of the North Sea. The risk of disruptive societal impact increases strongly if river runoff and storm-surge peak occur near-simultaneously. To understand the risk due to compound floods in the Dutch coastal regions, the

fourth and final study of this thesis investigates the possibility of finding near-simultaneous storm surge and extreme river discharge using an extended dataset derived from a storm surge model and two hydrological river-discharge models forced with conditions from a high-resolution regional climate model in ensemble mode. The probability for finding a co-occurrence of extreme river discharge at Lobith and storm surge conditions at Hoek van Holland is found to be four times higher than random chance for a broad range of time lags (-2 to 10 days, depending on the exact threshold). Other than previous studies, based on historical observations or proxies such as precipitation (for discharge) and winds (for storm surge) instead of a real impact variable, i.e., discharge, results reveal that model uncertainties make it necessary to consider a range of lag days rather than a fixed time lag of six days. The physical modelling approach used to investigate the joint occurrence of high discharge and water level in this study confirms that the correlations have a physical basis. This study conceptually shows that a strong storm whose winds set up a storm surge will need time to reach the Rhine headwaters where heavy rainfall will find its way to the river mouth after multiple days of travel time. However, in reality, this simple rationale is blurred by natural variability where multiple storms and anomalous travel times may lead to very different correlation lag times. This highlights that the hazard of co-occurrence of high river discharge and coastal water levels cannot be neglected in a robust risk assessment.

The studies included in this thesis cover several relevant topics related to a complete flood risk chain (from mountains to coasts) and their impact on water resources in regions around the world (i.e., Europe and Asia). This thesis highlights the importance of an integrated process-based physical modelling approach (atmospheric, hydrological and hydrodynamic) for the proper investigation of future flood risk. A new valuable insight on the mechanisms of compound floods and its potential impact on water resources (both for historical and future climate) has been gained with novel modelling approaches. The outcomes generated from this thesis might contribute to support climate change adaptation policy planning and outreach programs in these climate change hotspots, i.e., the mountains and deltas. Finally, this thesis outlines the challenges, limitations and possibilities required to further improve the understanding of compound flood risk and its impact on water resources in climate change hotspots around the world.

Samenvatting

Extremen hebben een grote impact op onze samenleving en ecosystemen, aangezien deze de leefomgeving vaak zeer ernstig beïnvloeden. Onder andere hydro-klimatologische extremen zoals overstromingen en droogte, hebben een grote impact vanwege de vaak grote ruimtelijke spreiding en hoge (financiële) gevolgschade. Hydro-klimatologische extreme gebeurtenissen zijn vaak het gevolg van één extreme situatie of van zogenaamde samengestelde extremen: het samenvallen van meerdere milde of extreme hydro-klimatologische situaties wat tot een versterkt effect leidt. De samengestelde extremen zijn veelzijdig, complex en worden vaak geassocieerd met specifieke regio's en verschillende spatio-temporele schalen. Het gelijktijdig voorkomen van rivieroverstromingen in combinatie met een verzadigde bodem, of een sterke wind die de stormvloed langs de kust versterkt, zijn typische voorbeelden van samengestelde extremen in kustgebieden. Een typisch voorbeeld van samengestelde extremen in de bergen is bijvoorbeeld het gelijktijdig voorkomen van hevige neerslag in combinatie met hoge temperaturen wat kan leiden tot zware sneeuw- en ijssmeltafvoer of een verzadigde bodem. De maatschappelijke en economische gevolgen van samengestelde extremen zijn over het algemeen veel groter dan de gevolgen van individuele extremen. De afgelopen decennia is een toename in frequentie en omvang van samengestelde overstromingen op regionale en mondiale schaal waargenomen. Verwacht wordt dat door klimaatverandering de intensiteit, frequentie en duur van deze samengestelde overstromingen zullen toenemen. Informatie over de waarschijnlijkheid van optreden en voorspelling van tijd en locatie van samengestelde extremen is nodig om het toekomstige risico te beoordelen. Om de toekomstige impact van samengestelde overstromingen op verschillende spatio-temporele aggregatieniveaus en klimaatzones, d.w.z. bergen, uiterwaarden en kusten, te begrijpen, is het onvermijdelijk om de mechanismen van samengestelde overstromingen te onderzoeken. Daarom zijn er nieuwe modelleertechnieken ontwikkeld om de samengestelde overstromingsmechanismen en de gevolgen ervan in klimatologisch diverse regio's over de hele wereld beter te begrijpen.

Bergwater dat afkomstig is van het smelten van sneeuw, gletsjers en orografische neerslag wordt getransporteerd via riviersystemen en is een belangrijke watertoevoer voor miljoenen mensen die in de laaglanden wonen. De hooggebergtes van Azië (High Mountain Asia of HMA) dienen als een belangrijke waterbron en spelen een cruciale rol bij het voldoen aan de benedenstroomse watervraag van mens en natuur. Het klimaat van HMA is de afgelopen decennia onderhevig geweest aan veranderingen en dit heeft verschillende effecten gehad op de waterbeschikbaarheid in de regio. De complexe topografie en de zware omstandigheden zorgen voor problemen bij het beheer van meetstations op grote hoogte, waardoor de historische trends in het klimaat slecht worden begrepen. Vaak worden trends berekend met behulp van een beperkt aantal in-situ waarnemingen, voornamelijk waargenomen in de valleien, die niet de klimaatverandering op grote hoogte vertegenwoordigen. Eerdere studies die zijn uitgevoerd verspreid over de stroomgebieden, op nationaal en regionaal niveau, gebruikten verschillende gegevens, spatio-temporele resolutie en benaderingen. Variabiliteit in benaderingen, gegevens en methoden maakt het nog uitdagender om de veranderingen in verschillende regio's op één lijn te brengen en te vergelijken. Om deze reden gebruikt de eerste studie van dit proefschrift state-of-the-art hoge resolutie heranalyse ERA5 klimaatdata om overeenkomsten en contrasten in historische klimaatverandering over heel HMA te detecteren met behulp van één consistente methodologie. Uit de analyse blijkt dat de temperatuur in het gebied consistent sneller toeneemt dan het gemiddelde tempo van de opwarming van de aarde, en dat neerslagveranderingen niet uniform zijn en substantiële temporele en ruimtelijke variatie laten zien, met name op grote hoogte. Voor de centrale stroomgebieden (het Tibetaans Plateau en Tarim) zijn warmere winters en nattere zomers duidelijk waarneembare trends. Daarentegen worden de westelijke (de Indus, de Helmand, de Amu Darya, de Syr Darya en Balkash) en oostelijke (de Gele Rivier, de Yangtze, de Salween en de Mekong) stroomgebieden duidelijk droger. Een significant stijgende trend in hittegolven wordt waargenomen in alle regio's in HMA. De resultaten laten zien dat trends in dagen met hevige neerslag een grotere variabiliteit vertonen in de zuidelijke (de Ganges, de Brahmaputra en de Irrawaddy) en oostelijke stroomgebieden (de Gele rivier, de Yangtze, de Salween en de Mekong) in vergelijking met andere regio's in HMA. Hoewel neerslag- en temperatuurgerelateerde indicatoren verschillende trends

tonen, komen extreme temperaturen en neerslag vaak teglijk voorin de door de moesson gedomineerde stroomgebieden. Deze veranderingen in extreme klimaatindicatoren impliceren een aanzienlijke toename van extreme gebeurtenissen zoals overstromingen, aardverschuivingen en droogtes, die op hun beurt gevolgen kunnen hebben voor de economie en infrastructuur in de regio.

Veranderingen in klimaatvariabelen zoals neerslag en temperatuur leiden tot compenserende en contrasterende effecten op de rivierafvoeren in HMA. Deze compenserende en contrasterende effecten resulteren in niet-lineaire, niet-stationaire en niet-uniforme reacties van cryosferische en hydrologische variabelen zoals sneeuw, gletsjers, bodemvocht en grondwater, op verschillende ruimtelijke en temporele schalen. Het systemische effect van de combinatie van veranderingen in neerslag en temperatuur en de impact op seizoensgebonden trends op de totale waterbeschikbaarheid in HMA is grotendeels onbekend. Om de impact van de klimaatverandering in de 21e eeuw op de watervoorraden in HMA op verschillende tijdschalen robuust te kunnen beoordelen, is een cryosferisch-hydrologisch model met hoge ruimtelijke resolutie ontwikkeld voor HMA. Hiermee is het samengestelde effect van toekomstige veranderingen in neerslag en temperatuur gekwantificeerd, gebruikmakend van een ensemble van recente klimaatmodellen (CMIP6). Voor de tweede studie van dit proefschrift is een nieuwe parameterisatie ontwikkeld om een essentiële component van de waterbalans in bergachtige gebieden te kunnen schatten, namelijk sneeuwsublimatie. Om model equifinaliteit te vermijden, is een 3-staps kalibratiestrategie gebruikt om model parameters gereleateerd aan sneeuw-, gletsjer- en neerslagafvoerprocessen te kalibreren. Uit de analyse blijkt dat de contrasterende respons ten gevolge van klimatologische veranderingen van de rivieren in HMA voornamelijk worden bepaald door hun hydrologische regimes. Op de seizoenale tijdschaal veroorzaakt het vroeger in het seizoen smelten van sneeuw en ijs een verandering in de omvang en een verschuiving van de piek in waterbeschikbaarheid naar eerder in het seizoen. Op een grotere tijdschaal bezien (decennium tot een eeuw), zal het smelten van de gletsjers eerst versnellen, waarna dit afneemt tegen het midden (2036–2065) of het einde van de eeuw (2071–2100). Ondanks dat de hydrologische regimes van de verschillende rivieren in HMA een grote variabiliteit vertonen, wijzen de resultaten op de tijdschaal van decennia op relatief consistente veranderingen in waterbeschikbaarheid als gevolg van klimaatverandering. Hoewel de totale waterbeschikbaarheid in de rivieren toeneemt, lopen veranderingen in en de omvang van seizoenale verschuivingen sterk uiteen. Het is daarom belangrijk om deze veranderingen onder de aandacht te brengen en tegelijkertijd klimaatadaptatiemaatregelen in deze regio door te voeren waar voedsel- en energiezekerheid, biodiversiteit en het levensonderhoud van velen afhankelijk zijn van water vanuit HMA.

Vaak worden hydrologische systemen beïnvloed door eerder opgetreden processen op verschillende tijdschalen. Hydrologische processen worden bijvoorbeeld sterk beïnvloed door anomalieën in atmosferische omstandigheden die vervolgens worden weerspiegeld in opvolgende gebeurtenissen of perioden. Spatio-temporele variatie van hydrologische processen met een sterk vertraagde autocorrelatie (geheugen), zoals bodemvocht, sneeuwopbouw andere en hydro-klimatologische omstandigheden hebben een significante invloed op de hoogte van afvoergolven. Het negeren van deze processen en hun autocorrelatie leidt tot verkeerde voorspellingen van bijvoorbeeld de hoogte van rivierpeilen of de ernst van overstromingen. Rivierpeilen zijn erg gevoelig voor het optreden van samengestelde hydrometeorologische processen. De derde studie van dit proefschrift onderzoekt de rol van het geheugen in hydrologische en meteorologische systemen op verschillende tijdschalen voor het stroomgebied van de Rijn. Het hydrologische regime van de Rijn wordt gesimuleerd met behulp van een cryosferisch-hydrologisch model dat wordt gevoed met hoge resolutie meteorologische data van een ensemble van uitvoeren van een regionaal klimaatmodel. De bevindingen tonen aan dat smeltwater van extreme sneeuwval resulteert in een verschuiving van de afvoerpiek van de Rijn. Bodemvocht bepaalt de relatie tussen neerslag en afvoer: er wordt een sterke afvoerrespons gegenereerd wanneer het bodemvochtgehalte hoog is en de afvoerpieken worden gebufferd bij een laag bodemvochtgehalte. Resultaten tonen aan dat meteorologische autocorrelatie (die zich manifesteert door het optreden van geclusterde neerslaggebeurtenissen) een sterke invloed heeft op de omvang van de piekafvoer. Het verwijderen van meteorologische autocorrelatie op tijdschalen langer dan vijf dagen vermindert de piekafvoer met 80% ten opzichte van het referentieklimaat. Op tijdschalen langer dan 30 dagen verliest de meteorologische autocorrelatie zijn belangrijke rol bij het genereren van hoge afvoeren. Ten slotte

illustreert de studie hoe het hydrologische geheugen van sneeuwopbouw en bodemvocht een aanvulling vormt op het genereren van extreme afvoeren. Deze bevindingen zijn relevant bij het onderzoeken van het effect van extreme afvoeren die worden veroorzaakt door het samen voorkomen van deze aansturende mechanismen.

Gebieden langs de kust lopen een groter risico op overstromingen als gevolg van samengestelde extremen vanwege het extra risico van stormvloeden. Risico op overstromingen van rivieren in laaggelegen landen zoals Nederland, waar waterkeringen het dichtbevolkte achterland beschermen, doen zich doorgaans alleen voor tijdens het winterseizoen wanneer Atlantische lagedruksystemen grote hoeveelheden neerslag genereren boven de Europese Alpen en Centraal-Europa. De bijbehorende frontale systemen leiden tot grote hoeveelheden neerslag, wat kan leiden tot rivierafvoeren die kritische drempels overschrijden. Vaak hebben deze lagedruksystemen het potentieel om aanzienlijke stormvloeden te veroorzaken langs de kust van de Noordzee. Het risico van een verstorende maatschappelijke impact neemt sterk toe als de rivierafvoerpiek en stormvloedpiek vrijwel gelijktijdig plaatsvinden. Om het risico op overstromingen door samengestelde extremen in de Nederlandse kustgebieden beter te begrijpen, wordt voor het het vierde en laatste hoofdstuk van dit proefschrift onderzocht hoe de kans op het gelijktijdig voorkomen van stormvloed en extreme rivierafvoer te kan worden bepaald met behulp van een uitgebreide dataset afgeleid van een stormvloedmodel en twee hydrologische modellen. -Deze modellen worden gevoed met ensembles van uitvoer van een regionaal klimaatmodel met hoge resolutie. De kans op het gelijktijdig voorkomen van een extreme rivierafvoer bij Lobith en stormvloedcondities bij Hoek van Holland blijkt vier keer hoger te zijn dan de willekeurige kans voor een breed scala aan tijdsvertragingen (-2 tot 10 dagen, afhankelijk van de exacte drempel). In tegenstelling tot eerdere studies gebaseerd op historische waarnemingen of proxies zoals neerslag (voor afvoer) en wind (voor stormvloed) in plaats van een echte impactvariabele (afvoer), laten de resultaten van deze studie zien dat modelonzekerheden het noodzakelijk maken om rekening te houden met verschillende tijdsvertragingen in plaats van een vast tijdsverloop van zes dagen. De fysische modelleringsbenadering die is gebruikt is om het gezamenlijk voorkomen van piekafvoer- en waterstand te onderzoeken, bevestigt dat de correlaties een fysieke basis hebben. Deze studie toont conceptueel aan dat een hevige storm waarvan de wind een stormvloed veroorzaakt tijd nodig heeft om het bovenstroomse deel van het stroomgebied van de Rijn te bereiken en dat zware regenval in het Rijn stroomgebied na meerdere dagen reistijd zijn weg naar de monding vindt. In werkelijkheid wordt deze versimpelde weergave echter vertroebeld door natuurlijke variabiliteit, waarbij meerdere stormen en afwijkende reistijden van afvoergolven kunnen leiden tot zeer verschillende correlatie-vertragingstijden. Dit benadrukt dat het gevaar van het gelijktijdig optreden van hoge rivierafvoeren en kustwaterstanden niet kan worden verwaarloosd in een robuuste risicobeoordeling.

De hoofdstukken in dit proefschrift hebben betrekking op verschillende onderwerpen die verband houden met de complete overstromingsrisicoketen (van bergen tot kusten) en hun impact op watervoorraden in Europa en Azië. Dit proefschrift benadrukt het belang van een geïntegreerd proces-gebaseerde benadering middels fysische modellering (atmosferisch, hydrologisch en hydrodynamisch) voor onderzoek naar toekomstige overstromingsrisico's. Nieuwe waardevolle inzichten in de mechanismen van samengestelde overstromingen en de mogelijke impact ervan op watervoorraden (zowel voor historisch als toekomstig klimaat) zijn verkregen met nieuwe modelleringstechnieken. De resultaten die in dit proefschrift zijn gegenereerd kunnen bijdragen aan het ondersteunen van het maken van beleid in de gebieden die het meest gevoelig zijn voor klimaatverandering, namelijk de bergen en delta's. Ten slotte schetst dit proefschrift de uitdagingen, beperkingen en mogelijkheden om overstromingsrisico’s bij samengestelde extremen te leren begrijpen en de impact ervan op watervoorraden in de gebieden die het meest gevoelig zijn voor klimaatverandering over de hele wereld verder te verminderen.

1

Chapter 1

Introduction

1 Introduction

1.1 Background: Extreme events

An event which is rare and unexpected or has a low probability to occur, at a particular place and time is an extreme event (Coles, 2001). Statistically, extreme events occur in the tails of the probability distribution that define the occurrence of events of a given magnitude. The nature of such extreme events may vary from place to place and tend to influence the environment more than common conditions. Even though the probability of occurrence of extreme events is low and further decreases with the increase in magnitude of events, such rare events are of great importance to the society (Birkmann et al., 2010; Black et al., 2013). Examples of extreme events are natural (floods, droughts, hurricanes, dam breaks, earthquakes and societal impacts caused by pandemics such as COVID), technical or mechanical breakdowns (power outages, explosions, chemical contaminations, infrastructure failures) and economical (stock crash and insurance loss). Examples of historical high-impact extreme events are the storm surge of 1953 in the Netherlands (Gerritsen, 2005), the fluvial flooding events of 1993 and 1995 in the Netherlands (Tol and Langen, 2000), the European 2003 heat wave (D'Ippoliti et al., 2010; Robine et al., 2008), the Sumatra 2004 earthquake (Ammon et al., 2005), the 2005 Hurricane Katrina (Kates et al., 2006), and the Nepal 2015 earthquake (Kargel et al., 2016). The damage and cost of protection is high for such extreme events. Information on the probability of occurrence and prediction of time and location of such events are necessary to assess the future risk. Representation of an extreme event in an analysis or modelling framework is not only useful for explaining it, but also ultimately being able to reproduce it. A common problem in many areas of science is to answer the question how likely it is that a specific event occurs in the future and how society can be protected from these events considering global interdependencies of economy and technology.

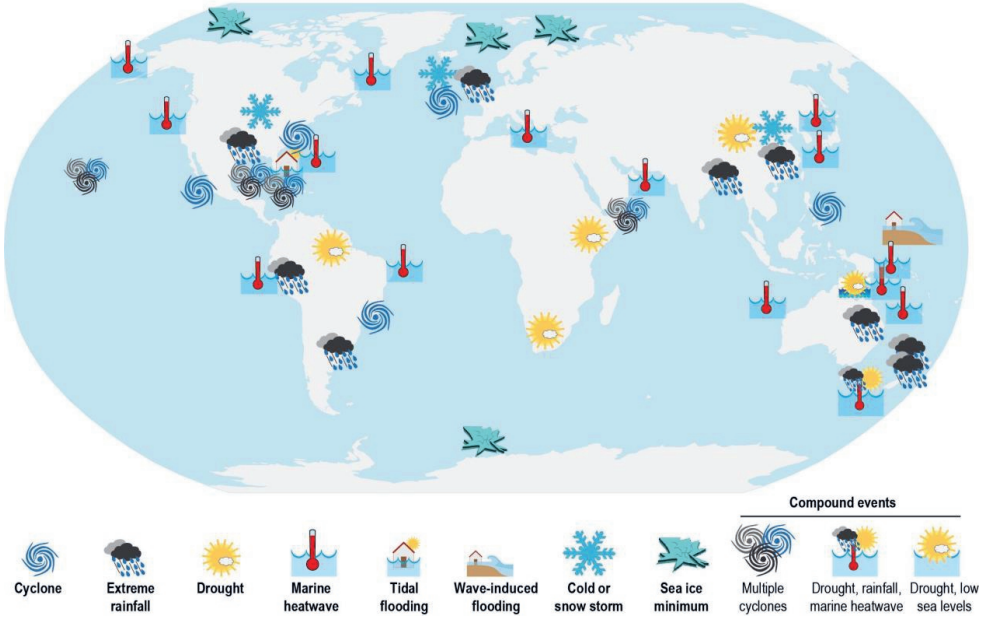

Figure 1.1: Overview of extreme events linked with mountains and coastal environments (Collins et al., 2019)

The occurrence of extreme events can be purely random, due to complex interaction of the states of the system, or the combination of both. These occurrences could also arise due to natural reasons, human induced reasons or could be triggered by the combination of both. Further, the occurrence of extreme events could be due to one extreme state or amplification due to many other contributing mild or extreme states, also known as compound events (see Figure 1.1). The extreme events are multifaceted, complex, and subjected to various interpretations and time scales, therefore their definition is influenced by the underlying cause-and-effect mechanisms. Studies have used subjective definitions to define the extreme events (McPhillips et al., 2018). From the science perspective, an objective definition is required to remove the subjectivity imposed on the definition of extreme events. Since the extreme events are rare, defining a mathematical quantity or physical threshold is difficult and requires an adequate knowledge of the physical processes that make the event extreme. To bridge the gaps in knowledge, the events are characterized based on the analogies, processes, mechanisms, statistical and dynamical properties (Zscheischler et al., 2020). One approach is to characterise events based on the potential for impact and change. With this approach, the event is considered extreme only if it causes loss to life, society and environment. The other approach characterises events based on uniqueness, unpredictability, and mechanisms of huge deviations from normal state and emphasises on process understanding.

In both approaches, the observations provide a firm base for a proper scientific analysis of extreme events. Statistical inferences can be made from observations. For extreme events, the unprecedented deviations compared to the mean or normal state are important. So, these events are in general too infrequent to handle with standard statistical tools and therefore demand a special methodology. A distribution function, mostly data driven, for such extreme events is required, but a lack of extreme event observations often hinders the correct parameterization of the distribution function (Castellarin et al., 2012; Renard et al., 2013). It is often referred to as “the curse of few observations”. A practical example is flood return period analysis based on 100 years of observed discharge data for dike establishment that aims for flood protection. The objective here is to predict discharge levels for the return period of 1250 years. A natural way to solve this issue is to use statistical extrapolation methods, such as flood frequency analysis, to estimate the discharge levels for a return period of 1250 years. Estimation of probability of an event that is more extreme than any event that has already been observed, demands extrapolation based on specific methods (extreme value statistical methods, data pooling and bootstrapping). However, the reliability of such extrapolations is often questioned by practitioners. Therefore, the appropriate methodology to answer the question requires physical modeling approaches as well. Physical modeling approaches are deemed helpful for both diagnostic (what has happened) and prognostic (what will happen) purposes. Moreover, physical modeling simulations are helpful for a long-term multiple scenario-based analysis which requires a correct representation of the dynamic state of the system.

The aim of this thesis is to assess the future risks (floods, droughts and water resources availability) induced by compound drivers of hydrological extremes. In this thesis, I focus on physical modeling configurations to understand weather, climate, hydrological and compound extremes at different temporal and spatial scales. The introduction section describes modeling approaches, physical model configurations, observational data, timescales, uncertainties in the approaches and provides a detailed description of the objective of this study.

1.2 Modeling framework

1.2.1 Statistical approach

1.2.1.1 Univariate extremes

Univariate extremes (UE) are expressed as scalar quantities exceeding a certain threshold or quantile, mainly summarized and characterised by a single variable. Typical examples of such UE events are heavy precipitation, high temperature, extreme wave height, storm surge, river water levels and wind speeds. The UE’s may have tangible and direct ethical, social, economic and environmental impacts,

which triggered the development of advanced statistical theories and methods to explore such events in the past (Gomes et al., 2016). The development of advanced methods for the estimation and prediction of UEs has contributed to risk assessment and modelling of climate, earthquakes and other environmental phenomena, with high potential impact and very low probabilities (Sillmann and Sippel, 2020). To analyse the UE's statistically, there are mainly two methods. The first method relies on fitting the data to statistical linear and non-linear models, as for instance additive, multiplicative and exponential models, and then look at extreme quantiles by simulating from the model multiple times (Chandler, 2005; Gilleland and Nychka, 2005). The second method relies on fitting the data to one of the generalised extreme value (GEV) distributions which constitutes the Gumbel, Fréchet or Weibull distribution (Coles, 2001; Embrechts et al., 2013; Katz and Brown, 1992; Resnick, 2007). The latter method is carried out by either fitting block maxima or peaks over threshold to one of the GEV distributions. The differences in behaviour of the tails makes each GEV distribution unique (Gilleland and Katz, 2006). The tail in the Weibull distribution is limited to a maximum finite value whereas the Gumbel distribution can yield infinite maximum values. Nevertheless, the probability of such high values decreases exponentially. On contrary, the Fréchet distribution is heavy tailed in which the maxima have higher probability compared to Gumbel.

EVT provides a robust means of statistical modeling of UE's thus making it suitable to use for hydro-meteorological applications (Katz, 2002; Lettenmaier et al., 1987; Towler et al., 2010). However, there are several underlying fundamental assumptions that restrict its applicability. The amount of data imposes a serious implication on the use of EVT (Vanem, 2015). EVT requires sufficiently long historical data series to be able to estimate the extreme return levels, but in practice such long historical datasets are not available for most applications. Limited data used to fit the distribution will lie near the mode of distribution and thus give poor fit of tails or extreme. The choice of blocks or threshold greatly influences the outcomes of fitting the data to GEV distributions. For instance, choosing a large block size (usually annual) discards too much data and exploits only a small subset of data in the block maxima approach. Too high or too low thresholds can lead to a higher variance and bias and therefore increasing uncertainty in the estimates. The fundamental assumption of independence in the point over threshold method, is often unreasonable because high values in hydro-meteorological processes are often auto-correlated (Entin et al., 2000; Koutsoyiannis, 2005a; Lorenz, 1969; Pelletier and Turcotte, 1997; Vinnikov et al., 1996; Wanders et al., 2018; Wu and Dickinson, 2004; Yue et al., 2002).

1.2.1.2 Multivariate extremes

In most real-world situations, the link between multiple variables is important to establish as they can jointly impact the state of the system. It is important to understand the effect of a combination of several individual extreme processes and infer the interrelationship. The assumption of independent and identical distributed (IID) random variables, as for UE, is often unrealistic for hydro-meteorological processes as the variables are generally dependent (Salvadori et al., 2007). To deal with such dependency issues, extensions of the univariate threshold and block maxima approaches are developed for multivariate distributions (Coles, 2001; Ledford and Tawn, 1996, 1997, 2003; Tawn, 1990). Amongst others, parametric distribution, copula, entropy and non-parametric models are widely used to construct the multivariate distributions (Hao et al., 2018).

Hydrological processes are characterized by correlated variables, for instance, the peak, volume and duration of flood events, the peak, mean intensity, duration and volume of hyetographs, severity, duration and areal extension of droughts, which therefore require a multivariate assessment of the dependence structure (Brunner et al., 2016; Chebana and Ouarda, 2009; Favre et al., 2004; Shiau, 2003, 2006). Ignoring the dependencies may lead to severe over or under estimation of the risk (Klein et al., 2010; De Michele et al., 2005). In recent years, copula models have been widely used to understand extremes as they provide more in-depth information compared to conventional univariate analysis (AghaKouchak et al., 2014; Bevacqua et al., 2017; Durante and Salvadori, 2010; Seneviratne et al., 2012; Zscheischler and Seneviratne, 2017). Copula models provide an efficient mathematical formulation to combine several univariate marginal cumulative distribution functions into joint

cumulative distribution functions (Sklar, 1959). The copula model transforms a complex problem into a unit square (0,1) and uniform marginals. An example of such a problem is to find the joint probability distribution between the maximum water level and the number of flood events. The marginal distribution is known a priori or can be selected based on the data. Copula transforms the marginals to joint distribution based on user specified multivariate joint distribution and specific correlation structure. Likewise, copulas can also decompose a joint probability distribution into marginals. Hydrological and water resources applications of copula models can be summarized under the following broad themes: rainfall frequency analysis, flood frequency analysis, drought analysis, sea storm analysis and streamflow simulations (Chen and Guo, 2019).

However, the use of multivariate copula models becomes difficult for higher dimensional problems where it is not possible to model all mutual interdependencies, especially in the tails of the extreme distributions (Aas et al., 2009; Kurowicka and Cooke, 2006). Fitting a parametric distribution function to the data is a complex process and choosing the family of distribution function is even more difficult (Bedford et al., 2016; Daneshkhah et al., 2016).

The number of observations in hydrological and water resource applications is usually sparse. Fitting distributions through a sparse number of observations leads to a large error, in particular for the tails of the distributions, which is an area of great interest for a whole range of risk analyses (Serinaldi, 2013). Furthermore, these multivariate models rely on many assumptions to simulate the joint behaviour or distribution. The joint distribution of the variables is difficult to estimate beforehand and thus a physical modeling framework that represents the physical correlations and memory components directly is needed.

1.2.2 Physical modeling

A model is a simplified replica of the real system where knowledge about a system is condensed in mathematical equations (Beven, 2012). Hydro-meteorological processes are often very complicated to model due to limited information of catchment characteristics, system states, boundary conditions, governing equations, and underlying heterogeneity (Beven, 2012; Blöschl and Sivapalan, 1995). Hydrological models (HMs) represent intricate relations between input and output signals, through intermediate fluxes and states, satisfying mass, energy and momentum balances (Fatichi et al., 2016; Sorooshian et al., 2008). Often hydrological fluxes and storages, such as evaporation, ground water, soil moisture, snow and riverine storage, are associated with memory and dependence at various spatio-temporal scales and these complex interactions are represented by HMs. A well configured and calibrated HM serves as a robust and reliable tool to estimate the magnitude and frequency of extreme hydro-meteorological events for both current and future climate (Krysanova et al., 2018). The propagation of uncertainty, in magnitude, spatial extent, and time, from the climate driver to the hydrological response and impact can be estimated well with HMs. Substantial efforts have been made to reduce the model output uncertainty, using different sources of information and data (Hrachowitz and Clark, 2017; Singh, 2018). However, there are several challenges posed on the use of HMs

1.2.2.1 Model structure

HMs can be defined both in terms of processes and spatial complexity across model elements (Clark et al., 2017; Hrachowitz and Clark, 2017). The HMs can be categorised in to two broad categories, i.e. conceptual, and physically based models. A HM based on the understanding of processes, their interactions and overall system behaviour are conceptual HMs (Arnold et al., 1998; Bergström, 1992; Martinec and Rango, 1986). These HMs require calibration and validation to comply with the purpose of use and if the model does not meet it objective the model should be revised and amended. Thus, conceptual HMs represents a top-down approach where the uncertainty of the processes in a catchment is defined in priori. On the other hand, physically based HMs are based on bottom-up approach which assumes overall performance is the result of a combination of all small-scale processes where each of these processes are defined based on physical laws and equations (Ragettli and Pellicciotti, 2012;

Schulla, 2017). The physically based HMs incorporate the space-time variability of precipitation, radiation and variation in physiographic characteristics and also resolve the spatial heterogeneity issues (Fatichi et al., 2016). The intermediate stages (buckets) and parameters in conceptual HMs may not have a complete physical resemblance to the actual system, thus are difficult to link with ground-based observations. However, the states and parameters in physically based HMs are physically justified and theoretically can be measured. In an ideal situation, physically based HMs do not require any parameter calibration, however, such a model is not available. HMs can also be categorised based on their ability to model processes at different spatial scales, i.e., lumped and distributed (also semi-distributed). Lumped HMs consider the whole system (or catchment) as a single entity. On the contrary, distributed HMs are lumped models applied at grid scale and account for distributed forcing and catchment characteristics (Kampf and Burges, 2007). Distributed HMs provide a better understanding of the spatial variability in system behaviour and thus provide additional information on the spatio-temporal processes of the system (Smith et al., 2004b). Based on data availability, parameters in distributed HMs can be varied spatially (Beven, 2001). The lack of spatial observations mostly limits the application of distributed HMs (Grayson et al., 2002). Often physically based distributed HMs have many parameters and are associated with high computational time and cost (Koch et al., 2016). The choice of HMs depends on the objective of the study and it still remains a matter of debate if conceptual lumped HMs model are better than physically based distributed models (Holländer et al., 2014; Vaze et al., 2011). Studies have concluded that conceptual lumped HMs are as good in representing discharge as physically based distributed HMs (Reed et al., 2004; Refsgaard and Knudsen, 1996; Vaze et al., 2010, 2011). Conceptual lumped HMs perform well in simulating discharge at the outlet but are subject to equifinality and they do not provide any insights in the spatial hydrology, which is the key advantage of distributed, physically based models (Beven, 2001). Moreover, the use of a single conceptual HMs is often questionable due to large variability in outcomes (Eregno et al., 2013; Orth et al., 2015).

1.2.2.2 Representation of key cryosphere and catchment related processes

Melt modeling

Melt estimation, from snow-covered or glacierised area, is a key element in assessment of river runoff, flood risk, water resources and cryosphere related changes associated with climate change (Hock, 2003). A robust river runoff simulation, in mountainous environment, requires proper representation of snow and ice melting processes in HMs (Pellicciotti et al., 2012). A degree day approach (also known as temperature index model), based on the empirical assumption between near surface-air temperature and melt rates, is commonly used in HMs to simulate the melt (Braithwaite and Zhang, 2000; Hock, 2003). This approach has been widely used due its simplicity and parsimony in data requirement (Pellicciotti et al., 2005). However, this method is sensitive to the time integration process of daily mean temperatures (use of different periods and time frame used to calculate the average) and unable to capture the diurnal changes. For instance daily mean temperature could be zero or negative indicating no melt, but the melt conditions may fluctuate during the day (Tobin et al., 2013). HMs generally assume a constant degree day factor over entire spatial modeling domain. The spatio-temporal variability, due to changes in seasons, topographic characteristics (slope, aspect and shading), albedo changes, and atmospheric conditions, should be considered while calculating the melt rates (Hock, 2003). The other approach to calculate melt requires estimation of all the relevant fluxes based on physical equations, which often require numerous input data at fine spatial and temporal scale (Cazorzi and Dalla Fontana, 1996; Che et al., 2019; Hock, 2005; Hock and Holmgren, 2005). Energy balance models are able to resolve the complex interaction between the fluxes and internal states that could not be resolved by temperature index models (Cazorzi and Dalla Fontana, 1996; Hock, 2005).

However, implementation of energy balance scheme in HMs is cumbersome and computationally expensive task. Moreover, many variables in energy balance models are still abstract, far from being easy to identify from measurements and indirectly estimated thus increase the uncertainty in the results (Essery et al., 2013; Günther et al., 2019; Hock, 2005).

Snow sublimation

Snow sublimation is found to be one of the important components of the water cycle in high altitude regions, and thus requires proper representation in HMs (Lv and Pomeroy, 2020; Sexstone et al., 2018; Stigter et al., 2018; Strasser et al., 2008). Studies have reported that snow sublimation in mountainous areas is highly variable and ranges between 10–90% of winter snowfall (Groot Zwaaftink et al., 2011; Lv and Pomeroy, 2020; MacDonald et al., 2010; Montesi et al., 2004; Pomeroy and Gray, 1995; Reba et al., 2012; Sexstone et al., 2016, 2018; Stigter et al., 2018; Strasser et al., 2008). Snow sublimation is a local scale process which depends on the available energy for the turbulent flux, vapor pressure gradient between the snow and atmosphere, wind speed and exposure (MacDonald et al., 2010; Sexstone et al., 2018). Direct measurement of sublimation is a difficult task and only gives estimate at point scale (Bowling et al., 2004). Sublimation of snow is categorised into surface sublimation (representing water vapor fluxes between the atmosphere and the snowpack surface), canopy sublimation (representing intercepted snow held within the forest canopy), and blowing sublimation (representing snow that is transported by wind) (Groot Zwaaftink et al., 2011; Sexstone et al., 2018; Strasser et al., 2008). The degree day approach, often used by HMs, is representative only when the surface melt is the only dominant ablation component as ablation represents the ensemble of the processes such as melt, evaporation, wind and gravity driven transport and sublimation (Litt et al., 2019; Mott et al., 2018; Saloranta et al., 2019; Stigter et al., 2018; Wagnon et al., 2013). Empirical relationship between sublimation and meteorological variables is generally used for scaling of sublimation processes from point level to catchment scale is (Stigter et al., 2018). However, these empirical relationship are often region specific and thus requires more sophisticated energy balance approach (Clark et al., 2015a; Knowles et al., 2012). Lack of data (for e.g. albedo decay time scale and aerodynamic roughness length) and difficulty in measurement of parameters in reality hinders implementation of energy balance schemes and models in HMs (Bowling et al., 2004; Günther et al., 2019).

Permafrost

Permafrost constitutes any type of ground (soil, sediment, or rock that extends vertically from a few feet to few miles beneath ground) that has been frozen (< 0 °C) continuously for a minimum of two years (e.g., Dobinski, 2011). A quarter of the Northern hemisphere and 17% of the earth land surface (exposed) is covered by permafrost (Biskaborn et al., 2019). The hydrological processes such as quick surface runoff, movement of water in soil layers, storage, exchange of surface and subsurface water is affected by the low hydraulic conductivity of permafrost (Dobinski, 2011; McNamara et al., 1998; Woo and Winter, 1993). The increasing warming rates, higher at polar and high elevation regions compared to global average, impact permafrost and associated hydrological processes (Lafrenière and Lamoureux, 2019; Pepin et al., 2015; Quinton and Baltzer, 2013). Degradation in permafrost (or thawing), either from climate or human induced changes, can change surface drainage patterns by generating ponding, inducing soil skin flow and gullying effects (Lafrenière and Lamoureux, 2019; Walvoord and Kurylyk, 2016). Understanding hydrologic changes and permafrost-carbon feedback mechanisms in response to permafrost degradation and climate change is critical for ecosystems (Lawrence et al., 2015; Schuur et al., 2015; Walvoord and Kurylyk, 2016). Permafrost processes are associated with diurnal changes, microclimate, physiographic characteristics and spatio heterogeneity aspects(Gao et al., 2021). Permafrost processes are difficult to implement in HMs as they require sophisticated energy balance and phase transformation schemes (Walvoord and Kurylyk, 2016).

Evaporation

Evaporation is an important constituent of the water and energy balance. It affects weather and climate through its influence on boundary layer dynamics and thermal dynamics (Clark et al., 2015b). Globally only 30-35% of the total inland precipitation ends up in rivers (or river systems) and the remainder is evaporated (Rodell et al., 2015). Evaporation, which constitutes surface evaporation, transpiration, evaporation from interception and open water evaporation, strongly influences the hydrological conditions (Savenije, 2004). Evaporation is not only affected by meteorological conditions (radiation, wind speed, atmospheric humidity and air temperature), but also depends on hydrological (soil moisture

availability) and biological factors (such as type and growing stage of vegetation). Most HMs use potential evaporation (or actual evaporation if available) to calculate the water balance (Zhao et al., 2013). Spatially distributed HMs often require evaporation information at grid level, which is not available as it is measured at point scale. Also, the relative contributions of various evaporation types are not well understood (Coenders-Gerrits et al., 2014; Nelson et al., 2020; Sutanto et al., 2014). Thus, more data measurement efforts are required to improve the understanding of evaporation processes (Harrigan and Berghuijs, 2016). It is found that the hydrological simulations which include explicit biological processes predict lower future droughts and small evaporation changes in a warmer climate (Prudhomme et al., 2014). Thus, evaporation should not be separated from the physical and biological process it connects. There are vast arrays of methods and equations available, differing in complexity and data require, to estimate the potential evaporation (Oudin et al., 2005). The potential evaporation estimation methods depending on the approach can be of divided into energy-based, temperature-based and mass transfer-based. The energy-based implementation of evaporation processes in HMs is cumbersome as it requires large array of input data compared to the other two methods.

Flow routing

Flow routing, i.e., transport of water from upstream cells (source) to downstream cells (sink) through a river network, in physically based distributed HMs is a difficult task as it requires solving Saint-Venant equations (Beven, 2012; Chaudhry, 2007; Te Chow, 2010). The physical method requires solving complex partial differential equations (i.e., continuity and momentum), and often have high data requirements related to river geometry, morphology and flood plain, which are often not available for large spatial scales (Singh and Woolhiser, 2002). Several simple numerical approximations to these complex partial differential equations have been proposed and implemented in several HMs in the past (Beven, 2012; Chanson, 2004; Cunge, 1969). The choice of routing scheme has a significant influence on the timing of simulated river discharge and its peak values (Hattermann et al., 2017; Zaherpour et al., 2018; Zhao et al., 2017).

1.2.2.3 Data availability

The availability and quality of spatial ground-based information is crucial for the choice of HM (Clark et al., 2017). In past decades, many efforts have been made improve the technology, quantity and quality of data required for HMs (Singh, 2018). Advancement in remote sensing technology, such as satellites and radars, made it easier to model the hydrological characteristics of ungauged or data scarce regions. However, for most hydrological processes, e.g. snow sublimation, avalanching, glacier melt and characteristics (debris, ponds and cliffs), permafrost, groundwater processes and routing processes, such spatial data do not exist (Beniston et al., 2018; Dobinski, 2011). The use of HMs, especially in high mountains where the hydrological processes vary considerably with altitude, is hampered due to the limited qualitative data availability at higher and remote regions (Klemeš, 1990).

It is extremely challenging to preform reliable streamflow simulations in particular for ungauged catchments and data scarce regions such as high mountain Asia (HMA) (Immerzeel et al., 2015b; Wortmann et al., 2018). Existing hydro-meteorological stations, mostly located in valleys lower than 4000m, are sparsely and unequally distributed in the region (Palazzi et al., 2013; Qin et al., 2009). The point-based station data are not representative of the complex surrounding in HMA. The low quality and limited availability of data at high altitude imposes difficulty in spatial interpolation and often leads to strong underestimation of HMA precipitation (Immerzeel et al., 2015b; Li et al., 2017; Palazzi et al., 2015).

To cater for these data scarcity issues, HMs either use a calibration parameter or an approximation based on limited data obtained from location specific studies (e.g. glacier mass balance, snow sublimation and hydraulic conductivity). Most of the processes are often measured or modelled at small scale (time and space). However, the real application requires estimation of these processes for long term and large region (such as lifetime of a hydraulic structures). Conversely, some local studies use regional and global-scale coarse data and parameters. The use of these approximations make the outcome from HMs

uncertain (Bierkens et al., 2001; Blöschl and Sivapalan, 1995; Peters-Lidard et al., 2017; Seyfried et al., 2009).

Remote sensing and satellite data provide better geographical coverage compared to sparse point-based station data and has been extensively used in the past decades to provide better understanding of the states and variables related to hydrological cycle and water resources (Wagner et al., 2009; Xu et al., 2014). Integration of remote sensing information with HMs provides a better uncertainty assessment of water resources and water-related issues and therefore in-depth exploration of the accuracy of such data is required (Emery and Camps, 2017).

1.2.2.4 Spatio-temporal resolution

The response time of hydrological processes varies from a few minutes (snow melt, snow avalanche) to multiple decades (glacier dynamics, groundwater flow in aquifers) (Hock, 2003, 2005; Koutsoyiannis, 2005b; Marshak, 2008). The choice of the appropriate modeling timestep for hydrological simulation again depends on availability of the data (temporal resolution of the forcing), dominant hydro-meteorological processes, geophysical characteristics of the catchments and objective of the study (Bastola and Murphy, 2013; Littlewood and Croke, 2008; Ostrowski et al., 2010; Smith et al., 2004a; Syed et al., 2003). For urban drainage processes a sub-hourly resolution time step is recommended whereas for irrigation a monthly resolution is found to be sufficient (Blöschl and Sivapalan, 1995). For the simulation of highly dynamic processes such as floods, a sub-daily time step is required to represent the high intermittency of convective precipitation and fast catchment response time which depends on basin physiographic characteristics such the size, drainage network, steepness, and percentage of impervious area (Ochoa-Rodriguez et al., 2015). The spatial resolution of HMs can vary from less than a meter resolution (for unsaturated flow processes) to few hundred kilometers (monsoon circulation). The coarse spatial resolution of HMs could be an important source of error in mountainous areas due to the missing interactions between the topography and atmospheric processes required for small scale processes (Beniston et al., 2018; Blöschl and Sivapalan, 1995; Sillmann et al., 2013).

1.2.2.5 Computational time

The use of physically based HMs is limited due to huge computational requirements (Huintjes et al., 2015; Koch et al., 2016; North, 1975; Paul and Kotlarski, 2010; Reid and Brock, 2010). On the other hand, conceptual HMs are becoming popular due to lower data and computation resources requirements (Koch et al., 2016). The advances in computational capacity in the recent decades made it possible to model the desired system, keep track of the state and fluxes of a system at any given time and spatial scale (Fatichi et al., 2016). However, computing remains a present-day challenge as the expectations have also increased beyond limits (Bierkens et al., 2015; Clark et al., 2017). The issues related to the tradeoff between the process complexity, spatial complexity, domain size, ensemble size, the time period of simulation, single deterministic simulation and model inter-comparisons still persist (Clark et al., 2017; Wood et al., 2011).

1.2.2.6 Uncertainties

Communicating predictive uncertainties with hydrological predictions are essential for water resources and other relevant decision-making processes (Georgakakos et al., 2004; Liu and Gupta, 2007). HMs involve many processes, and each component brings an uncertainty which ultimately contribute to the total uncertainty. Uncertainties in HMs stem from parameters, model structure, input data, initial conditions and calibration (Lindenschmidt et al., 2007; Papacharalampous et al., 2019; Renard et al., 2010; Sudheer et al., 2011; Troin et al., 2016; Wilby, 2005). Parameter uncertainty in HMs is a result of conceptual simplification which arises due to inadequate process understanding, over approximations, limited data, inability to measure or estimate a process (e.g. hydraulic conductivity can be measured at point scale but varies considerable for catchment scale), natural process variability, and observational errors (Beven, 2012). The structural uncertainty, sometimes referred to as “model uncertainty”, in HMs

mainly arises due to the simplified representation of hydrological processes (Lindenschmidt et al., 2007; Moges et al., 2021; Troin et al., 2016). HMs structural uncertainty also includes alternative conceptualizations related to surface and subsurface processes (Refsgaard et al., 2012). The input uncertainty in HMs is governed by uncertainty in forcing (sampling and measurement error in rainfall and temperature, large variability among the reanalysis, satellite derived and merged products), elevation, soil characteristics and other catchment related information. HMs require calibration of different parameters (including snow, glaciers and rainfall-runoff) and states based on the availability of ground-based observations. The errors emerging from unsatisfactory calibration and imperfect observations (for e.g. systematic error in stage and runoff measurements, rating curve extrapolations and hysteresis errors) contribute to the calibration and observational uncertainty of HMs (Domeneghetti et al., 2012; Kiang et al., 2018). Parameters calibrated to a stationary climate also add uncertainty in the hydrological prediction used to assess climate change impacts (Brigode et al., 2013; Wilby, 2005). Model structural uncertainty is found to be the dominant source of the predictive uncertainty in HMs under both stationary and non-stationary climate (Højberg and Refsgaard, 2005; Mendoza et al., 2015; Rojas et al., 2008). The input uncertainty, especially in data scarce mountain environments where the data involves interpolation, scaling and derivation from other measurements, constitutes about 10–40% of the predictive uncertainty (McMillan et al., 2018). To adequately assess and reduce the uncertainty from HMs, it is important to understand and quantify it (Liu and Gupta, 2007).

1.2.2.7 Coupling of models

Complexity is often required to understand the interaction between nature and human systems (Nobre et al., 2010). Often the overall response of the system doesn't provide key knowledge on how the principal components of the system interact. Earth system processes have their unique feedback mechanism and proper understanding of the system requires in depth modeling of these interactions and feedback mechanisms. The need for an integrated approach where the models integrate several aspects of the climate, ecology, hydrology and socio-economic system is increasing (Ning et al., 2019). The integration of feedback mechanism from several processes is achieved via coupling (or cascading) of models, i.e., atmospheric, hydrological, hydraulic, hydrodynamic and socio-economic models.

In flood risk assessment or forecast modeling, coupling is generally composed of a numerical weather prediction model for meteorological variables (precipitation, temperature and humidity etc.), a HM to assess runoff generation and water storage, hydraulic model for flow routing and a hydrodynamic model for the floodplain inundation (Grimaldi et al., 2019; Pappenberger et al., 2005). For flood risk assessment at various spatial scales, i.e., from catchment to global scale, rainfall to runoff conversion and routing are crucial components (Alfieri et al., 2017; Biancamaria et al., 2009; Dottori et al., 2018; Laganier et al., 2014; Lian et al., 2007; Ward et al., 2015). Hydraulic models, which solve equations of fluid motion to replicate the movement of water, are used for routing of flow components. These models can be a simple one-dimensional scheme which assume flow along the river channels in one direction only. However, that assumption is not valid when the flow is expected to spread around the flood plain. A fully two-dimensional hydraulic model, with plethora of data dependencies, is often required for an accurate operational flood forecasting system (Bates et al., 2018; Emerton et al., 2016; Schumann et al., 2016; Vorogushyn et al., 2018). Moreover, flood risk assessments at low lying coastal regions require an ocean hydrodynamic model for robust assessment of water levels (Barnard et al., 2019; Ganguli et al., 2020; Ikeuchi et al., 2015; Pasquier et al., 2019; Vousdoukas et al., 2018).

The integration (or coupling) between hydrological, hydraulic and hydrodynamic (or ocean) models is achieved by either (a) one-way coupled; where output from one model is used as input for another (Torres et al., 2015) (b) loosely coupled; where models run separately and some information is exchanged between the model (Goodall et al., 2011) (c) tightly coupled; where models are combined into one framework and full transfer of information among the models is possible (Loftis et al., 2016; Tang et al., 2013) (d) fully coupled; where the governing equations of all the physical processes are considered and solved simultaneously (Bilskie and Hagen, 2018; Santiago-Collazo et al., 2019; Sulis et al., 2010). The one-way and loosely coupled methods are easy to implement, require less computational time and effort compared to tightly coupled methods. However, they neglect the interaction of flood

generation mechanisms such as storm surge/quick surface runoff, storm surge/out-of-bank flow, storm surge/backwater flow and storm surge/streamflow.

Risk analysis depends on complex interaction and feedback mechanism of many physical processes represented by impact model (or chain of models) for instance droughts, where precipitation and evaporation interact via a land-atmosphere feedback mechanism. Another example of such interaction is coastal flood where large scale circulation patterns bring both storm surge and precipitation over the estuaries. The circulation pattern characteristics, local topography, lag-time relations and spatio-temporal correlation dictate the simultaneous occurrence of storm surge and river floods. Modeling of such a system requires an integrated framework where the physical processes can interact with each other.

The coupling of such vast arrays of models in an integrated system requires an internal consistency (space and time) and conservation of mass, energy and momentum components among the individual models (Santiago-Collazo et al., 2019). In most of the situations, these disparate models are never designed nor intended to be coupled together (Bilskie et al., 2014; Bilskie and Hagen, 2018). Moreover, each of these models are subject to different uncertainties (for instance model structure, parameters and inputs). Understanding the propagation of these uncertainties through the modeling cascade is a rigorous task and practically not feasible (Pappenberger et al., 2005; Ward et al., 2015).

1.3 Compound events

1.3.1 Definition

Hydro-meteorological extreme events (e.g., floods, droughts, heatwaves and wildfires), arise from the complex interaction of several natural processes at multiple spatio-temporal scales (Leonard et al., 2014; Zscheischler et al., 2020). For instance, hazards such as floods can occur from either anomalous precipitation, wind or temperature conditions leading to snow and glacier melt, rain on snow, saturated soil conditions and high groundwater levels, although not all these drivers and conditions need to be extreme. In coastal environments, storm surge from the sea adds an additional flood risk when combined with riverine floods. Unusual combinations of processes are difficult to foresee as they are rare and frequently do not have observed historical analogues (Blöschl et al., 2020; Milly et al., 2002). Superposition of multiple drivers and/or hazards may overamplify the impacts to society (Zscheischler et al., 2018). Conventional univariate hydro-meteorological analyses, related to weather and climate extremes, focus on single variable such as precipitation, temperature and river discharge and are not always able to resolve all the necessary conditions that lead to a significant impact (Fischer and Knutti, 2013; van den Hurk et al., 2015; Leonard et al., 2014; Orlowsky and Seneviratne, 2012; Trenberth et al., 2015). Changes in any of these variables over time will affect flood risk. For instance, meteorological variables, such as extreme precipitation and temperature, have been widely used to understand floods and droughts both for the current and future climate (Alexander et al., 2006; Dai, 2013; Donat et al., 2014; Dunn et al., 2020; Kokkonen et al., 2006; Kundzewicz et al., 2014; O'Gorman, 2015). It is not clear if increases in precipitation extremes would result in increased flood magnitudes as studies find more evidence of decreases than increases in flood magnitudes (Archfield et al., 2016; Blöschl et al., 2017; Do et al., 2017; Hall et al., 2014). An extreme precipitation event does not always lead to flooding. For example, 36% of extreme precipitation events lead to a corresponding extreme discharge across regions in the United States (Ivancic and Shaw, 2015). However, precipitation conditional on the catchment being wet before the start of the event increased the probability of extreme discharge to 62% compared to 13% when the moisture conditions before the event are dry (Sharma et al., 2018).

Thus, such hydro-meteorological events (or compound events) require an in-depth understanding of the dependence structure of multiple drivers (weather, climate and hydrological) that are involved in making an event extreme in magnitude and extreme in impact to society and ecology at appropriate spatio-temporal scales (van den Hurk et al., 2015; Kew et al., 2013; Leonard et al., 2014; Wahl et al., 2017; Zscheischler et al., 2018). To this end, first, a concise definition is required to characterize compound

events and establish a concrete framework that is helpful to assess future risks. The Intergovernmental Panel on Climate Change (IPCC) special report on managing the risks of extreme events and disasters to advance climate change adaptation (SREX) (Seneviratne et al., 2012), first defined compound events as:

"(1) two or more extreme events occurring simultaneously or successively, (2) combinations of extreme events with underlying conditions that amplify the impact of the events, or (3) combinations of events that are not themselves extremes but lead to an extreme event or impact when combined. The contributing events can be of similar (clustered multiple events) or different type(s)."

This definition proposed by the IPCC was ambiguous and unable to define the role of conditions (if such conditions are part of the compound event definition or they just amplify the event), the associated scale (both space and time) and event descriptors (if a single event can be a compound event of multiple drivers or if a compound event is made of two or more distinct events). These ambiguities made it difficult to develop concrete and discrete sets of methodology for quantifying the risk (Leonard et al., 2014).

The definition of compound events has evolved over time (Leonard et al., 2014; Zscheischler et al., 2018) and the IPCC's special report on the ocean and cryosphere in changing climate (SROCC) (Collins et al., 2019) reformulated the definition as:

"a combination of multiple drivers and/or hazards that contributes to societal or environmental risk"

where drivers are defined as any natural or human-induced factor that directly or indirectly causes a change in a system and may span over multiple spatial and temporal scales. Hazard refers a natural or human-induced physical event or trend or physical impact driver that may cause loss of life, injury, or other health impacts, as well as damage and loss to property, infrastructure, livelihoods, service provision, ecosystems and environmental resources. Risk, a product of hazard and its consequences, refers to the potential for consequences when something of value is at stake and the outcome is uncertain, recognizing the diversity of values.

To understand the risk associated with compound events it is important to have detailed information about: (a) what are contributing variables (also drivers and hazards)? (b) Are there any physical mechanism associated with the contributing variables? (c) How does dependence between the variables affect the magnitude of the event? (d) How does magnitude and occurrence of such events differ under present and future climate? A clear and coherent typology (or classification) of different types of compound events is required to answer these questions. In the following subsection, I present a typology of compound events related to weather and climate.

1.3.2 Typology of compound events

To understand weather and climate related typology, I corroborate definitions and examples from Zscheischler et al., (2020b). From weather and climate perspective, the compound event can be classified in to four categories:

(a) Preconditions that cause or lead to an amplified effect
(b) Multiple drivers of hazard cause an impact
(c) Sequence of hazard in time causes an impact
(d) Spatially co-occurring hazard cause an impact.

In the first category, impact is caused by the preconditions by weather or climate drivers. For instance the floods in Europe and USA are often caused due to a combination of saturated soil conditions or extensive snow cover (a precondition) and precipitation and/or snow melt (Berghuijs et al., 2016, 2019). Other examples of such preconditioning are: rain-on-snow flood events in the Swiss Alps, where snowfall leading to excessive snow cover is a precondition and the resulting flood is a hazard (Rössler

et al., 2013); low soil moisture conditions (a precondition) from the previous year leading to forest fires in Siberia (Forkel et al., 2012), wild fire in France leading to droughts in the northern Mediterranean (hazard) (Ruffault et al., 2018); and flash flood in a Ugandan mountain valley (hazard) triggered by mild precipitation but preconditioned by upstream fire and landslide (Jacobs et al., 2016).

In the second category, multiple drivers can cause one or more hazards/impacts or, alternatively, a single driver can cause multiple correlated hazards/impacts. Examples of such events are: compound coastal flooding in Italy (Bevacqua et al., 2017), the Netherlands (van den Hurk et al., 2015; Klerk et al., 2015) and the USA (Moftakhari et al., 2017; Wahl et al., 2015) which arises due to the combination of storm surge, waves, quick runoff and high river discharge; concurrent drought and heat waves caused by co-occurring precipitation and temperature extremes at multiple time scales (Cai et al., 2018; Hao et al., 2019; Hoerling et al., 2013; Schumacher et al., 2019; Zscheischler and Seneviratne, 2017), hot and dry conditions leading to wild fires (Ruffault et al., 2018), thermoelectric power plant failure (Cook et al., 2015), crop failure (Coffel et al., 2019), tree mortality (Allen et al., 2015; Goulden and Bales, 2019); and impacts caused by co-occurring wind and precipitation extremes (Fink et al., 2009; Hillier and Dixon, 2020; Liberato, 2014; Lin et al., 2010; Martius et al., 2016; Raveh-Rubin and Wernli, 2015).

The third category refers to the successive hazards that leads to, or amplify, an impact when compared with a single hazard. The successive hazards can be either similar type (for instance multiple tropical cyclones (Villarini et al., 2010), heat wates (Baldwin et al., 2019; Hughes et al., 2019), heavy precipitation events (Barton et al., 2016)) or different type (for instance flood (Wang et al., 2019) or tropical cyclone (Matthews et al., 2019) followed by a heatwave). The hazards in this category can be correlated via common drivers (Tilloy et al., 2019).

The last category refers to those events which cause an impact, either the by same or different hazard, at multiple connected location within a limited time window. The hazard impacts at multiple locations (near or distant) are physically linked in this category. Typical examples of such events are: hazards and impact imposed by large scale modes of climate variability such as El Niño–Southern Oscillation (Anderson et al., 2019; Singh et al., 2018); atmospheric teleconnections (Boers et al., 2019; Sun et al., 2014); or driven by circumpolar-wave patterns (Kornhuber et al., 2019), synchronous crop failure due to spatially co- occurring hazards (Kornhuber et al., 2020), individual weather systems such as atmospheric blocking which caused widespread floods in 2010 in Pakistan (Lau and Kim, 2012) or storms (Guisado-Pintado and Jackson, 2018; Wernli et al., 2002), weather conditions that lead to low energy output from wind turbines in multiple region concurrently and thus increasing the risk of power failures (van der Wiel et al., 2019), co-occurring climate hazards such as floods which damages road and rail network significantly (Koks et al., 2019) and concurrent storm surge along a coastline affecting ports and supply chains (Haigh et al., 2016).

1.3.3 Compound event and risk analysis framework

Compound events are analysed under the general risk framework which links hazard, exposure and vulnerability aspects (Figure 1.2). Exposure refers to the elements (population and values of assets) in an area where a hazard event may occur whereas vulnerability is the propensity or capacity of exposed elements to cope with the adverse effects of hazards. Exposure is intrinsically linked with the human environment (Thywissen, 2006). For instance, flood exposure can only have negative consequences in environments with human influences such as settlements, livelihood, landuse, agriculture and economic activities (Schanze, 2006). Adaptation and risk management strategies depend on a rigorous understanding of the dimensions of hazard, exposure and vulnerability, and proper assessment of changes in those dimensions (Collins et al., 2019; Koks et al., 2015; Kron, 2005).

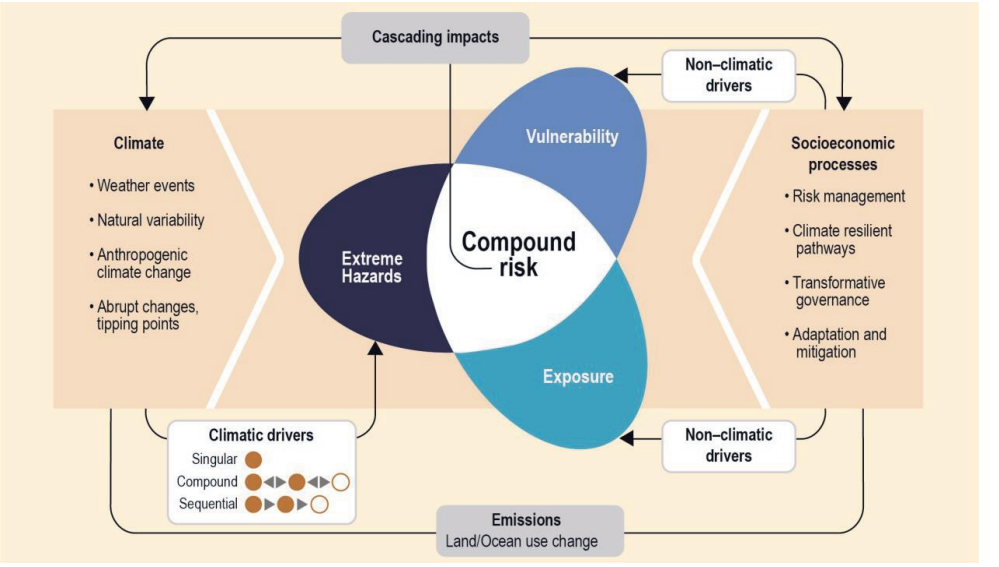

Figure 1.2: *Climate related compound event analysis framework proposed by Intergovernmental Panel on Climate Change (Collins et al., 2019).*

A first step in compound event analysis is the identification of drivers (or hazards or preconditions) of a system whose risk needs to be estimated. In most cases drivers can be clearly identified. For instance, temperature and humidity are the main drivers causing heat stress in humans (impact) (Deschenes, 2014; Kjellstrom et al., 2016). However, in some cases the drivers of impact are unknown or caused by many drivers and their interactions. A typical example of such system is coastal flooding which arises due to either one or a combination of multiple drivers and hazards i.e., storm surge combined with astronomical tides, locally generated waves, quick surface runoff from frozen and saturated ground and river discharge (Hendry et al., 2019; van den Hurk et al., 2015). To identify the drivers, their combination, sequence, system boundaries and associated spatio-temporal scales, a proper understanding of the overall system is required.

The system characterization in compound event analysis depends on the spatial extent of the drivers (hazard or impact) (see Figure 1.3). For instance, van den Hurk et al., (2015) used a relatively small system where excessive inland water from a water board close to Dutch coast, i.e., Noorderzijlvest, is drained off gravitationally to the North Sea though a combination of pumps and reservoirs. A series of low-pressure systems passing over the North Sea resulted in 60 mm of precipitation accumulated over 5 days in January 2012. The combination of five consecutive tidal period and storm surge in the same period did not permit any gravitational drainage to occur. High inland water level led to precautionary measures such as evacuation and use of emergency overflow areas. The authors demonstrated that the high tails of both storm surge and precipitation are driven by one or multiple active low-pressure systems which set up a strong Northerly wind leading to a storm surge, while at the same time the associated frontal systems produced high amounts of precipitation. The authors found a clear correlation structure between accumulated precipitation and single minimum sea level for a smaller aggregation period (1 day) compared to a larger aggregation period of 5 days where no correlation was found. The authors did not use any lag time correlation, i.e. time required for the translation of precipitation to discharge at the outlet, in their system as the area was close to the coast. Another example is the Rhine delta where discharge delay plays a key role as the precipitation from the same frontal system which sets up storm surge requires a travel time of a few days (6 days) to reach the coast (Klerk et al., 2015). In large systems such as the Rhine, where soil moisture, snow and glacier storage in the headwaters play an important role in determining the flow regime, extreme antecedent rainfall or snowfall can contribute to elevated

risk of high discharge, leading to coastal and fluvial flooding. Therefore, a clear distinction of space and time scales is required for the compound event analysis.

The next step is to identify the dependence structure and strength of the identified variables (or hazards or preconditions). Methods such as regression (Berghuijs et al., 2019; Forkel et al., 2012), event compositing (Ruffault et al., 2018), physically based modeling (Sippel et al., 2017), copula fitting (Bevacqua et al., 2017; Moftakhari et al., 2017), event clustering (Barton et al., 2016) and semi variograms (Davison et al., 2012) are used to investigate the complex and varying spatio-temporal dependence structure required for quantifying compound effects (Zscheischler et al., 2020). The next step involves projection of key dependencies to potential impacts. This is done by choosing the appropriate hazard scenario which is subjective and depends on personal judgement (thresholds), event characteristics, objective and available data (Durante and Salvadori, 2010; Moftakhari et al., 2017; Zscheischler and Seneviratne, 2017). For instance, at the confluence of two rivers, floods can be due to occurrence of flood in one river, or the other, or both hazard scenarios and both 'OR' and 'AND' hazard scenario can be constructed to deal with the problem (Bender et al., 2016; Salvadori et al., 2016). Similarly, for hydraulic infrastructures like dam and spillway, damages can be caused by either flood peak or flood volume or both exceeding a certain magnitude or threshold (Shiau, 2003; Volpi and Fiori, 2014; Xu et al., 2017). Concurrent extreme droughts and heat waves (AghaKouchak et al., 2014), wind speed and duration of storm dust (Li et al., 2013), hydrological drought duration and severity (Zhang et al., 2013) and water level and waves (Masina et al., 2015) are some examples where either 'AND' or 'OR', or both hazard scenarios are used. Multivariate hazard scenarios could also be constructed using a "Kendal", "Survival Kendall" and "Structural" approach (Salvadori et al., 2016). Finally, the exposure and vulnerability aspect are juxtaposed with hazards to understand the risk.

1.3.4 Compound event under climate change

The climate change response of different hydrological processes depends strongly on spatio-temporal scales and varies from catchment to basin and sub-daily to decadal-scale (Hock et al., 2019a). While rainfall-runoff processes respond quickly to climatic changes, glacier melt generation responds at longer timescales of decades to centuries and strongly depends on the available ice volume and the time scale considered. For snow, different processes combine in response to warming: a higher temperature accelerates snowmelt but reduces the fraction of precipitation that falls as snow, which eventually will lead to a decrease of snowmelt as a contributor to total runoff. However, the response time for snow processes under climate change varies from seasonal to annual time scales. Via compensating and contrasting impacts of precipitation and temperature on the discharge volume from the headwaters, changes in these climatic variables give rise to nonlinear, non-stationary, and non-uniform responses of cryospheric and hydrological variables such as snow, glaciers, soil moisture, and groundwater, at varying spatial and temporal scales (Blöschl et al., 2017; Hall et al., 2014). Understanding the likely causes of changes in these state variables and antecedent conditions are necessary to assess the hydrological risk in future.

To quantify the impacts of climate change on economic and societal sectors such as agriculture (Moore et al., 2017; Rosenzweig et al., 2014), water resources (Schewe et al., 2014), energy supply and demand (van Vliet et al., 2016), human health (Whitmee et al., 2015) and ecosystem services (Pecl et al., 2017), impact models are required (Schewe et al., 2019). Impact models which are simple and parameterized based on the past and current climate might not provide correct estimates both under anthropogenic climate change and land surface changes (Manning et al., 2018; Zscheischler et al., 2017).

For instance, traditional simple flood frequency analysis is representative only when drivers of flooding are stationary over time and not appropriate for designing infrastructure under future climate change. In events-based HMs for instance, antecedent soil moisture conditions, evaporation factors and routing coefficients are treated as calibration parameters whereas the flood generating relationship may change in the future. This is critical to systems where the compound nature of impact may emerge in the future due to the changes in the distribution of drivers (Maraun and Widmann, 2018). For instance, coastal settlements located close to a river mouth which are only affected by river floods under the current

climate may be affected additionally by sea level rise under climate change (Bevacqua et al., 2020; Wahl et al., 2015).

Figure 1.3: *Schematic representation of different systems i.e. mountains (area within red dashed line where drivers of hazard such as extreme rain, high temperature, snow and glaciers melt components affect floods) and coastal environment (area within blue dashed line where drivers of hazard form mountainous catchment as well as storm surge and wave from sea affect floods) (sketch credit: Kriti Shrestha).*

A good compound analysis framework will not always succeed in bringing a multivariate problem (drivers, hazards) to a univariate dimension (impact). Therefore, future risk assessment based on a single impact model accounting for river discharge may not be sufficient. A good understanding of the physical processes that lead to such compound events is necessary. Thus, robust approaches and impact models based on physical understanding of the system are required to simulate the impact of future climate change.

1.4 Research objectives and thesis outline

From the preceding sections, it is evident that several key challenges related to compound floods need to be addressed to better understand the historical and future water resources in mountain and coastal environments. Flood related processes require a proper investigation of the characteristics of temporal and spatial scales involved. For instance, the compound impact of high temperature and high precipitation in a mountainous basin are different than in a similar sized sub-basin at lower altitude. These differences in response across space and time are primarily due to various flood generation mechanisms since for headwaters snow, glacier melt and hillslope processes are important, whereas

antecedent soil moisture conditions, groundwater conditions and human development in the catchment predominantly influence the runoff generation mechanisms at lower altitudes and coastal estuaries. It is important to understand how the interplay between atmospheric (precipitation and temperature) and catchment processes (snow, glaciers, rainfall-runoff, soil moisture and antecedent conditions) across time and space influences flood regimes and the occurrence of extreme floods. Improved knowledge of key processes across time and space will help to better understand the future flood risk and climate change impact on water resources.

In this thesis, I address the research gaps mentioned in previous sections to understand the compound floods in mountain and coastal environment. I have selected four case studies in large river basins in Europe and Asia (Figure 1.4), which I elaborate in the next chapters of this thesis.

The main objective of this PhD thesis is

Mapping future floods and water resources by modeling compound drivers at multiple spatial and temporal scales

Forthcoming from the main objective and the identified challenges, the following research questions (RQs) are formulated:

RQ1 *Under which conditions are hydrological risk assessments based on multivariate analysis methods more realistic than assessments based on univariate methods?*

RQ2 *What is the best approach to combine proxy-based flood indicators with process-based modeling to study the role of compounding events in hydrological risk assessments?*

RQ3 *Can we improve the understanding and prediction of hydrological extremes if memory effects and compounding events are incorporated?*

RQ4 *What is the impact of improved process understanding and analysis techniques on the assessment of future climate risks?*

The chapters in this thesis are arranged based on increasing order of modeling complexity (see Table 1.1). First, historical climate trends of key drivers, i.e. precipitation, temperature and their compound occurrence, at different temporal (seasonal and annual) and spatial scales (gridded, basin and regional aggregates), over nineteen sub-basins across High Mountain Asia (HMA) are assessed in **Chapter 2** using the consistent and state-of-the-art ERA5 high-resolution reanalysis data. This chapter covers **RQ1** and includes the typology of compound events where multiple drivers of hazard cause an impact. Second, impact of these climatic trends on hydrological characteristics and water resources, which are influenced by spatio-temporal changes of many other state variables and fluxes, i.e. soil moisture content, evapotranspiration, glaciers, snow, ground water, antecedent conditions assessed in **Chapter 3.** A fully distributed cryospheric-hydrological model for fifteen sub-basins across the HMA region is used to simulate the impacts of climate change on the hydrological cycle and water resources at varying spatio-temporal scales. The compound impact of changes in precipitation and temperature on peak water availability and shifts in hydrological regimes for different combinations of future climatic changes are assessed in this chapter. This chapter covers **RQ1** and **RQ2** and includes compound events where preconditions (snow fall, glacier melt and soil moisture) cause or lead to an amplified effect. Third, the effect of memory component within hydro-meteorological systems which are responsible for the generation of extreme discharges are investigated for the Rhine basin using a fully distributed cryospheric-hydrological and hydraulic model in **Chapter 4**.

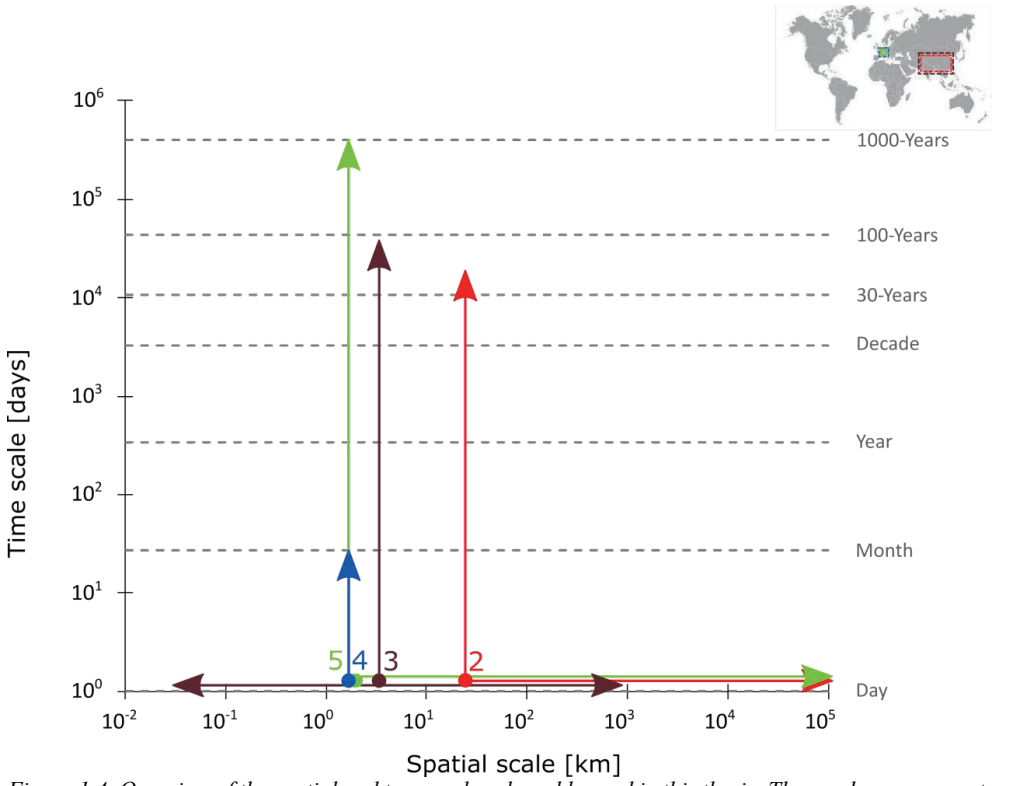

Figure 1.4: *Overview of the spatial and temporal scales addressed in this thesis. The numbers represent the chapters. The colored dots represent the spatial and temporal resolution of the models used in the chapters. The arrows represent the scales (time and space) covered in each study. The rectangle and inset map (right top) show geographical extent of each study presented in this thesis*

The role of meteorological autocorrelation is assessed by perturbing the time-correlation of the meteorological time series which is used as forcing for streamflow simulations. Furthermore, the role of snow and soil moisture memory in the hydrological regime of the Rhine is quantified in this chapter. This chapter covers **RQ3** and includes compound events where preconditions (snow fall and antecedent soil moisture) cause or lead to an amplified effect and includes sequence of hazard (extreme precipitation events) in time causes an impact. Finally, the possibility of finding compound flood events, i.e., near-simultaneous storm surge and extreme river discharge is explored in **Chapter 5.** Two hydrological models, a hydraulic model and a storm surge model are used to demonstrate the importance of proper physical model configurations to correctly assess the lag time correlation for compounding high coastal water level and high discharge events in the Rhine basin. These models use output from a large ensemble of a high-resolution regional climate model to assess the temporal dependence structure of compounding extreme coastal water level and river discharge for the Rhine basin. This chapter covers **RQ2** and **RQ4** and includes compound events where multiple drivers of hazard (storm surge, waves, quick runoff and high river discharge) cause an impact (coastal flooding). In **Chapter 6** the main findings and answers to the research questions of the PhD research are synthesized and discussed, and an outlook is provided on possible future research directions.

Table 1.1: Summary of the chapters in this thesis

Chapter	Time frame	Region	Data	Approach And models	Drivers	Typology	Impact
2	Historical	HMA	Reanalysis (ERA5)	Univariate, Bivariate meteorological extremes	Precipitation and temperature	-Multiple drivers of hazard cause an impact	Floods and droughts
3	Historical /Future	HMA	Reanalysis (ERA5)	Hydrological modeling (SPHY)	Rainfall, temperature snowfall, and glacier melt	-Preconditions that cause or lead to an amplified effect.	Hydrological extremes, water availability, Seasonal shifts
4	Historical	Rhine	GCM-RCM ensemble (EC-EARTH)	Hydrological (SPHY) and hydraulic modeling (PCR-GLOBWB2)	Rainfall, snowfall, soil moisture and discharge	-Preconditions that cause or lead to an amplified effect -Sequence of hazard in time causes an impact	Floods and hydrological extremes
5	Historical	Rhine	GCM-RCM ensemble (EC-EARTH)	Hydrological (SPHY and HBV) hydraulic (PCR-GLOBWB2) and hydrodynamic modeling (RACMO)	Storm surge, waves, quick runoff and high river discharge	-Multiple drivers of hazard cause an impact	Coastal floods and hydrological extreme

2

Chapter 2

Historical climate trends over High Mountain Asia derived from ERA5 reanalysis data

2 Historical climate trends over High Mountain Asia derived from ERA5 reanalysis data

The climate of High Mountain Asia (HMA) has changed in recent decades. While the temperature is consistently increasing at a higher rate than the global warming rate, precipitation changes are inconsistent, with substantial temporal and spatial variation. Climate warming will have enormous consequences for hydro-climatic extremes. In particular for the higher altitudes of the HMA, which are a significant source of water for the large rivers in Asia. Often trends are calculated using a limited number of in-situ observations mainly observed in valleys, which do not represent the climatic changes at high altitude. This study explores the changes in mean, extreme, and compound-extreme climate variables and their seasonality along with the full altitudinal range in HMA using daily ERA5 reanalysis data. Our results show that winter warming, and summer wetting dominates the interior part of HMA, whereas the western and eastern basins are drying. Our results indicate a coherent significant increasing trend in the occurrence of heatwaves across all regions in HMA. The number of days with heavy precipitation shows higher variability in southern and eastern basins than other areas of HMA. The dry-period occurrence shows a distinct demarcation between lower and higher altitude regions and is increasing for most basins. While precipitation and temperature show variable tendencies, their compound occurrence is coherent in the monsoon dominated basins. These changes in indicators of climatic extremes imply substantial increases in the future occurrence of hazards like floods, landslides, and droughts, which in turn may impact economic production and infrastructure.

Chapter based on:

Khanal, S., Tiwari, S., Lutz, A. F., Hurk, B. van den., Immerzeel, W. W; Historical climate trends over High Mountain Asia derived from ERA5 reanalysis data, Journal of Applied meteorology and climatology (JAMC), 2021 (under review)

2.1 Introduction

High Mountain Asia (HMA) serves as a major water source for large rivers in Asia (Immerzeel and Bierkens, 2012). HMA consists of the Tibetan Plateau, surrounded by the mountain ranges of Tien Shan, Pamir, Hindu Kush, and the Karakoram in the West, the Himalayas in the South and Southeast, and Qilian Shan in the East. Over 1.4 billion people in various countries, including Afghanistan, Bangladesh, Bhutan, China, India, Kazakhstan, Kyrgyzstan, Mongolia, Myanmar, Nepal, Pakistan, and Tajikistan, depend on water originating from HMA. The topography and atmospheric circulation patterns mainly define climate variability (Maussion et al., 2014; Schiemann et al., 2009; Webster et al., 1998). The region has a strong longitudinal (West-East), latitudinal (North-South), and vertical climate gradients (Yao et al., 2012a). The climate of HMA is driven by the interaction of the Indian summer monsoon, dominant in the south-eastern parts, while winter westerly winds dominate the climate in the western region. The steep north-south orographic results in strong temperature gradients which drives the moisture-laden winds from the Indian Ocean to the landmass, and ultimately the moisture is released under the orographic influence.

Consequently, the southern and eastern parts of HMA receive nearly 80% of the yearly precipitation from June to September during the monsoon season, which occurs as rainfall at low altitude and snow at high altitude (Bookhagen and Burbank, 2010). Conversely, the westerly winds in the West, originating from the Mediterranean, contribute around 50% of annual precipitation during winters, mainly falling as snow (Bao and You, 2019; Rees and Collins, 2006). The interaction of the monsoon and westerlies, where the monsoon has a dominant role in the summer months and westerlies in the winter months, influences the climate of the interior Tibetan Plateau (TP) (Frauenfeld et al., 2005; Yang et al., 2014; You et al., 2015b).

The climate of HMA has witnessed many changes in recent decades. There are spatially consistent and statistically significant warming trends over the different regions of HMA (Krishnan et al., 2019; Liu and Chen, 2000). Studies based on ground-based observations have consistently reported warming trends over the TP in the past (Kosaka and Xie, 2013; Liu and Chen, 2000; Yan and Liu, 2014). Tien Shan, Central Asia, and the Hindu Kush Himalayas (HKH) region have observed similar warming trends (Aizen et al., 1997; Hu et al., 2014; Ren et al., 2017). In contrast to temperature, precipitation shows a more considerable interannual variability, and inconsistency in trends for different regions in HMA (Fowler and Archer, 2006; Palazzi et al., 2013; Ren et al., 2017; Shrestha et al., 2000; You et al., 2015b; Zhan et al., 2017). The climate variability in recent decades resulted in changes in the cryosphere (glaciers, snow cover, permafrost) and hydrology (water availability, seasonality, hydrological extremes like floods and droughts), which in turn affects society (Bolch et al., 2012; Immerzeel, 2010; Jin et al., 2020; Kääb et al., 2012; Kang et al., 2010; Shean et al., 2020; Wijngaard et al., 2017; Yang et al., 2010; Yao et al., 2012b).

Past studies used monthly scale station data to derive the historical trends for different regions in HMA (Cao et al., 2013, 2017; Duan and Xiao, 2015; Guo and Wang, 2012; Khattak et al., 2011; Liu and Chen, 2000; Shrestha et al., 1999, 2000; Xu et al., 2018; Yan and Liu, 2014; Yang et al., 2014). Attempts were made with remote sensing techniques to calculate trends (Qin et al., 2009; Salama et al., 2012; Zhong et al., 2011). Some recent studies used the general circulation model (GCM) data downscaled with fine resolution regional climate models (RCM) to calculate the long term trends (Amato et al., 2019; Zhang et al., 2017). Moreover, some studies combined in-situ and reanalysis data to understand the spatial pattern of historical climate change (An et al., 2017; Krishnan et al., 2019; Madhura et al., 2014). However, these studies are either scattered around the basin, national and regional level. Further, these scattered studies use different data, coarser spatio-temporal resolution, and approaches. Variability in approaches, data, and methods makes it even more challenging to align and compare the changes around different regions in HMA. Studies that use consistent, observed, and remotely sensed data integrated with numerical models at a higher spatial resolution over the entire HMA region are required to resolve the climate variability in the region.

Existing hydro-meteorological stations, mostly located in valleys lower than 4000m, are sparsely distributed in the region (Qin et al., 2009). The complex topography and harsh conditions in the mountains impose difficulties in managing the ground stations. Therefore, climate signals are biased towards these station observations at lower elevations (An et al., 2017; Palazzi et al., 2013). Remotely sensed satellite measurements from geostationary thermal infrared and polar-orbiting passive microwave sensors are useful for deriving precipitation measurements based on cloud-top brightness temperature and spectral scattering due to large ice particle, respectively. However, the uncertainty is high due to sensor signals' limitations in penetrating the clouds and correctly estimating the precipitation falling as snow at high altitudes (Immerzeel et al., 2015a). Nevertheless, remotely sensed products, in the recent decades, have proven to be a cost-effective and reliable tool to understand precipitation patterns and trends at various spatial and temporal scales (Gehne et al., 2016). Among other remotely sensed products, the Asian Precipitation Highly Resolved Observational Data Integration Towards Evaluation (APHRODITE), the Tropical Rainfall Measuring Mission (TRMM), the Climate Hazard group Infrared Precipitation (CHIRPS), the Multi-Source Weighted-Ensemble Precipitation (MSWEP), the Climate Prediction Center MORPHing product (CMORPH) and the Precipitation Estimation from Remotely Sensed Information using Artificial Neural Network (PERSIANN) and are most commonly used in HMA region for wide range of applications (Ashouri et al., 2015; Beck et al., 2017; Funk et al., 2015; Huffman et al., 2007; Joyce et al., 2004; Yatagai et al., 2012). The direct use of such products to derive climatological and hydrological trends often requires validation and correction based on in situ observations (Gebregiorgis and Hossain, 2015; Gehne et al., 2016). The correction is often hampered by mismatch in resolution and insufficient geo-statistical interpolation accuracy of situ data caused due to sparse gauge distribution. Moreover, these global remotely sensed products have higher uncertainty in assessing correct precipitation amount in an environment with complex mountainous topography such as HMA (Cheema and Bastiaanssen, 2012; Mei et al., 2014). A common scientific consensus, based on a plethora of studies, could be made that all these remotely sensed data have large and variable biases

compared to the gauge data in HMA (Andermann et al., 2011; Cheema and Bastiaanssen, 2012; Guo et al., 2015; Tong et al., 2014; You et al., 2015a).

A gridded reanalysis product, which is a result of data assimilation from multiple sources; airborne balloons, scatterometers radiosonde, dropsonde, aircraft measurements, satellites, and ground-based radar-gauge composite, provides an alternative to the sparse and inconsistent point scale observations to find spatial patterns of change especially at higher altitudes (Alexander et al., 2006). Even though biases between reanalysis and in situ observations are present, the reanalysis products have shown good reliability in resolving the climatological mean, anomalies, and normalized trends (Donat et al., 2014; Simmons et al., 2010). Given the high variability in climate of HMA, this paper aims to assess trends in annual and seasonal air temperature and precipitation and a range of climate change indices for the high-altitude regions. We use the state-of-the-art ERA5 high-resolution reanalysis data to derive the trends (Hersbach et al., 2020). These trends help us detect similarities and contrasts in recent climate change over the entire HMA using one consistent dataset.

2.2 Study Area

The HMA, consisting of the TP and its surrounding high mountain ranges along with its 18 downstream river basins, is considered for this study (Figure 2.1). Within this region, the Hindu Kush Himalayan (HKH) range along with the TP covers an area of over 5 million km^2 with an average elevation of ~4000 m asl (above sea level) (Yao et al., 2012b). The areal extent considered in this study is 57° −113° E and 22° − 47° N. Given the large extent of the study area, the overall climate is variable. For example, in the West, the Helmand, Amu Darya, and Syr Darya river basins have a dry continental climate characterized by cold winters and hot summers (Chen et al., 2011), while in the East, the Yangtze basin has a sub-tropical climate with maximum rain between April and October (Gu et al., 2018). The north-western basins, Balkash, Junngar, and Alaguy are influenced mainly by mid-latitude westerlies and cold inflows from the polar region. The TP, generally below 0 °C and temperature decreasing from East to West, experiences cold winters and dry summers, with maximum precipitation during July and August (Frauenfeld et al., 2005). Climatic differences enhance the spatial variation within each basin's higher and lower altitudes (Krishnan et al., 2019; You et al., 2017). A significant part of the south-eastern basins' precipitation is from the southwestern Indian monsoon between June, July, August, and September. Winter monsoon brings rain to the north-western part of the HKH. At the high altitudes, precipitation mainly falls as snow, while at the lower altitudes as rain. The Central Asian basins receive annual precipitation of ~211mm, ranging from less than 50 mm in the desert areas and higher than 2000 mm on the windward slopes (Deng and Chen, 2017).

2.3 Data and Methods

We use historical climate data from the European Centre for Medium-Range Weather Forecasts (ECMWF) ERA-5 dataset covering the years 1979–2018 (40 years) (Hersbach et al., 2020). The ERA-5 is an improved (atmosphere, ozone, land, and ocean waves component) and high-resolution successor of the ERA-Interim (Dee et al., 2011). The ERA5 uses observations from over 200 satellite instruments or conventional data types, including ground-based radar–gauge observations, PILOT, radiosonde, dropsonde, buoys, and aircraft measurements. The ERA5 data are available at an hourly time scale and 31 x 31 km spatial resolution for 137 vertical pressure levels. Surface or single-level data are also available, containing two-dimensional parameters such as precipitation, 2m temperature, top of atmosphere radiation, and vertical integrals over the entire atmosphere. The daily aggregated surface level precipitation sum and mean temperature are used in this study to derive historical climate indicators as described in Table 2.1. We analyse each climate indicator on an annual scale and seasonal scale, (a) Winter (December, January, and February) (b) Summer (March, April, and May) (c) Monsoon (June, July, August, and September), and (d) Post-Monsoon (October, November).

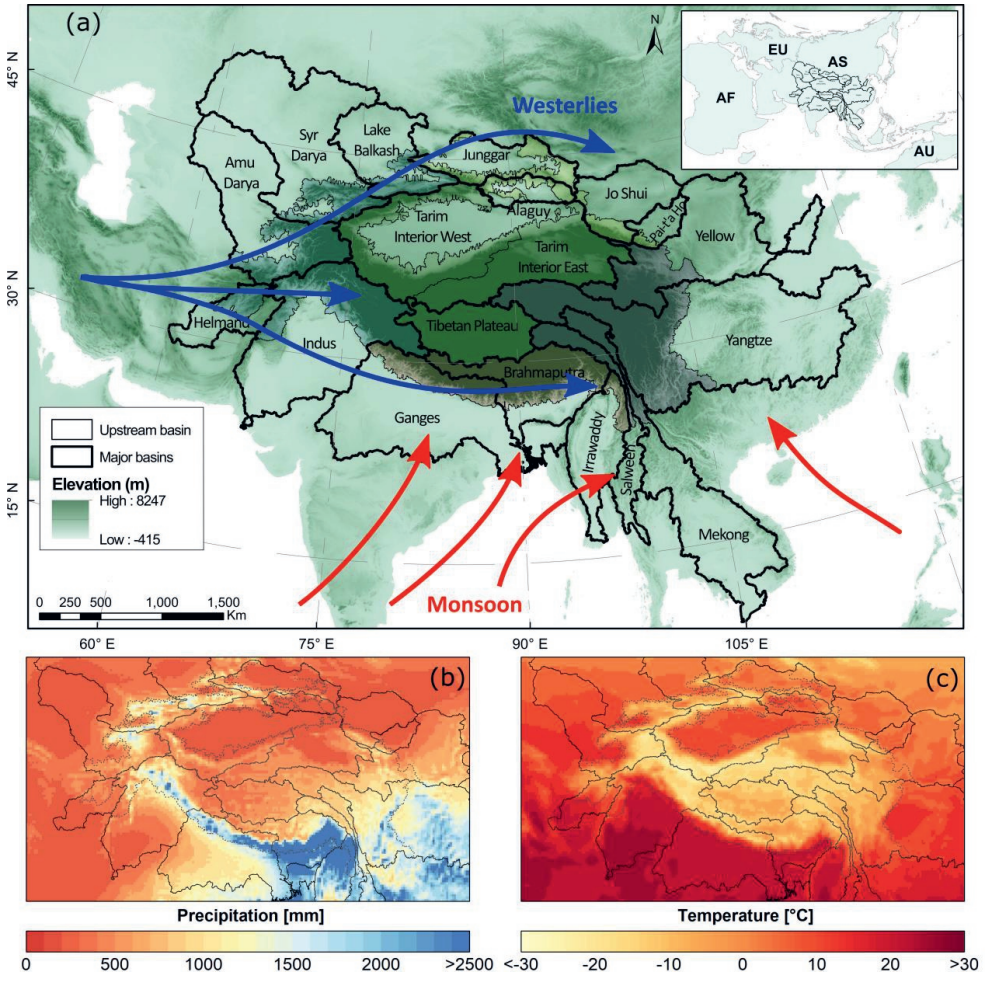

Figure 2.1: (a) The river basins analysed in this study (black boundaries). Grey lines represent the upstream region of each major river basin. The background represents the elevation of the region. The arrows represent the major atmospheric circulation system, red for monsoon and blue for westerlies, in HMA (arrows adapted from Yang et al., (2014)). Panels (b) and (c) show the spatial distribution of mean annual precipitation (mm) and temperature (°C) during 1979-2018 across HMA.

The climate indicators analyzed for this study are consecutive dry days (CDD), heatwave duration index (HWDI), highest five-day precipitation amount (RX5), heavy precipitation days (R10), wet days precipitation (R95P), and compound indices (COMP95). The first five indices used are defined and described in Zhang et al., (2011). We define COMP95 as the number of days when both precipitation and temperature are greater than the 95th quantile values of their distributions. For convenience, we use CDD and HWDI as the proxy for droughts and its related hazards, and R10, RX5, R95P, and COMP95 as a proxy for flood-related hazards.

Table 2.1: Climate indices used in this study

Indicator	*Definition*	*Unit*	*Related hazards*
Consecutive Dry Days (CDD)	The largest number of consecutive days with less than 1 mm precipitation	days	Drought
Heat Wave Duration Index (HWDI)	Number of days, in intervals of at least 6 consecutive days, when the maximum temperature is more than 5 degrees larger than the normal maximum temperature (TXnorm*)	days	Drought
R10	Number of heavy precipitation days (precipitation >10 mm)	days	Floods
RX5	Annual highest five-day precipitation sum	mm	Floods
R95P	Wet days precipitation (precipitation >1 mm) when daily precipitation is greater than 95th percentile of all wet days.	mm	Floods
COMP95	The number of days when both precipitation and temperature are greater than the 95th percentile of their distribution.	days	Floods

*TXnorm is the mean of maximum temperatures of a five-day window centered on each calendar day of a given climate reference period, here, 1981-2010.

We calculate the magnitude of the trend for each index using Thiel-Sen's slope estimate, and its significance at 5% ($p < 0.05$) using the non-parametric Mann-Kendall's significance test (Mann, 1945; Sen, 1968). It is preferred over other parametric tests since the data does not need to be normally distributed or homogeneous, and the effect of outliers is reduced as it is based on median values rather than means (Gilbert, 1987). The Thiel-Sen's slope method involves calculating the slope its median for each data point in time to calculate the trend. The slope for each data point is calculated as:

$$Q = \frac{x_i' - x_i}{i' - i} \quad (1)$$

where, x_i' and x_i are data values at times i' and i, respectively and where $i' > i$. Finally, the median of Q represents Thiel-Sen's trend. Before trend analysis, the data are checked for autocorrelation and corrected based on Yue and Wang (2002). We focus our analysis on the high-altitude upstream parts of each river basin. The upstream region used in this study is defined as all areas above 2000 m and is

delineated using the HydroSHEDS digital elevation model (Lehner et al., 2008b). Further, we categorize river basins in HMA by climatic regions (Table 2.2). Since the Tarim basin exhibits different climatic characteristics, we make a further distinction between the Tarim interior East (TIE) and the Tarim interior West (TIW). Unless specified the Tarim basin represents the whole of TIW and TIE. All the results presented in this study will represent the upper or upstream region unless specified explicitly. The basin average trends are calculated for the area aggregated basin average time series.

2.4 Results

2.4.1 Climatic characteristics

The HMA region shows considerable variability in climatic characteristics, as shown in Table 2.2. The monsoon dominated southern river basins generally receive the highest amounts of precipitation (Figure 2.2b). The Irrawaddy (3593 mm), Brahmaputra (1978 mm), and Ganges (1755 mm) basins are the wettest basins, whereas the Alaguy (218 mm) and Helmand (367) are the driest basins in HMA. The steep elevation gradient along the north-south and the monsoon are the main reasons for southern basins to receive most orographic precipitation. The average temperature in the region shows a distinct difference between the higher, colder mountain regions and the warmer plains (Figure 2.2b). The northern basins are coldest of the whole HMA. The relatively cold temperature is mainly due to higher mean elevation than other basins in HMA (Table 2.2). The monsoon dominated downstream areas of the Ganges, Indus, Irrawaddy, and Salween basins show the highest temperature. These regions are known to experience warm summers with extreme heat events and cold winters (Im et al., 2017). Given the large extent of the study area, the overall climate is variable.

Table 2.2: Average basin and climatic characteristics calculated for the upstream part of the major river basins. The climate of the basin can be of monsoon or westerly or mixed type. The upstream area represents the % of major river basins used as the upstream part in this study. The number inside the parenthesis represents the trend, and the bold number represent a significant trend at the p<0.05 level.

BASIN	*Region*	*Climate*	*Mean elevation (m asl)*	*Area (km^2)*	*Upstream Area (%)*	*Mean precipitation ($mm\ yr^{-1}$)*	*Mean temperature °C*
Brahmaputra	Southern	Monsoon	4003	400	75.7	1978 (-2.25)	1.7 (**0.03**)
Ganges	Southern	Monsoon	3090	202	17.8	1755 (**5.03**)	6.8 (**0.03**)
Irrawaddy	Southern	Monsoon	2109	49	12.6	3593 (**-24.73**)	12.9 (**0.02**)
Mekong	Eastern	Monsoon	3968	111	13.7	1035 (-1.37)	0.8 (**0.03**)
Salween	Eastern	Monsoon	4430	119	44.4	1096 (-2.31)	-2.1 (**0.04**)
Yangtze	Eastern	Monsoon	3678	687	38.5	1108 (-0.13)	1.9 (**0.03**)
Yellow	Eastern	Monsoon	3389	273	31.8	740 (-0.06)	0.5 (**0.04**)
Amu Darya	Western	Westerly	2930	268	33.6	678 (-1.29)	0.8 (**0.03**)
Balkash	Western	Westerly	2144	121	27.2	877 (-0.28)	1.2 (**0.02**)
Helmand	Western	Westerly	2355	74	29.7	367 (-2.11)	9.8 (**0.05**)
Indus	Western	Westerly	3511	473	42.4	837 (-1.98)	0.6 (**0.04**)
Syr Darya	Western	Westerly	2331	173	15.5	941 (1.10)	2.5 (**0.03**)
Alaguy	Northern	Westerly	1506	75	51.8	218 (-0.47)	6.8 (**0.03**)
Pai-t'a Ho	Northern	Westerly	2664	16	14.4	633 (-1.07)	0.6 (**0.05**)
Jo-Shui	Northern	Westerly	2575	66	18.8	395 (0.57)	1.3 (**0.05**)
Junggar	Northern	Westerly	1778	152	44.9	387 (-0.18)	3.0 (**0.02**)
Plateau of Tibet	Interior	mixed	4996	415	100	444 (**3.57**)	-3.2 (**0.03**)
Tarim Interior East	Interior	mixed	3842	600	37.8	305 (**1.63**)	-2.4 (**0.04**)
Tarim Interior West	Interior	mixed	3301	481	30.3	371 (0.14)	-0.9 (**0.03**)

2.4.2 Trends in temperature and temperature-derived indices

2.4.2.1 Mean air temperature

The annual temperature trends are coherent and statistically significant over the entire region (Figure 2.2a and Table A1). The cooling of irrigated Indo-Gangetic plains is in line with the finding that an increase in irrigated areas can lower the magnitude of climate change and extremes (Puma and Cook, 2010; Thiery et al., 2017). The averaged annual trend (0.05 °C yr^{-1} ~ 2.12℃ over 40 years) in the Helmand basin is inline with 2.2℃ increase reported by Krishnan et al., (2019) (Figure 2.2a and Table 2.2). The annual warming of regions in HMA is higher compared to Northern Hemisphere (0.024 °C yr^{-1} for land and Oceans and 0.033°C yr^{-1} for land) and the global average (0.017 °C yr^{-1} for land and Oceans and 0.03°C yr^{-1} for land) calculated for time 1979–2018 using Global Historical Climatology Network (NOAA, 2020). The seasonal spatial trends show that the increase (0.08–0.10 °C yr^{-1} ~ 3.2–4.0℃ over 40 years) is most apparent in the headwaters of the southern, monsoon dominated basins of the Ganges, the Brahmaputra, and the interior basins in winter (Figure 2.2b). The winter warming trend is higher for eastern TP, for which an increase of 0.61℃ per decade (~2.44℃ over 1961-2006) is reported (Liu et al., 2009). Strikingly, the northern basins, Junggar, Alaguy, and Balkash show a decreasing winter temperature trend. Several studies report a similar winter cooling in the Northern Hemisphere and attribute it to the increase in Eurasian snow cover contributed by the warmer moisture laden arctic atmosphere in the autumn season (Cohen et al., 2014, 2020, 2012). A relatively smaller warming trend is observed in the monsoon season compared to summer and winter seasons (Figure 2.2b, 2c, and 2d). The irrigated downstream region of the Indus shows a significant decrease in temperatures during the monsoon season, implying that most of the annual decline in temperature trend is contributed by the monsoon season.

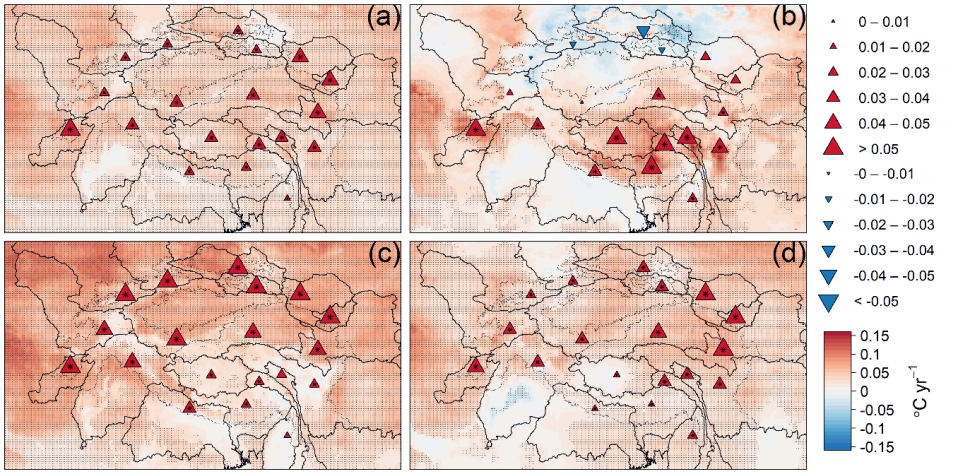

Figure 2.2: (a) Average daily mean temperature over the entire TP during 1979-2018. (b), (c) and (d) represent winter, summer, and monsoon trends of mean temperature estimated using Sen's Slope (°C yr^{-1}). Black dots represent areas with Kendall's significance at p<0.05. The triangles, red-upward for the increase and blue downward for decrease, represent the upper basin averaged temperature trends. The presence of black asterisks in the triangle indicates areas with Kendall's significance at p<0.05 for upper basin averaged temperature trends.

2.4.2.2 Heat Wave Duration Index

The annual average HWDI is relatively low in most parts of the study region except the lower regions of the westerly dominated basin (Figure 2.3 and Table A2). We find high HWDI "hotspots" in the southern and eastern monsoon dominated basins of the Brahmaputra, Ganges, Salween, the Mekong, and the Yangtze. We further investigate the annual anomalies of HWDI for two different climatic regions, the westerly dominated the Helmand basin and the monsoon-dominated Salween basin, to understand these high HWDI "hotspots" (Figure 2.3b and c). We found the maximum HWDI in the Salween basin in 2016 correlates with the century's strongest El-Nino event (Cai et al., 2018). The spatial annual HWDI trend, in general, does not show significant changes in HMA apart from the lower regions of western and eastern basins (Figure 2.3d). Interestingly, the smaller "hotspots" in the Salween and the Mekong do not show a consistent trend, indicating that the high values are reached due to large scale climate events such as the El-Nino that are known to influence the climate of the Indian Sub-continent (Krishnan et al., 2019). Again, the upper basin averaged annual HWDI trend shows minimal changes with the maximum increase seen in Helmand, 0.44 days yr^{-2}, and for most regions, the values range between 0.1–0.2 days yr^{-2} (Figure 2.3d).

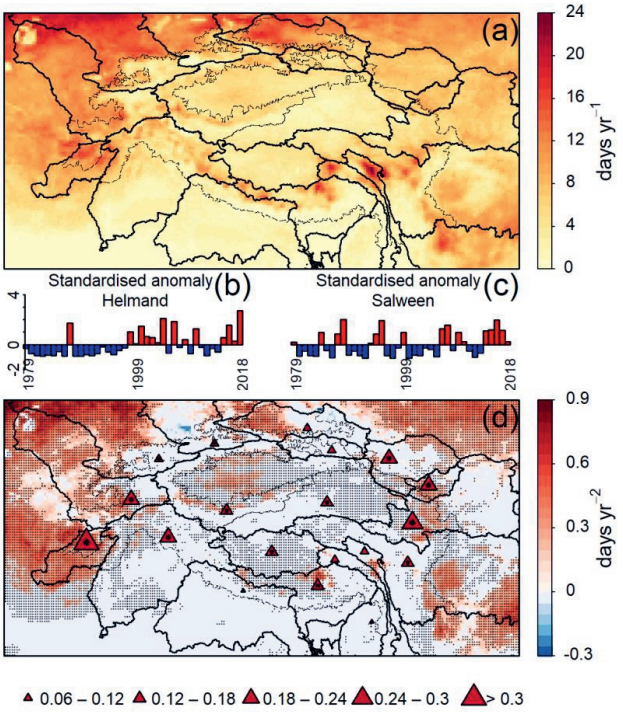

Figure 2.3: *(a) Average of annual HWDI over the entire HMA during1979–2018 (days yr-1). (b) and (c) represent standardised anomalies of annual HWDI for the Helmand and the Salween respectively. (d) Annual HWDI trend estimated using Sen's Slope (days yr^{-2}). Black dots represent areas with Kendall's significance at $p<0.05$. The triangles, red-upward for the increase and blue downward for decrease, represent the upper basin averaged HWDI trends. Black asterisks denote areas with Kendall's significance at $p<0.05$ for upper basin averaged HWDI trends.*

2.4.3 Trends in precipitation and precipitation-derived indices

2.4.3.1 Annual precipitation

Even though annual precipitation shows a higher variability in HMA, the trends are only significant for four basins (Table 2.2). The western basins show a decreasing annual precipitation trend, except for the Syr Darya, where annual precipitation increases by 0–5 mm yr^{-1} (Figure 2.4a). In contrast to the western basins, the monsoon-dominated southern and interior basins show an increasing annual precipitation trend. Strikingly, the western and eastern regions of Brahmaputra show contradictory trends in annual precipitation. The western Brahmaputra shows a significant increasing trend (5–15 mm yr^{-1}), whereas the eastern part shows a significant decreasing annual precipitation trend (50–70 mm yr^{-1}). The significant decreasing trends in regions such as the eastern Brahmaputra and upper Irrawaddy basin correlates with areas that receive the highest precipitation. The lower parts of eastern basins show statistically significant decreasing trends (5–15 mm yr^{-1}) compared to the increasing trends for upper regions. The relative precipitation increase is highest for the interior basin compared to the other regions in HMA (Figure 2.4b). The trends found in this study are in line with those reported by Cuo et al., (2013) based on in situ observations for the Northern TP. The upper basin average annual trend reflects the highest decreasing trend of ~25mm yr^{-1} in the Irrawaddy.

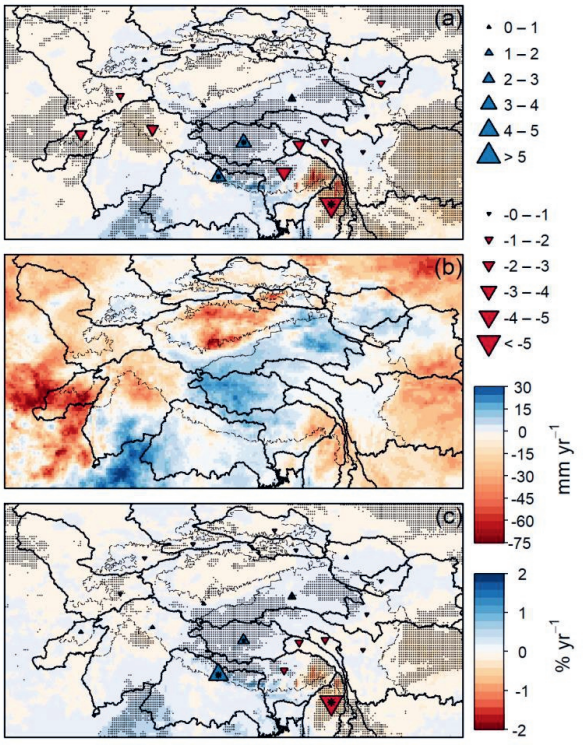

Figure 2.4: *(a) Mean annual average trend for precipitation estimated using Sen's Slope (mm yr^{-1}). (b) Same as (a) but expressed in % yr^{-1} (c) Mean annual average trend for monsoon precipitation estimated using Sen's Slope (mm yr^{-1}). Black dots represent areas with Kendall's significance at $p<0.05$. The triangles, blue-upward for the increase and red downward for decrease, represent the upper basin averaged precipitation trends.*

The West to East opposite pattern of precipitation trend in the entire upper Brahmaputra basin ultimately results in an overall decreasing trend of -2.2 mm yr^{-1}, where the strong negative trend in the East clearly dominates the western Brahmaputra trend (Table 2.2). The monsoon months strongly dictate the annual precipitation trends in HMA (Figure 2.4c and Table A3).

2.4.3.2 Heavy precipitation days (R10)

The annual spatial R10 shows a higher variability in the upstream part of the southern and eastern basins compared to other regions (Figure 2.5a). The Irrawaddy followed by the Brahmaputra, and Ganges shows the highest annual R10 (112.3, 55, 51.2 days) in the entire HMA (Table A4). The northern and interior basins have low R10 values when compared to the other basins. Higher variability and contradictory trend patterns within the basins are observed for the Brahmaputra and Ganges basins (Figure 2.5b). Overall basin average R10 trend values in the Ganges (0.1–0.2 days yr^{-2}) and Brahmaputra (0–0.1 days yr^{-2}) basins show an increasing trend. Irrawaddy basin shows a spatially consistent decreasing trend similar to precipitation trends. The eastern basins show consistent decreasing trends except for the Yangtze basin. The lower Yangtze basin shows significantly decreasing trends than the middle reaches, where the trends are slightly positive.

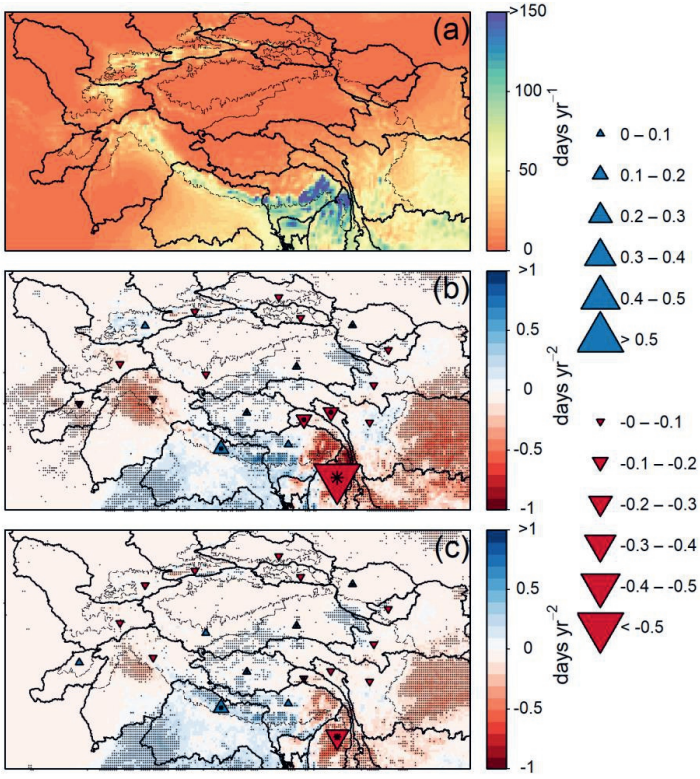

Figure 2.5: *(a) Mean annual average R10 (days yr-1) over HMA for 1979–2018. The trend in R10 for (b) Annual and (c) Monsoon season estimated using Sen's Slope (days yr^{-2}). Black dots represent areas with Kendall's significance at $p<0.05$. The triangles, blue-upward for the increase and red downward for decrease, represent the upper basin averaged R10 days trends.*

All western basins show coherent decreasing trends with the highest decrease in the western parts of Indus, except for the Syr Darya. Monsoon months contribute to most of the annual trends in the region (Figure 2.5c). The monsoon trends are mostly coherent with the annual trends except in Helmand and the Syr Darya, where the sign of trends are reversed. The westerly precipitation regime is responsible for this reversal of trends.

2.4.3.3 Annual maximum five-day precipitation (RX5)

The southern basins show the highest RX5 day values in the entire HMA (Table A5). The foothills of the upper Ganges, Brahmaputra, and Irrawaddy basins receive higher RX5 than high altitudes (Figure 2.6a). The low annual precipitation in the northern and interior basins is again reflected for annual RX5. The RX5 shows a decreasing annual trend, especially in the Brahmaputra and Irrawaddy basins (Figure 2.6b). The weakening of the Indian summer monsoon is the primary reason for the decreasing RX5 trend in these basins. The upper Brahmaputra shows both significant spots of positive and negative trends; however, the latter is of a higher order of magnitude. In contrast, the Ganges basin shows an increasing trend for most of the upstream region.

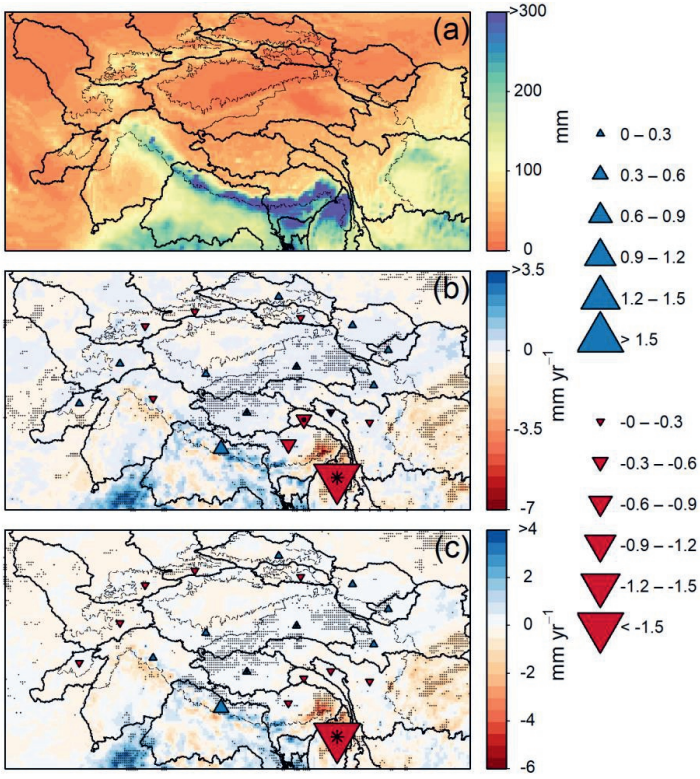

Figure 2.6: *(a) Mean annual maximum RX5 precipitation sum over HMA for 1979-2018 (mm). The trend in RX5 for (b) Annual and (c) Monsoon season estimated using Sen's Slope (mm yr^{-1}). Black dots represent areas with Kendall's significance at p<0.05. The triangles, blue-upward for the increase and red downward for decrease, represent the upper basin averaged RX5 precipitation trends.*

The upper basin average RX5 shows mixed trends in the southern basins as the Irrawaddy and the Brahmaputra show negative trends, whereas the Ganges basin shows positive trends. However, only in Irrawaddy, the trend (-1.8 mm yr^{-1}) is statistically significant at level $p < 0.05$. Among the eastern basins,

a minor negative trend is observed for the Mekong, Salween, and Yangtze, and a positive trend is seen in the Yellow River basin. Most of the annual trend in RX5 is contributed by the monsoon months precipitation (Figure 2.6c and Table A5). A similar pattern to annual trends is observed for monsoon months in entire HMA except for the western basins where the winter and spring precipitation regime are dominant.

2.4.3.4 WET DAYS PRECIPITATION (R95P)

A clear demarcation between the upper and lower basins, as seen in annual precipitation, R10, and RX5 is also detected for R95P (Figure 2.7a). The largest values of R95P are observed in the upper regions of the Irrawaddy, Ganges, and Brahmaputra basins (Table A6). The lower irrigated plains in the eastern part of the Ganges basin show a coherent increasing trend in contrast to the urban western part, which shows mostly decreasing trends.

The annual spatial trends also show high variability, especially in the southern, eastern, and western parts (Figure 2.7b). While the Ganges basin shows consistent and significant increases in R95P trends in the upstream regions, the Brahmaputra basin shows an increase in the western part and a significant decrease in the eastern parts. For some grid cells, the decrease in R95P is exceptionally high (30–40 mm yr-1). However, the basin average annual R95P trends show a decreasing trend of 2–4 mm yr-1, which is again due to the spatial aggregation. The lower reaches of the Yangtze and the Yellow show a higher degree of decreasing trends as compared to the upper and middle reaches.

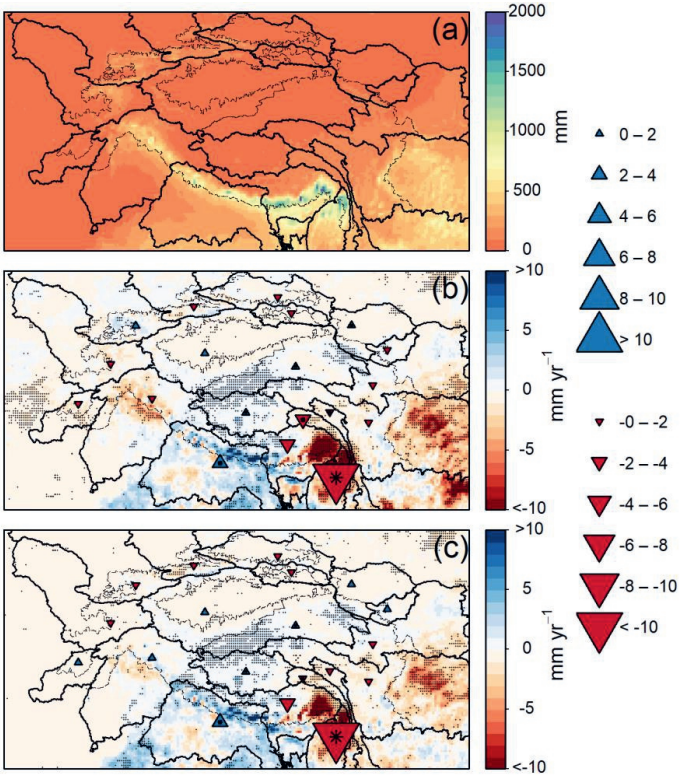

Figure 2.7: (a) Mean annual average R95P precipitation over TP for 1979-2018 (mm). The trend in R95P for (b) Annual (c) Monsoon estimated using Sen's Slope (mm yr^{-1}). Black dots represent areas with Kendall's significance at p<0.05. The triangles, blue-upward for the increase and red downward for decrease, represent the upper basin averaged R95P precipitation trends.

The Kunlun Mountains regions of the eastern Tarim show a considerable increase in R95P as compared to the decreasing trend in the western Tien Shan mountainous regions. The western basins show decreases in R95P, although the trends are not spatially coherent. The urban area of the Indus, especially around Islamabad and Lahore in Pakistan shows a significant reduction in R95P. Interestingly, the lower irrigated regions in the Indus basin show a slight increase in R95P. Monsoon and annual R95P patterns similar apart from western basins where the direction of the trend is reversed (Figure 2.7b).

2.4.3.5 Consecutive number of Dry Days (CDD)

On an annual scale, the upper and lower part of the catchments shows distinct differences in CDD in particular for the western and interior basins (Figure 2.8a). The average number of CDD is highest in the upper Helmand basin, 135 days yr^{-1}, followed by the interior basins and the lowest (~19 days yr^{-1}) in the Balkash basin (Table A7). Shi et al., (2018) reported similar values for the Tarim basin.

The spatial annual trend patterns over the region correlate with the average CDD distribution, as the areas with higher CDD have higher trends (Figure 2.8b). The Helmand basin, which has the highest number of annual CDD, shows the highest positive trend of 0.55 days yr^{-2} (Table A7). The basin average trend in western basins show heterogeneous signals as the Helmand and Amu Darya basins show a large increasing trend (0.16–0.32 days yr^{-2}) compared to a small (0–0.08 days yr^{-2}) decreasing trend in the Indus, Syr Darya, and Balkash basins (Figure 2.8b). The decreasing trend in the TP is consistent with the increasing trends in annual precipitation, R10, RX5, and R95P. Sigdel and Ma (2017) reported a trend of 4.2 days $decade^{-1}$ for the southern slope of the Central Himalayan region of Nepal which is comparable to our findings of 0.25–0.75 days yr^{-1} (Figure 2.8b). However, the authors reported a smaller but significant trend of 0.9 days $decade^{-1}$ for the northern slope of Central Himalayas in the TP in contrast to this study. Their estimates were based on the simple average of data from three observed stations with opposite trends, and it could be a possible reason for the differences. Our results in the middle and lower reaches of Yangtze are in line with the observed trend of -2–2 days $decade^{-2}$ reported for 1961–2015 (Shi et al., 2018).

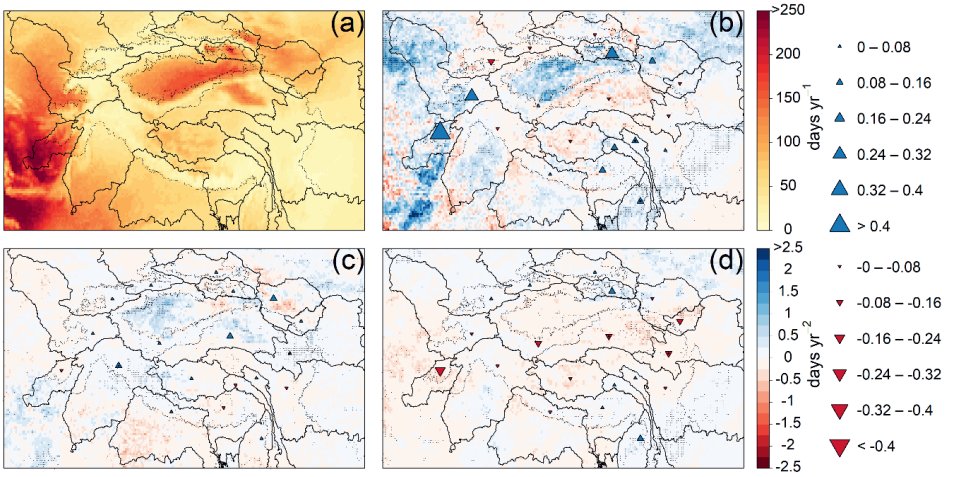

Figure 2.8: *(a) Mean annual average CDD over entire TP for 1979–2018 (days). The trend in CDD for (b) Annual, (c) summer, and (d) Post monsoon estimated using Sen's Slope (days yr^{-1}). Black dots represent areas with Kendall's significance at $p<0.05$. The triangles, blue-upward for the increase and red downward for decrease, represent the upper basin averaged CDD trends.*

All western, interior, and northern basins show increasing summer CDD trends except the Helmand (Figure 2.8c). The spatial patterns summer trends are significant for the eastern part of Indus among the western basins. Interestingly, the Yangtze basin among the eastern basins shows a consistent significant

increase in summer CDD for all upperparts. In the post-monsoon season, all the interior basins show a decreasing trend in contrast to the summer CDD (Figure 2.8d).

2.4.4 Trends in compounding extremes of temperature and precipitation

All the western basins show decreasing spatial trends in the number of days when the 95th quantile of precipitation (P95) is exceeded except for the Syr Darya basin (Figure 2.9a). The interior basins show a significant increase in P95 except for a decrease in the TIW basin. Among the southern basins, the Ganges and Irrawaddy basin show a significant increase and decrease in P95, respectively. Again, the Brahmaputra shows mixed patterns in the spatial P95 trend in the eastern and western regions. The eastern basins show a mixed pattern in P95 trends as the upper Yangtze and Yellow shows a small increase while the others show decreasing P95 trends.

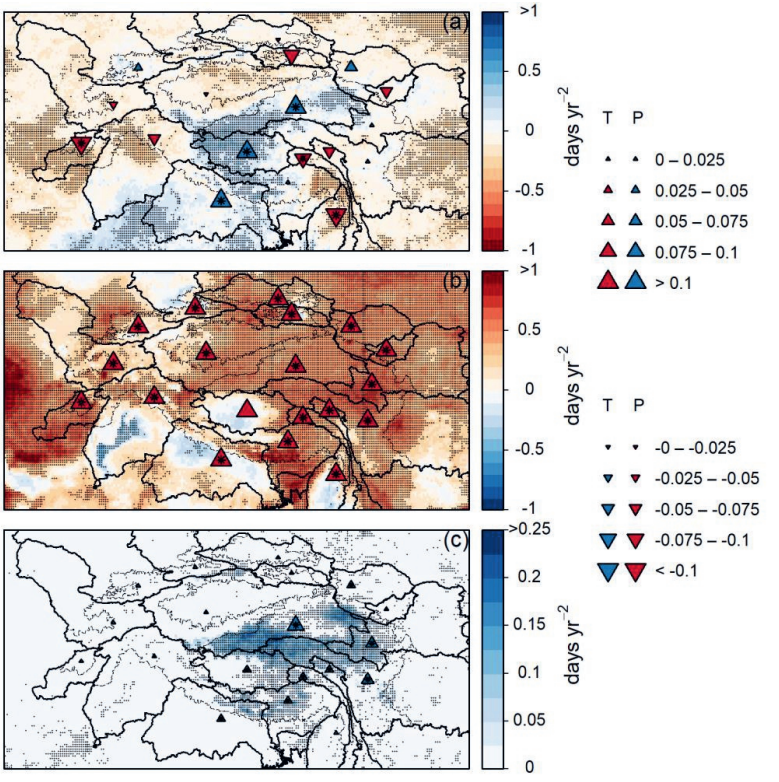

Figure 2.9: Trend for (a) precipitation and (b) temperature greater than 95th quantile over the entire TP for 1979–2018 (days yr^{-2}). (c) Trend when both precipitation and temperature exceed 95th quantile (days yr^{-2}). Black dots represent areas with Kendall's significance at p<0.05. The triangles (blue upward for precipitation (P) and red upward for temperature (T) increase and vice versa) represent the upper basin averaged COMP95 trends.

In contrast to P95, the days when the 95th quantile of temperature (T95) shows a consistently increasing trend over the entire HMA. All the upper basins show significant increases in T95. Interestingly, the lower Indo-Gangetic plains show a decrease in the number of T95. Non-homogeneous spatial patterns

are observed in the TP where the western part shows a decrease in T95 as compared to an increasing trend for the eastern part.

COMP95 shows a significant increasing trend for the interior, southern, and eastern basins. The western part of TIE shows the highest increase (0.2–0.25 days yr^{-2}) in COMP95 trends over the entire HMA as reported by other studies (You et al., 2008; Zhao et al., 2010). Among the eastern basins, the Yangtze and Yellow basin show higher and substantial trends in COMP95. While the COMP95 trends are significant in the eastern part of Ganges, the Brahmaputra, on the other hand, shows a significant trend for the western part.

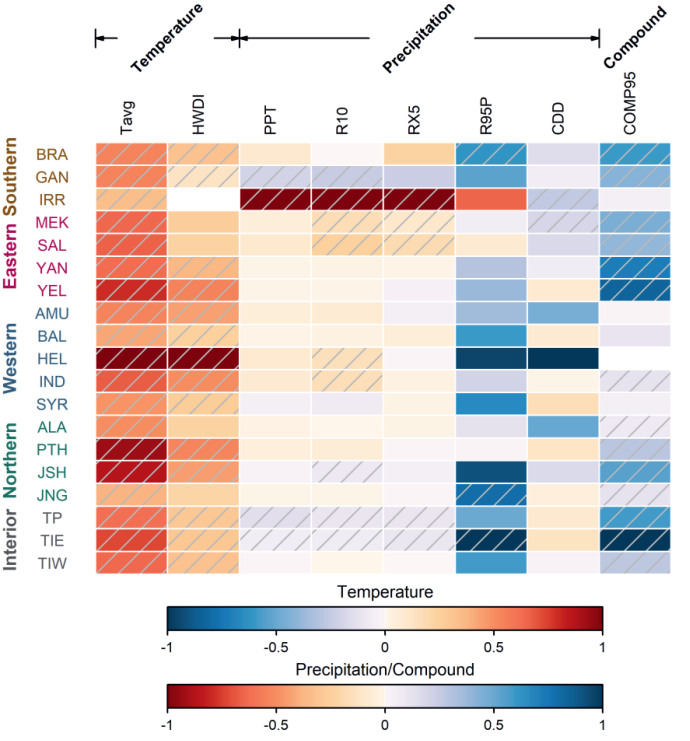

Figure 2.10: *Summary of upstream area aggregated annual trends. For each indicator, the trends are scaled with the absolute maximum value among the basins. The grey inclined lines represent the significance of the trend at $p<0.05$.*

2.5 Discussion

2.5.1 Regional patterns in ERA5 and comparison to previous findings

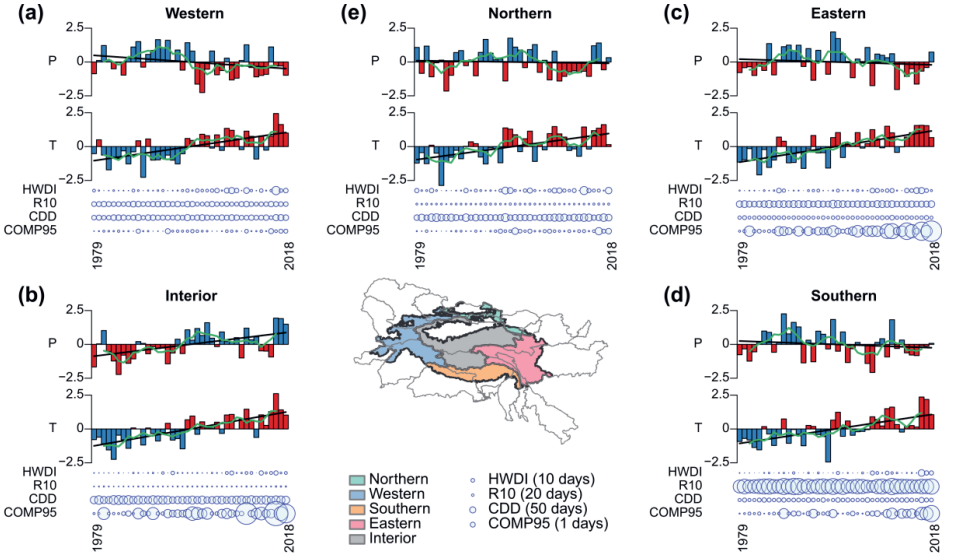

Figure 2.11: *Area aggregated trend in precipitation and temperature and the annual value of extreme indices for different regions, as shown in the central base map (a–d). The first two rows in each plot represent the standardised precipitation and temperature anomalies. The blue (red) colour represents a positive (negative) anomaly for precipitation or temperature. The X-axis represents the years 1979–2018. The black line represents the linear trend, and the green line represents the moving 5-year average. The bubbles represent the annual value of each extreme indices with different linear scaling as specified in the legend.*

2.5.1.1 Interior basins

For the TP, we find a warming trend that is predominant in winter. Yan and Liu (2014) based on observed data reported a trend of 0.32 °C decade^{-1} (~1.58 °C increase for 1961–2012), lower in magnitude as compared to our estimate of ~2.12 °C (Figure 2.2b and Table A1). Further, they reported the highest warming trend in winters, similar to our results. Enhanced warming trends over TP are also reported by recent regional and global studies (Duan and Xiao, 2015; Pepin et al., 2015; Ren et al., 2017). However, at altitudes above 5000 m asl, Gao et al., (2018) did not find any elevation-dependent warming trend for the past (1984–2011) and future. Warming trends calculated from ERA5 at high altitudes do not show any evidence of enhanced warming (Figure A1). Chen et al., (2006), based on observed station data, reported the temperature has increased for the Tarim basin at the annual rate of 0.03 °C yr^{-1} for 1955–2000. We find similar positive increasing trends for the TIE (~0.04 °C yr^{-1}) and TIW (~0.03 °C yr^{-1}) (Table A1). The seasonal trends are also comparable with results based on observed station data (Xu et al., 2010).

The second important finding for the TP is the increase in precipitation (Figure 2.10 and Figure 2.11). Precipitation changes in the region are less consistent than the temperature changes. Zhong et al., (2019), reported an increase in precipitation of 0.78 mm yr^{-1} for 1980–2014, resulting in a ~27 mm increase over the period. This trend is much lower than our estimate 3.57 mm yr^{-1} (~140 mm increase over the 40 years). Besides, the authors reported a different trend of 1.23 mm yr^{-1} for 1999–2014, which

still is lower than our estimates. A wetting trend for TP, similar to results from this study, are also widely reported (Yang et al., 2011; Zhang et al., 2019a).

Similarly, an increasing precipitation trend (0.69 mm yr^{-1}), based on observed station data, is reported for the Tarim basin (Chen et al., 2006). We report a positive trend for TIE (1.63 mm yr^{-1}) and TIW (0.14 mm yr^{-1}). Even though absolute values differ, either due to different levels of spatial and temporal aggregation or biases in the ERA5, the direction of the trends is in line with our findings. A similar positive increase is seen for Rx5, R10 and R95P for all interior basins. The interior basins, in contrast to other regions, show a decreasing trend in annual CDD. Moreover, COMP95 shows a consistent increase in the number of extremely warm and wet days over the interior basins.

The annual standardised precipitation anomaly (SPA) over the entire interior basin shows an increasing trend, in contrast to all the other regions, which show a significant decrease in precipitation (Figure 2.11a). A similar increasing trend is observed for the annual standardised temperature anomaly (STA). The HWDI and COMP95 occurrences also show a rising frequency in recent years. The combination of increasing precipitation with no significant changes in R10 implies mainly low to medium rainfall episodes are increasing in the region. Therefore, the TP has become warmer and wetter in recent decades, and this trend has been reported to continue in the future (Bonekamp et al., 2020; Krishnan et al., 2019; Li et al., 2010). Even though the precipitation related spatial and seasonal trends are non-homogenous, the basin aggregated annual trends show an increase in precipitation extremes in the Tarim basin. While the reported projected changes in the future vary significantly, on the whole, the precipitation and temperature are projected to increase in the future in the interior basins (Su et al., 2013; Zhou et al., 2014).

2.5.1.2 Western basins

For this region, we find a general warming and drying trend that is not consistent across all seasons and indicators. Limited observed station data from this region has resulted in a limited number of studies when compared to other parts of the HMA. Other studies have reported a warming trend (0.1–0.2 ºC $decade^{-1}$) and a small increasing precipitation trend in the Helmand region of Afghanistan (Krishnan et al., 2019; Qutbudin et al., 2019). Similarly, Aich et al., (2017), reported an increase of 0.7 ºC (1980–2010) and 1.2 ºC (1950–1980) in temperature along with a 0–10% change in precipitation in the Helmand region. Our results show a relatively higher warming trend of ~0.05 ºC yr^{-1} and a similar small wetting trend for precipitation in this region. The consistent warming trends for the Amu Darya, Syr Darya, Balkash basins are in line with an observed increasing trend of 0.032 ºC yr^{-1} between 1975–2005 (Zhang et al., 2019c). Likewise, for RX5, they reported an increasing trend (0.55 mm yr^{-1}), which is in line with our findings (0.3–0.6 mm yr^{-1}). The warming trend of 0.30 ℃ $decade^{-1}$ (for 1961–2005) reported for central Asia is comparable with the trends reported for the western and interior basins in our study (Peng et al., 2019). Even though there are discrepancies in the spatial patterns, the Indus and Balkash basins show consistent decreases for basin-aggregated indices for all precipitation related indicators.

The annual SPA and STA show decreasing trends for both precipitation and temperature (Figure 2.11a). While R10 and CDD frequencies show smaller variability, HWDI, and COMP95 show large variability in recent years. Given the above findings, it is clear that the western basins are warming for the most part. However, a general regional drying or wetting precipitation trend is harder to establish.

2.5.1.3 Southern basins

The temperature-related indices show a clear warming trend in annual and seasonal time scales. The warming trends reported here are in line with the findings based on ground-observations (Dash et al., 2007; Dash and Mamgain, 2011). There is a clear decreasing trend especially in the eastern Brahmaputra and Irrawaddy across all precipitation indices during the monsoon season in this region. The greenhouse gas (GHG) and anthropogenic aerosols induced warming of the Indian ocean leading to the weakening of the Indian summer monsoon explains the negative trends in annual precipitation in the southern basins

(Ramanathan and Carmichael, 2008; Saha et al., 2014; Saha and Ghosh, 2019). Despite the variability in absolute numbers, the decreasing trends in the monsoon months for the historical climate have been reported by several studies in the Brahmaputra and the Ganges basin (Bisht et al., 2018; Choi et al., 2009; Dimri et al., 2019; Immerzeel, 2008; Khandu et al., 2017; Mishra and Singh, 2010; Palazzi et al., 2013). Contrastingly, Roy and Kaur, (2000) reported no trend in monsoon precipitation in the upper Irrawaddy basin and did not find any direct correlation between El-Nino and monsoon precipitation. Consistent with our findings, no significant trends for RX5 were reported for the historical climate in the upper Irrawaddy basin (Caesar et al., 2011; Ghimire et al., 2019).

Similar decreasing and increasing trends are observed for SPA and STA for the southern basins, respectively (Figure 2.11d). Interestingly, for the past decade, the SPA and STA show higher negative and positive anomalies which would suggest more dry and warm conditions favouring the heatwave and droughts. The R10 index is highest for southern basins compared to other regions in HMA. While CDD remains in-general similar, the HWDI and COMP95 occurrences show increasing trends in the recent past. Thus, the warming trends are evident in the region. However, drying or wetting trends are harder to establish.

2.5.1.4 Eastern basins

Warming trends are coherent in all the eastern basins. The warming trends (0.03–0.04 °C yr^{-1}) reported here are comparable to the observed trends (Cao et al., 2013, 2017; You et al., 2008). The temperature-related extreme indices unanimously show increasing trends in all the basins except the Yellow basin. Similarly, drying trends are also coherent in all the eastern basins, a decrease of 2–4 mm yr^{-1} in the Salween and Mekong basins are comparable to the observed trends (Fan and He, 2015; Li et al., 2010). The drying patterns are consistent with trends in the extreme indices in all the basins except the Yellow basin. Again, the SPA and STA show decreasing and increasing trends for precipitation and temperature, respectively. However, the former is not statistically significant (Figure 2.11d). CDD frequencies are the lowest among the other regions in HMA. While variability in CDD and R10 occurrences are small, the COMP95 and HWDI occurrences show an increasing trend for the most recent years. Given the above findings, it is clear that the East Asian basins are warming and drying for most parts.

2.5.1.5 Northern basin

The annual temperature trends are coherently increasing (0.02–0.05°C yr^{-1}), in all the northern basins and are in line with observed trends (0.2–0.4°C $decade^{-1}$) reported for the Junggar and Alaguy basins (Xu et al., 2018). The winter temperature trends are decreasing in these basins in contrast to other regions of HMA. These winter trends are also in contrast with the trends reported by Xu et al., (2018). They reported a consistent increase at all the observed station locations, across all the seasons. While HWDI increases coherently for the northern basins, the annual and monsoon precipitation decreases except for Jo Shui. The annual and monsoon precipitation is also in contrast to the trends at some locations, as reported by Xu et al., (2018). They mostly report increasing precipitation trends (5–10 mm $decade^{-1}$) in the middle and eastern Tien Shan. Our results show similar trends, however, for smaller spatial patches (Figure 2.4). We found a decreasing trend for R10 and an increasing trend for RX5 and COMP95. While SPA shows no changes, STA increases. The HWDI and COMP95 frequencies have increased in the recent past. Given the above findings, it is clear that the northern basins are warming. However, a general drying or wetting trend is again harder to establish.

Additionally, the spatial patterns and trends in annual and seasonal temperature and precipitation and a range of climate change indices for large regions; HKH, entire TP (TPE), and HMA are consistent with the trends reported by previous studies (Figure A2).

2.5.2 Implications for extreme events and hazards

2.5.2.1 Floods

While increasing precipitation and temperature conditions would favour floods, decreasing precipitation and increasing temperature would result in conditions favourable for droughts. During the monsoon months, especially the Indus, southern and eastern basins experience severe concurrent floods. Precipitation indices; RX5 and R95P, over the interior and southern basins show a small increasing trend except for the significant decreasing trends in the eastern Brahmaputra and upper Irrawaddy. The decreasing trend in precipitation indices could mean less severe floods. Among others, climate change and local conditions such as river morphological changes, river depth, and socio-economic development will determine if this trend does result in lower floods. In the southern and eastern Tibetan Plateau, hydrological trends based on observed data, show decreasing trends and mainly attributed to decreasing precipitation and increasing evaporation trends (Cong et al., 2010; Yang et al., 2014). However, for future, frequent floods of lower magnitude in a 1.5℃ and 2℃ warmer world are projected (Uhe et al., 2019). Additionally, studies based on glacio-hydrological modelling show general seasonal shifts and increases in the frequency and intensity of the extreme discharge in the upper Indus, Ganges, and Brahmaputra basins in the future (Lutz et al., 2016; Wijngaard et al., 2017).

A consistent increase in temperature and related indices will have significant impacts, especially for the cryosphere of HMA. These cryospheric changes include shrinkage of glaciers, reduction in snow cover, permafrost degradation, changes in seasonally frozen grounds, and increases in the frequency of snow and ice avalanches (Ballesteros-Cánovas et al., 2018; Bolch et al., 2012; Kang et al., 2010). Increased temperature-related changes result in the accelerated melting of glaciers and snow (Immerzeel, 2010; Kraaijenbrink et al., 2017; Lutz et al., 2014; Maurer et al., 2019a). Consequently, rapidly increasing glacial lakes (both area and water level) further exacerbate the risk of glacial lake outburst floods (GLOF) (King et al., 2019; Liu et al., 2014b; Zhang et al., 2015). Moreover, regional and global studies show a significant increase in flood risk in Asia and its socio-economic impacts (Hirabayashi et al., 2013; Kundzewicz et al., 2014; Winsemius et al., 2016).

2.5.2.2 Droughts

In recent decades, droughts have occurred with higher amplitude and severity levels (Mishra and Singh, 2010). Positive STA and negative SPA in the recent decade in the western, eastern, and southern regions also suggest favourable conditions for droughts. Increases in the CDD trend over the western (Helmand and Amu Darya), eastern (Mekong and Salween), and southern (Brahmaputra and Ganges) basins combined with increasing temperature trends may have resulted in increasing magnitude and frequency of droughts (Dai, 2013). Our results are also in line with recently reported drought events in the Indo-Gangetic plains (2002, 2009, and 2015) and China (2005, 2007, 2010, 2013, 2014, and 2015) (EMDAT, 2020; Mishra et al., 2018; Udmale et al., 2020; Zhang et al., 2019b) Further drought days are expected to increase significantly in the future (Dai, 2013; Hirabayashi et al., 2008). Global and regional studies have found positive linkages between CDD and drought in the past for different spatial and temporal scales (Alexander et al., 2006; Duan et al., 2017; Frich et al., 2002; Groisman and Knight, 2008; Orlowsky and Seneviratne, 2012). Increasing the magnitude and frequency of droughts will have a profound impact on agricultural production and food security (Biemans et al., 2019; Elliott et al., 2014; Im et al., 2017; Nelson et al., 2014; Yu et al., 2018). Basins dependent on melt from snow and glaciers are at higher risk in the future either due to changes in seasonality or decrement in water availability for irrigation (Barnett et al., 2005). The regions with increasing temperature and less precipitation, especially, the arid western and northern basins are at higher risk among the other regions in HMA (Qin et al., 2020).

2.5.2.3 Heatwaves

The number of extreme humid heatwaves is doubled in frequency in recent decades (Raymond et al., 2020). The concurrence of high temperatures and low precipitation in association with occurrences of heatwaves can have a severe impact on society. These impacts include losses in agricultural production, livestock security, high water, and energy demands, an increase in wildfire frequencies, and degradation of human health and the ecosystem (Lutz et al., 2019; Perkins-Kirkpatrick and Lewis, 2020). Studies based on observations show an increase in frequency and magnitude of heatwaves, especially in India and Pakistan (Im et al., 2017; Rohini et al., 2016). The heatwaves of 2003 (Andhra Pradesh, India), 2010 (Gujarat, India), 2013 (China), 2015 (India and Pakistan), 2018 (China), 2020 (India and Pakistan) are recent examples of extreme heatwave events (BBC, 2020; EMDAT, 2020; Ren et al., 2020; Rohini et al., 2016). Severe and long-lasting heatwaves in the Indus and the Ganges are mainly attributed to the delay in the onset of monsoon caused by the El-Nino. Our results also indicate a consistent and significant increase in basin annual average HWDI for the entire HMA in recent decades. An increased possibility of heatwaves is expected in the interior and northern basins; the TP, Tarim and the Junggar, the Alaguy and the Jo-Shui during the 21st century, (Li et al., 2019).

2.5.2.4 Landslides and debris flows

HMA is a global hot spot for landslide and debris flow hazards. Changing climatic conditions will have contrasting effects on landslide hazards (Gariano and Guzzetti, 2016; Huggel et al., 2012). An increase in extreme seasonal rainfall in the future will exacerbate the rate of landslide activity, especially in the regions with glaciers and lakes (Kirschbaum et al., 2020). Studies have shown that glacial lakes are already increasing at alarming rates and will continue to grow in the future due to warming (Cook and Quincey, 2015; Song et al., 2017; Veh et al., 2020). Consequently, increasing the possibility of landslide events will result in cascading hazards downstream (Kargel et al., 2016; de Ruiter et al., 2020).

2.5.3 Uncertainties, limitations, and outlook

This study uses reanalysis data as an alternative to limited ground-based observations to calculate trends in extreme climate indices. Spatial inferences from the limited observed station data over the HMA are challenging to establish due to the highly variable climate. The ERA5 Reanalysis products provide a good alternative for regions with data scarcity. This study shows that the trends derived from the ERA5 are consistent with the trends based on the model and observed data and confirms its applicability in the region. The results of this study rely heavily on the ERA5 data and potentially inherit the fundamental limitations of it. Even though the ERA5 has shown improved performance over its predecessors for many applications, studies have found a cold bias in the ERA5 temperature especially in mid-latitudes (Cao et al., 2020; Ji and Yuan, 2020; Orsolini et al., 2019; Yan et al., 2019). Most importantly, a cold bias in the order of 5 °C in winter months for the eastern part of TP has been reported by several studies (Beck et al., 2020; Cao et al., 2020; Yan et al., 2019). The annual trends for threshold related temperature indices, i.e. HWDI, will be affected by the cold biases in the ERA5 temperature. The cold biases in the winter temperature will lower the annual average temperature, thus underestimating the number of days exceeded by TXnorm plus 5 °C criteria used in HWDI calculation. However, the seasonal HWDI trends except winter would remain unaffected. If the cold bias persists consistently over the entire time period, then the winter HWDI trends would also remain unchanged as it will also lower the TXnorm.

In future, improved higher resolution reanalysis products would help to a better understanding of the changes at an even smaller spatial scale, in particular for mountainous regions like HMA. For example, ERA5-Land (9 km), or the High Asia Reanalysis v2, which is based on ERA5 downscaled with WRF (Wang et al., 2020), could provide an improved understanding and more reliable estimates of the trends. Furthermore, the hydrological implications derived in this study are based solely on the meteorological drivers, i.e. precipitation and temperature. The changes in climate extreme and their co-occurrence will have a nonlinear impact on the hydrological system. Hydrological processes memorise past anomalies, and their effects are reflected in subsequent events or periods (Anon, 2019; Delworth and Manabe, 1988;

Dirmeyer et al., 2009; Liu et al., 2014a; Shinoda, 2001). A cascade of hydrological and hydraulic studies are required for more reliable and adept flood risk and droughts in the region (Khanal, et al., 2020, under review).

2.6 Conclusions

In this study, we derive annual and seasonal historical trends in precipitation, temperature, heatwave duration index (HWDI), heavy precipitation days (R10), highest five-day precipitation sum (RX5), wet days precipitation (R95P), consecutive dry days (CDD) and the number of days when both precipitation and temperature are greater than 95th percentile of their distribution (COMP95) in HMA using daily ERA5 reanalysis. We conclude ERA5 is a useful dataset to perform a region-wide, consistent historical climate analysis. We demonstrate that the trends have spatial and interannual variability. Our results show that winter warming and summer wetting is dominant in the interior basin (Plateau of Tibet interior and Tarim). In contrast, the western (the Indus, the Helmand, the Amu Darya, the Syr Darya, and the Balkash) and eastern basins (the Yellow, the Yangtze, the Salween, and the Mekong) are coherently drying. A coherent and significant increasing trend in heatwaves is observed across all regions in HMA. The results reveal that trends in heavy precipitation days show higher variability in southern (the Ganges, the Brahmaputra, and the Irrawaddy) and eastern basins as compared to other regions in the HMA. The trends in consecutive dry days show a distinct demarcation at the boundary between lower and upper regions and are generally increasing for most basins. While the precipitation and temperature showed variable trends, their compound occurrence shows a consistently increasing trend, in particular for the monsoon dominated basins. The trends found in this study suggest an increase in frequency and magnitude of extreme events and are consistent with trends reported for flood, heatwaves, and droughts. A reported decreasing trend of floods, under the current climate, in the southern and eastern Tibetan Plateau will likely increase in the future and requires an in-depth state-of-the-art climate scenario analysis. Moreover, if these historical trends persist in the future, a most likely scenario, an increase in the flood, drought, heatwave, landslide, and compound hazards can be expected. These hazards will have severe impacts on the overall livelihood and ecosystem of the High Mountain Asia and thus requires urgent adaptation policies at the local and regional level.

Acknowledgments

The project received funding from the Strategic Priority Research Program of the Chinese Academy of Sciences, Grant No. XDA20100300. This project was also partly funded by the European Union's Horizon 2020 Research and Innovation Program under the Marie Skłodowska-Curie grant agreement no. 676027.

3

Chapter 3

Variable 21st century climate change response for rivers in High Mountain Asia at seasonal to decadal time scales

3 Variable 21st century climate change response for rivers in High Mountain Asia at seasonal to decadal time scales

The hydrological response to climate change in mountainous basins manifests itself at varying spatial and temporal scales, ranging from catchment to large river basin scale and from sub-daily to decade and century scale. To robustly assess the 21st century climate change impact for hydrology in entire High Mountain Asia (HMA) at a wide range of scales, we use a high resolution cryospheric-hydrological model covering fifteen upstream HMA basins to quantify the compound effects of future changes in precipitation and temperature based on the range of climate change projections in the CMIP6 climate model ensemble. Our analysis reveals contrasting responses for HMA's rivers, dictated by their hydrological regimes. At the seasonal scale, the earlier onset of melting causes a shift in the magnitude and peak of water availability, to earlier in the year. At the decade to century scale, after an initial increase, the glacier melt declines by the mid or end of the century except for the Tarim river basin, where it continues to increase. Despite a large variability in hydrological regimes across HMA's rivers, our results indicate relatively consistent climate change responses across HMA in terms of total water availability at decadal time scales. Although total water availability increases for the headwaters, changes in seasonality and magnitude may diverge widely between basins and need to be addressed while adapting to future changes in a region where food security, energy security as well as biodiversity, and the livelihoods of many depend on water from HMA.

Chapter based on:

Khanal, S., Lutz, A. F., Kraaijenbrink, P. D. A., van den Hurk, B., Yao, T., & Immerzeel, W. W. (2021). Variable 21st century climate change response for rivers in High Mountain Asia at seasonal to decadal time scales. Water Resources Research, 57, e2020WR029266. https://doi.org/10.1029/2020WR029266

3.1 Introduction

High Mountain Asia (HMA) has the world's largest ice and snow reserves outside the polar regions and is an important source of water for the major river systems in Asia, providing water for a population of more than a billion people, which is increasing rapidly (Immerzeel, 2010; Immerzeel et al., 2020; Stocker et al., 2013). The HMA region is characterized by contrasting atmospheric circulation patterns (Bookhagen and Burbank, 2006; Cannon et al., 2016). Midlatitude westerlies and Asian monsoon systems supply most moisture as snow or rain in the western and eastern parts of HMA, respectively. The variability in the climate, hypsometry, and cryosphere distribution leads to characteristic glacial, nival, pluvial, and mixed hydrological regimes in HMA's rivers.

In the past decades, HMA has experienced many climatic changes (Krishnan et al., 2019; Yan and Liu, 2014; Zhan et al., 2017). Past climate change led to changes in the cryosphere and hydrological cycle (Bolch et al., 2012; Kang et al., 2010; King et al., 2019; Sakai and Fujita, 2017; Yao et al., 2012a). These changes include rapid glacier shrinkage, reduction in snow cover, permafrost degradation, changes in area of seasonally frozen grounds, and increases in the frequency of snow and ice avalanches (Ballesteros-Cánovas et al., 2018; Bolch et al., 2012; Kang et al., 2010). The changes in climate and cryosphere lead to shifts in timing and magnitude of river discharge (Immerzeel, 2010; Lutz et al., 2014; Maurer et al., 2019b). Furthermore, climate change lead to increases in area and volume of glacial lakes has further exacerbated the risk of glacial lake outburst floods (King et al., 2019; Liu et al., 2014b; Zhang et al., 2015).

In the future, climate change is expected to lead to further changes in cryospheric storages and subsequently impact the hydrological cycle (Kraaijenbrink et al., 2017; Lutz et al., 2014; Maurer et al.,

2019b; Wijngaard et al., 2017). The climate change response of different hydrological processes depends strongly on spatio-temporal scales and varies from catchment to river basin scale and sub-daily to decadal timescales (Hock et al., 2019a). While rainfall-runoff processes respond quickly to climatic changes, glacier melt generation responds at longer timescales of decades to centuries and strongly depends on the presently available ice volume and the time scale considered. As long as sufficient ice is present, further warming will continue to increase glacier melt, but a decreasing glacier area will lead to a gradual reduction of melt generation in the long run. The time it takes to reach the melt peak increases with ice volume (Huss and Hock, 2018). For snow, different processes combine in response to warming: a higher temperature accelerates snowmelt but reduces the fraction of precipitation that falls as snow, which eventually will lead to a decrease of snowmelt as a contributor to total runoff. The response time for snow processes under climate change varies from seasonal to annual time scales. Via compensating and contrasting impacts of precipitation and temperature on the discharge volume from the HMA headwaters, changes in these climatic variables give rise to nonlinear, non-stationary, and non-uniform responses of cryospheric and hydrological variables such as snow, glaciers, soil moisture, and groundwater, at varying spatial and temporal scales (Blöschl et al., 2017; Hall et al., 2014). The systemic effect of the compound occurrence of extreme precipitation and temperature and their impacts on the seasonality and trends in total water availability for HMA is largely unresolved (Zscheischler et al., 2018, 2020; Zscheischler and Seneviratne, 2017).

Recent studies have focused on glacier melt to derive the impact of either historical or future climate change on melt water availability on a regional and global scale (Brun et al., 2017; Hock et al., 2019b; Huss and Hock, 2018; Kaser et al., 2010; Kraaijenbrink et al., 2017; Marzeion et al., 2020; Maurer et al., 2019b). Many studies have investigated the impact of historical and future climate change on the melt water and streamflow contributors in HMA for fragmented regions varying from sub-basin to basin-scale (Immerzeel, 2008; Immerzeel et al., 2013; Lutz et al., 2016; Nepal, 2016; Ragettli et al., 2016; Sorg et al., 2014). Only a few studies have investigated the impact of climate change on streamflow contributors (i.e., hydrological regime) on a regional scale in HMA (Armstrong et al., 2019; Immerzeel, 2010; Lutz et al., 2014; Miller et al., 2012; Wijngaard et al., 2017). These basin-scale and regional studies use different data and approaches. Variability in approaches, data, and methods makes it difficult to align and compare the effects of climate change on future melt contribution and water availability across HMA. A consistent, high-resolution, long-term modeling approach is required for a robust and spatially consistent assessment of climate change impacts for cryospheric and hydrological processes and their states in HMA at different spatial and temporal scales.

In this study, we bridge scale, variability in approaches, data, and methodological issues by implementing a consistent large-scale high-resolution cryospheric-hydrological model for the entire HMA region to simulate the impacts of climate change on the hydrological cycle at varying spatial and temporal scales. First, we simulate hydrological processes for the historical climate and categorize river basins by their hydrological regimes based on the contribution of glacier, snow, and rainfall-runoff for fifteen upstream basins. Second, we assess the compound impact of changes in precipitation (referred to as dP hereafter) and temperature (referred to as dT hereafter) on peak water availability and shifts in these hydrological regimes for different combinations of future climatic changes. Third, we assess the seasonal and decadal changes in hydrological processes for different hydrological regimes. Lastly, we investigate the changes in total water availability for different spatial scales.

3.2 Study area

We define HMA as the region within 57°−113° E and 22°− 47° N encompassing the Tibetan Plateau and the adjacent mountain ranges Tien Shan, Pamir, Hindu Kush, and Karakoram in the West, the Himalayas in the south and southeast and Qilian Shan in the East. We focus our analysis on the high-altitude upstream parts of fifteen major river basins in HMA (Figure 3.1). The upstream region defined in this study includes all areas above 2000 m asl (meters above sea level) (details in supporting information Text S1). The HMA region has strong longitudinal (West-East), latitudinal (North-South), and vertical climate gradients, therefore making the climate highly diverse (Figure 3.2). The fifteen upstream river basins analyzed in this study are the Amu Darya (AMU), Balkash (BAL), Brahmaputra

(BRA), Ganges (GAN), Helmand (HEL), Indus (IND), Irrawaddy (IRR), Mekong (MEK), Plateau of Tibet Interior (TP), Salween (SAL), Syr Darya (SYR), Tarim interior east (TIE) Tarim interior west (TIW), Yangtze (YAN), Yellow (YEL) (Figure 3.1). Overall, the HMA region includes 97,590 glaciers covering 98,534 km2 (Farinotti et al., 2019). The IND and TIW basins have the highest glaciated area covering over 29,700 km2 (6.3% of total upstream basin area) and 27,700 km2 (5.8%) (Figure 3.2).

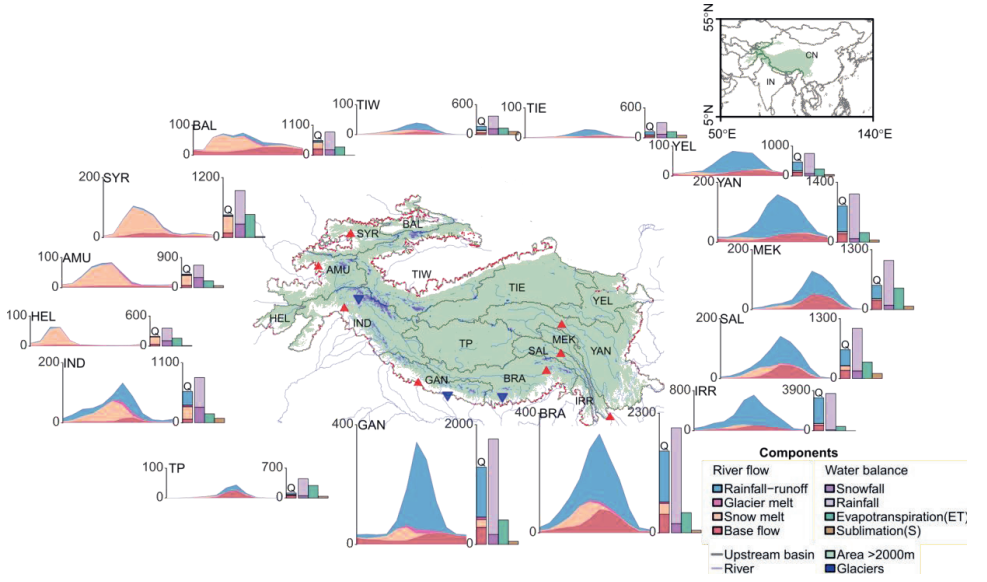

Figure 3.1: The upstream mountainous basins of HMA analyzed in this study (grey boundaries). The green color represents the area above 2000 m. Shown are 1985–2014 mean seasonal cycles of discharge (Q, in mm yr-1) contributed by baseflow (red), snowmelt (orange), glacier melt (magenta), and rainfall-runoff (blue). Stacked bar plots aside show the average annual contributions of the discharge components (Q, 1st bar), the precipitation (P, 2nd bar) falling as rain (light purple) and snow (purple), the actual evapotranspiration (light green, 3rd bar), and sublimation (brown, 4th bar). The red triangles in the geographical map represent the station locations used for the calibration and validation of the hydrological model with observed discharge. The blue downward triangles represent the station locations where independent model validation with observed discharge is performed. Note the difference in vertical scale for each of the basins.

3.3 Data, and Methods

3.3.1 Glacio-hydrological model

In this study, we use the Spatial Processes in Hydrology (SPHY) v3 model, which is a spatially distributed (raster-based) "leaky-bucket" type water balance model (Terink et al., 2015). The model is designed for large scale cryospheric-hydrological studies and integrates different hydrological processes, including (i) rainfall-runoff, (ii) cryospheric processes, (iii) evapotranspiration, and (iv) soil hydrological processes. SPHY can operate at flexible spatial scales (sub-basin, basin, regional).

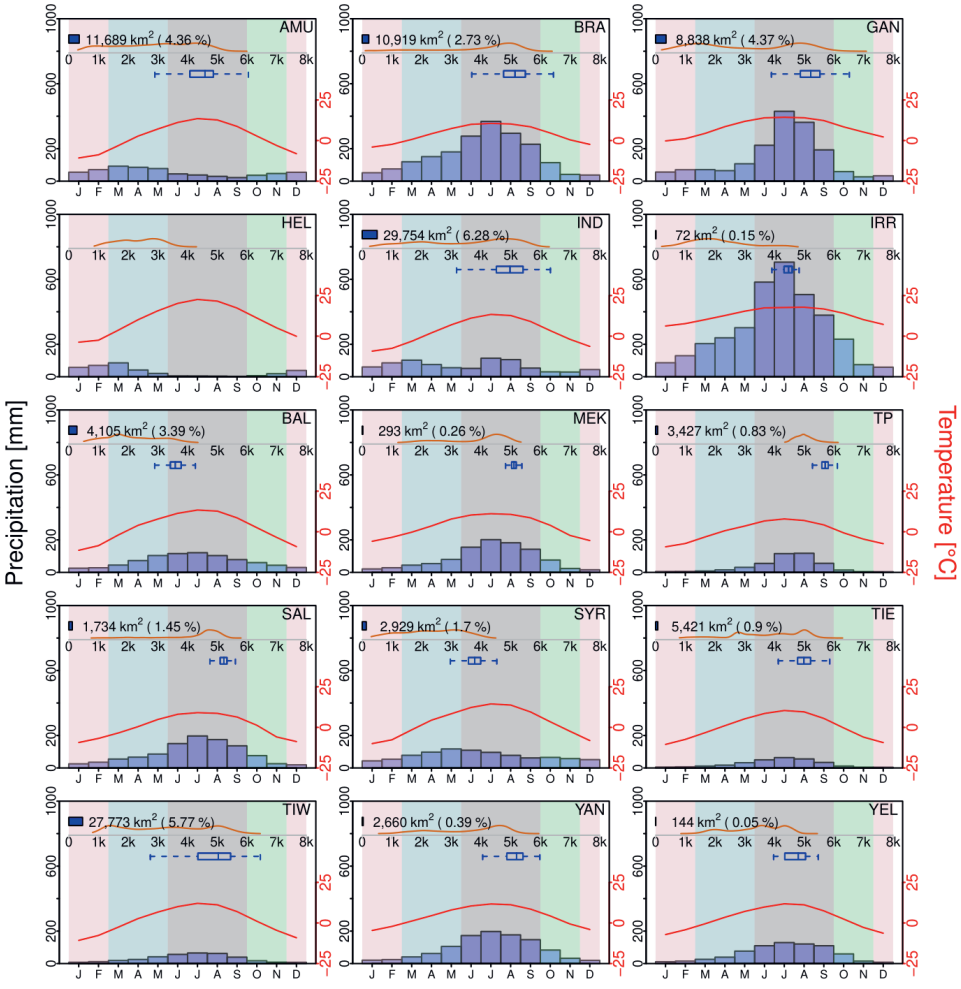

Figure 3.2: Climate setting and relevant characteristics of each basin. The blue histogram (bottom half) represents the average monthly precipitation for the full ERA5 period (1979–2018). The red line (bottom half) represents the average monthly temperature for the same period (right axis). The orange line (top half) represents the elevation distribution of the upper basins (scaled between 0–1 on the y-axis). The horizontal blue box plot (top half) represents the elevation distribution of the glaciers in the basins (except HEL). The width of the blue bar (top left) represents the percentage of glacierized area relative to the total upstream basin area (scaled to 0–100% on the x-axis). The text on the right of the blue bar (top left) gives the total glacier area (km2) and the number in parenthesis gives the percentage of glacier area relative to the upstream basin area. The pale background color represents four seasons: winter (DJF), spring (MAM), monsoon (JJAS), and autumn (ON).

For this study, the model runs at a daily time step at 5x5 km spatial resolution covering fifteen upstream river basins in HMA. The total runoff (Q_{Tot}) for each grid cell at any time step in the model is the sum of glacier-melt runoff (Q_{GM}), snowmelt runoff (Q_{SM}), rainfall-runoff (Q_{RR}), and base flow (Q_{BF}).

$$Q_{Tot} = \sum (Q_{GM}, Q_{SM}, Q_{RR}, Q_{BF}) \quad (2)$$

For each grid cell, a dynamic snow storage, soil water storage, and ground water storage are maintained. Snow melt runoff is calculated for the snow-covered grid cell over the land surface. The snow melt runoff over the glacier surface is defined as glacier runoff. A degree-day approach with calibrated melt rates is used to calculate the snowmelt. For each time step, before melt is calculated, sublimation is estimated using a large-scale parameterization for sublimation and removed from the snow storage. Subsequently, snow melt is calculated and removed from the snow storage at each time step. The model also accounts for the refreezing of melt water within the snowpack. When the snow melt exceeds the storage threshold, snow melt runoff is generated. Rainfall-runoff is calculated as the sum of surface runoff from rainfall and lateral flow from the soil water storage layer. Surface runoff is calculated based on saturation excess runoff. The reference evapotranspiration is calculated using the Modified Hargreaves reference evapotranspiration method (Hargreaves and Samani, 1985). The resulting soil moisture, depending on the soil properties, is subjected to evapotranspiration, influenced by the land use type and capillary rise, while the remainder (if any) contributes to the river discharge through lateral flow or surface runoff. The ground water storage releases delayed base flow runoff. Each of these runoff types are routed downstream using a simple recession coefficient method. While the runoff contributors are self-explanatory, in the next section we discuss the glacier module in detail.

3.3.1.1 Dynamic glacier module

The model takes sub-grid variability into account by calculating the snow and glacier melt runoff from glaciers at a 50x50 m sub-grid. By intersecting the Randolph Glacier Inventory glacier outlines with the 5x5 km model grid, we identify the glaciers or parts thereof (fraction) that lie within each model grid cell (RGI Consortium, 2017). Each (part of a) glacier is assigned a unique-id. To simulate future changes in glaciers, we simulate the glacier mass balance of each individual glacier, which can occupy multiple model grid cells. We distinguish debris-covered and debris-free parts for each glacier based on the classification by Kraaijenbrink et al. (2017). We assign the initial ice thickness and volume for each (part of a) glacier parts using ice volume data from Farinotti et al. (2019). For each (part of a) glacier, we derive its mean elevation from a 30x30 m digital elevation model, to lapse daily air temperature from the 5x5 km model grid cell mean elevation to the glacier's mean elevation (Farr et al., 2007). Daily precipitation and temperature serve as input for the glacier module to calculate accumulation and melt. The module uses a degree-day approach to calculate the glacier ice melt (Hock, 2003). Different calibrated melt rates are applied to debris-covered and debris-free glaciers (Bolch et al., 2012; Gardelle et al., 2013; Scherler et al., 2011). Future changes in (parts of) glaciers in response to the precipitation and temperature are taken into account by using a mass conserving ice redistribution approach. The ice redistribution is done once per year at the end of the hydrological year, which is also the end of the melting season (1st of October). At that moment the accumulated snow in the accumulation zone is transformed into ice and distributed downwards to the ablation area. The net imbalance (I), i.e., the difference in the volume of total snow accumulated ($SnowS$) and total volume of melt generated from the glaciers (GM), forms the basis of ice redistribution:

$$\boldsymbol{I_{n,j} = SnowS_{n,j} - GM_{n,j}} \quad (3)$$

where the subscript n is the glacier id, and j is a unique-id. Only when the net imbalance is negative, the volume of ice is redistributed (Vred) over the ablation zone according to:

$$\boldsymbol{Vred_{n,j}} = \begin{cases} \mathbf{0} & , \quad \boldsymbol{j \epsilon B_{n,j}} \\ \sum_{\boldsymbol{j \epsilon B_{n,j}}} \boldsymbol{I_{n,j}} \times \dfrac{\boldsymbol{Vini_{n,j}}}{\sum_{\boldsymbol{j \epsilon A_{n,j}}} \boldsymbol{Vini_{n,j}}}, & \boldsymbol{j \epsilon A_{n,j}} \end{cases} \quad (4)$$

where A_j is the part of the glacier with a negative imbalance, B_j is the part of the glacier with a positive imbalance in any glacier-id n. The redistribution is proportional to the initial total volume of ice (Vini).

i.e., glacier parts with a larger initial ice volume will receive a large volume of accumulated ice from the accumulation zone to the ablation zone.

3.3.1.2 Snow sublimation

We use a large-scale parameterization to estimate the sublimation from the snow storage. Although snow sublimation is an essential component of the water balance in mountainous regions, its magnitude is still uncertain and poorly understood (Stigter et al., 2018). To understand and quantify sublimation from snow, we use an estimate of the theoretical incoming shortwave radiation, the topographic exposure to wind calculated based on the angle of inflection, and elevation (Fu and Rich, 1999; Winstral and Marks, 2002). We calculate the monthly probability of sublimation (P_{sub}) as:

$$\boldsymbol{P_{sub} = SW \times (1 - e) \times h} \quad (5)$$

where SW is the incoming shortwave radiation in W m^{-2}, e is topographic exposure, a dimensionless number which ranges between 0–275, and h is the elevation in m. The elevation is scaled between 2500 and 6500 m to restrict the snow sublimation. The resulting P_{sub} is further scaled between 0–1; with higher values indicating a higher probability of sublimation. The theoretical maximum sublimation (Smax) is calculated as:

$$\boldsymbol{Smax = (1 - \alpha) \times SW \times L} \quad (6)$$

where, α is albedo (a unitless number varying from 0 to 1), and L is the latent heat of sublimation (2.838 kJ kg^{-1}). Sublimation is strongly dependent on wind, temperature, and humidity (Hood et al., 1999). There are several constraints to the conditions favorable for sublimation; for instance, the melting snow surface temperature cannot exceed 0 °C, and vapor partial pressure at the surface cannot exceed 6.11 hPa (Strasser et al., 2008). Here, we use a proxy of humidity conditions by assuming low precipitation intensity (P<1 mm d^{-1}) to be favorable for the sublimation to occur. The favorable sublimation condition (Scon) in the model is calculated as:

$$\boldsymbol{Scon = (T <= 0) \,\&\, (SnowS > 0) \,\&\, (P <= 1)} \quad (7)$$

where T is the mean air temperature, $SnowS$ is the snow storage (mm), and P is the precipitation (mm). $Scon$ is a binary value where 0 represents grid cells with no sublimation, and 1 represents grid cells with sublimation. Finally, the actual sublimation (Sact) is calculated as:

$$\boldsymbol{Sact = Sfact \times Scon \times P_{sub} \times Smax} \quad (8)$$

where the sublimation factor (Sfact) is a calibration parameter that ranges between 0 and 1.

3.3.2 Data

3.3.2.1 Climate data

The SPHY model is forced with precipitation and temperature fields from the European Centre for Medium-Range Weather Forecasts (ECMWF) ERA5 climate data (Hersbach et al., 2020). The ERA5 data are available for 1979–2018 at an hourly time scale and 31x31 km spatial resolution (hereafter referred to as ERA5 resolution). ERA5 hourly precipitation is aggregated to daily precipitation sum and then interpolated to 5x5 km model grid using a cubic spline interpolation. Similarly, mean, maximum (max), and minimum (min) daily temperature aggregates were created from the hourly ERA5 data and spatially resampled using a cubic spline interpolation. The resampled temperature fields (T_{cor}) are spatially downscaled using the digital elevation model (DEM, see section 3.2.3) and vertical temperature lapse rates (VLR). A linear regression method is applied to calculate the monthly VLR from ERA5

temperature climatology at the original ERA5 resolution for a 5x5 grid cell window around each grid cell in the model domain. The resampled monthly vertical lapse rates are then aggregated over the basins and used to correct air temperature at 5x5 km model resolution as in eq (9).

$$\boldsymbol{T_{cor,t} = T_{res,t} \times VLR_{m,t} \times (h1 - h2)} \quad (9)$$

where $T_{\mathrm{cor},t}$ is the corrected temperature at time step t, $T_{\mathrm{res},t}$ is the resampled temperature from ERA5 resolution to model resolution, VLR_t is the resampled vertical lapse rate for a corresponding month (m), $h1$ is the elevation aggregated to 5x5 km model resolution, and $h2$ is elevation aggregated to the original ERA5 grid resolution and smoothed to the model resolution.

We used projected changes in temperature (dT) and precipitation (dP) from the Coupled Model Intercomparison Project Phase 6 ensemble (CMIP6) to generate the future climate forcing (Eyring et al., 2016). Several recent studies have investigated dP and dT in the Asian and Tibetan plateau regions with the available CMIP6 models (Almazroui et al., 2020; Na et al., 2020). Based on the ranges in the projections of the CMIP6 ensemble for these regions, we select -30% to +40% for dP and 3 °C to 8 °C for dT as change by the end of the century (2100) compared to the reference period. Over these ranges, increments of 1°C for dT and 10% for dP, were used to generate 48 different combinations of future climate change projections. The dT and dP in each combination were assumed to change linearly between the start of the century (2015) and the end of the century (2100). Future time episodes are generated by random sampling from the full ERA5 years historical model forcing (1979–2018) without replacement, in three blocks of 40 years each, to generate a transient sequence of 86 years (2015–2100). The annual incremental increase (or decrease) is added to the temperature fields and multiplied with the precipitation fields to generate the future forcing for corresponding daily time steps of the resampled years. In this way, we generate transient future forcing for the entire region, from 2015 until 2100, for the 48 different future combinations.

For parts of the analysis, we categorize the 48 climate runs in to four groups of 12 combinations each; warm-wet (dT from 6°C to 8°C, dP from 10% to 40%), cold-wet (dT from 3°C to 5°C, dP from 10% to 40%), warm-dry (dT from 6°C to 8°C, dP from -30% to 0%) and cold-dry (dT from 3°C to 5°C, dP from -30% to 0%) (Figure B1). Any positive (negative) increment in precipitation is defined as a wet (dry) scenario. Further, a distinction is made for a wet (dry) scenario, based on the temperature either as cold-wet (cold-dry) or warm-wet (warm-dry) (Lutz et al., 2016). While the wet scenarios (i.e., positive precipitation increment) are self-explanatory, the temperature scenarios were distributed evenly (3°C to 5°C as cold and 6°C to 8°C as warm). To show the seasonal and decadal changes for different hydrological regimes, we focus on three specific future runs: high dT (dT = 8°C and dP = +0%), high dP (dT=3°C and dP= +30%) and high dPdT (dT = 8°C and dP = +30%).

Unless explicitly specified, we use 30 years (1985–2014) as a reference period throughout the study. To investigate the climate change impacts in the future, we divide the future period into two slices of 30 years; mid-century (hereafter referred to as MC, 2036–2065) and end of century (hereafter referred to as EOC, 2071–2100). Furthermore, to assess seasonal changes, we divide the year into four seasons: winter (from December to February, DJF), spring/premonsoon (from March to May, MAM), summer/monsoon (from June to September, JJAS), and autumn/postmonsoon (October and November, ON).

3.3.2.2 Discharge data

The discharge data in this study were obtained from the Nepal Department of Hydrology and Meteorology (DHM), Pakistan Water and Power Development Authority (WAPDA), Bhutan National Centre of Hydrology and Meteorology (NCHM), Central Asian Waterinfo portal (CAWater, 2020) and Global Runoff Data Centre (GRDC, 2020) as shown in Table 3.1.

*Table 3.1: The stations used for the calibration and validation in this study. The type 'C', 'V', and 'IV' indicates calibration, validation, and independent validation. The basins with * represent the missing year in the discharge time series.*

Basin	*Names*	*Station*	*Calibration*	*Validation*	*Missing*	*Frequency*	*Data source*	*Type*
Amu Darya	AMU	Nurek inflow	2001-2004	2005-2010	-	Daily	CAWATER	C,V
Brahmaputra	BRA	Nu Xia	1979-1982	-	-	Daily	GRDC	C
Brahmaputra	BRA	Wangdirapids	-	2004-2008	-	Daily	NCHM	IV
Ganges	GAN	Chisapani	2001-2004	2011-2014	-	Daily	DHM	C,V
Ganges	GAN	Devghat	2001-2004	2011-2014	-	Daily	DHM	IV
Indus*	IND	Dainyor	2001-2004	2006-2010	2005–2007	Daily	WAPDA	IV
Indus	IND	Tarbela inflow	2001-2004	2006-2010	-	Daily	WAPDA	C,V
Mekong*	MEK	Jiajiu	1979-1983	1984-1987	1986	Daily	GRDC	C,V
Salween*	SAL	Jia yu qiao	1980-1983	1984-1987	1981,1983,1986	Daily	GRDC	C,V
Syr Darya	SYR	Toktogul	2001-2004	2005-2010	-	Daily	CAWATER	C,V
Yangtze	YAN	Zhimenda	1981-1985	1990-1997	-	Daily	GRDC	C,V

3.3.2.3 Other data

We use the hydrologically conditioned 30 arc-second resolution (~1km) DEM from HydroSHEDS, resampled to 5x5 km model resolution in order to calculate the slope, cell drainage direction, and for lapsing of temperature fields (Lehner et al., 2008a). We also use the 1 arcsec (~ 30 m) Shuttle Radar Topography Mission (SRTM) elevation data to calculate the mean glacier elevation used for the glacier melt calculation (Farr et al., 2007). The MODIS MOD10CM006 (hereafter referred to as MODIS) snow cover data (2001–2017) is used to calculate the monthly snow persistence (Hall and Riggs, 2015). The glacier outlines defined in RGI6.0 for the RGI regions 13 (Central Asia), 14 (South Asia West), and 15 (South Asia East) were used in this study (RGI Consortium, 2017). The initial ice thicknesses for individual glaciers are derived from modelled glacier ice depths (Farinotti et al., 2019). Geodetic glacier mass balance data (Brun et al., 2017) is used to calibrate snow and glacier melt parameters over glaciers. Hydrological subbasin boundaries from HydroBasins dataset (referred to as hydro-basins) at spatial level 05 are used to aggregate specific glacier melt to hydrological units for model calibration purposes (Lehner and Grill, 2013). Hydraulic soil properties used in this study were derived from HiHydroSoil (1x1 km) and resampled to model resolution (Boer, 2016). Landuse data used in the model are derived from the European Space Agency Climate Change Initiative (ESA CCI) dataset (Kirches et al., 2014).

3.3.3 Methods

3.3.3.1 Bias correction of ERA5 temperature data

Several studies have found a cold bias in ERA5 temperature in mid-latitudes and on the TP (Cao et al., 2020; Ji and Yuan, 2020; Orsolini et al., 2019; Yan et al., 2019). Cold biases in the order of 5 °C during winter months have been reported in the eastern part of the TP (Yan et al., 2019). We used MODIS-derived snow persistence to bias correct the temperature fields in ERA5. Snow persistence is defined as the fraction of time that a grid cell is covered by snow. The SPHY model is run from 2001 to 2017, and the temperature is corrected for individual grid cells to match the simulated snow persistence from

SPHY to observed snow persistence from MODIS. We use a minimum threshold of 5 mm of snow storage to limit the very shallow and infrequent snow cover in SPHY. Parameters related to snow processes in SPHY; the critical snow temperature (Tcrit), which controls the snow and rain differentiation, and degree-day factor for snow (DDFs), were assumed to be 0 and 4.5 mm °C^{-1} day^{-1} (Table B1). We aggregate the snow persistence from SPHY and MODIS to a 100x100 km grid and calculate the difference in snow persistence. We iteratively increase the temperature fields by +1 °C until the difference in snow persistence from SPHY and MODIS is within ±10%. We only implement a one-way bias correction, to a maximum of +5 °C consistent with the reported cold bias over the TP. The bias-correction factors are spatially smoothed from 100x100 km to 5x5 km model resolution.

3.3.3.2 Model calibration

To avoid the pitfalls of model equifinality, we use a three-step modeling strategy to calibrate the snow, glaciers, and rainfall-runoff processes in the model (Pellicciotti et al., 2012). First, parameters related to snow processes are calibrated to observed MODIS snow cover data. Second, parameters related to glacier melt are calibrated to observed geodetic glacier mass balance data. Third, rainfall-runoff and routing parameters are calibrated to observed streamflow (Table B1).

Snow cover calibration

After the bias-correction of the temperature fields, we calibrate Sfact in the sublimation routine for each upstream basin to optimize simulated snow cover. Sfact is optimized to minimize the difference between the mean annual simulated and observed snow persistence in SPHY and MODIS, respectively (Table B1). Here, we use a maximum ±10% difference in snow persistence as an optimization target for the calibration.

Glacier mass balance calibration

The geodetic glacier mass balance database from Brun et al., (2017) is used as the observed mass balance data (hereafter "observed") to calibrate the glacier melt parameters; debris-free (DDF_{ci}) and debris-covered (DDF_{dc}). The observed database consists of mass balance information of 92% of the glaciers in HMA for period 2000 to 2016.

In the first step, the melting factors (DDF_{ci} and DDF_{dc}) for glaciers are adjusted. DDF_{dc} and DDF_{ci} are assumed to be proportional as shown in (10).

$$\boldsymbol{DDF_{dc} = 0.2 \times DDF_{ci}} \quad (10)$$

Factor 0.2 is incorporated to represent the reduced melting rates of debris-covered glaciers relative to debris-free glaciers (Östrem, 1959). DDF_{ci} is varied between 3 and 7 mm °C^{-1} day^{-1}, consistent with melt rates found in other studies in the region (Braithwaite, 2008; Immerzeel et al., 2012; Singh et al., 2000; Zhang et al., 2006). For each run from 2001-2017, the simulated glacier area-specific mass balance is calculated and compared with the observed area-specific mass balance data. We calibrate at the spatial aggregation level of sub-basins, as defined by the level 05 data in the hydro-basins dataset (Figure B2). The DDF values are optimized until the difference between observed and simulated glacier mass balance is within ±0.05 m. w.e yr^{-1}.Where calibration of degree-day factors does not lead to sufficient accuracy in the simulation of the glacier mass balance, we calibrate the glacier VLR used in the glacier melt calculation. The initial monthly VLRs used in the glacier module are estimated from the ERA5 described in section 3.2.1. The range of the VLR after calibration is confined between 0 and -0.011 °C m^{-1}. We correct the VLR with an annual correction factor to preserve the seasonal patterns in the VLR.

Discharge calibration

As the final calibration step, the parameters related to rainfall-runoff processes (Soilfactor, Rootdepth, crop coefficient multiplier, baseflow recession coefficient, ground water recharge delay time,and routing recession coefficient) are calibrated (Table B1) The model is calibrated against observed discharge at a daily timestep for the locations where the discharge data is available (Table 3.1). In the BRA river basin

(at Nu Xia), there were only four years (1979 to 1982) of discharge data; the model is calibrated for those four years and independently validated at Wangdirapids for a different period (2004–2008). In the GAN river basin, we calibrated and validated the model at Chisapani and independently validated it at Devghat. Similarly, in the IND river basin, we calibrated and validated model at the inflow of Tarbela dam and independently validated it at Dainyor bridge. The rainfall-runoff parameters were calibrated for each individual basin as shown in Table 3.1.

3.4 Results

3.4.1 Bias correction

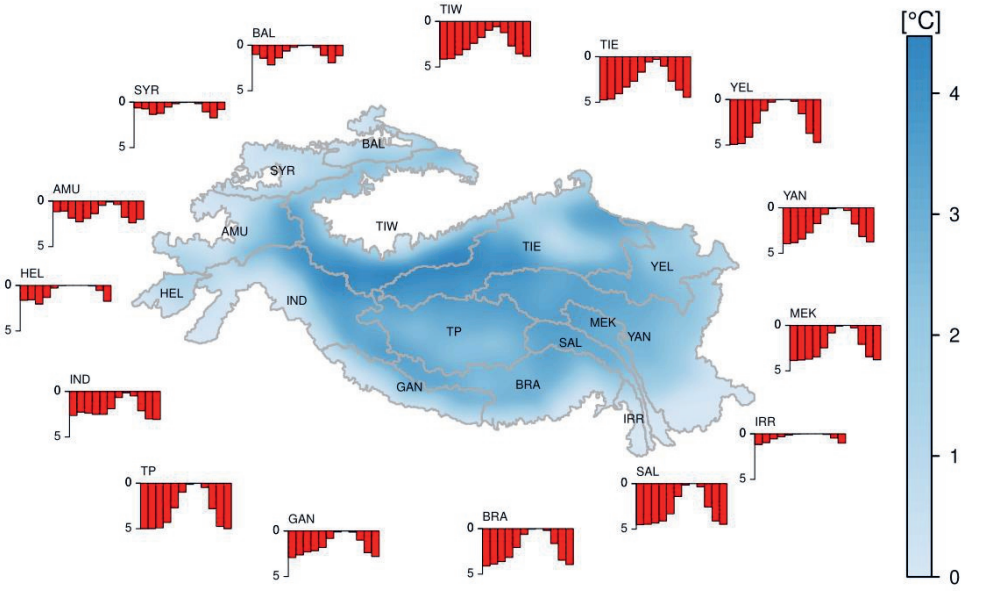

Figure 3.3: Basin averaged temperature bias-correction values (°C). The bars (red) represent the monthly temperature correction applied to each basin. The base map represents the annual averaged correction for the entire HMA.

The bias correction results show high variability, among the basins in HMA (Figure 3.3). For instance, there are differences in the monthly variation and absolute values between the western and eastern parts. The basin averaged biases reflect significant seasonal variability in the basin as the correction is highest in winter and lowest in the summer season. The higher altitude areas show higher bias correction as compared to the lower altitude areas. The higher biases are found in the winter months, in particular for the higher altitude regions, where the temperatures are below 0°C (Figure B3). The seasonal and spatial variability in bias can be mainly attributed to the spatio-temporal variability of temperature in the basins (Figure B3). The interior river basins TIW, TIE, and TP show higher monthly corrections as compared to the other river basins in HMA. The IRR and HEL river basins have low average bias correction among all the other basins in HMA. In general, the southern (GAN, BRA) and eastern basins (MEK, SAL, YAN, YEL) show higher correction as compared to the westerly dominated river basins (IND, HEL, AMU, SYR, and BAL). The seasonal variability of bias correction factors (higher for winter months and lower for summer months) from this study are in line with those based on the average of 33 observed meteorological stations (Orsolini et al., 2019). Thus, we conclude that bias corrected results of this study are realistic and satisfactory for use in further analysis.

3.4.2 Model calibration and validation

3.4.2.1 Calibration to observed snow cover

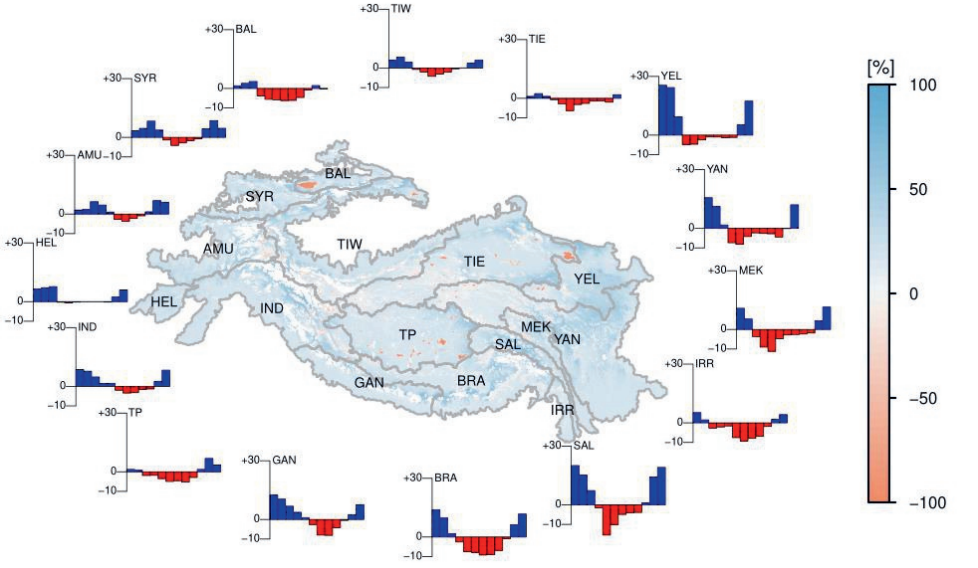

Figure 3.4: Difference in simulated and observed snow persistence between SPHY and MODIS for 2001–2017. The bars represent the monthly average differences in snow persistence for each basin after calibration. The blue (red) bar indicates SPHY overestimating (underestimating) the MODIS snow persistence. The base map represents the annual difference in snow persistence for the entire HMA.

The snow persistence calibration results also show a large spatial and seasonal variability. For instance, there is less variability for western basins compared to eastern parts (Figure 3.4). While SPHY overestimates snow persistence for the winter and spring seasons, the summer snow persistence is underestimated. The eastern (MEK, SAL, YEL, and YAN) and southern (GAN, BRA) river basins show higher variability as compared to the western (IND, HEL, AMU, SYR, and BAL) and interior river basins (TP, TIE, and TIW). The western and interior river basin snow persistence values are within the threshold of ±10% whereas eastern and southern river basins show higher overestimation. However, higher overestimation is only seen for the winter months in these basins. The overestimation of snow cover in winter months could be attributed to either the presence of cold biases in the ERA5 (even after the bias correction), too little sublimation or due to omission of other transport mechanism such as avalanching and snow redistribution by wind in the SPHY model which could eventually result in excessive snow accumulation and higher simulated snow cover. Overestimation of snow cover extent could potentially lead to an overestimation of snow runoff calculation. Given the scarcity of the snow related data in HMA, snow redistribution, avalanching or a physically explicit modelling of sublimation is computationally impossible. Moreover, the actual snow melt calculation depends on the snow water equivalent (SWE), which depends on snowfall. Though, there are spatial differences between observed and modelled snow cover, at basin scale this effect will be less pronounced.

3.4.2.2 Calibration to observed glacier mass balance

The glacier parameter calibration results are presented in Table 3.2. In general, the simulated mass balance after model calibration is in close agreement with the geodetic mass balance observations reported by Brun et al., (2017). However, for some river basins, the aggregated SPHY simulated glacier mass balance is too negative (TIE) or too positive (IND, BAL, and TIW). The underestimation in glacier mass balance can be attributed to lower snow degree-day factors and cold biases in ERA5 temperature. The lower temperature over the glacier surface results in the accumulation of seasonal snow in the winter and thus delays the glacier ice melt process.

Table 3.2: Simulated and observed glacier mass balance aggregated to the entire upstream basin after calibration of glacier melt parameters.

Basin	Simulated (Gt yr^{-1})	Observed (Gt yr^{-1})
AMU	-1.12	-1.02
BRA	-4.44	-5.08
GAN	-2.13	-2.62
IND	-3.02	-3.92
IRR	0.00	-0.03
BAL	-0.54	-0.91
MEK	-0.11	-0.08
TP	-0.36	-0.47
SAL	-0.62	-0.75
SYR	-0.36	-0.38
TIE	-0.38	-0.19
TIW	2.14	0.15
YAN	-0.30	-0.40

3.4.2.3 Calibration to observed discharge

To estimate the efficiency of the calibration to discharge, we use the Nash-Sutcliffe efficiency criterion (NSE), percent bias (PBIAS), and coefficient of determination (R^2) as performance indicators (Nash and Sutcliffe, 1970). The daily NSE for the calibration period in the GAN, IND, BRA, AMU, SAL, and YAN river basins are 0.86, 0.85, 0.69, 0.66, 0.76, and 0.59 (Figure 3.5). The discharge calibration performance in most of those basins is 'very good' and in others, it is 'satisfactory' (Moriasi et al., 2007). However, there is a large overestimation of the flow in the MEK (PBIAS = 29%) and SAL (PBIAS =13%) river basins for the calibration period and even higher for the validation period. The overestimation in discharge can most likely be attributed to overestimation in precipitation amounts in ERA5 over these basins. A similar overestimation of precipitation in ERA5, leading to higher biases in simulated discharge, has been reported in several other studies (Cucchi et al., 2020; Shaun Harrigan, 2020). The overestimation of precipitation can be related to the spatial distribution and the sparse density of meteorological stations in HMA used for the ERA5 reanalysis (Jiang et al., 2020). Further, extremely large rainfall totals, to some extent, can be attributed to 'rain bombs' in the numerical weather prediction model (NWP) used in ERA5 (Shaun Harrigan, 2020). Similarly, studies have reported large biases (PBIAS) up to 44% in ERA5 precipitation compared to ground-based observations in the Pamir region (Zandler et al., 2019). Moreover, overestimation of discharge for the calibration period (PBIAS = 19.6%,Figure 3.5) and validation period (PBIAS = 19.8%, Figure B4) in the SYR river basin are likely due to the precipitation overestimates of ERA5. The discharge simulations in westerly-dominated and monsoon-dominated basins show different responses to the overestimation of precipitation. In the MEK and SAL river basins, which are monsoon dominated catchments, the overestimation of precipitation in the monsoon season causes quick overland flow, which leads to the large overestimation of discharge mainly in the monsoon season. However, in the westerly-dominated SYR river basin, the dominant

winter precipitation leads to the storage of solid precipitation in the snowpack. The overestimation of winter precipitation in ERA5 leads to excessive snowmelt in spring and the summer season. Furthermore, the coarse spatial resolution (5x5 km) and a simple routing scheme might also contribute to the overestimation of the simulated flow.

Additionally, the contributions of snow melt, glacier melt, rainfall-runoff and baseflow to overall discharge were compared to several other smaller-scale studies in the region (Table B2). For the Hunza subbasin at Dainyor, Mukhopadhyay and Khan, (2014) analysed annual hydrographs and reported a combined 74% of snow and glacier melt contribution to the total discharge, compared to our estimates of 86%. Shrestha et al., (2015) used WEB-DHM-S, a distributed biosphere hydrological model, and estimated 33% glacier melt and 49% snow melt contribution (average of 3 years 2001–2003), compared to our estimates of 37.4% and 48.7% for glacier and snow melt respectively. Wijngaard et al., (2017) used a 5x5 km resolution SPHY hydrological model with a dynamic glacier mask for Hunza at Dainyor and reported a glacier and snow melt contribution of 18% and 69%, respectively. Similarly, Lutz et al., (2014) used a 1x1 km resolution SPHY hydrological model with a static glacier module and estimated largely different results, 81% and 10% from glacier and snow melt respectively. This discrepancy can be largely attributed to their choice of a static glacier boundary which does not differentiate between glacier melt, snow melt and rainfall-runoff from glaciers, but defines all runoff from glacier areas as glacier melt. The dynamic glacier module in our study updates glacier boundaries at the end of the accumulation season every year.

The runoff contribution estimates from Wijngaard et al., (2017) for the Ganges basin at Devghat comprise 3.4% for glacier melt (compared to 4.1% for this study), 12.4% (9%) for snow melt, 63.4% (65.9%) for rainfall-runoff and 20.8% (21.0%) for base flow, which are all in close agreement with values reported in this study. A similar close agreement in runoff partitioning was reported for the Brahmaputra catchment at Wangdirapids. Given the differences in scale, time period, modeling approach and input data, the runoff contribution estimates align well with past studies in this region. Considering the close agreement of runoff contributions compared to past studies, uncertainties in the ERA5 input data and the large spatial model domain, we conclude the model performance is satisfactory for our purpose.

Either limited or no discharge data availability for the hydrological model calibration is a key issue in the data scarce HMA region. Due to the lack of available discharge data for other basins, we adopt a "vector teams" approach to transfer the parameters for the ungauged basins (Bárdossy, 2007). The basins adjacent to each other with similar climatic and physiographic characteristics tend to hydrologically behave in a similar manner (Merz and Blöschl, 2004; Patil and Stieglitz, 2014). We transfer the parameter sets between them as this approach has been widely used in several sub-basin, basin, and regional scale studies in the HMA region (Lutz et al., 2014, 2016; Nepal et al., 2017; Wijngaard et al., 2017). We transfer the rainfall-runoff parameters from the BRA to TP, SAL to IRR, YAN to YEL and TIE, IND to TIW, and AMU to HEL and BAL river basins. Further, we validate the plausibility of transferred parameters by analyzing the patterns of annual and seasonal variability in discharge reported in the public domain for those basins. Finally, we conclude that the parameter transfer approach from a gauged basin to neighboring ungauged basins in HMA is applicable.

3.4.3 Hydrological regimes

The climate in the western mountain ranges (Karakoram, Hindu Kush, Pamir, and parts of Tien Shan and Kunlun) is primarily influenced by westerly disturbances and characterized by large amounts of snowfall in the winter season (Figure 3.2). This snow melts and contributes to the river flow in the spring and summer in the AMU, SYR, HEL, BAL, and IND river basins (Figure 3.1). A considerable amount of precipitation falls as snow (% of annual precipitation) in the AMU (45%), SYR (29%), HEL (30%), IND (35%), and BAL (24%) basins (Table B3). These basins are also characterized by vast glacierised areas, particularly in the IND (6.3% of total upper basin area). Therefore, the hydrology in these basins is dominated by snow and glacier melt (Figure 3.6). The total melt contribution to runoff, from snow

and glaciers, in the AMU (79%), SYR (74%), HEL (78%), and IND (45%) is higher than in other river basins (Table 3.3).

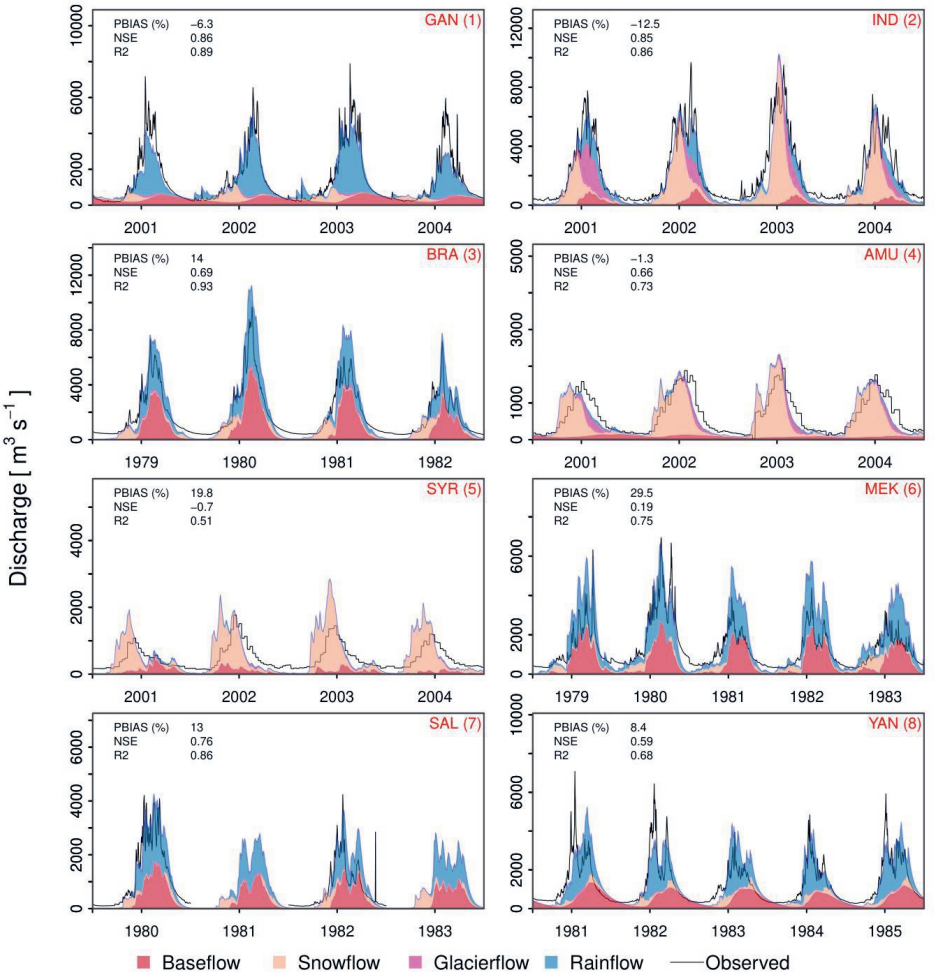

Figure 3.5: Observed and simulated discharge with the distinction of flow components at calibration locations shown in Figure 3.1 and Table 3.1 for the calibration time period. Each panel shows values for model performance indicators; Nash-Sutcliffe efficiency criterion (NSE), percent bias (PBIAS), and coefficient of determination (R2) at the top left corner.

In contrast, the hydroclimate in the southern and south-eastern basins is dominated by the Indian monsoon. Most of the annual precipitation falls during the summer monsoon months (June, July, August and September) in the GAN (71%), BRA (60 %), IRR (62%), MEK (66%), and SAL (63%) basins (Table B3). The hydrology in these Himalayan rivers is dominated by the rainfall-runoff component (Figure 3.1). A large amount of monsoonal precipitation over the GAN river basin explains the relatively small melt contribution (13%) despite having a relatively large area covered by glaciers (4.4%). A similar rainfall-runoff dominated regime can be observed in the wet eastern HMA in the YAN (71%) and YEL (64%) river basins. In these eastern river basins, the melt contribution is small due to the small glacier area coverage (0.4% and 0.1%, respectively) and little precipitation falling as snow (7% and

11%). The endorheic basins on the interior of the Tibetan Plateau (TP) show a stronger monsoonal precipitation pattern than other river basins in the Himalayan arc. The spring, autumn, and winter seasons are very dry, and 80% of the annual precipitation falls during the monsoon period (Bookhagen and Burbank, 2010). Even though the average elevation of the TP is above 4500 m, only 12% of annual precipitation falls as snow in the region, since most precipitation falls during summer when T is above 0°C (Figure 3.1and Figure 3.2), even at this a high altitude. Consequently, a rainfall-runoff regime, with 89% of the total annual flow occurring during the monsoon, is prevalent in the region. The northern basins, TIW and TIE, surrounded by the Pamir in the West, Karakoram in the South-East, Kunlun Shan in the East, and Tien Shan in the North, are among the driest basins in the entire HMA. These basins have a continental climate with high evapotranspiration rates (35% and 41% of annual precipitation) in the central dry region and high sublimation (17% and 18% of annual precipitation) on the surrounding mountain parts. The higher melt contribution to the runoff in the TIW (34%) as compared to TIE (21%) can be explained by the relatively larger glacierised area (5.8%) in TIW as compared to TIE (0.9%).

We define four different (single and mixed) hydrological regimes based on the dominant contributors: Nival (N; snowmelt dominated), Pluvial (Pl; rainfall-runoff dominated), Glacial-Nival (GN; snow and glacier melt dominated), and Nival-Pluvial (NP; snowmelt and rainfall-runoff dominated). We use three different thresholds for the snowmelt (15%), glacier melt (3%), and rainfall-runoff (40%) contribution to categorize the regimes. The baseflow contribution is excluded from hydrological regime distinction. The runoff contributions for each basin (Table 3.3) are recalculated excluding baseflow contribution. If two or more threshold criteria are exceeded, then it is considered as a mixed hydrological regime. We find five basins with a nival-glacial regime (AMU, GAN, IND, BAL, and TIW), six basins with a nival-pluvial regime (BRA, MEK, TP, SAL, TIE, and YEL), two basins with a nival regime (HEL and SYR) and two basins with a pluvial regime (IRR and YAN). These thresholds were selected to ensure the basins with a large fraction of glacier areas compared to upstream basin area (e.g., IND, TIW and AMU) stand out with a nival-glacial regime. For some basins, in particular BRA, even though the glacier area is greater than 10000 km2, the overall contribution of glacier melt was less than 3% and thus was not included in nival-glacial regime. The thresholds selected were subjective to the upstream basin boundaries used in this study.

Table 3.3: Basin characteristics for the reference period (1985–2014). The basin represents the upstream catchment area, as shown in Figure 3.1. Acronym CV represents the coefficient of variation.

							% contribution to total runoff				
Basin	Precipitation (mm yr^{-1})	Area (Km^2)	Glacier area (%)	Runoff (mm yr^{-1})	Runoff coef. -	CV of runoff (%)	Glacier melt	Snow melt	Rainfall runoff	Base flow	Melt (%)
Amu Darya (AMU)	676	268,280	4.36	407	0.60	89	4.4	74.4	5.4	15.8	78.8
Brahmaputra (BRA)	2018	400,182	2.73	1575	0.78	85	1.8	13.2	62.1	22.8	15.0
Ganges (GAN)	1763	202,420	4.37	1293	0.73	101	3.1	10.3	64.7	22.0	13.4
Helmand (HEL)	360	74,334	0.00	195	0.54	140	0.0	77.5	5.2	17.4	77.5
Indus Basin (IND)	832	473,494	6.28	577	0.70	83	5.1	39.7	43.9	11.4	44.7
Irrawaddy (IRR)	3638	49,029	0.15	3223	0.88	87	0.0	5.1	78.2	16.7	5.1
Lake Balkash (BAL)	856	121,185	3.39	543	0.62	43	2.2	46.3	9.3	42.3	48.5
Mekong (MEK)	1066	110,678	0.26	528	0.49	101	0.3	7.4	55.1	37.2	7.7
Plateau of Tibet Interior (TP)	451	415,197	0.83	117	0.25	162	2.3	15.3	32.8	49.6	17.6
Salween (SAL)	1091	119,377	1.45	627	0.57	94	1.4	14.7	55.7	28.3	16.1
Syr Darya (SYR)	942	172,704	1.70	456	0.48	97	1.3	72.9	5.6	20.2	74.2
Tarim Interior East (TIE)	305	600,182	0.90	126	0.42	93	1.1	20.2	49.7	29.0	21.3
Tarim Interior West (TIW)	373	481,481	5.77	166	0.45	103	5.8	28.4	44.4	21.4	34.2
Yangtze (YAN)	1127	687,150	0.39	849	0.75	76	0.2	5.5	71.0	23.3	5.7
Yellow (YEL)	751	272,857	0.05	468	0.62	77	0.1	9.6	63.9	26.5	9.6

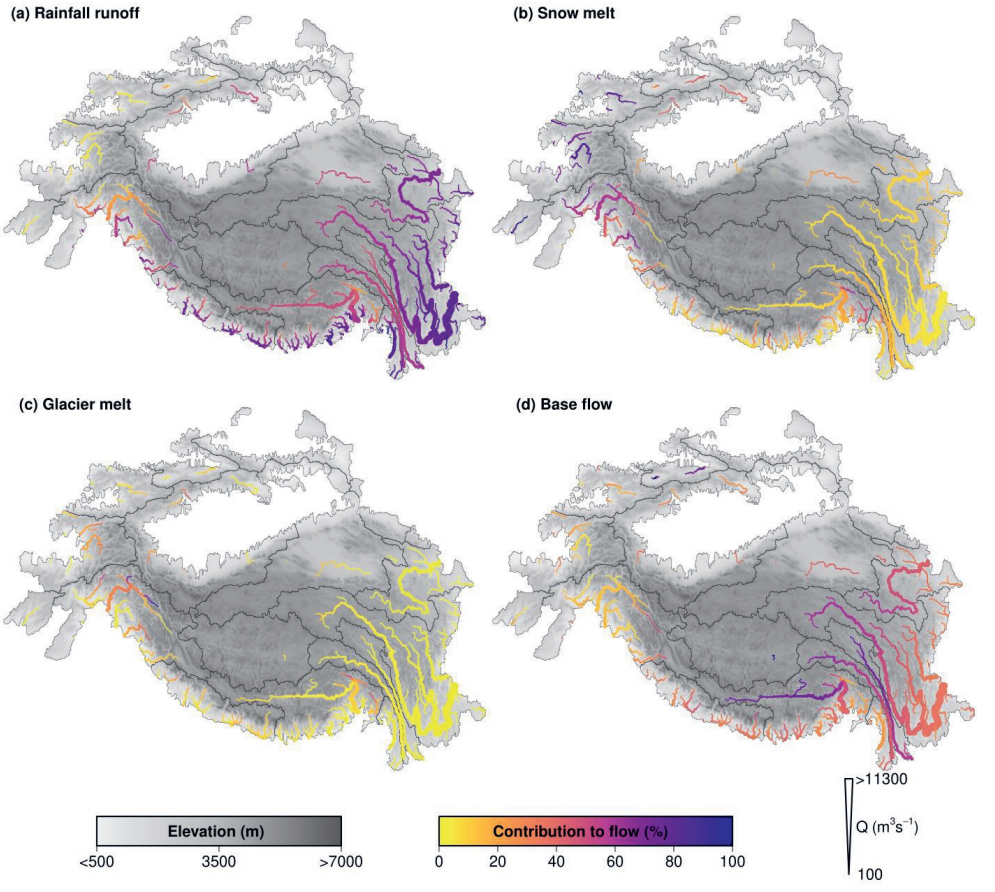

Figure 3.6: Flow components of the average annual total runoff for the reference ERA5 period (1985–2014). The magnitude of total annual flow is represented by the thickness of the line, color indicates the relative contribution to the total annual flow.

3.4.4 Hydrological responses at different time scales

3.4.4.1 Seasonal shifts in flow peaks

Here we investigate the shifts in peak timing, and magnitude changes in basin aggregated total runoff between the EOC and the reference period for the four different hydrological regimes. The increasing fraction of liquid precipitation attributed to climate warming results in a faster translation of precipitation to runoff and results in a higher magnitude of peak runoff in all the basins. Four out of fifteen basins show a clear shift in peak flow timing of total runoff. Basins with GN hydrological regimes, in particular the AMU, IND, and BAL basins, show changes in the total runoff patterns for the EOC period (Figure 3.7). For these basins, the onset of snow (Figure B5) and glacier melt runoff (Figure B6) starts earlier in the spring season in the EOC period. This results in an earlier peak flow as compared to the reference period. In the AMU basin, the peak of total runoff is shifted from June in the reference

period to April for the EOC warm-wet, warm-dry, and cold-dry and to May for the cold-wet scenario. A significant increase in peak total runoff is also projected for the AMU basin in the future. Although all runoff components contribute to the peak total runoff, the snowmelt runoff contribution dominates, compared to the glacier and rain-runoff (Figure B5Figure B6 Figure B7). An early total runoff peak that is mainly due to snow and glacier melt, as observed for the IND basin, is also observed in the BAL basin for future scenarios. While the IND basin shows no changes in the timing of peak total runoff, interestingly, a bimodal hydrograph is observed for the future period. The first peak is mainly attributed to the early snow and glacier melt while the second peak is primarily due to the rainfall-runoff during the monsoon. In contrast, the peak of total runoff in the TIW basin is shifted to later in the year (July) as compared to the reference period (June). This is predominantly due to the earlier onset of melt and removal of seasonal snow from the ice surface, resulting in rapid glacier ice melt in combination with increased monsoon precipitation in the future.

Among other basins with a GN hydrological regime, the GAN basin does not show changes in seasonality for total runoff in the future. Even though the snowmelt runoff in the GAN shows a clear shift to earlier onset of snowmelt in spring, like all basins in HMA, this effect is not reflected in the total runoff due to the dominant contribution of rainfall-runoff in the monsoon season. For the basins with an NP hydrological regime, there are no shifts observed in the timing of total runoff in future scenarios. Interestingly, for the BRA basin, a decrease in the hydrograph's rising limb slope is observed after a small peak in the total runoff in the months (MAM) for the future. This reduction in slope is mainly due to reduced snowfall resulting in a decrease in snowmelt contribution in future scenarios. A similar slope reduction is observed in all the basins with an NP hydrological regime. Basins with an N regime do not show specific changes in seasonality except the SYR for the warm-dry scenarios in the EOC period. The HEL and SYR basins initially show a significant increase in total runoff, mainly due to the rapid melting of seasonal snow in the early spring months and increased rainfall runoff contribution as compared to the reference conditions. Basins with a Pl regime do not show any significant changes in seasonality as most of the changes are associated with increases in rainfall-runoff during the monsoon season. Although same future projections (dP and dT) were imposed, the response of individual runoff components (Figure B5Figure B6 Figure B7) and total water availability is different in magnitude and peak timing for basins across HMA (*Table 3.4*). The differences in total water availability are due to the combined effect of changes in individual runoff components. Climate change response on the overall water budget of a region is primarily driven by the climatic characteristics but also by physiographic characteristics, human interventions, and socioeconomic changes. The changes reported here represent the combined effect of climatic and physiographic changes related to snow and glacier processes.

A first-order second moment (FOSM) uncertainty analysis (see Supplementary text S2 for details) suggests that uncertainty estimates for some basins (BAL, TIW, BRA, TP, HEL, and SYR) are higher than the others (AMU, GAN and IND) (Figure 3.7). To understand the underlying reasons for the variability in uncertainty estimates, the contribution of variance in individual parameters to the total variance is calculated (Figure B8). The uncertainty in meteorological forcing input (precipitation and temperature) is an order of magnitude higher compared to the model parameter uncertainty (DDFCI and DDFS). The precipitation uncertainty is highest in all basins, except for TIW and BRA, followed by uncertainty in T, DDFS, and DDFCI. The analysis suggests a large uncertainty in reference climate of the HMA region which limits the interpretation of climate change scenarios.

The seasonal shifts shown in Figure 3.7 represent the changes across several climatic combinations. Averaging the results in these broad categories, does not reveal the changes for the individual scenarios. Still, several clear trends of shifts in timing of the peak melt runoff, the overall change in contribution of runoff contributors are similar for basins with a similar hydrological regime. To illustrate changes at the seasonal scale for different time horizons, we take one basin from each of the hydrological regimes as an illustrative example: IND basin for GN, TP for NP, SYR for N, and YAN for Pl. We show these changes for the MC and EOC periods for the high dT, high dP, and high dPdT scenarios. For basins with a GN hydrological regime under the high dT scenario in both the MC and EOC periods, the seasonal changes are mainly driven by an initial increase in snowmelt runoff in the spring months followed by a decrease in snowmelt and an increase in glacier melt in the monsoon months (Figure 3.8 and Figure

B10). The initial increase in snowmelt results from earlier melting of seasonal snow due to an increase in temperature. Moreover, an increase in temperature will further reduce the likelihood of precipitation falling as snow and intensifies the glacier ice melt process, thus increasing the glacier melt contribution. Clearly, the magnitude of change varies in the two future periods and is higher for the EOC than for the MC period. For the high dP scenario, changes are mainly driven by an increase in rainfall-runoff and snowmelt contribution, whereas for the high dPdT scenario, the changes are driven by an increase in rainfall-runoff, as well as snow and glacier melt contributions outside the monsoon season. A similar decrease of snowmelt runoff during the monsoon season is observed in the high dPdT scenario.

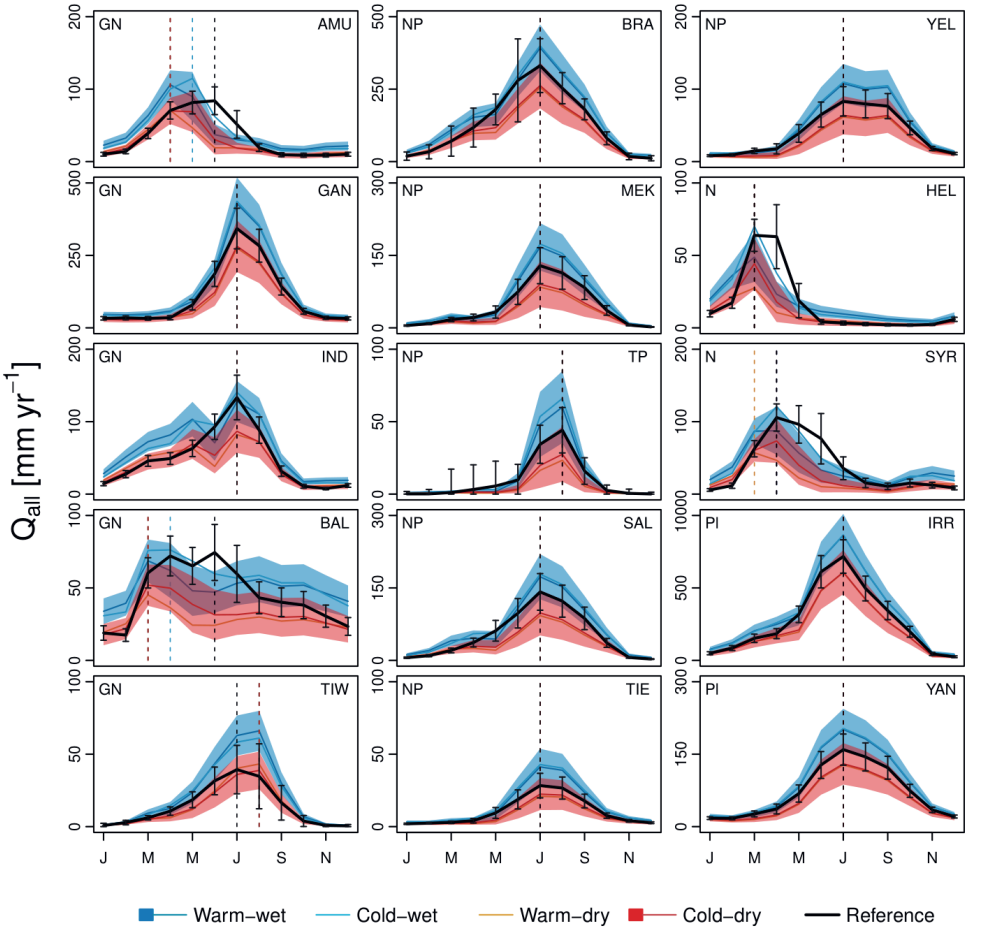

Figure 3.7: Changes in the mean annual cycles of total runoff by the end of the century (2071–2100) for the four hydrological regimes. The colored lines represent the mean of four groups of future scenarios, consisting of twelve dT/dP combinations each; warm-wet (6°C to 8°C, 10% to 40%), cold-wet (3°C to 5°C, 10% to 40%) , warm-dry (6°C to 8°C, -30% to 0%) and cold-dry (3°C to 5°C, -30% to 0%). The color shadings represent ±2 standard deviation for a group of scenarios (only shown for warm-wet and cold-dry). The black solid lines represent the reference (1985–2014) mean annual cycle of total runoff. The vertical black error bar represents the total estimated variance calculated using first order second moment method for the reference climate for period 1985–2014. The vertical dashed lines represent the peak flow months for each group of scenarios. The text on the top-left and top-right gives the hydrological regime and basin name, respectively.

For river basins with a N regime, changes in snowmelt contribution are mainly driving the changes in the future, for all three scenarios. These changes include a significant reduction of snowmelt contribution and shifts in peak melt water timing. While the changes in the future, for both time horizons and across all scenarios, are mainly driven by the snowmelt and rainfall-runoff contributors for river basins with aNP regime, rainfall-runoff drives the changes in river basins with a Pl regime, especially in the monsoon season. The scenarios with precipitation changes, i.e. high dP and high dPdT, show a higher magnitude of rainfall-runoff change compared to high dT scenarios for basins with a Pl regime. The snow melt related changes are insignificant in the Pl regime compared to all other regimes where snow plays a dominant role in driving future changes. Thus, at the seasonal scale, changes are mainly driven by either change in snowmelt, rainfall-runoff, or a combination of both.

Table 3.4: *Relative changes in the magnitude (%) for mean annual total runoff for the future end of century time period (2071-2100) as compared to the reference period (1985–2014). The values in the parentheses represent the standard deviation (±1).*

	WARM-WET	***COLD-WET***	***WARM-DRY***	***COLD-DRY***
AMU	19.6 (14.4)	24.3 (14.6)	-27.2 (12.9)	-23.4 (13.2)
GAN	23.0 (13.4)	25.5 (13.4)	-22.4 (13.0)	-20.1 (13.1)
IND	29.7 (13.5)	28.4 (13.4)	-15.7 (12.9)	-16.6 (12.8)
BAL	10.3 (14.8)	19.9 (14.9)	-37.8 (13.5)	-29.1 (14.0)
TIW	58.0 (19.5)	50.9 (19.2)	-4.9 (17.0)	-11.3 (17.1)
BRA	18.2 (12.7)	21.0 (12.7)	-24.5 (12.2)	-22.0 (12.3)
MEK	26.4 (19.8)	32.4 (20.0)	-37.2 (17.0)	-32.5 (17.5)
TP	24.4 (28.0)	40.4 (29.7)	-53.2 (17.3)	-44.1 (19.6)
SAL	22.8 (17.6)	27.9 (17.8)	-34.9 (15.8)	-30.8 (16.2)
TIE	37.8 (21.3)	45.4 (21.5)	-29.6 (17.9)	-23.5 (18.5)
YEL	22.5 (15.6)	26.7 (15.7)	-29.7 (14.9)	-25.9 (15.1)
HEL	0.9 (15.2)	12.9 (15.7)	-46.8 (13.0)	-36.0 (13.7)
SYR	0.1 (16.6)	15.0 (17.6)	-49.0 (12.6)	-37.8 (14.0)
IRR	19.8 (11.4)	20.8 (11.4)	-19.7 (11.6)	-18.6 (11.6)
YAN	22.7 (13.4)	25.1 (13.4)	-23.2 (13.3)	-20.8 (13.4)

3.4.4.2 Changes in decadal time scales for runoff contributors

In contrast to the high dP scenario, under the high dT scenario, a significant impact is observed for the snow and glacier melt contributions in river basins with a GN regime, at yearly to decadal scales (Figure 3.8). Glacier melt in the basins with a GN regime shows a slower melting response and smaller changes for the high dP scenario as compared to the high dT scenario. Moreover, the glacier melt contribution for basins with a GN regime shows an initial increase and the peak of glacier melt is reached by the end of the MC period, which is then followed by a strong decline by the start of the EOC period. The initial increase results from warming induced melt, which eventually is offset by a reduction in available ice volume. In particular, smaller glaciers will reach the glacier melt peak in the next few decades or by the MC period, followed by a permanent loss in glaciated area except for the TIW where glacier melt has not reached its peak melt by the EOC and contributes strongly to the peak total runoff (Figure B9). Interestingly, the increases in glacier melt runoff, rainfall-runoff, and baseflow contributions are offset by a significant decrease in snowmelt contribution in river basins with a GN regime. This results in almost no change in the total runoff for the high dT scenario. While the glacier melt keeps increasing by the EOC period in river basins with a GN regime, the initial increase eventually starts decreasing by the MC or EOC periods for basins with other hydrological regimes. An explanation is that most of the basins have either passed or are approaching the peak in glacier melt runoff. For all the regimes, the high dP scenario leads to an increase in rainfall-runoff and baseflow contribution, which leads to a consistent increase in total runoff in the future. On the other hand, the high dPdT scenario shows a nonlinear response on the longer time scales when compared to either the high dP or high dT scenarios

for all the regimes. In the high dPdT scenario, a significant increase in the rainfall-runoff and baseflow contributions is observed across regimes. An increase in liquid P as a result of high T and an increase in precipitation are the main factors causing the increase in rainfall-runoff and baseflow. The high dPdT scenario results in an increased total runoff in all regimes except the N regime as the increase in rainfall-runoff is offset by the decrease in glacier and snowmelt runoff.

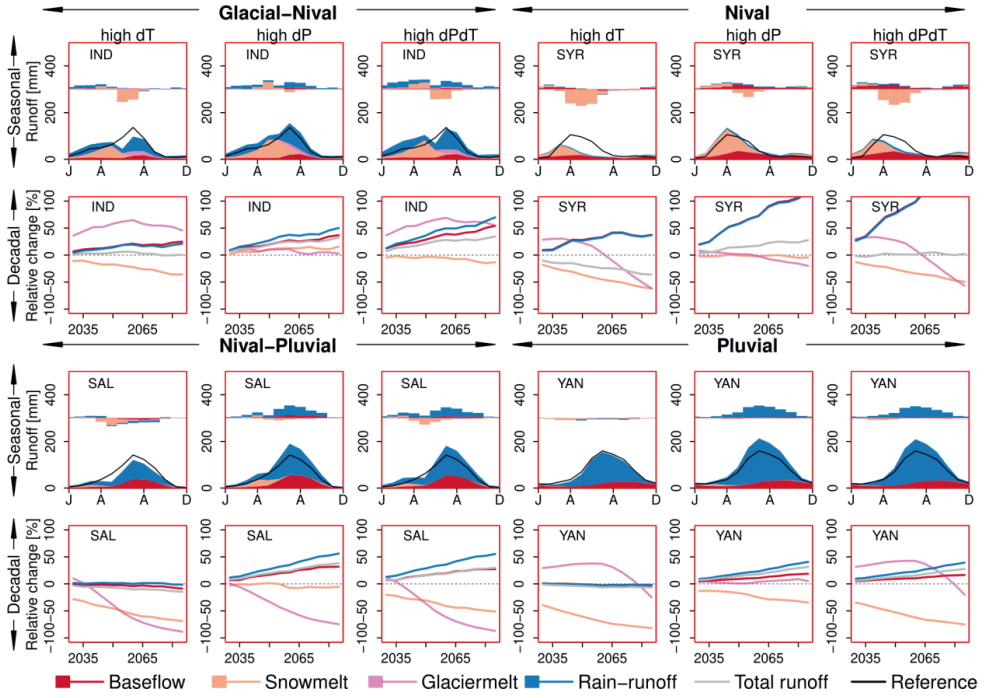

Figure 3.8: Hydrological response to climate change at seasonal (row 1 and 3) and decadal time scales (row 2 and 4). The seasonal hydrographs and changes in flow components (bars) are plotted for the end of century period (2071-2100) for one illustrative basin from each hydrological regime i.e., Glacial-Nival (IND), Nival-Pluvial (SAL), Nival (SYR), and Pluvial (YAN). Changes in the flow regime are assessed for three different future scenarios i.e., high dT, high dP, and high dPdT. The bars in seasonal plots represent changes per-flow component relative to the reference period (1985–2014). The black solid lines in seasonal plots represent the reference mean annual cycle of total runoff. The lines in decadal plots represent the transient 30-yr running mean relative changes in annual sums of rainfall-runoff, glacier melt, snowmelt, baseflow and total runoff. The 30 years mean is calculated at 5-year intervals.

3.5 Discussion

3.5.1 Climate change response at smaller spatial scales

The climate change response of hydrological processes explored here is highly scale dependent. It varies both spatially from catchment to basin-scale and temporally from the seasonal to the decadal scale. The responses vary strongly in the climatically and hydrologically diverse HMA region, where runoff generated at higher altitude depends strongly on snow and glacier melt, whereas rainfall-runoff and baseflow processes dominate runoff generation at lower altitudes. In HMA, the changes in total water availability are larger at higher altitudes than at lower altitudes for the different hydrological regimes except in the HEL and MEK basins (Figure 3.9). Even though the scenarios show similar patterns, the

magnitude differs. Magnitudes are higher for the warm-wet and cold-wet scenarios as compared to the warm-dry and cold-dry scenarios. For higher altitudes, the total water availability increases either due to increased melt or an increase in the liquid precipitation fraction. Both conditions are mainly driven by increased temperature or precipitation. The differences in the magnitude of flow components and total water availability for high altitude regions are well visible in two extreme scenarios; warm-wet (Figure B11) and cold-dry scenarios (Figure B12). However, this increased water availability levels off and decreases when lower altitude regions are considered as well. The TIW and TIE show the strongest changes for the higher altitudes among all the basins in HMA. This is mainly due to the increase in future total water availability driven by a stronger increase in monsoon precipitation (Figure B7) and glacier melt (Figure B9) in those basins.

Even though the total water availability at higher altitudes increases, the changes in timing and magnitude of peak water availability and seasonality impose a serious threat on the livelihood of people. In particular, agricultural productivity at high altitude regions which depend on the timing of melt from snow and glaciers are strongly exposed to cryospheric changes and will be impacted by future changes in hydrological regime and peak melt water availability for irrigation (Qin et al., 2020).

3.5.2 Hydrological regimes at smaller spatial scales

The characterization of hydrological regimes depends on the choice of thresholds of runoff contributors and the spatial aggregation level. To demonstrate this, we show the distinction of hydrological regimes differs for a varying spatial aggregation level. We compare hydrological regimes at three spatial aggregation levels: (i) river basins (i.e., the fifteen upper basins), (ii) subbasins as defined in the hydro-basins dataset at aggregation level 06, and (iii) subbasins as defined in the hydro-basins dataset at aggregation level 08 (Figure B2). At each of these aggregation levels, we plot the contribution from rain, snow, and glacier melt runoff in a ternary plot (Figure 3.10). At the river basin aggregation level, the contribution from rain and snow dominates due to the substantial reduction in the relative contribution of glacier melt water with water from these sources (Figure 3.10a). Defining the hydrological regime based on the relative contributions of stream flow contributors will result mostly in rain or snow dominated flow regimes. However, the contribution changes with the finer spatial aggregation levels (Figure 3.10). For aggregation level 08, the glacier and snow contribution increases. For instance, the GAN river basin at basin aggregation level suggests a mostly rain dominant (80%) regime (Figure 3.10a). But at aggregation level 08, a higher number of subbasins have higher contribution from snow and glacier melt, despite the majority of subbasins being rain-dominated (Figure 3.10c). This highlights the importance of spatial scale in the distinction of hydrological regimes. In this study, we use basin and the relative contributions from rain-fall runoff, snow melt runoff, and glacier melt runoff at the river basin scale aggregation for the distinction of hydrological regime. The use of different thresholds and spatial scales would change the hydrological regime characterization and consequently the analysis.

3.5.3 Comparison with other studies

The differences in spatial and temporal aggregation, time horizons, models, and reference and future climate forcing make a comparison to other studies not straightforward. Even though the absolute magnitude of projected changes cannot be directly compared with studies that use inputs from either regional or global climate models, the patterns and direction of change are similar and comparable. The patterns of future change in seasonality and peak melt water in this study align with the other regional and global studies (e.g., Huss and Hock, 2018; Lutz et al., 2014; Wijngaard et al., 2017). Future increases in total water availability from this study (summarized in *Table 3.4*) are comparable to those reported at basin outlets by Wijngaard et al., (2017) for the similar future EOC period (i.e., 29–41% for the GAN, 24–49% for the BRA and 4–51% for the IND under RCP4.5 - RCP8.5). The total water availability for the BRA basin in this study is also comparable to the values reported by Lutz et al., (2014): -15–60% for combined RCP4.5 and 8.5 emissions scenarios. The changes in seasonality and early melt dominated regimes found in this study are in line with previous basin and sub-basin scale studies (Lutz et al., 2014;

Ragettli et al., 2016; Sorg et al., 2014). The peak glacier melt timing found in this study are also consistent with the results of Huss and Hock. (2018).

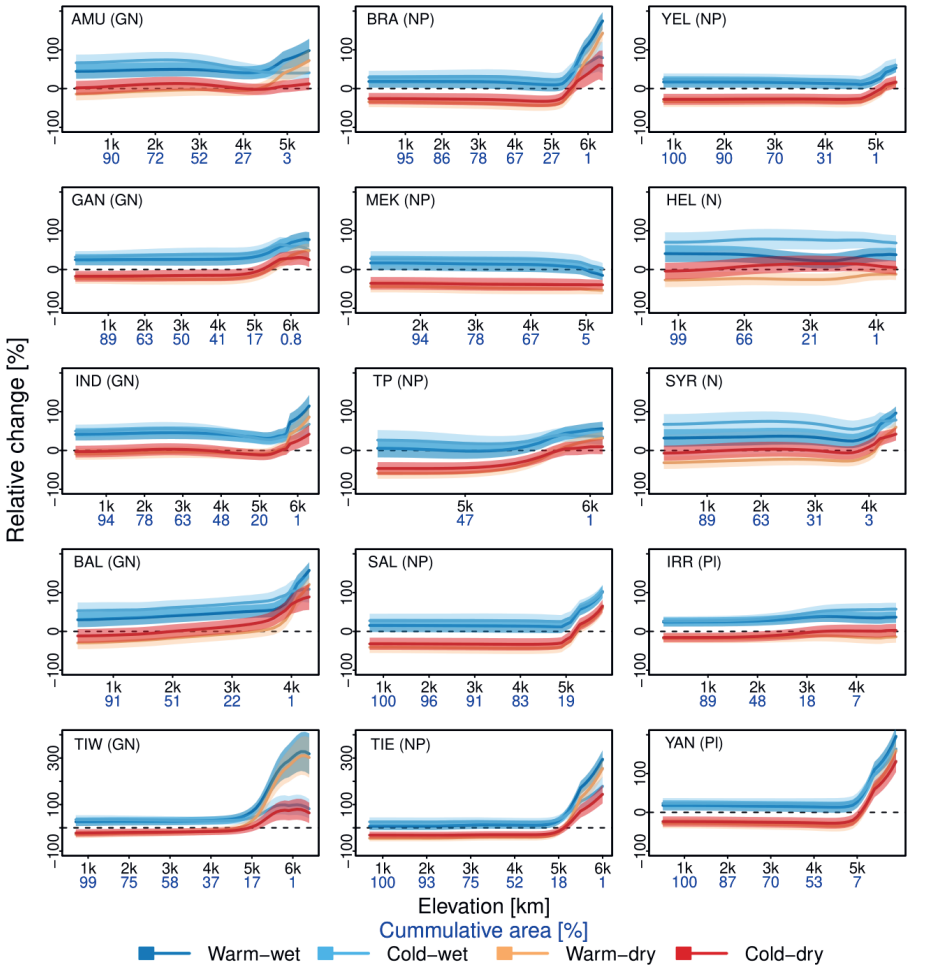

Figure 3.9: *Relative changes in total runoff as a function of elevation by end of century (2071–2100). The black and blue x-axis labels represent the elevation [km] and cumulative area fraction above each 100 m elevation bin [%]. The color represents 4 future scenarios; warm-wet (6°C to 8°C, 10% to 40%), cold-wet (3°C to 5°C, 10% to 40%), warm-dry (6°C to 8°C, -30% to 0%) , cold-dry (3°C to 5°C, -30% to 0%). The solid line indicates the mean of the model combination, and shading represents ±1 standard deviation (only shown for warm-wet and cold-dry). The text on the top right represents basin names with hydrological regimes in parentheses. Note the different scaling used for TIW and TIE.*

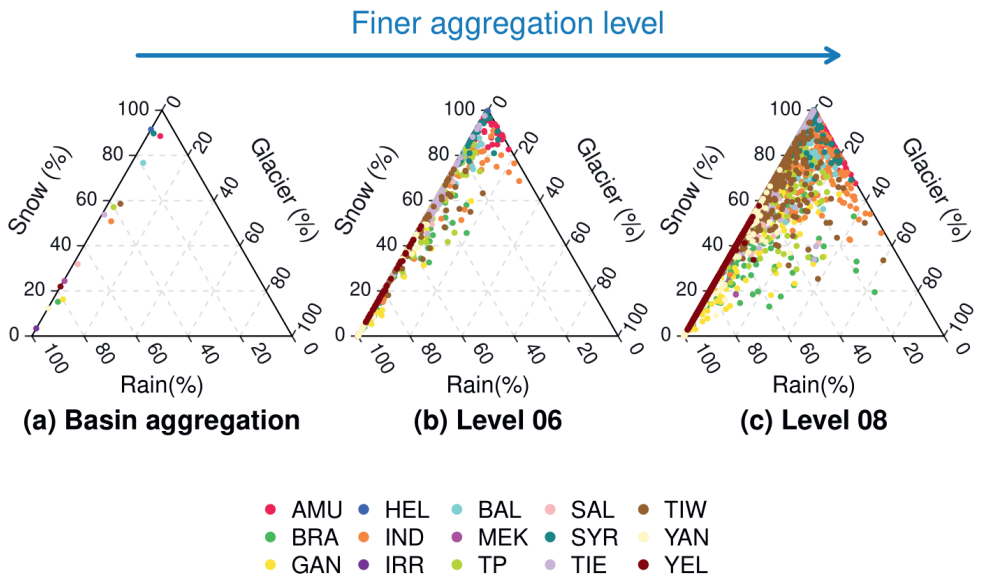

Figure 3.10: Ternary plot for hydrological regimes at the basin and hydro-basins (Lehner and Grill, 2013) aggregation levels 06 and 08. The axes give the different flow contribution (snow, glacier, and rainfall-runoff) to the total flow expressed in percentage [%]. The colored points represent the temporal aggregation for each spatial aggregation level.

3.5.4 Uncertainties and limitations

The results of this study heavily rely on the ERA5 reanalysis data and are therefore subject to limitations in those. In particular, the overestimation of precipitation in the monsoon dominated HMA regions results in overestimation of historical total water availability in those regions. However, the relative changes in future total water availability will not deviate significantly due to the historical overestimation. Computed changes in the absolute amount of glacier melt are also sensitive to the initial glacier states such as areas and ice volumes, which are subject to large uncertainties. The limited discharge data availability for the model calibration and parameter transfer approach is associated with uncertainties in the results. To reduce the uncertainty due to the parameter transfer approach, we use neighboring basins with similar climatic and physiographic characteristics in the approach and further validate the mean monthly climatological discharge values with those available in the public domain.

Furthermore, the range of projected changes in precipitation and temperature we use are based on a subset of 27 members of the CMIP6 model ensemble (Almazroui et al., 2020), and therefore may not cover the full range of uncertainty in future projections of the final CMIP6 ensemble. Nevertheless, the chosen ranges provide a good indication of the potential range of future changes. Moreover, the aggregated projected change over the entire region does not entirely resolve the micro-scale changes in the region where climate varies over short distances. Also, the use of a linear transformation of the historical climate to the future climate poses limitations. Seasonal variation in the climate change signals as well as non-uniform changes across the frequency distributions of temperature and precipitation are not considered, which may play a key role in future climate change response. Moreover, the uncertainty ranges for future runoff presented in this study represent the uncertainty from the range in future climate projections solely and do not include uncertainties in the input data and structural model uncertainty. Therefore, they represent the lower bound of uncertainty.

Apart from the improvement in simulation of physical processes, such as snow avalanching and sublimation, glacier melt and dynamics (debris, ponds, cliffs), groundwater processes and flow routing, future work must focus on developing a homogenized and representative climate data archive for HMA. More research is needed to improve the inadequacies and missing processes in the reference climatology, representation of key precipitation and temperature related processes in complex terrain like HMA. In-depth understanding of the full spread amongst CMIP6 models will be necessary to improve the interpretation of the highly space and time-dependent projections. Further, a more complex uncertainty analysis (e.g., a full Monte-Carlo or Bayesian approach) would be helpful to disentangle model input and structural uncertainty which is quite important for better interpretation of future climate change.

3.6 Conclusions

We show contrasting climate change responses across High Mountain Asia's upstream river basins, dictated by the present-day variability in climate and hydrological regimes. At the large, river basin scale, the upstream basins of fifteen rivers in High Mountain Asia can be grouped into four hydrological regimes: glacial-nival, nival-pluvial, nival, and pluvial. Our results show that an increased fraction of liquid precipitation due to climatic warming results in higher peak total runoff in all the basins. Despite clear shifts at the seasonal scale in peak snowmelt runoff to earlier in the year in most cases, at the decadal to century scale only basins with glacial-nival hydrological regimes show shifts in the timing of peak runoff by the end of century. The snowmelt runoff decreases significantly for most of the basins towards the end of the century except for basins with a glacial-nival hydrological regime. This is found even for scenarios with moderate temperature increase. We demonstrate that all basins have either passed or are approaching the peak glacier melt runoff except the Tarim interior West basin, for which glacier melt continues to increase even by the end of the century. At the seasonal scale, the changes are mainly driven by changes in either snow or rainfall-runoff but at the decadal scale, the responses are rather consistent and mainly driven by precipitation changes. Finally, we illustrate that the changes in total water availability are stronger in magnitude for the headwaters than at lower altitudes. It is the change in seasonality and changes in peak melt runoff that will pose the main challenge to be addressed in adapting to future changes in a region where food security, energy security as well as biodiversity, and the livelihoods of many depend on water from the mountains. These findings provide important information to support climate change adaptation policy planning in this climate change hotspot.

Acknowledgments

The project received funding from the Strategic Priority Research Program of Chinese Academy of Sciences, Grant No. XDA20100300. This project was also partly funded by the European Union's Horizon 2020 Research and Innovation Program under the Marie Skłodowska-Curie grant (agreement no. 676027), by the European Research Council (ERC) under the European Union’s Horizon 2020 research and innovation programme (grant agreement number 676819), and by the Netherlands Organization for Scientific Research under the Innovational Research Incentives Scheme VIDI (grant agreement 016.181.308). The authors thank Fanny Brun for providing the glacier mass balance data for high mountain Asia. The authors also thank the Nepal Department of Hydrology and Meteorology (DHM), the Pakistan Water and Power Development Authority (WAPDA), and the Bhutan National Center of Hydrology and Meteorology (NCHM) for providing discharge data. Streamflow data are also obtained from the Global Runoff Data Center (GRDC) (https://www.bafg.de/GRDC/EN/). We thank 3 anonymous reviewers for their constructive comments that helped to improve the manuscript. We would also like to thank Rene Wijngaard for helpful discussions.

4

Chapter 4

The Impact of Meteorological and Hydrological Memory on Compound Peak Flows in the Rhine River Basin

4 The Impact of Meteorological and Hydrological Memory on Compound Peak Flows in the Rhine River Basin

Spatio-temporal variation of hydrological processes that have a strong lagged autocorrelation (memory), such as soil moisture, snow accumulation and the antecedent hydro-climatic conditions, significantly impact the peaks of flood waves. Ignoring these memory processes leads to biased estimates of floods and high river levels that are sensitive to the occurrence of these compounding hydro-meteorological processes. Here, we investigate the role of memory in hydrological and meteorological systems at different temporal scales for the Rhine basin. We simulate the hydrological regime of the Rhine river basin using a distributed hydrological model (SPHY) forced with 1950–2000 atmospheric conditions from an ensemble simulation with a high resolution (0.11°/12 km) regional climate model (RACMO2). The findings show that meltwater from antecedent anomalous snowfall results in a time shift of the discharge peak. Soil moisture modulates the rainfall-runoff relationship and generates a strong runoff response at high soil moisture levels and buffers the generation of runoff peaks at low levels. Additionally, our results show that meteorological autocorrelation (manifesting itself by the occurrence of clustered precipitation events) has a strong impact on the magnitude of peak discharge. Removing meteorological autocorrelation at time scales longer than five days reduces peak discharge by 80% relative to the reference climate. At time scales longer than 30 days this meteorological autocorrelation loses its significant role in generating high discharge levels.

Chapter published as:
Khanal, S.; Lutz, A.F.; Immerzeel, W.W.; Vries, H.d.; Wanders, N.; Hurk, B.v.d. The Impact of Meteorological and Hydrological Memory on Compound Peak Flows in the Rhine River Basin. Atmosphere 2019, 10, 171. https://doi.org/10.3390/atmos10040171

4.1 Introduction

In many natural systems memory effects play a prominent role. Although the memory of atmospheric processes generally does not entail more than a few days (Entin et al., 2000; Lorenz, 1969; Vinnikov et al., 1996; Wu and Dickinson, 2004), atmospheric autocorrelation is propagated to the slow hydrological storage reservoirs such as soil moisture (hereafter referred to as SM), snow pack, glaciers, groundwater and riverine storage (Pelletier and Turcotte, 1997; Wanders et al., 2018). Hydrologic processes with longer time scales "remember" past atmospheric anomalies and their effects are reflected in subsequent events or periods. For instance, a storm event may persist within the soil columns for a long time even after the external forcing has ceased. Similarly, accumulation of heavy snowfall may persist for a long time ultimately affecting the hydrological regime of a region.

Hydrological systems are governed by processes with memory at different time scales (Koutsoyiannis, 2005a). Examples are evaporation (Delworth and Manabe, 1988; Scott et al., 1997), ground water (Amenu et al., 2005; Güntner et al., 2007), SM (Seneviratne and Koster, 2012; Wu and Dickinson, 2004), snow dynamics (Bojariu and Gimeno, 2003; Cohen and Fletcher, 2007; Xu and Dirmeyer, 2011) and riverine storage (Wanders et al., 2018) having memory of days to up to several years. Similarly, the long term persistence—or 'Hurst phenomenon'—has triggered many studies supporting engineering applications such as design discharge for hydraulic infrastructure (Hurst, 1951), lake inflows (Montanari et al., 1997), river inflows (Koutsoyiannis, 2002), the regional hydrological cycle (Blender and Fraedrich, 2006), floods (Mudelsee et al., 2003) and droughts (Bunde et al., 2005). Predictability studies have addressed SM memory effects (Dirmeyer et al., 2009; Koster and Suarez, 2001; Orth and Seneviratne, 2012), ground water memory (Amenu et al., 2005; Bierkens and van den Hurk, 2007; Güntner et al., 2007; Van Lanen et al., 2013) and snow memory (Cohen and Rind, 1991; Shinoda, 2001; Xu and Dirmeyer, 2011). In reality, many phenomena act simultaneously, and their compound

occurrence is highly influential in determining the final state of the system (Zscheischler et al., 2018). For instance, persistence in SM may lead to a drought during warm periods (Nicholson, 2000; Wu and Dickinson, 2004) but can similarly increase the likelihood of severe floods during cold periods (Bonan and Stillwell-soller, 1998; Liu et al., 2014a). Likewise, snowfall from a prior season can strongly modulate subsequent stream flow.

The co-occurrence of hydro-climatic extremes may propagate disproportionally to extreme hydrological events. For instance, the co-occurrence of heavy precipitation with heavy snowmelt, high SM or high groundwater levels can lead to extreme discharge. This compounding nature of extreme events may be crucial to understand the background of extreme hydrological events (van den Hurk et al., 2015; Kew et al., 2013; Khanal et al., 2019; Leonard et al., 2014; Wahl et al., 2017). Hydrometeorological compound events (CEs) are increasingly receiving scientific attention (Hazeleger et al., 2015; Seneviratne et al., 2012; Zscheischler et al., 2018). This study primarily focuses on compound hydrometeorological events and their intensification by the memory of hydrological processes. For Dutch coastal areas, several studies describe CEs for storm surges in combination with wind (Kew et al., 2013), precipitation (Hazeleger et al., 2015; van den Hurk et al., 2015; Kew et al., 2013; Ridder et al., 2018b) and discharge (Khanal et al., 2019; Pinter et al., 2006). These studies confirm a clear correlation structure among the compound occurrence of storm surges and discharge (precipitation). Further, they share some shortcomings emanating from using limited observation records, reanalysis products or model simulations, and/or focusing on a limited dynamic range of the lagged signals contributing to the CEs (van den Hurk et al., 2015; Kew et al., 2013; Khanal et al., 2019; Klerk et al., 2015; Ridder et al., 2018b). Moreover, these studies focused on a predefined timescale without explicitly exploring the role of process memory in the governing hydrometeorological systems. In a large river basin like the Rhine, where basin SM and snow storage in the Alps and upper Rhine play an important role in determining the flow regime, extreme antecedent rainfall or snowfall can contribute to elevated risk of high discharge, leading to coastal or fluvial flooding. A significant part of the precipitation during the winter months (DJF) is temporarily stored as snow in the upper/alpine part of the Rhine (te Linde et al., 2010; Pinter et al., 2006). The stored snow releases the meltwater with a certain time delay (Junghans et al., 2011), and contributes annually around 34% to the discharge at Lobith (Stahl et al., 2016). The co-occurrence of snowmelt either with a persistent single low depression or sequence of low depressions extending over multiple weeks can result in high discharge volumes (Engel, 1997). Extreme rainfall on frozen or saturated soil can also generate extreme floods in the Rhine (Disse and Engel, 2001). In addition, high discharge of the Rhine at Lobith requires a series of moisture laden low pressure depressions passing over the basin (Hegnauer et al., 2015; Kew et al., 2011). The most destructive floods in Netherlands in 1926 (heavy rainfall episodes leading to dike breach), 1993 (heavy rainfall episodes on saturated soil), and 1995 (rain on frozen soil) are examples of CEs. A good understanding of the memory processes and their nonlinear interaction with extremes is required to correctly estimate risk imposed by these CEs.

A deeper analysis for such CE's requires a consistent long spatial-temporal dataset for soil moisture, snowfall and snowmelt. There are no such datasets available for historical periods. It is a challenging task to analyze the CE's from a limited observed record (van den Hurk et al., 2015). Several studies have shown that long and realistic simulations of hydrodynamic processes and events can bypass the limitation posed by the limited observation record and improve the accuracy of estimation of the statistical properties of compound extreme events (van den Hurk et al., 2015; Kew et al., 2013; Klerk et al., 2015). However, the climate data requires downscaling and bias correction of precipitation and temperature fields before it could be used for the hydrological impact studies (Brienen et al., 2010; Kleinn et al., 2005; Minville et al., 2013).

In this study we synthesize to what extent memory within hydro-meteorological systems affects the generation of extreme discharge. We particularly investigate memory effects at monthly to seasonal timescales. To achieve this, first, we explore the role of meteorological autocorrelation by perturbing the time-correlation of the meteorological time series used as forcing for streamflow simulations by a hydrological and hydraulic model system. Next, we investigate the role of snow and SM memory in the

hydrological regime of the Rhine. Finally, we analyze the role of memory in the hydro-meteorological system that leads to intensification of the hydrological extremes.

4.2 Study Area

The Rhine basin covers an area of 185,000 km2 and runs over 1320 km from its source in the Alps to the North Sea. The largest fraction of the basin (about 2/3rd) is located in Germany, amongst the nine countries through which the Rhine flows (Figure 4.1). Along its course, the Rhine collects water from major tributaries like the Aare, Neckar, Main and Moselle. The mean annual precipitation across the Rhine basin varies from about 500 (Rhine valley) to 2000 mm (Alpine region), and the mean annual discharge at Lobith is about 2200 m^3s^{-1}. During summer the streamflow for the upper part of Rhine at Basel is dominated by snowmelt and rainfall-runoff from the Alps (Viviroli, Daniel; Messerli, 2003). However, for the lower parts at Lobith, the Netherlands, streamflow is dominated by rainfall resulting in streamflow peaks during winter. The annual mean hydrograph shows a change of the discharge peak from summer to winter when descending from the upper Rhine at Basel down to the lower Rhine at Lobith (Disse and Engel, 2001; Photiadou et al., 2011). The annual mean contribution of snowmelt to total streamflow at Lobith is around 34% (Stahl et al., 2016), while discharge from the area upstream of Basel consists of snowmelt for almost 50% (Kwadijk and Deursen, 1999). The travel time of the flood wave between Basel and Lobith is around five days (Hegnauer et al., 2014). Downstream of Lobith, the Netherlands is protected by numerous dikes measuring a total length about 22,000 km.

The highest discharge ever recorded in the Rhine at Lobith is about 12,000 m^3s^{-1} during the floods of January 1926, which was primarily caused by multi-day episodes of rainfall after a period of moderate rain filling up the SM reservoir, in combination with melting of snow stored over the previous winter. Similarly, in December 1993 a flooding was caused by an extreme 10-day rainfall sum on saturated soil. In January 1995 an anomalous high temperature episode following a cold spell caused a coincidence of precipitation falling as rain on frozen soil and melting of snow leading to a strong discharge peak. Current protection levels for flood infrastructure in the Netherlands are designed to withstand a flood event of a strength that has a recurrence time of 1250 years (Ward et al., 2017). This leads to a so-called "design discharge" of 16,000 m^3s^{-1}. Discussions to increase this level to higher discharge volumes, to account for changing climate and socio-economic conditions, are ongoing.

4.3 Data, Model and Methods

4.3.1 Data

In this study we used daily output from a 16-member ensemble of climate model simulations with the Global Climate Model (GCM) EC-Earth for the period 1951–2000 (Hazeleger et al., 2012). The 12 km resolution Regional Climate Model (RCM) RACMO2 was used to dynamically downscale the GCM ensemble (van Meijgaard et al., 2008). E-OBS v14 daily gridded precipitation data at 0.25° resolution were used for the bias correction of outputs from the RCM (Haylock et al., 2008). Daily temperatures were adjusted to local topography using a vertical lapse rate of −6.5 °C km^{-1}. The downscaled data were used as input for the hydrological model.

4.3.2 Hydrological Model

In this study we used the Spatial Processes in Hydrology (SPHY) hydrological model (Terink et al., 2015). SPHY is a conceptual, spatially distributed (raster-based) "leaky-bucket" type model. The model integrates dominant hydrological processes like (i) rainfall–runoff; (ii) lake/reservoir outflow, (iii) cryospheric processes (snow, ice, glaciers) (iv) evapotranspiration and (v) soil hydrological processes. SPHY requires input data as fixed state and dynamic variables. Digital Elevation Model (DEM), land use type, glacier cover, reservoirs and soil characteristics are the relevant fixed state variables. The main dynamic variables are metrological data such as precipitation and temperature (maximum, minimum and average). The model contains sub-grid variability (e.g., cells can be glacier-free or partially to fully

covered with glaciers) and melt generation is based on the widely used degree-day melt modeling approach (Hock, 2003). The snow storage at each time step is updated with snow accumulation and/or snowmelt. Precipitation is segregated in the form of rain or snow, depending on the temperature. Precipitation can be intercepted by canopy and in part or in whole evaporated. The reference evapotranspiration is calculated using the modified Hargreaves method (Hargreaves and Samani, 1985).

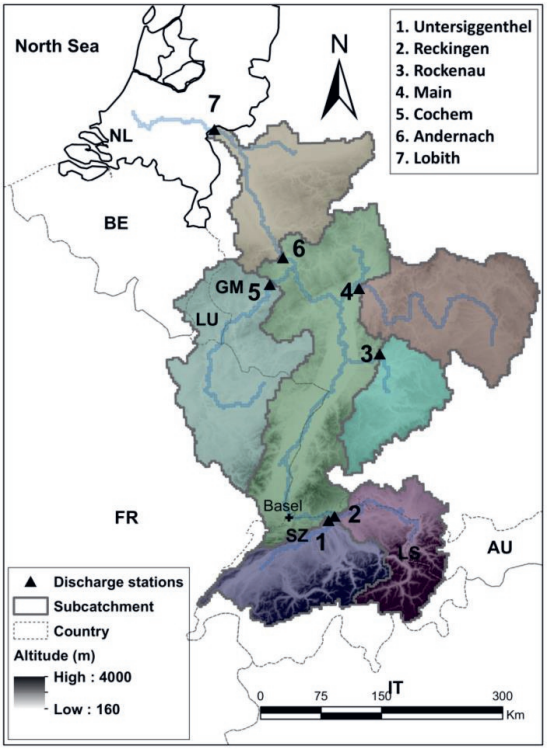

Figure 4.1: The Rhine basin, with seven sub catchments used for the calibration.

A fraction of the liquid precipitation contributes to the surface runoff, whereas the remainder infiltrates into the soil. The resulting soil moisture, depending on the soil properties and fractional vegetation cover, is available for the evapotranspiration, while the remainder contributes in the long-term to river discharge by means of lateral flow from the first soil layer, and base flow from the groundwater reservoir. Glacier ice melt contributes to the river discharge by means of a slow and fast component, being (i) percolation to the groundwater reservoir that eventually becomes base flow, and (ii) direct runoff. The cell specific sum from surface runoff, lateral flow, base flow, snowmelt and glacier melt is further routed. It is coupled to the PCRaster Global Water Balance model (PCR-GLOWB2) kinematic wave routing scheme to represent the hydrodynamic processes in the basin (Sutanudjaja et al., 2018). SPHY is calibrated and validated against observed daily discharge, obtained from the Global Runoff Data Centre, at seven locations (Figure 4.1). along the Rhine for the period of 1989–2000 (GRDC, 2016). The model is calibrated for the time period 1989–1995 and validated for 1996–2000. The calibration was done sequentially for five independent upstream locations and subsequently for the two downstream locations Andernach and Lobith. We used the mean square error (MSE) as the objective function and maximum likelihood estimation (MLE) to calibrate the model parameters (Khanal et al., 2019). The generated daily specific fluxes from SPHY for each grid cell are then routed through the river network using the simple kinematic wave scheme from PCR-GLOBWB 2 model (hereafter

referred to as 'routing model'). The routing model is calibrated for the Manning's n value using the observed discharge.

4.3.3 Snow Memory Effects

To investigate the effects of snow memory on the hydrological regime of the Rhine, we used a conditional sampling approach. From the 16 ensemble simulations we sampled hydrological years with above average and below average snowfall in separate bins, and assessed the discharge characteristics for the two sets of years. To account for snow accumulation and ablation the hydrological year runs from October until September in the next year.

4.3.4 Soil Moisture Memory Effects

Conditional sampling was also applied to study the impact of SM memory effects. The SM calculated is only confined to the top rootzone layer. The rootzone layer, a calibration parameter in SPHY model, varies from 50 (Alpine parts) to 500 mm (lower valley) along the basin. We used the fraction of actual water stored in the top rootzone layer and the potential capacity of rootzone layer to calculate the dimensionless SM. Winter and summer months which are preceded by a 10-day precipitation sum exceeding the long-term 95% percentile value are separately stored and analyzed. This selection reflects anomalously high initial SM values that limit the soil infiltration capacity for subsequent rainfall events.

The interaction of PPT in combination with SM on discharge was assessed based on the multi-conditional sampling method. First, two groups of PPT samples, high (HPPT) and low (LPPT), were separated by above and below median 10-day cumulative PPT values. Then from each of PPT groups two sub groups, climatological and anomalously low (<10% quantile, LSM) and high (>90% quantile, HSM) initial (beginning of 10 day) SM, were segregated. We thus created four groups of 10-day samples, namely LPPT_LSM (low precipitation and low SM), LPPT_HSM (low precipitation and high SM), HPPT_LSM (high precipitation and low SM) and HPPT_HSM (high precipitation and high SM). Finally, we compared the discharge characteristics in each of these samples and evaluated the effect of antecedent SM conditions on discharge. While analyzing the data it was ensured that the SM and discharges were segregated at the beginning and end of the 10 days period of each event respectively.

4.3.5 Meteorological Autocorrelation

Meteorological autocorrelation results from the occurrence of clustered rainfall events, e.g., series of low depressions passing the Rhine basin. We tested the sensitivity of the occurrence of peak discharge in the Rhine basin to the length of the autocorrelation time scale of the sequence of daily weather events. The evaluation was carried out by removing autocorrelation at chosen time scales by reconstructing the meteorological time series using a randomized selection from the 800 years of model data. In this reconstruction, precipitation and temperature fields were selected jointly without replacement, retaining consistency between these meteorological variables, and the structure of the spatial patterns (Beersma, 2007; Rajagopalan and Lall, 1999). This is analogous to a non-parametric resampling weather generation method. The reshuffling procedure does preserve the probability density distribution of the original time series.

The shuffling was applied using five different time scales. All autocorrelation exceeding a daily time scale was removed by randomly resampling daily meteorological fields. Autocorrelation at the five-day time scale is retained by resampling five-day blocks of meteorological fields, thereby removing all autocorrelation beyond a five-day time scale. Similar procedures were applied to time scales of 10, 30 and 180 days. Figure 4.3 illustrates the procedure. These sets of weather sequences serve as input forcing for SPHY and the routing model.

Finally, in a set of specific case studies, we analyzed a number of synoptic meteorological patterns leading up to an extreme hydrological event. We selected two synoptic meteorological patterns that lead

to the generation of extreme discharge, one for the original and one for the shuffled simulations using one-day selection blocks. The comparison of these anecdotal situations provides insight in the role of memory in the meteorological systems for the generation of extreme discharge. We investigated the climatology and anomaly of mean sea level pressure (SLP), wind speed, precipitation, rainfall, SM and temperature corresponding to the extreme discharge for each of the two cases. We also investigated the role of compounding snow, rain and SM to generate the extreme discharge.

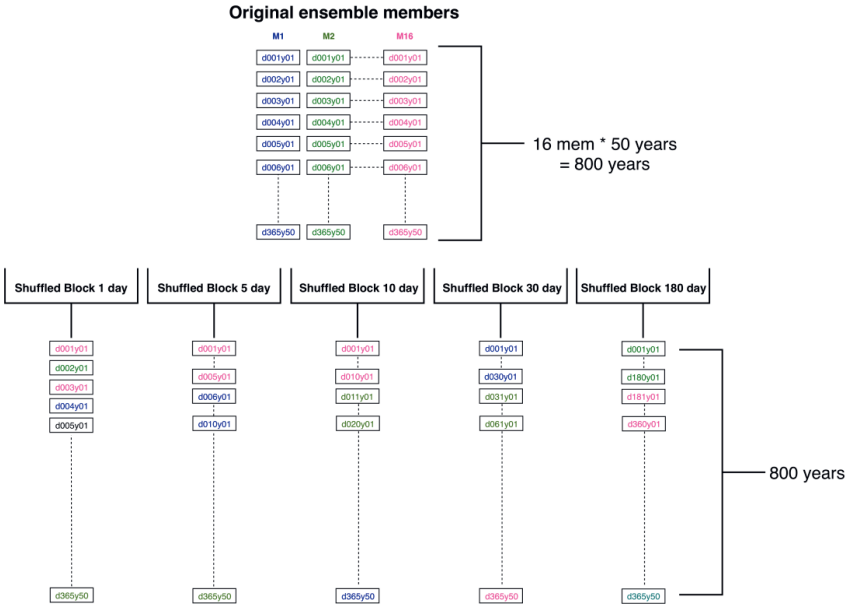

Figure 4.2: The resampling technique used in the study. 'd' stands for the calendar day, 'y' stand for the year and 'M' stands for the ensemble member number. The color designates the sequences of days kept together as per the block and data from the same ensemble member is used. For instance, in the block of five days, the five days memory is preserved both in temperature and precipitation. The block containing day one (d001) to day five (d005) has been taken from a given ensemble member (16). For the subsequent five day block (d006–d010) another ensemble member (01) is randomly chosen.

4.4 Results and Discussion

4.4.1 Performance of the Hydrological Model

We assessed the performance of the hydrological and routing model in two steps. First the daily flow at Lobith was compared to observations. Next, the temporal characteristics of the flood wave were assessed to check the ability of the model to generate realistic peak discharge features.

4.4.1.1 Daily Flows

First, we compared the simulated discharge at Lobith to the observed time series separately for the calibration and validation period as shown in Table 4.1 (GRDC, 2016). During the calibration period, the model simulates the observed discharge values fairly well, with an overall bias and Nash Sutcliffe Efficiency (NSE) of 3.3% and 0.78, respectively (Nash and Sutcliffe, 1970). The 95th quantile of discharge is overestimated on average by 4.5%, which is acceptable given the fact that the timing during these events is essential to obtain a good performance score (Figure 4.3). The validation of the model shows similar performance.

Table 4.1: Performance index for the coupled Spatial Processes in Hydrology (SPHY)PCR-GLOBWB2 hydrological model on a daily time scale for 1989–1995 (calibration) and 1996–2000 (validation). The 95% quantiles represent Q > Q95th (4425 m3s-1) of the observed flow.

	Calibration		Validation	
	Full Time Series	**95% Quantile**	**Full Time Series**	**95% Quantile**
BIAS (%)	3.3	4.5	–0.8	7.3
NSE	0.78	0.31	0.64	0.3
RMSE (m^3s^{-1})	598	1475	650	1784
R^2	0.84	0.65	0.79	0.51

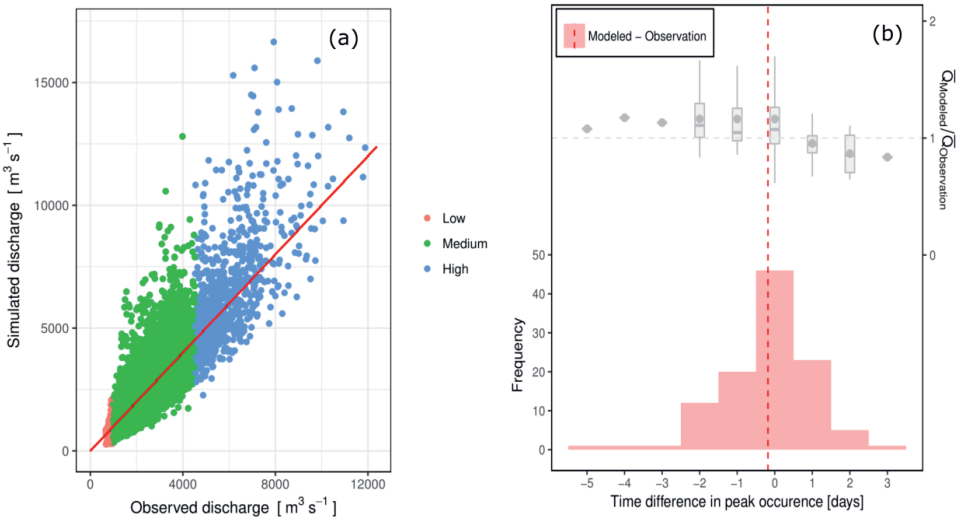

Figure 4.3: (a) Observed versus modeled daily discharge at Lobith for the period between 1951 and 2000. Colors indicate three ranges based on observed percentiles: Low (<5%, red), Medium (5%–95%, green) and High (>95%, blue). The solid red line represents the 1:1 slope. (b) Distribution of the difference between observed and modelled time of occurrence of discharge wave peak (red columns). The red dashed line represents the mean time error. The box plot represents the ratio of modeled and observed mean discharge for all wave peaks within a time difference interval. The grey line represents a mean ratio of 1. The grey point represents the mean of the ratio for each interval.

4.4.1.2 Flood Wave Timings

To assess the performance of the hydrological and routing model, the calibrated SPHY and routing models were forced with E-OBS daily precipitation and temperature data for the period 1951–2000. We evaluated the amplitude, timing and duration of extreme discharge events by using a simplified threshold approach to identify discharge waves (Khanal et al., 2019). A discharge (or flood wave) event is defined as a series of consecutive days (minimum of two days) with daily discharge exceeding the 95th quantile of the discharge. The length of each flood wave (in days) is calculated as the time difference between the onset (flow exceeds the threshold) and offset (flow falls below the threshold). Following this segregation method, we found 116 flood waves, on average just over two flood waves per year. The direct comparison of the timings for peak discharge (Figure 4.3b) shows that most of the simulated discharge waves reach the outlet at the same time as the observed discharge waves. Almost 80% of the flood waves reach the outlet within ±1 day. Furthermore, the ratio between modelled and observed mean discharge is close to 1, suggesting that the wave volumes are estimated fairly well.

4.4.2 Snow Memory Effects

Figure 4.4a shows the effect of separating the snowfall events in low and high values on peak discharge. The years with above average snowfall tend to produce higher peak discharge than years with below average snowfall. Longer return periods are dominated by the years with above average snowfall, and similarly below average snowfall corresponds to shorter return periods (Figure 4.4b). The ratio between the cumulative number of points below average and total show an exponential decay with increasing return time, confirming that higher discharges are dominated by above average snowfall years.

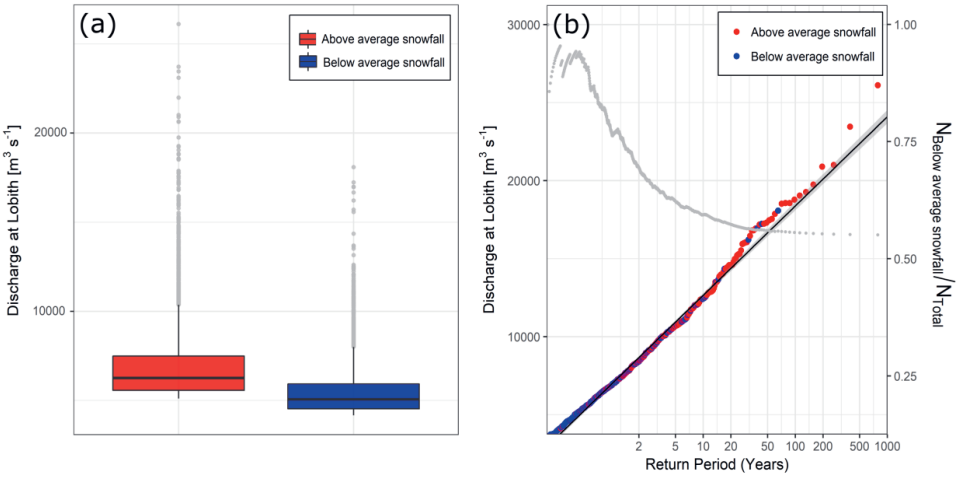

Figure 4.4: (a) Box plots for the discharge events exceeding the 95th quantiles for the year above and below average snowfall. (b) Generalized extreme value (GEV) plot of annual maximum discharge for years above and below average snowfall years. The grey point shows the fraction of below average snowfall samples. Its exponential decay shows a clear preference of below-normal snowfall events for the lower discharge return periods. The grey band around the line shows the confidence interval of the linear fit.

The seasonality of the snowfall and melting process play significant roles for the extent and seasonality of discharge extremes (Sivapalan et al., 2005). Figure 4.5 shows that years with above average snowfall have high discharge for January and February. The peak discharge regime is prolonged compared to years with below average snowfall. Snow accumulated in December in combination with fresh snow in January and February leads to this regime shift.

4.4.3 Soil Moisture Memory Effects

In summer, SM content is generally low. This gives a high infiltration capacity of the basin resulting in low to medium discharge response to extreme precipitation (Figure 4.6a). High SM is a default state in winter, which generates a stronger discharge response to precipitation (Figure 4.6b). The above analysis shows the effect of seasonal variation of SM on discharge, but significant variability in the SM–discharge–precipitation interaction prevails. To explore this interaction further, we applied a conditional sampling approach.

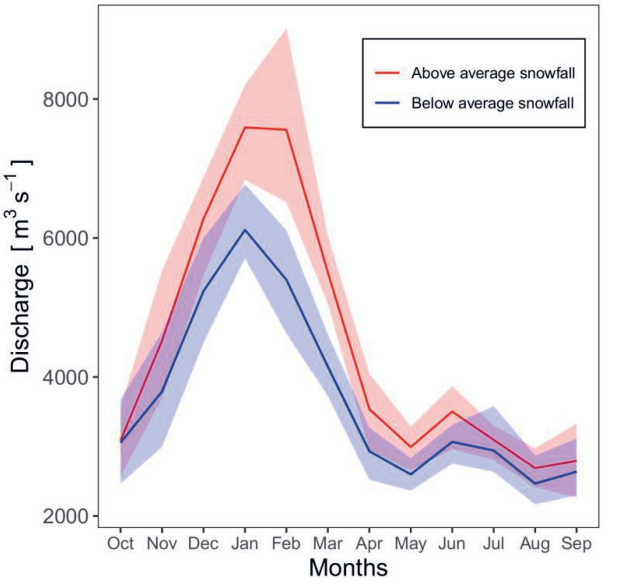

Figure 4.5: The seasonal cycle of discharge for the years above and below average snowfall. The solid lines are the mean of the 95th percentile of discharge for each ensemble member and the shaded area represents the spread of the ensemble (between 5th and 95th quantiles).

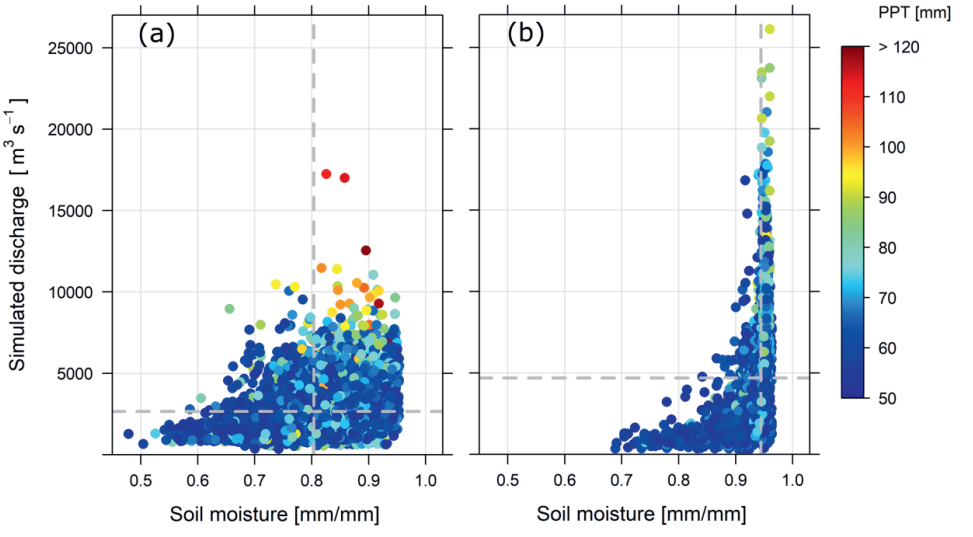

Figure 4.6: 10-day mean of soil moisture plotted against the corresponding discharge at the end of each 10 day interval, shown for 10-day precipitation events exceeding the 95% quantile for (a) summer (Mar–Sep) and (b) winter (Oct–Mar). The color scale represents the 10-day sum of precipitation (PPT) for the events shown. The dashed line represents the mean of the points for soil moisture and discharge.

Figure 4.7 shows that low precipitation on low initial SM results in the generation of low discharge values. The left two low precipitation (grey box plots within the red and blue partition) samples show

the similar distribution implying that the discharges are solely driven by the SM conditions rather than the precipitation. The same applies for the right-hand side two high precipitation samples (grey box plots within the black and green partition). For both low and high precipitation values the effect of initial SM is evident: low SM values reduce the discharge volume strongly. Low precipitation on high SM results in higher discharge scenarios than high precipitation on low SM. SM controls the overland flow processes and is non-linearly related to the rainfall-runoff response (Mcgrath et al., 2007; Zehe and Sivapalan, 2009). High SM limits vertical infiltration in the soil, and precipitation will be routed towards saturation excess runoff triggering overland flow (Dunne, 1978). The results from this study are in line with the studies describing the antecedent SM controls on rainfall-runoff response (Beven, 2004; Blöschl and Zehe, 2005; Zehe et al., 2010).

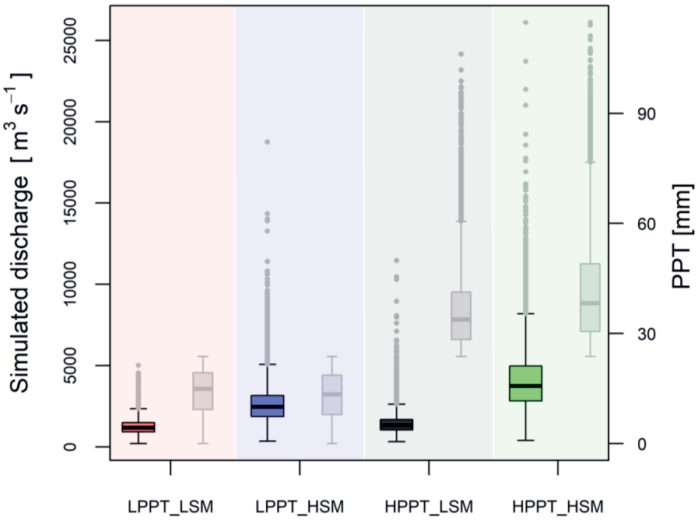

Figure 4.7: Simulated discharges for four different sampling scenarios: LPPT_LSM indicates below median 10-day precipitation in combination with climatological low initial soil moisture (<10% quantile), HPPT_HSM high precipitation/high soil moisture (>90% quantile), and HPPT_LSM and LPPT_HSM show corresponding combinations. The colored boxes show the distribution of discharge in each bin, the grey boxes the distribution of 10-day precipitation sums (right axis scale).

4.4.4 Meteorological Autocorrelation

4.4.4.1 Importance of Autocorrelation

The role of autocorrelation between meteorological events is shown in Figure 4.8 and Table 4.2, demonstrating the significance of meteorological memory for extreme hydrological events. Removing the memory in the meteorological system (shuffled time series using a one-day block; red line) reduces the slope of generalized extreme value (GEV) annual maximum discharge distribution down to 45% of the original non-shuffled simulation (black line), e.g., the associated peak discharge becomes 45% lower.

Removing all correlation at length scales exceeding a single day leads to a GEV slope that is more than 50% lower than the original (Table 4.2). This shows that high discharge peaks originate from multi-day precipitation events, generated by synoptic systems that generate rainfall for a subsequent period of time. Indeed, preserving the meteorological memory for five days retains almost 80% of the original GEV slope. This is a time scale that can be associated with large low pressure systems that are slowly moving over the basin. Virtually all peak discharge events are well reproduced when autocorrelation at

the monthly timescale is retained. Shuffling the data with half-yearly blocks increases the GEV slope slightly, but primarily by generating lower discharge at low return periods (see Figure 4.8). Differences in the model runs are mainly due to the other memory processes in the hydrological system such as snowfall, SM, and snowmelt.

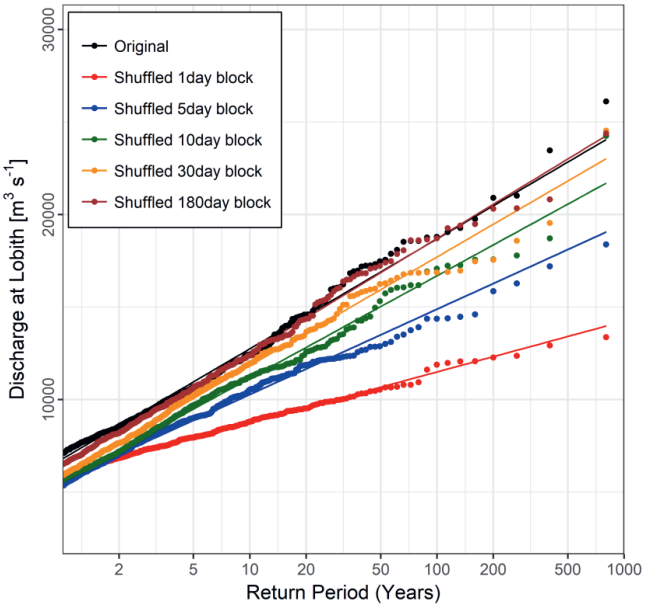

Figure 4.8: GEV fit of annual maxima discharges of the different meteorological shuffling experiments. The points (colored) represent the distribution and the solid (colored) line represent the linear fit on a logarithmic scale.

Table 4.2: Slope of the GEV shown in Figure 4.8, and lower and upper bound of the linear fit. Results are normalized relative to the original unshuffled simulation.

Shuffling	Slope	Lower bound	Upper bound
Original	1	0.978	1.022
Shuffled one day block	0.462	0.457	0.467
Shuffled five days block	0.777	0.761	0.793
Shuffled 10 days block	0.933	0.916	0.949
Shuffled 30 days block	0.99	0.972	1.008
Shuffled 180 days block	1.035	0.995	1.049

The monotonic decrease in maximum discharge with incremental reductions in the block length shows a relatively large step (from 0.78 to 0.46) timescales of one and five days (Table 4.2). This implies that most of the memory in the meteorological system in the Rhine basin is present at time scales around five days. This includes the possibility of high discharge events affected by sequences of storms. Memory characteristics at longer time scales can also include effects of accumulating snow, SM and groundwater processes. Particularly the difference between retaining 10-day or 30-day memory is related to snow processes. At this timescale, snow in the higher Alpine areas of the Rhine can be stored. At the half-yearly time scale the seasonal cycle of snow accumulation and ablation, and the dynamics of SM storage, become prominent.

4.4.4.2 Case Studies

For a number of hydrological extreme events, we analyzed the synoptic meteorological patterns leading up to these events, and how the events develop in time. Following earlier studies exploring the relation between peak discharge from the Rhine and the precipitation time scale (Beersma et al., 2008; van den Brink et al., 2005; van den Hurk et al., 2015; Kew et al., 2013), we analyzed the meteorological situation for the 10-day period preceding an extreme discharge event. Anomalous circulation characteristics and associated land surface fields were evaluated for extreme discharge events, both for the original and for the shuffled (one-day block) simulations. The comparison of these anecdotical situations was carried out for the most extreme events in these two simulations.

Floods occurring during the winter half of the year in the western part of Europe are primarily due to zonal westerly circulation systems (Jacobeit et al., 2003). Synoptically the most extreme event in the standard simulation is characterized by a strong low-pressure system moving from Iceland to the Scandinavian region (van den Hurk et al., 2015). The persistent low pressure over the Iceland region results in development of strong westerly winds. These are characterized by humid Atlantic moisture conditions and transport moisture towards the Alps (Figure 4.9a).

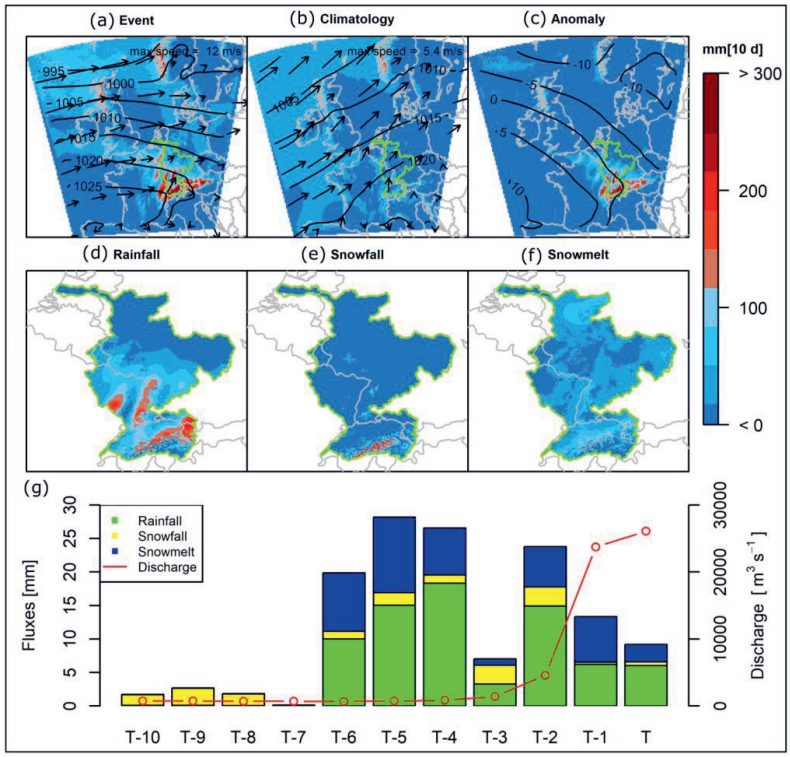

Figure 4.9: Meteorological circulation patterns leading up to the most extreme discharge event in the control simulation (date: 1953-12-27; member 10). Fields shown are composed of 10-day mean sea level pressure (SLP) and near surface wind and 10-day accumulated precipitation, rainfall, snowfall and snowmelt. Panel (a) shows the accumulated 10-day precipitation during the event together with the 10-day mean wind (arrows) and SLP (contours). Panel (b) shows the climatology of the event for the same 10-day episode in the ensemble. Panel (c) shows the anomaly of the event. Panels (d–f) show the rainfall, snowfall and snowmelt anomalies respectively. Panel (g) shows the sums of basin mean daily averaged fluxes of the hydrological budget terms during the event (colored bars) together with discharge (red line).

The climatological flow of the period in which this event took place has a more south westerly direction resulting in less rainfall than during the event (Figure 4.9b). The patches of high precipitation in the

upper Rhine and Alpine regions are aligned with the N-S orientation of the Black forest and Vosges mountain range (Figure 9c). The moisture laden westerlies result in topographically induced rainfall and snowfall in the mountainous region of the Black forest and Alps (Figure 4.9d and Figure 4.9e).

In the shuffled simulations the circulation anomalies for the most extreme event are much less pronounced than in the control simulation (Figure 4.10a). The south westerly winds are aligned parallel to the mountain ranges and result in less precipitation than the winds in the control simulation that are aligned nearly perpendicular to the mountains. The rainfall anomalies are positive mainly in the middle Rhine, Cochem and Main catchments (Figure 4.10d). Conversely, there are no significant differences in snowfall and snow melt anomalies in the region.

The temperature evolution 10 days prior to the event reveals that most of the region is cold (below 0 °C) for multiple days early in that period (a), thus resulting in precipitation falling as snow (Figure 4.9g). The precipitation event, mainly characterized by the sequence of moderate rainfall episodes, continued for about six days prior to the extreme discharge event. Accumulated snowfall at T-10 to T-8 served as a source of snow melt later in the period, when temperatures reached values above 0 °C. Snowmelt thus occurred jointly with snow/rain and contributed to the peak discharge (Figure C1b). In some areas (mainly higher alpine regions and the Neckar region) low temperatures prevailed during the entire 10-day period thus triggering rain on snow processes (Figure C2). A saturated antecedent SM state, which is normal in this time of the year (Figure C3) aggravated the magnitude of the discharge generating processes (Merz et al., 2014; Nied et al., 2014; Sivapalan et al., 2005). Therefore, the coincidence of persistent meteorological patterns resulting in multiple episodes of rainfall events, warmer temperature activating snow melt, high antecedent SM in combination with rain on snow processes, and preceded by several days of snowfall together resulted in an extreme discharge event.

Contrary to the extreme discharge generation mechanism from the control simulation, shuffled simulations show a different magnitude and different types of discharge generation processes (Figure 4.10). The striking difference in magnitude of the discharge peak is notable (Figure 4.10g). The complete removal of memory from precipitation resulted in the reduction of the discharge peak by nearly 50%. The precipitation is mostly in the form of rain except for six days prior to the peak discharge event, consistent with the evolution of the region's temperature (Figure C2). The lower and middle part of the Rhine experience cold temperatures and this results in the accumulation of snowfall. The temperature throughout the basin is found to be above zero except one day before the discharge event. The event is solely dominated by rainfall-runoff mechanism. The rainfall event stretching for multiple days in combination with the saturated antecedent SM (Figure C4) generates the peak discharge. The snow memory effect hardly plays a role in this event.

4.5 Discussion and Conclusions

Though this study overcomes the limitations posed on the past studies for instance limited observation records, reanalysis products or model simulations, and/or focusing on a limited dynamic range of the lagged signals contributing to the CEs, it still has a number of potential caveats. First, the analysis is based on the cascade of meteorological, hydrological and routing models, which all are imperfect and biased. Downscaling of GCM simulations may impart the extreme meteorological signal (Christensen et al., 2008; Ehret et al., 2012; Sippel et al., 2016). The choice of routing scheme has a considerable influence on the timing of simulated river discharge and its peak values (Hattermann et al., 2017; Zaherpour et al., 2018; Zhao et al., 2017). Furthermore, the limitations in the hydrological model structure and hydraulic model to correctly simulate the timing and magnitude of flood waves add to the uncertainty from downscaling of climate data (Adam et al., 2016; Franz et al., 2014; Heinke et al., 2011; Wiltshire et al., 2013).

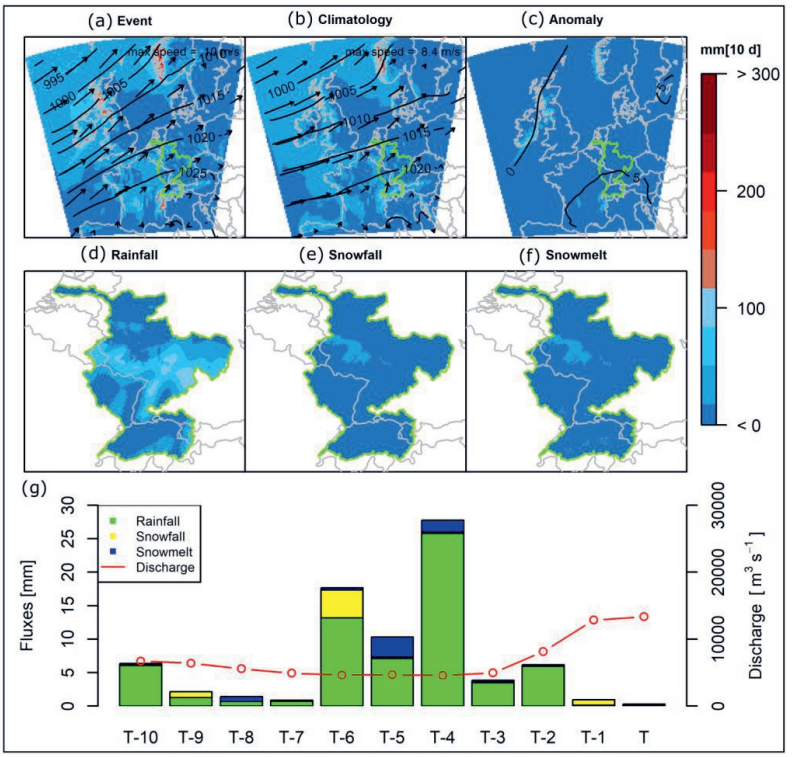

Figure 4.10: As for Figure 4.9, for the most extreme event in the one-day block shuffled simulation (date: 1982-01-15; member 12).

The meteorological shuffling represents a combination of, and interaction between, memory from the meteorological and hydrological systems. To exclusively isolate the contribution of hydrological memory from the meteorological memory a random SM or snow storage state could be considered at each time step of the model run. This ensures that any system memory in the hydrological system is removed, and remaining memory is resulting from the meteorological autocorrelation. The riverine memory, for instance off-channel, canals, lakes and reservoir storages of the hydrological systems, are not modeled in this study. Though the ground water interacts and modulates with the SM and base flow, the explicit contribution to the peak generation is not assessed. The ground water memory (Amenu et al., 2005; Güntner et al., 2007; Lo and Famiglietti, 2010; Wu and Dickinson, 2004), a contributing memory component for the generation of extreme flood in Rhine (Middelkoop et al., 2001), is not directly attributed here. Further, the SM calculations are only limited to the top rootzone layer and it lacks the effects of progressively deeper SM memory processes.

The most extreme discharge in the control simulations (representative for a return period of once in 800 years) at Lobith is around 26,000 m^3s^{-1} which is around 50% higher than the current design discharge of 18,000 m^3s^{-1} (for a return period of once in 1250 years) (Hegnauer et al., 2015). This high estimate can be partly attributed to biases in EOBS, calibration of the hydrological and hydraulic model and the atmospheric models used in the study. However, the high estimate could also be the result of an unprecedented extreme event that has not been realized in the limited observational records and cannot be estimated by extrapolation of the observational record. The use of a large ensemble overcomes this limitation posed by the short-term observations and therefore the possibility of occurrence of such an

extreme event cannot be neglected. Additionally, the systematic biases are not expected to have a large impact on the correlation structures of the processes and events studied here.

The findings confirm that the years with annual snowfall above average tend to generate anomalous high discharge. The snow accumulated in the basin serves as an additional source of meltwater for the discharge resulting in a significant shift of the discharge peak. A strong asymmetric rainfall-runoff response is triggered by the sensitivity to the initial SM state. Additionally, our results show that meteorological autocorrelation has a strong impact on the magnitude of peak discharge. The higher discharge peaks tend to level off (flatter slopes) in the hypothetical and shuffled weather scenarios where all the correlations in the meteorology are removed. The shuffling randomizes the sequence of the weather events, and thus deletes the memory of the meteorological system. A monotonic increment in extreme discharges with longer memory time scales is found. The results highlight that removing any meteorological autocorrelation occurring at time scales longer than five days reduces peak discharge by 80% relative to the control simulations. Autocorrelation at time scales longer than 30 days plays a minor role. Most memory in the meteorological system in the Rhine basin is found at time scales around five days. Furthermore, we show how hydrological memory from snow accumulation and SM complements the generation of extreme discharges. These findings are relevant when exploring the effect of extreme discharge events that are caused by a compound occurrence of drivers. The time scales identified do diagnose the time scale at which compounding drivers need to be considered in order to contribute to a meaningful analysis of compound events.

Author Contributions:

Conceptualization, Sonu Khanal and Bart Hurk; Data curation, Sonu Khanal; Formal analysis, Sonu Khanal; Funding acquisition, Bart Hurk; Investigation, Sonu Khanal; Methodology, Sonu Khanal, arthur lutz, walter immerzeel and Hylke Vries; Project administration, Sonu Khanal; Resources, Sonu Khanal and Niko Wanders; Software, Sonu Khanal and Niko Wanders; Supervision, arthur lutz, walter immerzeel and Bart Hurk; Validation, Sonu Khanal; Visualization, Sonu Khanal; Writing—original draft, Sonu Khanal; Writing—review & editing, Sonu Khanal, arthur lutz, walter immerzeel, Hylke Vries and Niko Wanders.

Funding:

This research was funded by the European Union's Horizon 2020 research and innovation programme under the Marie Sklodowska-Curie grant agreement No 676027. The project has also received funding from the European Research Council (ERC) under the European Union's Horizon 2020 research and innovation program (grant agreement number 676819) and the Netherlands Organization for Scientific Research under the Innovational Research Incentives Scheme VIDI (grant agreement 016.181.308).

Acknowledgments:

The authors would like to thank the IMPREX project, in particular Erik van Meijgaard, for providing the downscaled RACMO simulations. The authors would like to acknowledge Nina Ridder for her contribution to discussions during this study.

Data availability:

The code of the SPHY model is publicly available at https://github.com/FutureWater/SPHY. The PCR-GLOBWB 2.0 model is publicly available at https://github.com/UU-Hydro/PCR-GLOBWB_model. The datasets that are produced in this study are available upon request from the corresponding author.

5

Chapter 5

Storm surge and extreme river discharge: a compound event analysis using ensemble impact modelling

5 Storm surge and extreme river discharge: a compound event analysis using ensemble impact modelling

Many winter deep low-pressure systems passing over Western Europe have the potential to induce significant storm surge levels along the coast of the North Sea. The accompanying frontal systems lead to large rainfall amounts, which can result in river discharges exceeding critical thresholds. The risk of disruptive societal impact increases strongly if river runoff and storm-surge peak occur near-simultaneously. For the Rhine catchment and the Dutch coastal area, existing studies suggest that no such relation is present at time lags shorter than six days. Here we re-investigate the possibility of finding near-simultaneous storm surge and extreme river discharge using an extended data set derived from a storm surge model (WAQUA/DCSMv5) and two hydrological river-discharge models (SPHY and HBV96) forced with conditions from a high-resolution (0.11°/12 km) regional climate model (RACMO2) in ensemble mode (16x50 years). We find that the probability for finding a co-occurrence of extreme river discharge at Lobith and storm surge conditions at Hoek van Holland are up to four times higher (than random chance) for a broad range of time lags (-2 to 10 days, depending on exact threshold). This highlights that the hazard of a co-occurrence of high river discharge and coastal water levels cannot be neglected in a robust risk assessment.

Chapter published as:
Khanal S, Ridder N, de Vries H, Terink W and van den Hurk B (2019) Storm Surge and Extreme River Discharge: A Compound Event Analysis Using Ensemble Impact Modeling. Front. Earth Sci. 7:224. doi: 10.3389/feart.2019.00224

5.1 Introduction

Floods are a major cause of casualties due to natural disasters, with over 6.8 million deaths globally during the 20th century (Doocy et al., 2013), and an annual average loss of 104 billion US$ (Blöschl et al., 2017). Rivers floods are the result of a complex chain of atmospheric and surface hydrological processes (Hall et al., 2014; Merz et al., 2014). Atmospheric circulation patterns distribute the necessary precipitation on a variety of spatial scales and intensities (Prudhomme and Genevier, 2011). Following the characteristics of the local hydrology the water then aggregates into streams and rivers, ultimately transporting river runoff to coastal estuaries. On its way to the sea, the main river is fed from several sub-catchments and receives input from reservoirs that act on longer time scales than runoff routing processes. These long time scales introduce a dependence on antecedent conditions, for example ice and snowmelt from high-altitude glaciers and/or snow reserves located in the headwaters, soil moisture retention, and baseflow processes. In low-lying countries like the Netherlands, flood defense infrastructure protects the densely populated hinterland. Risk of river flooding therefore typically only occurs in the winter season when deep Atlantic low-pressure systems (extratropical cyclones) precipitate large amounts of water over the European Alps and Central Europe.

Traditionally floods are defined by a set of correlated random variables like flood peak, flood volume, and duration (Brunner et al., 2016; Chebana and Ouarda, 2009). However, in the assessment of flood events this univariate approach to discharge is only suitable when dependencies between the contributing variables are known or absent (Serinaldi et al., 2015; Yue and Rasmussen, 2002). Ignoring the dependencies may lead to severe over or under estimation of the flood risk (De Michele et al., 2005).

Coastal regions are threatened not only by river flooding. Storm surges and sea-level rise provide additional risk to flooding (Olbert et al., 2017; Wahl et al., 2017). Atlantic cyclones are prime candidates to cause both storm surges and large-scale precipitation over western and central Europe (Hawcroft et al., 2012; Ulbrich et al., 2009). Since storm surges find their origin in the very same Atlantic winter storms that also bring large amounts of precipitation, possible relations between the two factors play a major role in the assessment of flood risks. If high coastal water levels occur simultaneously with

extreme river discharge events, flood risk increases as the river is not able to discharge its water at the outlet, eventually causing river water levels to rise (van den Hurk et al., 2015). Further, projected sea-level rise will strongly amplify this risk (van den Hurk et al., 2014; Vries et al., 2014; Wahl et al., 2015). Previous studies investigated the probability of joint occurrence of storm surge and precipitation/river floods based on observed data along the British, Australian, and US coasts and Dutch coasts (Geerse, 2013; Svensson and Jones, 2004; Wahl et al., 2017; Zheng et al., 2013). In literature, these sets of joint extreme events are categorized as compound events. Their societal importance and association to risk are well discussed by Hazeleger et al. (2015), Leonard et al. (2014) and Seneviratne et al. (2012).

Inclusion of tail dependence, i.e. the probability that a given variable exceeds a certain threshold given the exceedance probability of a threshold by another variable, is necessary for the investigation of joint extremes events (Joe, 1997). Poulin et al. (2007), who used families of copulas to study the joint behavior of river flood peaks and flood volumes, demonstrated that resulting joint return periods are significantly sensitive to the choice of the copula model and inclusion of tail dependence in the analysis. Recent studies, such as Bevacqua et al. (2017) and Moftakhari et al. (2017) for the Italy and US coasts respectively, further explored the importance of multivariate (copula) analysis of compound events related to coastal flooding including sea water level and river discharge. Also, these studies confirmed a substantial decrease in return periods if the compound occurrence probability of related events was considered.

For the Rhine river catchment, previous studies have investigated those compound events based on observations, reanalysis products and model simulations. By using a coarse-resolution global climate model ensemble, Kew et al. (2013) showed that low pressure systems over the North Sea can lead to compound occurrence of extreme storm surges and precipitation affecting the Dutch coast. Proxies for storm surge and river runoff were used, namely north-westerly winds and multi-day precipitation sums. In an attempt to use more realistic data to assess the statistical relationship between surge and river discharge, Klerk et al. (2015) subsequently used variables diagnosed from hydrological, hydraulic and storm surge models. In their coarse-resolution dataset covering the relatively short historical period from 1981–2010 they found a clear correlation between the two variables, but only when a substantial time lag of six days was taken into account. This is the time scale needed to transport excess precipitation peak in the Rhine catchment to the river outlet. Accordingly, they conclude that there is no increased risk at simultaneous occurrence (zero lag). However, an in-depth investigation of the uncertainty introduced by the hydrological and storm surge model to the time dependence correlation was not performed.

Here, we build on the findings of the previous studies and extend them by including the application of (a) a fine resolution climate model, (b) a large sample of data (800 years) obtained from a climate model ensemble, and (c) two different regimes of hydrological models. The use of large sample of data obtained from a fine resolution climate model ensemble provides a better insight into the statistical connection between the two variables (Wahl et al., 2015; Wu et al., 2018) than possible in previous assessments in Rhine which used either samples from observations limited to the past 30–40 years or used coarse resolution climate model simulations. Furthermore, by applying two hydrological models, we demonstrate the importance of proper physical model configurations to correctly assess the lag time correlation for compounding high coastal water level and high discharge events. Using a methodology developed by van den Hurk et al. (2015), we force three impact models (one storm surge model and two hydrological models) with output from a large ensemble of a high-resolution regional climate model avoiding the necessity of proxies as applied in some of the previous assessments. Further, this approach provides us with a large dataset ensuring a solid statistical assessment of the problem. The combination of these improvements, i.e. the use of real impact variables rather than proxies, different regimes of discharge models and a longer timeseries obtained from a high-resolution climate model ensemble, improve our ability to draw more consistent conclusions than possible in previous studies.

5.2 Data and methods

5.2.1 Study area

The Rhine basin covers an area of 185,000 km^2 and runs over 1320 km from its source in the Alps to the North Sea. The streamflow in the Rhine is mainly dominated by snowmelt and rainfall-runoff from the Alps during summer for the upper part of Rhine (Viviroli, Daniel; Messerli, 2003). However, for lower parts at Lobith, streamflow is mostly dominated by rainfall resulting in streamflow peaks during winter. A peak-shift in the average annual hydrograph is observed from summer to winter from the upper Rhine at Basel (50 km downstream of Untersiggenthal as shown in Figure 5.1 and lower Rhine at Lobith (Engel, 2001; Photiadou et al., 2011). The snowmelt contribution to the streamflow at Lobith is significant and total annual contribution to streamflow is around 30 percent (Stahl et al., 2016). The area upstream of Basel produces almost 50% of the discharge despite only covering around 20% of the total area of the Rhine catchment (Kwadijk and Deursen, 1999). The flood wave travel time from Basel to Lobith is around 5 days (Hegnauer et al., 2014). Further, the slow melt from snow and glaciers would require an additional day or two to reach Basel.

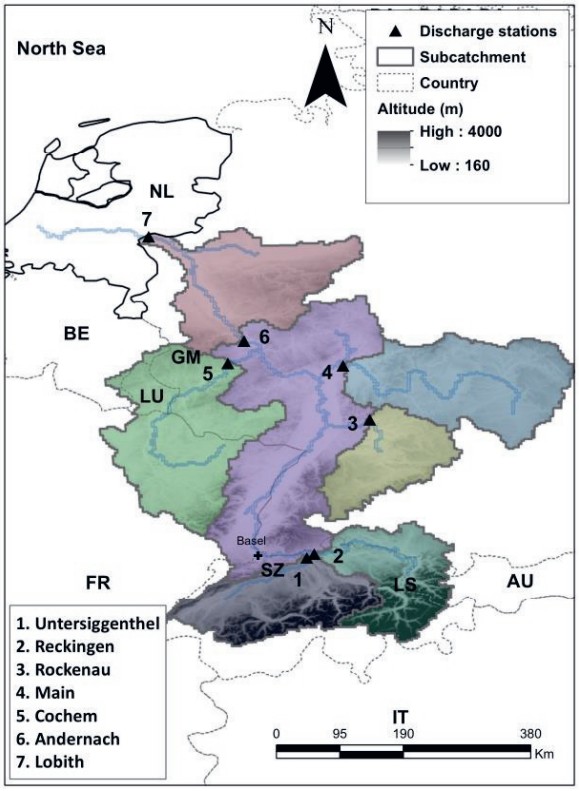

Figure 5.1: The Rhine basin, with seven sub catchments used for the calibration in the study. The triangles (black) represent the outlet of sub-basin used for the calibration. The two letter abbreviations are used to denote the countries. The blue line represents the Rhine and the tributaries. The black boundary represents the Netherlands outline.

The storm surges along the Dutch coasts are driven by meteorological conditions (Ridder et al., 2018b). in general, the most extreme storm surges are associated with low pressure systems in the North Eastern Atlantic area, depression trajectories with a south-east direction, along the jet stream over the North Sea

results in the development of persistent strong north-westerly winds and related surge conditions at the Dutch coast (van den Hurk et al., 2015). These stormy conditions in the North Sea area mainly develop during the winter season from October to March. Every year on average two strong storm events (winds higher than 19-20 m/s) are recorded at Hoek van Holland (Smits et al., 2005). Further, these depression systems are also characterized by humid Atlantic moisture conditions and primarily transport the moisture towards the Netherlands (Anon, 2019).

5.2.2 Observations and climate model data

We use data from a 16-member ensemble obtained with the Global Climate Model (GCM) EC-Earth (Hazeleger et al., 2012), created using a perturbed atmospheric initial-state approach (start in 1850). Each of the ensemble member is a plausible representation of possible climate states and differs from each other in their initial atmospheric conditions and model internal variability. The internal variability of the climate system is highly nonlinear, which causes significant variability between model runs. Thus, each of the ensemble member represents how climate can vary due to chaotic internal variability (Deser et al., 2012).

This study focuses on the period from 1951 to 2000. The GCM ensemble is dynamically downscaled using the regional climate model (RCM) RACMO2 at 12-km resolution (van Meijgaard et al., 2008). Daily precipitation output from RACMO2 is subsequently bias-corrected using gridded E-OBS V14 data at a 0.25° resolution (Haylock et al., 2008). The downscaled temperatures are further adjusted with a temperature lapse correction rate of -6.5°/Km. The dynamically downscaled and bias-corrected data serves as input for two conceptually different hydrological models for the Rhine basin (a) SPHY (Terink et al., 2015) (b) HBV-96 (Bergström, 1976) and a storm surge model; WAQUA/DCSMv5 (Gerritsen et al., 2013). The performance of the hydrological models is tested against observed mean daily Rhine river discharge at Lobith, where the Rhine enters the Netherlands and daily mean total water levels (the sum of the tidal contribution and the non-tidal residual including the meteorological effect referred to as TWL i.e. total water level) at Hoek van Holland (HvH) for the period 1951–2000 provided by Rijkswaterstaat and are available online (www.waterbase.nl/). The overall modeling framework of this study is presented in Figure 5.2.

5.2.3 Hydrological modeling of Rhine river discharge using SPHY and HBV-96

The application of two hydrological models allows the assessment of model-uncertainty in simulating discharge waves in relation to the natural variability due to e.g., dominant precipitation regions, and the sensitivity of different routing methods. To this end, we use different hydrological models to simulate the daily discharge of the river Rhine at Lobith. From this point on the flow of the river is highly regulated with the main part of the river discharge being directed to the coastal outlet at HvH. Since snowmelt runoff plays a significant role in defining the hydrological regime and annual cycle along the Rhine (Stahl et al., 2016), we use models that explicitly account for this process.

The Spatial Processes in HYdrology model (SPHY) is a spatially distributed, physically based “leaky-bucket” type model, which operates on a gridpoint basis. It integrates parameterizations of the dominant hydrological processes: (i) rainfall–runoff; (ii) lake/reservoir outflow, (iii) cryospheric processes (snow, ice, glaciers), (iv) dynamic vegetation, (v) evapotranspiration, and (vi) root-zone moisture content. It contains sub-grid variability (e.g., cells can be glacier-free or partially to fully covered with glaciers) and is based on the widely-used degree-day melt modeling approach (Hock, 2003). SPHY requires daily precipitation, and daily maximum, minimum and average temperature as forcing input. SPHY was calibrated against observed time-series of daily discharge (Obs), obtained from the Global Runoff Data Centre (http://grdc.bafg.de/), at seven locations along the Rhine for the period of 1989-2000. The calibration was performed sequentially; initially for five independent upstream (U/S) locations and subsequently for the two downstream (D/S) locations Andernach and Lobith.

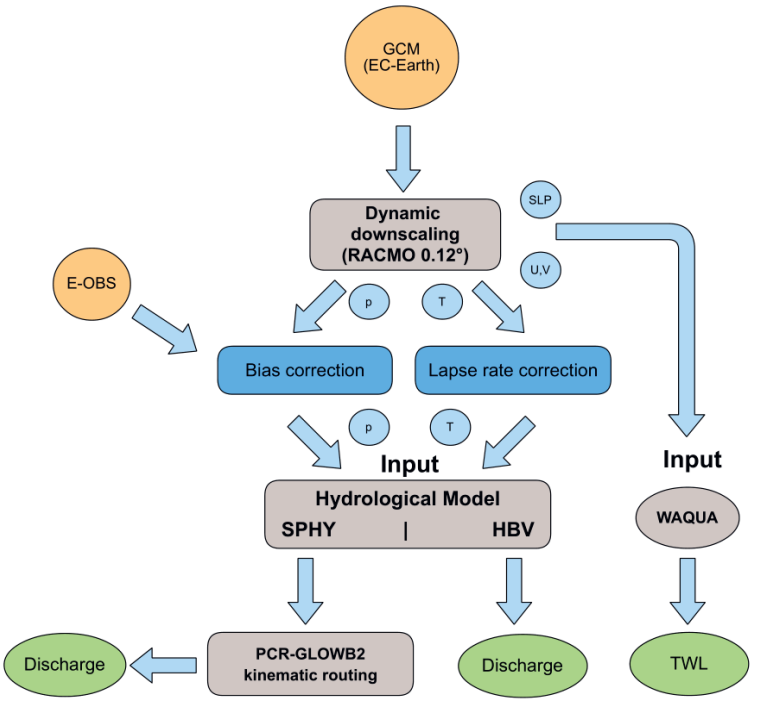

Figure 5.2: The research framework used in this study. The orange, green and gray color represents the input, output and the model used in the study, respectively. The P, T, SLP, U and V represents the precipitation, temperature, sea level pressure, zonal and meridional wind components, respectively. The blue color represents the intermediate steps followed like bias correction of precipitation and lapse rate correction of temperature obtained from downscaling EC-Earth.

We used the mean square error (MSE) as the objective function and maximum likelihood estimation (MLE) criteria to calibrate the model parameters. SPHY uses a simple flow recession coefficient (kx) to simulate the delay between generation of specific runoff within the catchment and reaching the outlet. The recession coefficient is used as a weighting parameter to calculate the routed flow at each pixel, which in SPHY is calculated as weighted average inflow of the current and previous day (Terink et al., 2015). The averaging used in SPHY causes the attenuation and delay of the floodwaves in the model. A simple accumulation of the fluxes over the drainage network is used to calculate the flow. This method is typically suitable when aggregation time period (month, year) is larger than the travel times of water along the longest river length. To simulate the realistic flood wave propagation, we use the stand-alone version of PCR-GLOBWB 2 kinematic wave routing scheme (here after referred to as routing model). SPHY is coupled one-way to the routing model as the outputs from SPHY serve as input for the routing model. More detail about routing model can be found in Sutanudjaja et al. (2018). The routing model is calibrated for Manning's n for the same time period as SPHY. The daily flux in mm/day generated by SPHY model is routed with the calibrated routing model to get the discharge. From now onwards the discharge or floods from SPHY mentioned in this study will refer to the routed discharge after the use of routing model. Calibration and performance of the upstream sub basins are provided in the appendix (Figure D1, Figure D2 and Figure D3). The extreme flooding events of 1993/1994 and 1995, dominated by precipitation and snowmelt respectively (Engel, 1997), are included in the calibration period.

The second hydrological model is HBV-96 (hereafter referred to as HBV) originally developed by Swedish Meteorological and Hydrological Institute (SMHI, Bergström, 1976) and updated to version

used here by Lindström et al. (1997). HBV is a "semi-distributed" conceptual model and, similar to SPHY, also includes parameterizations for processes such as snow accumulation and melt, evapotranspiration, soil moisture and runoff. Unlike SPHY, HBV contains a detailed routing procedure to model flow between sub-basins and through lakes. In this study, we use the version of HBV calibrated by Deltares (Kamer et al., 2008). The final discharge series at Lobith for both the calibration run and the 16-member ensemble were provided by Deltares.

5.2.4 Storm surge modeling of the North Sea using WAQUA/DCSMv5

The storm-surge model used in this study is WAQUA/DCSMv5 (hereafter referred to as WAQUA). WAQUA solves the two-dimensional shallow water equations on a (1/8)°x(1/12)° grid to simulate water levels for the North Sea and its coastal areas. For this, the model takes into account the astronomical tide, the wind-induced movement of water and the barometric effect (Olbert and Hartnett, 2010) associated with the locally prevailing sea level pressure. Therefore, when a low-pressure system travels over the North Sea, WAQUA responds to the main meteorological forcing components that affect shallow seas during such an event. Tidal effects, modified in amplitude and timing by geometry of the coast and the underlying bathymetry, are calculated separately to this meteorological forcing. To obtain the TWL, WAQUA is first run using only the harmonic components at the domain boundaries, while the meteorological forcing is neglected. In a second step, WAQUA uses the calculated tidal level from the previous step and applies the meteorological forcing to calculate TWL. The non-tidal residual (hereafter referred to as surge) is then derived by subtracting the tidal level from the TWL.

A detailed description of how surge and tides are computed in WAQUA can be found in Gerritsen et al. (2013). The model sensitivity and capability to represent relevant air-sea momentum transfer processes and annual extreme water levels is described in Ridder et al., (2018a). For the study presented here, the daily mean TWL (tide plus surge) at HvH is used.

5.3 Performance of the surge and discharge models

It is important to assess the basic quality of the surge and discharge models. For a validation of the storm surge model WAQUA the reader is referred to previous studies that present this assessment in detail (van Meijgaard et al., 2008; Ridder et al., 2018a). Since the aim of this study is the exploration of relations between river discharge at Lobith and coastal water level at HvH, the amplitude, timing and duration of (extreme) discharge events are particularly critical.

5.3.1 Hydrological models (SPHY and HBV)

To assess the performance of the two hydrological models, both HBV and SPHY (together with routing model) were forced with bias-corrected E-OBS daily precipitation and temperature data for the period 1951–2000. The output of both models thus produced (hereafter referred to as EOBS runs) is compared to the observed discharge at Lobith. The assessment focuses on the ability of the models to reproduce discharge amounts, duration of the flood wave (see section 5.3.3) and timing of flood peaks (see section 5.3.4). For this we use a simplified threshold approach to identify the flood waves in the discharge time series. In this study, a flood wave event is defined as a series of consecutive days with daily discharge exceeding the 95th percentile of the annual distribution. The length of each flood wave (in days) is calculated as the time difference between the onset (flow exceeds threshold) and offset (flow falls below threshold). The 95th quantiles are computed independently for the observations and the models based on the respective full-time series to account for model biases.

5.3.2 Basic metrics and distribution

Figure 5.3 shows the daily Rhine river discharge for the entire period 1951-2000 as modeled by HBV and SPHY compared to observations. HBV tends to slightly overestimate observed high peaks (flow greater than 95th percentile) by up to 420 m^3s^{-1} on average (> 3500 m^3s^{-1} in some cases). Similarly, SPHY overestimates the discharge by up to 390 m^3s^{-1} on average (> 8000 m^3s^{-1} in some cases). Modeled discharge in SPHY exceeds 16,600 m^3s^{-1} as compared to the observed discharge around 11,885 m^3s^{-1}, making it unsuitable as a forecast model for the Rhine river's discharge extremes without additional statistical post-processing (such as quantile correction). Nevertheless, both models show the ability to represent observed discharge values fairly well with an overall bias and Nash Sutcliffe Efficiency (NSE, Nash and Sutcliffe, (1970) see equation D1) of 0.3% and 0.69 for SPHY, and -10.3% and 0.87 for HBV (Table 5.1). HBV thus outperforms SPHY at all metrics except bias.

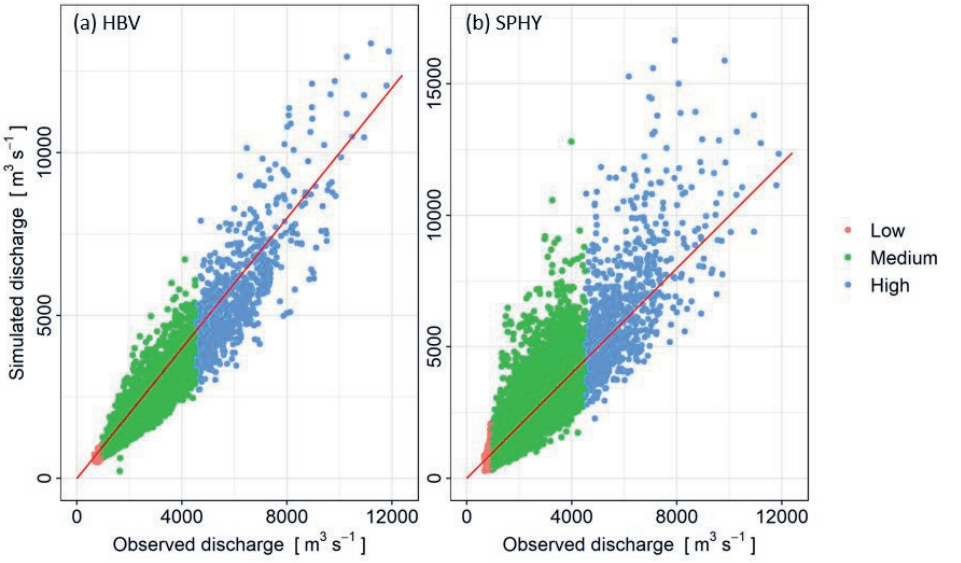

Figure 5.3: Observed versus modeled daily discharge at Lobith (a) HBV and (b) SPHY for the period between 1951 and 2000. Colors indicate three ranges based on observed quantiles: "Low" (<5%, red), "Medium" (5–95%, green), and "High" (>95%). The solid red line represents the 1:1 slope.

The normal quantile-quantile plot using observed and modeled discharge (Figure 5.4) shows that both HBV and SPHY overestimate the observed flow at low discharge values. At intermediate values (ranging from -1.5 standard deviation to +1.5 standard deviation of mean discharge) SPHY reproduces observations fairly well, while HBV clearly outperforms SPHY for values above 2 standard deviations. At the highest discharge extremes, observations lie below the discharges of HBV and SPHY with HBV following observations more closely.

5.3.3 Flood wave duration distribution

Using the definition of a flood wave event described in section 5.3.1, i.e. flows higher than the 95th percentile of the respective dataset, we find 92 (SPHY), 113 (HBV) and 116 (observations) flood waves in the 50 years between 1951 and 2000, just under two per year on average. Most of these events have occurred in the winter half year (October to March). Their duration ranges from one to up to 35 (in HBV), 40 (in Obs), and 50 (in SPHY) days (Figure 5.5a).

Table 5.1: Performance index for HBV and SPHY model on a daily time scale. The low, med and high represent the statistics for Q<Q(5th), Q(5th) < Q < Q(95th) and Q > Q(95th) quantile of the observed flow whereas, all, represents the overall flow series.

	HBV				SPHY			
Objective function	**Low**	**Med**	**High**	**All**	**Low**	**Med**	**High**	**All**
R2	0.52	0.87	0.65	0.91	0.19	0.65	0.44	0.77
PBIAS (%)	-18.3	-10.6	-7.3	-10.3	-20	-0.1	6.7	0.3
RMSE(m^3s^{-1})	180	359	1045	415	300	605	1732	695
NSE	-4.9	0.79	0.26	0.87	-5.26	0.59	0.2	0.69
Volumetric Efficiency	0.82	0.87	0.85	0.87	0.72	0.81	0.79	0.81
Flood wave timing (days)	-	-	-0.76	-	-	-	-0.18	-

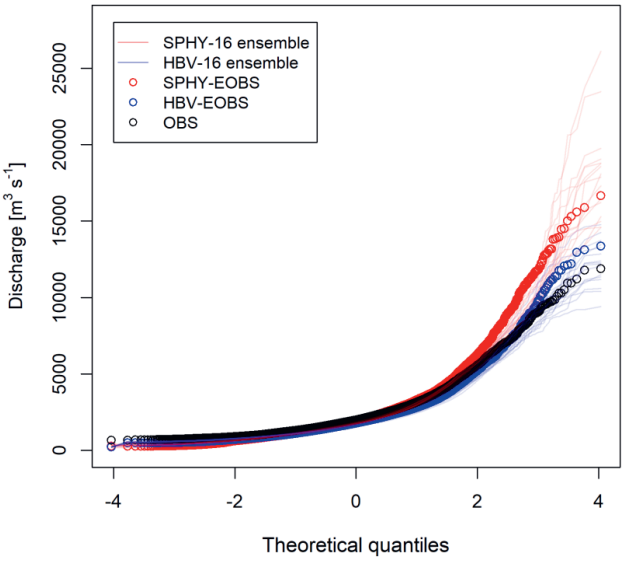

Figure 5.4: *Normal quantile plot for HBV (blue), SPHY (red) and Observation (black). On the horizontal axis, the distributions are centered and scaled (divided by the standard deviation). The light blue and red lines represent 16 ensemble members for HBV and SPHY.*

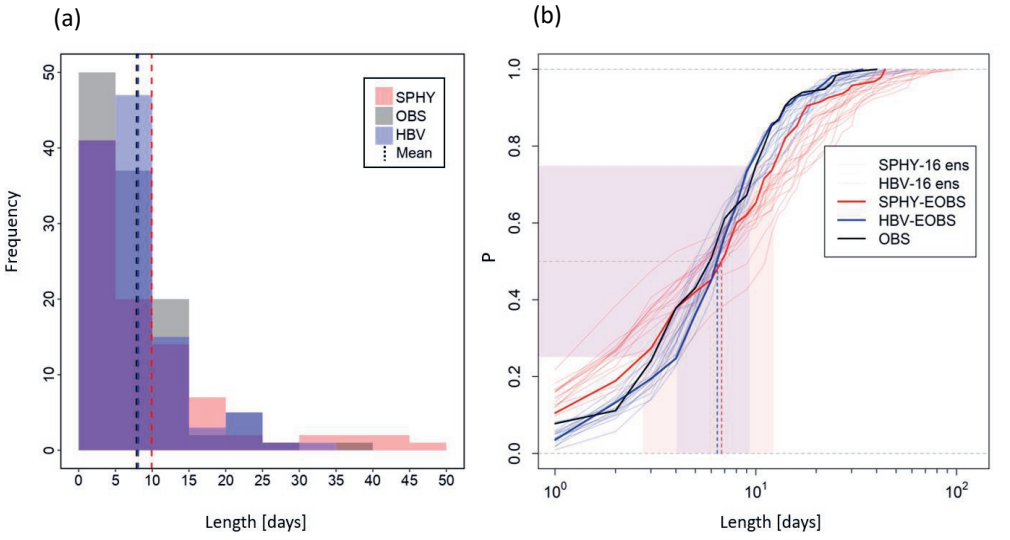

Figure 5.5: (a) Frequency plot for the flood wave length above 95th quantile threshold of discharge. The dash vertical lines show the mean of the flood waves for SPHY (red), HBV (black) and HBV (blue). (b) The Empirical cumulative distribution function (ECDF) plot for the floodwave length above 95th quantile threshold of individual time series discharge. The light red and the blue shaded area represents the 0.25 and 0.75 for SPHY and HBV, respectively.

As a result, HBV reproduces the observed mean flood wave length of approximately eight days fairly well while SPHY overestimates the mean duration. Note that the calculation of the mean flood wave length is based on the number of flood waves in the respective dataset. Therefore, in SPHY fewer occasions of overestimated flood durations affect the mean of the flood wave length more strongly than in HBV where a higher total number of flood waves can mask the effect of prolonged flood waves. This can be seen in the empirical cumulative distributions (ECDFs) of the flood duration for the hydrological models and observation (Figure 5.5b). The ECDFs of the two models show that half of the events (ranging from a probability of 0.25 to 0.75) last between 4–9 days in HBV and 2–9 days in SPHY (Figure 5.5b). Hence, there is no consistent overestimation of flood wave duration in SPHY but the overestimation of the mean is highly biased by a few long flood waves.

Adding the ECDFs of the different RACMO2 ensemble members (light blue and red lines) highlights the range of uncertainties in flood wave length. A comparison between ensemble members and observations is of course not possible. However, adding them alongside the ECDFs of the two EOBS runs (blue and red solid lines) gives an indication of the influence of random internal variations (see section 5.2.2) and highlights that the results of both models fall within the physically plausible flood wave durations.

5.3.4 Timing of onset and peak

In compound events, two or more variables reach high percentiles of their distribution simultaneously, or in rapid succession. Therefore, the ability of hydrological models to reproduce the timing of events in impact-parameter space (TWLs and discharge) is crucial. However, neither SPHY nor HBV are able to reproduce all observed flood peaks. Out of the 200 highest maximum discharge dates in the observations, 141 are realized in HBV, but only 115 in SPHY. A better match is reached if we allow for some flexibility in the timing, accounting for random errors in the meteorological forcing or runoff

generation process. The modeled arrival time of the peak of a flood wave is sensitive to many parameters, including intensity, duration and frequency of precipitation, soil moisture, the existence of basal flow (e.g. due to snow/ice melt upstream), river bathymetry and topography. Modeling and representation errors in each of these processes can explain part of the large difference in observed and modeled peak-flow days.

Here, we use the exact matching of the peak timing of the flood waves in observations and the models. The dates corresponding to local maxima within the onset and offset of the flood waves in the impact models are then compared with the observed peak dates allowing for a difference of ±5 days to match. Since taking longer than ±5 days might result in matching the flood peaks entirely from different events, we chose to use ±5 days here. From 116 floodwaves in total, the peaks that lie outside (2 in HBV and 8 in SPHY) of the ± 5 days range, are discarded. Figure 5.6 shows the distribution of arrival-time differences in peak timings of flood. Both models mostly have a negative time lag (implying that most peaks arrive earlier than in the observations) but in HBV the negative time lag (about one day) is larger than the value in SPHY (almost zero). This suggest that both the models have errors in estimating the timings of flood waves and HBV being the worst of two. Half of the data points lie between -1 and 1 for HBV and SPHY. The presence of positive values in the distribution indicate the models waves sometimes occur too late. The broad shape of the distribution of both HBV and SPHY reflects the complex interaction of the climatic and hydrologic processes. This wide distribution is a result of multiple drivers of flood rather than a single flood generation mechanism. The climatic mechanism includes persistent synoptic weather conditions favoring a very extreme event or episodes of moderate precipitation events resulting in a multiple day extreme event or extreme positive temperature anomaly causing a quick melt of snow in the catchment (Gaál et al., 2012; Nied et al., 2014; Prudhomme and Genevier, 2011). The hydrological processes such as antecedent soil moisture conditions, snow and ice storage in the catchment, rain on snow mechanisms, and antecedent ground water level play an important role in defining the magnitude and length of the flood wave (Merz and Blöschl, 2003, 2008). Further, the superposition of flood waves from different tributaries of the river also contributes towards the increased length and magnitude of the flood wave. Moreover, coincidence of any of the extremes from the climatic and hydrological processes results in amplification of the flooding magnitude and extent.

In summary, SPHY overestimates the peaks, while the flood waves in HBV reach the outlet earlier than observed flood waves. Both models have difficulties in reproducing the exact flood timing, and HBV generates flood waves that occur systematically too early. However, the distribution of timing errors is quite broad which makes correcting for this error difficult.

5.4 Dependencies between storm surge and river discharge

In this section, we assess the dependence between Rhine river discharge at Lobith (modeled by SPHY and HBV) and TWL at HvH (modeled by WAQUA). Since most storm driven high water levels and discharge events occur in winter, we focus our analysis on the winter half year only (October–March). Here we repeat the earlier analyses of Geerse, (2013) and Klerk et al. (2015), but account for a range of both positive (discharge event succeeded by TWL event) and negative (discharge event preceded by the TWL event) time lags in our assessment. A positive lag can account for the time required for the weather system to move inland including hydrological responses of the catchment. A negative lag may result from an unusual track of the passing weather system, or from natural variability where the events are shaped by a sequence of storms.

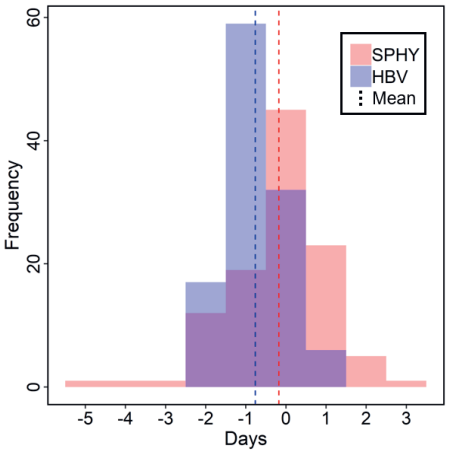

Figure 5.6: The frequency plot for the peak of the floodwave models compared with the observation. The X axis represent the lag in the peak of the wave as compared to the observed peak. The negative and positive value represents the peak of the modeled waves are earlier and later than the peak of observed floodwaves. The dash line (blue and red) represent the weighted mean of the distribution (HBV and SPHY).

The use of a range of time lags allows also to account for the inherent model uncertainty in reproducing the correct wave travel speed (Figure 5.6). To analyse the influence of the choice of time lag on the dependence structure of high discharges and high TWL, we base our assessment on extreme values in TWL. We use daily mean TWL instead of the maximum TWL to eliminate any possibilities of extreme sea levels driven by the astronomical tide. By using the daily mean TWL the effect of astronomical tide on total water level is neglected focusing our analysis on the meteorological driver only. Thus, we define a high/extreme water level event as a day where the daily mean TWL at HvH exceeds the 90th percentile of its distribution.

Figure 5.7 shows this composite for the RACMO based ensemble of WAQUA-HBV and WAQUA-SPHY. In absence of any correlation between TWL and Rhine discharge, the 90%-confidence bands of the percentiles of the lagged time series around a high-water event (shaded area) would overlap with the unconditional discharge percentiles. This is not the case. Depending on the hydrological model, and more importantly, depending on the discharge percentile considered, the composite shows elevated discharge levels for a range of lags. For the 90th percentile the discharge levels are significantly elevated at lags ranging from -2 days to >10 days. This indicates that there is dependence between the two variables starting two days before a high water (90th percentile) event and lasting up to ten days after the event. The elevated conditional discharge two days before a high TWL event possibly due to the twin or series of storm surge where the water level is already elevated by the first storm event. These ranges of lag are consistent with the time (i) the low-pressure system causing the conditions in both variables requires to move over the catchment area, affecting the fetch for surge and precipitation starting locally and moving further upstream, and (ii) the transformation of rainfall to runoff and the propagation of the runoff waves to the downstream location of Lobith, and (iii) natural variability in the dependence of discharge and TWL. The relationship between the discharge and TWL is not linear as the conditional discharge starts to rise with the positive lag and attains a maximum value around positive lag of 6 days (Figure 5.7). The dependence ceases afterwards with increase in the positive lag days ultimately levelling off with the climatology. Both HBV and SPHY show significantly elevated discharges at the 99% quantile for a lag of four to eight days. The 90th, 95th and 99th quantiles show a clear deviation from the climatology in both models.

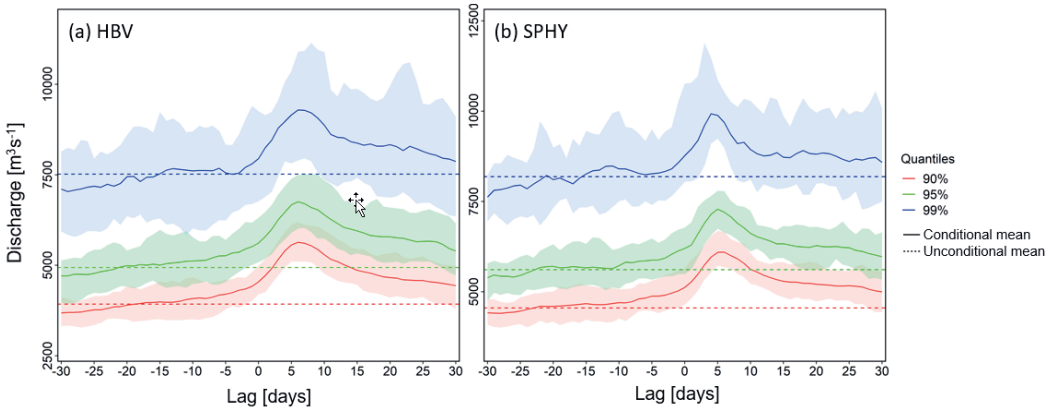

Figure 5.7: Mean temporal evolution of the 90th (red), 95th (green) and 99th (blue) quantile of discharge at Lobith for total water level events exceeding the 90th quantile at HvH in WAQUA as modeled by HBV (a) and SPHY (b). The lag in discharge at Lobith is relative to the peak in total sea water level at HvH. Negative and positive lag days indicate that the discharge peak occurs before and after the day of the high sea water event. The dashed lines are the unconditional discharge quantiles, i.e. discharge quantiles independent of water level; solid lines are the ensemble mean of the conditional quantiles. The shaded area represents 16 different lines for each ensemble and we only took the 5th and 95th quantile of those 16 lines to show spread of 16 ensemble members.

5.4.1 Dependence in the tail of the distributions

In this section, we examine how the upper tails of these two distributions are related. As mentioned in the introduction, tail dependence has been shown to be of particular importance for the influence of compound events on flood risk. Since tail dependence describes the degree of dependence in the tails of a multivariate distribution, we investigate the tail of the discharge distribution conditioned on the distribution of total water level and compare it with the unconditional tail of the discharge distribution. The result of this analysis determines whether or not there is any underlying correlation in the tails of the discharge and TWL distributions. The availability of 800 years of data provides us with sufficient confidence in analysing the extremes in the tail of the distributions.

Having determined the correlation for a range of time lags in discharge and TWL (Figure 5.8), we now examine the dependence in the tail of the distribution for a lag of three days, i.e. with a water level event at HvH occurring three days before the discharge peak at Lobith. This is a shorter time lag than applied by Klerk et al. (2015), who presented the dependence in the tail for a lag of six days. Despite this shorter time lag we find a similar relation between the two variables as Klerk et al. (2015) (Figure 5.8a and c). For this, we test the 50th and 90th percentile of the discharge distribution conditional on TWL and compare it to the respective unconditional discharge. We use seven different percentiles of the full water level distribution to determine the conditional discharge (50, 60, 70, 80, 90, 95 and 99). The conditional discharge values lie above the unconditional discharge. This suggests that the two variables show some correlation in the tail of their distribution even at a lag shorter than the six days. The background scatter points only serve as an illustration of the joint distribution of the two variables. Presence of red scatter points on the top right corner implies that two variables are dependent. However, discharge and TWL do not show any strong dependence, especially for very large values.

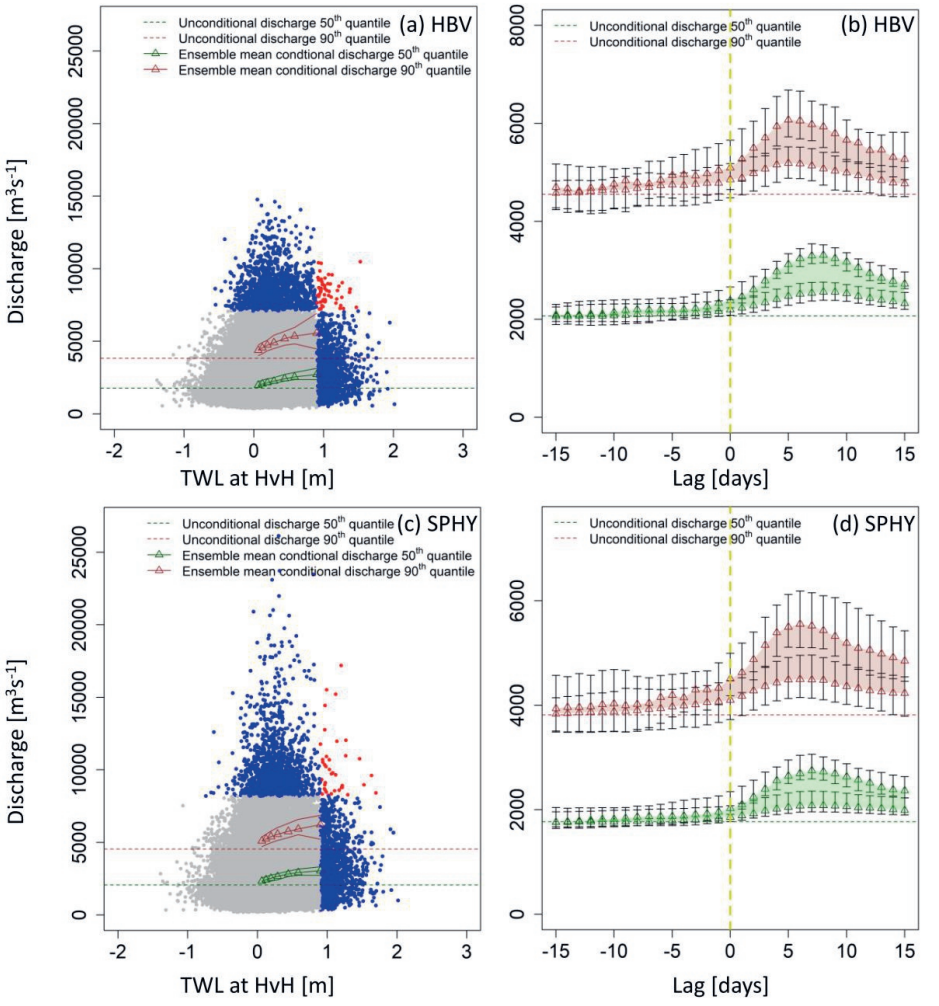

Figure 5.8: Scatter plot of coastal water levels and discharge for a lag of three days ((a) HBV and (c) SPHY) and 16 ensemble members. Events exceeding the 99th quantile of either of the variables are marked in blue. Events exceeding the 99th quantile of both variables are marked in red. The triangles (green/brown) represent the ensemble mean of the conditional discharge (50th and 90th). The green solid lines represent the spread of ensemble i.e. 5th and 95th quantiles of the conditional discharge (50th quantile). Similarly, the brown solid lines represent the 5th and 95th quantiles of the conditional discharge (90th quantile). Conditional discharge plot for 50th and 95th quantile of surge ((b) HBV and (d) SPHY). The green band, represents the conditional discharge distribution i.e. the discharge distribution between the 50th and 90th quantile only for the cases where the total water level is above 50th quantile. Similarly, the brown band represents the conditional discharge distribution i.e. the discharge distribution between the 50th and 90th quantile only for the cases where the total water level *is above 90th quantile. The upper and lower green triangle represent the mean of the 50th and 90th quantile of discharge conditioned on 50th quantile of TWL. Similarly, the upper and lower brown triangle represent the mean of the 50th and 90th quantile of discharge conditioned on 90th quantile of TWL. The vertical yellow dash line indicates the time lag zero. The error bar on triangle represent the confidence interval estimates of the mean (5th and 95th quantiles) from 16 ensemble members.*

Since the dependency in tail of these two-distribution is already realised at a lag of three days, we also assess if the correlation still holds for other choices of lag duration. For this, we investigate the discharge distribution conditioned on specific (50^{th} and $90^{th)}$ quantiles of TWL. We find that, due to the longevity of floodwaves and the natural variability within the system, this tail dependency can be shown to hold for a range of lags. To illustrate this, we chose the 50^{th} and 90^{th} quantile of TWL and again determined the part of the discharge distribution between 50^{th} and 90^{th} quantiles, i.e. the high tail of the conditional discharge distribution. Figure 5.8b and Figure 5.8d show the discharge conditioned on the 50^{th} and 90^{th} percentile value of TWL as function of time lags varying from -15 to 15 days. Two important aspects can be seen in this figure: (1) the width of the band increases with time lag, and (2) the timescales at which the band approaches the climatology, i.e. none of the ensemble members shows a correlation between discharge and TWL. The band width (brown and green area) represents the conditional discharge distribution (part of distribution between the 50^{th} and 90^{th} quantiles) for the respective TWL quantile. The increasing band width suggests a large variation in the distribution (between 50^{th} and 90^{th} quantiles) and vice versa. The band width is decreasing with increasingly negative lag days and approaches its climatological value quickly. This implies that discharge and TWL before a high coastal water level event are uncorrelated and their connection is not different than during normal climatological conditions. For positive lags the band width increases with increasing number of lag days and attains a maximum deviation from climatology around 4–8 days. This variability in bandwidth could be explained by the connection between TWL and river discharge for positive lags and indicates that both variables have the same origin, i.e. winter storms building high surge levels at the coast and dropping large amounts of precipitation to the catchment resulting in high river discharge levels after few days. The 90% confidence interval within the ensemble (i.e. 5^{th} and 95^{th} quantiles) in bandwidth and are calculated from the ensemble. The ensemble confidence is larger in estimating the bandwidth for 90^{th} quantile (brown band) than the 50^{th} quantile (green band). Like bandwidth, ensemble spread (bars) increases for 4–8 days positive lag, but are still higher than climatology. Conversely, at negative lags the uncertainties overlap with climatological values. The uncertainty bands are higher than climatology only after positive lag of two days for both HBV and SPHY.

Other than for negative lags, the bandwidth for large positive values does not reach the climatological values. This is mainly imposed due to the slow hydrological response of the catchment and large duration of the river floods. This means that local precipitation at the discharge location occurs within hours, while the precipitation over the upper regions of the catchment takes several days to be transformed into river discharge and travel downstream. Furthermore, a second low pressure system closely following the previous system can cause the initial increase in river flow by precipitating in the same local downstream region and later accumulating with the upstream precipitation from the previous system.

5.4.2 Joint distribution

In order to discard the possibility that the joint occurrence of high discharge and water level (red dots in Figure 5.8a and Figure 5.8c) are just based on coincidence, we follow the method applied in Kew et al. (2013) and van den Hurk et al. (2015). For this, the probability density function (PDF) of the full, physically related ensemble is compared to a “randomized version” where the statistical relation between the two variables is removed by combining random pairs of variables (Figure 5.9). Results are shown for a three-day lag, but similar results are found for all lags where tail-dependence was shown (see section 5.4.1).

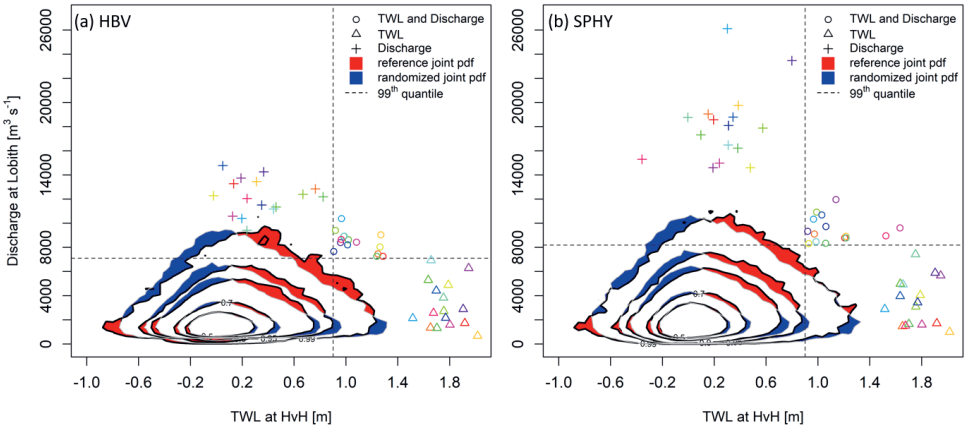

Figure 5.9: Joint probability density for total water level at HvH and discharge at Lobith (3-day lagged) for winter six months period (a) HBV and (b) SPHY). The contours show different quantiles of the joint distribution (50th, 70th, 90th, 95th and 99th). Shading is used to contrast density estimates from direct model output and randomized (shuffled) data, where correlations have been artificially removed. Red/blue shading indicates regions where model data is more/less populated than the shuffled data. The thin dashed lines show the 99% quantiles of each variable in the respective dataset. The colored points correspond to the highest TWL (Δ), discharge (+) and compound events (o) for individual ensemble members.

The shuffled dataset is derived from the original data in the following way. First, the 16 discharge ensemble members were shuffled (changing the order of ensemble randomly). Then this new data is paired with the TWL data from all other ensemble members. In this way fifteen shuffled sets of 800 years (16 ensembles * 50years) of paired data were created. The reference data set, in which the physical between the two variables is retained, links TWL to the discharge three days later. Maximum discharge from the reference and shuffled data sets are shown in Figure 5.9. Each ensemble member is shown using a different colour. Both hydrological models show similar joint distribution patterns for the reference dataset. However, SPHY reaches further into the high discharge area of the distribution than HBV. This is to be expected due to overestimation of high discharge events by SPHY (see section 5.3.2). The area of interest for the assessment of the connection between coastal water level and discharge is the area between quantile contours of the reference and randomized joint probability distributions.

Consistently probabilities of joint occurrence of high TWL and discharge levels are found in the reference data set exceed randomized joint probability density in the diagonal top direction, which indicates an increasing dependence with increasing return period. Conversely, combinations of high TWL/low discharge and vice versa are less likely than randomized joint probability density (diagonal perpendicular to the previous diagonal). This elongated shape of the joint distribution of the reference data along the diagonal indicates a positive correlation between the TWL and discharge volumes three days later. The same diagram for other lag days shows similar features suggesting that this correlation is not limited to one fixed choice of lag but exists over a range of time scales. The main differences between the different distributions depending on lag day is that the correlation is stronger for lag days around six days with the regions only covered by the reference distribution being bigger than for shorter time lags (Figure D4).

5.4.3 Compound probabilities

Up to now we have shown several aspects of the relation between lagged extremes in TWL and Rhine river discharge at Lobith. In this final section we compare the probability of Rhine discharge exceeding a certain level, given that TWL at HvH is also high. The unconditional probabilities here are referred to as "random chance" as these are not dependent on any pre-requisite threshold of TWL. The metric of interest is the conditional probability scaled with its random chance. For example, if TWL and discharge were completely uncorrelated, we expect a random probability x*y that TWL > x^{th} percentile and discharge > y^{th} percentile of their respective distributions. We calculate the random chance for different quantiles purely from the reference winter discharge distribution. The conditional discharge probability only for TWL higher than 97.5th quantile is then calculated for same quantiles again for winter discharge distribution. By scaling the conditional probabilities by the random chance, the inflation factor due to the tail-dependence is quantified. Figure 5.10 shows these scaled probabilities for TWL > 97.5% percentile of the winter distribution, and a range of discharge exceedance probabilities. Results are shown for various time lags. A value till one implies scaled probabilities do not exceed the random chance probability. These values near unity are found at all lags for the lowest discharge percentiles. However, for increasingly rare conditions (higher discharge percentiles), the scaled probabilities strongly increase. For HBV up to 2–5 times higher values are found for the higher discharge percentiles, for a broad range of time lags. This implies that it is 2–5 times more likely to get a high discharge once TWL is high. SPHY shows qualitatively the same result. Although its peaks reach lower values, the levels remain elevated for longer positive lags than in HBV. This is clearly related the generally longer duration of the floodwaves in SPHY.

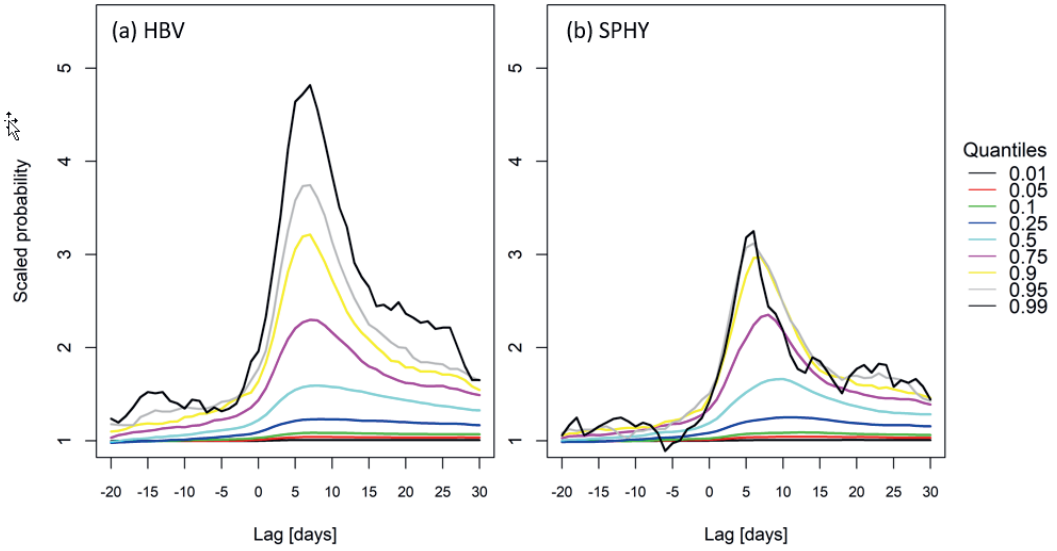

Figure 5.10: Probability for getting river discharge above a certain percentile (a) HBV and (b) SPHY, given that total water levels also exceed the 97.5% percentile. For each discharge percentile, the probability is scaled by the random probability of the event.

5.5 Discussion

Using the dynamically downscaled output of the EC-Earth ensemble, we obtain coastal water levels and associated river discharge from one state-of-the-art storm surge model (WAQUA/DCSMv5) and two hydrological river-discharge models (SPHY with routing model and HBV). The use of a physically

related 16-member ensemble provides us with a larger sample size (800 years), allowing a solid statistical assessment of physical relationship that cannot be carried out with observations alone, as applied in previous studies. The increased sample size is particularly important for the assessment of the high tails of the tail of two distributions and their joint distribution.

This study is limited by the performance of the applied models. The results presented here carry the bias of the meteorological and hydrological models. For instance, both hydrological models show discrepancies to observed high discharges. Both HBV and SPHY overestimates the discharge at high values. These large biases mainly emerge in the peak discharge events, characterized as multi-day events occurring roughly twice every year. The same is valid for the storm surge model WAQUA, which has been shown to reproduce observed coastal water levels and their extremes fairly well (Ridder et al., 2018a). Since the results presented here are based on quantile thresholds relative to the respective dataset, the biases in the model results do impact the findings concerning the statistical relation between the variables water level and river discharge. The results of two hydrological models with different bias allows evaluation of the impact of these bias on the correlation characteristics, and gives an indication of the contribution of model bias to uncertainty of this joint correlation.

The presented results are based on daily values, both in the analysis of the relevant variables as well as in the forcing of the hydrological models. Consequently, the data does not contain any diurnal variations in river discharge and surge/TWL. Averaging to daily values leads to smoothening of the response and to additional uncertainty in the timing of the peak onset and duration. Moreover, the effect of two or more consecutive precipitation events within a couple of days (analogous to two or more small depression passing over in quick succession) could be considered as one. This would result in underestimation of extreme events frequency, particularly in hydrological sense. Since with the current threshold approach to identify the flood wave, differentiation between the flood wave generated separately from multiple precipitation event in quick succession is not possible. More importantly, two storms in quick succession ("twin storms") where the second storm coincides with delayed high runoff could not be resolved completely and considered as one in the present setup. Although, the elevated conditional discharge 2 days before a high TWL event, to some extent, is explained by "twin storms" still it is not completely understood in this study. While it is unlikely that this has a significant impact on the probabilities of occurrence of compounding events it should be highlighted as it may lead to a (small) underestimation of the number of these events.

The impact models, especially HBV, are unable to resolve the exact timing of the observed floodwaves. SPHY tends to overestimate the flood peaks making it unsuitable to use for the forecasting purposes unless additional post processing is considered. To avoid a large mismatch of timing of floods peaks, we chose to define the peak as the local maxima between the onset and offset of the floodwaves. We found that both hydrological models are unable to simulate the correct timing of the flood peaks, but flood durations are well represented in both models.

The uncertainty due to downscaling from RACMO may introduce spurious biases in the results presented here. RACMO is known to release precipitation too close to the coastline (van Meijgaard et al., 2012) which makes it difficult to estimate the basin scale hydrological responses of the synoptic scale circulation pattern. This may lead to an overestimation of the local flood magnitude near coastal areas. Additionally, the most extreme wind speeds can only be generated at scales that are finer than those resolved by RACMO. Consequently, the modeled TWL may display a bias as well. The statistical bias correction methods do not always accurately preserve the properties of extremes and associated signals (Christensen et al., 2008; Ehret et al., 2012; Sippel et al., 2016). The possible alteration in extreme precipitation signals, due to bias correction of downscaled EC-Earth ensemble, may affect the results presented here.

Copula models, though rely on many assumptions, are very useful and powerful tools in simulating the dependence of variables in a multivariate environment. However, these statistical models rely on many assumptions to simulate the joint behaviour or distribution. The joint distribution of the variables is difficult to estimate beforehand and a physical modelling framework that represents the physical

correlations directly is needed. Our approach is focused on addressing the correlation using a physical model setup to generate the long time series. This indeed introduces model error. On the other hand, fitting distributions through the sparse number of observations lead to a large error, in particular for the tails of the distributions, i.e. the very extremes, which we are particularly interested in for this study. To this end, we adopt a methodology that directly assesses the compound nature of coastal water level and discharge, rather than indirect proxies. By using multiple hydrological models and fine resolution gridded climate data in ensemble mode, we ensure that the heterogenous variation of meteo-hydrological processes and the memory components of the system are well captured in this study while they were missing in earlier studies for the Rhine. We used a complete physical approach to investigate the joint occurrence of high discharge and water level to show that the correlations are not just by a chance. We conceptually show that a strong storm whose winds set up a storm surge will need time to reach the Rhine headwaters where heavy rainfall will find its way to the river mouth after multiple days of travel time. However, in reality this simple rationale is blurred by natural variability where multiple storms and anomalous travel times may lead to very different correlation lag times. Our ensemble high-resolution model set-up allows diagnosing this correlation range much better than studies that rely on observational records. Fitting distributions through the sparse number of observations leads to a large error, in particular for the tails of the distributions, i.e. the very extremes, which we are particularly interested in for this study. We believe a multivariate statistical fit on the model output data set will give more robust results but pretty similar to the current findings. Nonetheless, we show that the compound events, consisting of high discharges and high TWLs, are physically related to each other. This is an important finding to improve assessments of coastal flood risks.

5.6 Conclusion and recommendation

The temporal dependence structure of compounding extreme coastal water level and river discharge events has been analysed. Taking into account model uncertainty, natural variability and duration of flood peaks, we find that correlation between the discharge at Lobith and coastal water levels at Hoek van Holland occur at a range of time lags. Other than previous studies, which are based on historical observations, we find model uncertainties make it necessary to consider a range of lag days rather than a fixed time lag of six days. Thus, considering these uncertainties, the impact of co-occurring high river discharges and coastal surge levels cannot be neglected for large catchment areas as the Rhine basin, as was suggested in earlier studies. Our results show that even shorter time lags show significantly increased probabilities of joint occurrence. Neglecting these short time lags can lead to significant underestimations in return periods and thus flood risk. Finally, this study illustrates the importance of good physical models in compounding event analysis framework to allow for solid and reliable assessments of the events.

It is possible that the temporal dependence structure will be significantly altered when different subcomponents of discharge such as rain, snow melt and baseflow are considered separately. While we did not assess this in the present study, we believe it to be a valuable assessment and plan to follow up this line of investigation in a future study.

Code and Data Availability

The code of the SPHY model is publicly available at https://github.com/FutureWater/SPHY. The PCR-GLOBWB 2 source code is publicly available at https://github.com/UU-Hydro/PCR-GLOBWB_model. The WAQUA model codes are available upon request. The datasets that are produced in this study are available upon request.

Author Contributions

The study is designed by Bart van den Hurk, Hylke de Vries, Nina Ridder, Sonu Khanal and Wilco Terink. The SPHY model was run by Sonu Khanal and Wilco Terink. The analyses of the results were performed by Sonu Khanal, Hylke de Vries and supported by Nina Ridder. Sonu Khanal, Nina Ridder and Hylke de Vries prepared the manuscript text. The figures were prepared by Sonu Khanal. Finally, the proof-reading was performed by all (co-)authors.

Competing Interests

Author Sonu Khanal was employed by company FutureWater, Wageningen, Netherlands. All other authors declare no competing interests.

Acknowledgements

This project has received funding from the European Union's Horizon 2020 research and innovation programme under the Marie Skłodowska-Curie grant agreement No 676027. This study was also partly funded by the Netherlands Organisation for Scientific Research (NWO) as part of the project "Impacted by Coincident Weather Extremes" (ICOWEX; grand number 869.15.017). The authors would like to thank the IMPREX project, in particular Femke Davids and Erik van Meijgaard, for providing the data from two of the impact models. We also thank Ferdinand Diermanse, Arthur Lutz and Walter Immerzeel for their valuable comments and expert advice during the data analysis for this study.

6

Chapter 6

Synthesis

6 Synthesis

Hydro-climatic extremes are of prime importance to the society and ecosystem as they tend to influence the overall environment more than a common/regularly occurring event. The losses due to compound extremes can be more severe, leading to larger impacts to the environment than those from individual extremes alone. Recent decades have witnessed an increase in frequency and magnitude of compound events at regional and global scale (Bevacqua et al., 2020; Feng et al., 2020; Zhou et al., 2019). Furthermore, climate change is expected to exacerbate the intensity, frequency, and duration of these compound events. To understand the future impact of compound events at different spatio-temporal aggregation levels and climate zones it is inevitable to examine the mechanisms of compound events.

The studies included in this thesis cover several relevant topics related to a complete risk chain (from mountains to coasts) and their impact on water resources (flood, droughts and water resources availability) in regions around the world (i.e., Europe and Asia). This thesis highlights the importance of an integrated process-based physical modelling approach (atmospheric, hydrological and hydrodynamic) for the proper investigation of future flood risk. A new valuable insight on the mechanisms of compound floods and its potential impact on water resources (both for historical and future climate) has been gained with novel modelling approaches. The outcomes generated from this thesis might contribute to support climate change adaptation policy planning and outreach programs in these climate change hotspots, i.e., the mountains and deltas.

The research questions highlighted in this thesis (see section 1.4) are answered by analysing model outputs at multiple spatial levels, i.e. sub-basin, basin and regional scale. Data is analysed at different time scales, i.e. daily, seasonal and decadal, from several hydrological, hydraulic and hydrodynamic, models (see Table 1.1). A dynamically downscaled EC-EARTH ensemble (van Meijgaard et al., 2008) and ERA5 reanalysis (Hersbach et al., 2020) data are used to answer the research questions for climatically diverse regions such as river basins in Europe and High Mountain Asia (HMA).

In the following sub-sections, I will synthesize the research, discuss the main findings and limitations. I will end this chapter by providing key recommendations and potential future research directions.

6.1 Under which conditions are hydrological risk assessments based on multivariate analysis methods are more realistic than based on univariate methods?

In chapter 2, the trends in seasonal and annual extreme climate indices for historical climate in HMA are investigated using daily ERA5 reanalysis following both univariate and bivariate approaches. Analysis reveals while the temperature in the region is consistently increasing at a higher rate than the global warming rate, precipitation changes are not uniform, with substantial temporal and spatial variation in particular for the higher altitudes of HMA. While precipitation and temperature-related indicators show varying tendencies, the compound occurrence of indicators of temperature and precipitation extremes is coherent in the monsoon-dominated basins. This suggests a potential increase in flood related hazards due to co-occurring melt and extreme rain in monsoon dominated regions.

The hydrological implications derived in chapter 2 are based solely on the trends in meteorological drivers, i.e., precipitation and temperature. Attribution of changes in hydrological extremes from compound changes in meteorological drivers is not straightforward because of complex, nonlinear and dynamic relationship between the processes and spatio-temporal distribution of other state variables and fluxes, i.e. soil moisture content, evapotranspiration, snow storage, ground water and antecedent conditions. Hydrological processes memorise past anomalies, and their effects are reflected in subsequent events or periods (Delworth and Manabe, 1988; Dirmeyer et al., 2009; Liu et al., 2014a; Shinoda, 2001).

Therefore, univariate methods are not sufficient to explore changes in multivariate processes such as floods in a climatic diverse region such as HMA. For a better characterization of floods and droughts, understanding complexity of the relationships among the entire suite of hydro-meteorological variables that lead to the generation of flood extremes is required (Sharma et al., 2018). To this end, I used cascade of process-based models, i.e. hydrological, hydraulic and hydrodynamic models, in chapter 3, 4 and 5 to show that multivariate risk assessment methods are robust in assessment of hydrological risk compared to univariate methods that neglect memory component of hydro-meteorological systems.

6.2 What is the best approach to combine proxy-based indicators with process-based modeling to study the role of compound drivers in hydrological risk assessments?

In chapter 3, a study is presented that uses the SPHY model to assess the impact of compound changes in meteorological drivers, i.e. precipitation and temperature, in relation to historical and future hydrological changes in HMA. The study considered a wide range of relevant processes, i.e. snow, glaciers, evapotranspiration, rainfall-runoff and groundwater, which are necessary in assessing the impact of long-term hydrological changes due to compound changes in meteorological drivers at multiple time scales. The study illustrates contrasting climate change responses across HMA's upstream river basins, dictated by the present-day variability in climate and hydrological regimes. Results showed that an increased fraction of liquid precipitation due to climatic warming results in a higher peak of total runoff in all the basins. Despite clear shifts in peak snowmelt runoff (earlier in the year) in most cases, only basins with glacial-nival hydrological regimes show shifts in total runoff by the end of century. The snowmelt contribution decreases significantly for most of the basins towards the end of the century except for basins with a glacial-nival hydrological regime, even under moderate temperature increase. The study demonstrates that all basins have either passed or are approaching the peak glacier melt runoff except the Tarim interior West basin, for which glacier melt continues to increase even by the end of century. At the seasonal scale, the changes are mainly driven by changes in either snow or rainfall-runoff but at the decadal scale the responses are rather less variable and mainly driven by precipitation changes.

This study highlights that a combination of both meteorological (precipitation and temperature) and hydrological (glaciers, snow, soil moisture and antecedent conditions) drivers contribute to impacts compared to study in Chapter 2. The role of snow, glaciers and other states cannot be neglected in mountain ecosystem as it impacts water availability and hydrological regime characteristics. This study illustrates that the drivers of compound event differ depending on climate and physiographic characteristics of the catchment. For instance, in the eastern basins (IND and AMU) changes in snow and glaciers mainly drive changes in water resource availability and hydrological characteristics (magnitude and timing of peak) compared to predominantly precipitation in the eastern basin (YEL and MEK).

In chapter 5, a study is presented for the Netherlands, where storm surges and sea-level rise provide additional risk to fluvial flooding for the people living in the delta. In a delta, if high coastal water levels occur simultaneously with extreme river discharge events, flood risk increases as the river is not able to discharge its water at the outlet, eventually causing river water levels to rise (van den Hurk et al., 2015). For the Rhine river catchment, previous studies have investigated these compound events based on either proxies such as multi-day precipitation sums (a proxy for river discharge) and north-westerly winds (a proxy for storm surge) or limited hydrological observations and simulations using a coarse-resolution global climate model ensemble (Kew et al., 2013; Klerk et al., 2015). This study used a large sample of hydrological simulations (800 years) from different models (SPHY and HBV) forced with a high resolution climate model ensemble, which provides a better insight into the statistical connection between the two variables than what was possible in previous assessments for the Rhine (Wahl et al., 2015; Wu et al., 2018). By using multiple hydrological models and high-resolution gridded climate data in ensemble mode, I ensured that the heterogeneous variation of meteo-hydrological processes and the memory components of the system are well represented.

Different than previous studies, this study illustrated that model uncertainties, variability in weather and catchment response make it necessary to consider a range of lag periods rather than a fixed time lag of

six days for assessment of compound flood risk. This study conceptually showed that strong winds, which set up storm surge will need time to reach the Rhine headwaters from where heavy rainfall will find its way to the river mouth after multiple days of travel time. Results illustrated that the compound events, consisting of high discharges and high coastal water levels, are physically related to each other. The study showed that even for short time lags discharge probabilities conditional on total water level are increased compared to random chance which are not dependent on any pre-requisite threshold of total water level. Thus, considering these uncertainties, the impact of co-occurring high river discharges and coastal surge levels cannot be neglected for large catchment areas as the Rhine basin.

6.3 Can we improve the understanding and prediction of hydrological extremes if memory effects, and compound drivers are incorporated?

In chapter 4, a study is presented that investigates the role of memory in the hydro-meteorological system that leads to intensification of the hydrological extremes. It is achieved by perturbing the time-correlation of the meteorological time series, used as forcing for streamflow simulations by a hydrological and hydraulic model system. Results illustrate that snow accumulated in the Rhine basin serves as an additional source of meltwater for the discharge resulting in a significant shift of the discharge peak and the years with annual snowfall above average tend to generate anomalous high discharge. Initial low soil moisture values reduce the discharge volume strongly. However, low precipitation on high soil moisture states results in higher discharge scenarios than high precipitation on low soil moisture. Soil moisture controls the overland flow processes and is non-linearly related to the rainfall-runoff response (Mcgrath et al., 2007; Zehe and Sivapalan, 2009). Antecedent soil moisture triggers a strong asymmetric rainfall-runoff response (Beven, 2004; Blöschl and Zehe, 2005; Zehe et al., 2010).

Additionally, results showed that meteorological autocorrelation has a strong impact on the magnitude of peak discharge. The higher discharge peaks tend to level off (flatter slopes) in the shuffled weather scenarios where all the correlations in the meteorology are removed. The shuffling randomizes the sequence of the weather events, and thus deletes the memory of the meteorological system. A monotonic increment in extreme discharges with longer memory time scales is found. The results highlight that removing any meteorological autocorrelation occurring at time scales longer than five days reduces peak discharge by 80% relative to the control simulations. Autocorrelation at time scales longer than 30 days plays a minor role. These findings are relevant when exploring the effect of extreme discharge events that are caused by a compound occurrence of drivers. The time scales identified do diagnose the time scale at which compounding drivers need to be considered in order to contribute to a meaningful analysis of compound events. By using a cascade of process-based models and a fine resolution gridded climate data in ensemble mode, it is ensured that the heterogenous variation of hydro-meteorological processes and the memory components of the system are well captured in this study while they were missing in earlier studies for the Rhine (for e.g. Kew et al., 2013).

Climate change will affect the local hydrology and cryosphere of headwater catchments (see chapter 2 and 3). The hydrological and cryospheric changes that occur in HMA can most likely be related to climatic changes that occur on a regional scale. For example, large-scale atmospheric systems, such as the South and East Asian monsoon systems, dominate the regional climate and are large suppliers of precipitation for the mountain ranges in the respective regions (Lau and Kim, 2018; Li et al., 2018). Changes in the intensity and patterns of these atmospheric systems might have implications for the regional hydrology and the occurrence of hydrological extremes in mountainous domains, which, in turn, will pose serious threats for the livelihoods of people. There is a need to improve our understanding on the regional impact of climate change on hydrological extremes in mountainous domains. To this end, regional/basin scale modelling applications with a detailed representation of mountain-hydrological processes are required. The projected trends in hydrological extremes are not exceptional. Also in other mountain regions around the globe, such as the European Alps, it is likely that hydrological extremes as a result of climate change will occur more frequently (e.g. de Jong, 2015; see chapter 3).

6.4 What is the impact of using advanced models and analysis techniques on the assessment of hydro-meteorological risks?

A simple and parsimonious model is often preferred over a complex modeling framework. However, in many of the natural processes often complexity is necessary to understand how states and fluxes can lead to non-linear systems (Fatichi et al., 2016). Here, I illustrate the impact of improved process understanding on hydro-meteorological risk assessment.

In chapter 3, I focused on improving the glacier and snow sublimation processes which play an important role in snow hydrology and the high-altitude water cycle (Saloranta et al., 2019; Stigter et al., 2018; Strasser et al., 2008). A large-scale spatial parameterization is used to estimate the snow sublimation. This parameterization uses an estimate of the theoretical incoming shortwave radiation, the topographic exposure to wind calculated based on the angle of inflection, and elevation (Fu and Rich, 1999; Winstral and Marks, 2002). Inclusion of sublimation process in the simulation of HMA's hydrology significantly improves the snow cover mapping and consequently the water balance of the region. The endorheic basins in HMA, in particular the Tibetan Plateau, Tarim interior east and Tarim interior west, showed high basin averaged sublimation losses of 10, 17 and 18% (of total annual precipitation) respectively. This sublimation loss in the water budget will likely reduce the absolute magnitude of snow runoff and consequently the overall discharge. The hydro-meteorological risk such as flood, without the inclusion of snow sublimation processes, will be overpredicted. Moreover, in chapter 3 an improved version of a glacier module is used (Terink et al., 2017). A previous version of the glacier module in the SPHY model is not mass conserving but uses a large scale parametrization of glacier retreat to represent changes in glacier area. (Lutz et al., 2014, 2016). However, in reality glaciers are dynamic entities that can melt, accumulate, and redistribute ice. The changes in snow and glacier reserves will have a large impact on the runoff in the future (Huss and Hock, 2018; Immerzeel and Bierkens, 2012; Kraaijenbrink et al., 2017). Thus, these improvements are necessary for the robust assessment of future risk due to hydrometeorological extremes.

In chapters 4 and 5, the routing of the hydrological model (SPHY) is improved by coupling it to a stand-alone version of PCR-GLOBWB2 routing scheme (Sutanudjaja et al., 2018). The choice of routing scheme has a significant influence on the timing of simulated river discharge and its peak values (Hattermann et al., 2017; Zaherpour et al., 2018; Zhao et al., 2017). SPHY uses a simple flow recession coefficient to simulate the delay between the generation of specific runoff within the catchment and reaching the outlet. The recession coefficient is used as a weighting parameter to calculate the routed flow at each grid cell, which in SPHY is calculated as the weighted average of inflow of the current and previous day. The averaging used in SPHY causes the attenuation and delay of floodwaves in the model and is typically useful when the aggregation time period of the output (month, year) is larger than the travel times of water along the longest river stretch. To simulate a more realistic flood wave propagation, SPHY is coupled with a kinematic wave routing scheme and calibrated based on the Manning's n coefficient (Sutanudjaja et al., 2018). Even though the magnitude of the extreme discharge events is overestimated, the inclusion of a kinematic wave routing scheme significantly improved the exact timing of the peak events (see chapter 5). The timing of events is crucial in compound event analysis as two or more variables reach high percentiles of their distribution simultaneously. Thus, improving the routing scheme improves the simulation of the flood wave duration and timing of the onset and peak of flood events and thus improves compound flood risk assessment.

6.5 Research novelties

This thesis presents several research novelties:

- This thesis includes the meteorological (precipitation, temperature and strong wind induced storm surge) and hydrological (soil moisture content, evapotranspiration, snow storage, ground water and antecedent conditions) drivers of hazard related to compound hydro-meteorological

risk (floods, droughts, and water availability). The thesis highlights several relevant topics related to a complete risk chain (from mountains to coasts) and their impact on water resources in different climate zones around the world (i.e., the Rhine in Alps and high mountains in Asia). It illustrates the drivers of compound impact differ (chapter 3 and chapter 5) depending on climate, spatio-temporal scale of analysis and physiographic characteristics of the catchment. This thesis assesses compound hazards in different level of complexities: (a) based on the trends and patterns of climate extremes calculated from statistical methods in mountainous environment (chapter 2) (b) based on hydrological (multi-model i.e. HBV and SPHY) and hydraulic models (PCR-GLOBWB 2) in mountainous environment (chapter 3 and 4) (c) based on hydrological, hydraulic and hydrodynamic models (WAQUA/DCSMv5) in coastal environment (chapter 4 and 5). New insights are provided on impacts of climate change on the hydrological regimes, seasonality, and changes in water availability in the headwater and low-lying regions (chapter 3 and 5).

- Improvement of the simulation of physical processes, i.e. dynamic glaciers and snow sublimation (see chapter 3) and routing (see chapter 4 and 5), essential to calculate the water budget of high-altitude regions. These improvements will help to better assess the long-term changes in the cryosphere, and consequently on the water resources.

- Use of a cascade of process-based models to evaluate real impact variables (total sea water level and discharge) as compared to the proxies used by previous studies for the compound flood risk analysis (precipitation and temperature as proxies of hydrometeorological extremes as discussed in chapter 2 and use of wind speed and precipitation as a proxy of storm surge and discharge as discussed in chapter 5).

- Quantification of the memory effect and autocorrelation of hydro-meteorological system that leads to intensification of the hydrological extremes (chapter 4).

6.6 Recommendations and research outlook

The research presented in this thesis provides new and valuable insights in several aspects of flood risk and large-scale water resources assessments by modeling of compound drivers. However, there are several recommendations for further research which I will highlight in this section.

6.6.1 Improvement in understanding of the physical processes and its implementation in glacio-hydrological models

In this thesis, I focused on the use of physical modeling configurations (Chapter 3, 4 and 5) to understand hydrological extremes at different temporal and spatial scales. I used semi-distributed model (Chapter 5) to fully distributed physically based models (Chapter 3 and 4). Essential processes of the high-altitude water cycle, for instance glacier melt (Chapter 2), sublimation (Chapter 2) and routing (Chapter 3 and 4) were improved. Still, significant improvements are needed to have better understanding of water cycle, these are illustrated in the following sub-sections.

6.6.1.1 Cryospheric processes

The cryosphere (water in frozen state as snow, ice, lakes, glaciers and permafrost) plays a key role in global water cycle and affects water availability, weather, energy and agriculture (Hock et al., 2017; Huggel et al., 2015). Each of these components are associated with different response and spatio-temporal scale. A change in the state of these variables affects the overall water cycle differently (both in space and time), and thus requires proper understanding of the process and their current and future states.

Snow and ice melt

Degree day approach is used to simulate the melt throughout the thesis (chapter 3, 4 and 5). To account for the differences in melt processes for snow, clean ice and debris-covered ice, separate melt rates are applied in chapter 3, 4 and 5. However, temporal variability in degree day factors and its impacts on the melt volumes is not assessed in this thesis. The degree factor adjusted and re-calibrated to different seasons and climatic conditions will give more accurate estimates of the melt (Carenzo et al., 2009; Gabbi et al., 2014; Huss et al., 2009; Litt et al., 2019; Rango and Martinec, 1995; Tobin et al., 2013). Inclusion of other variables, such as solar radiation (incoming short wave), albedo and relative humidity, found to improve the spatial and temporal variability of melt simulations as compared to simple temperature index models which only depend on the near surface air temperature (Huss et al., 2009; Litt et al., 2019; Ohmura et al., 2007; Pellicciotti et al., 2005). Moreover, melt in high altitudes are sensitive to spatial and interannual variability of temperature lapse rates (He and Wang, 2020; Heynen et al., 2016; Kattel et al., 2015; Nigrelli et al., 2018; Shaw et al., 2020; Shea and Moore, 2010). A constant lapse rate (both in space and in time) is used in chapter 4 and 5 to calculate the melt, whereas in chapter 3 spatially variable monthly lapse rates are used. Inclusion of a spatio-temporal variable temperature lapse rate will decrease the uncertainty in melt simulation and requires further research. With technological advancement, use of such data and computation intensive approaches is feasible and needs further exploration.

Snow sublimation

Sublimation was not considered for the modeling exercise in chapter 4 and 5. Chapter 3 explicitly uses a large-scale parameterization to estimate sublimation from the snow storage. This method estimates sublimation using the theoretical incoming shortwave radiation, the topographic exposure to wind calculated based on the angle of inflection, and elevation (Fu and Rich, 1999; Winstral and Marks, 2002). However, the individual components of sublimation cannot be quantified by this method. Also, the method uses a fixed parameterization (calibration parameter) to calculate actual sublimation (based on potential sublimation), which requires re-calibration to different regions and climates. Energy balance snow models (Strasser et al., 2008), coupled atmosphere-mass balance models (Collier et al., 2013; Vionnet et al., 2014) and snow drift models (Groot Zwaaftink et al., 2011, 2013; Marsh et al., 2020) could be an alternative and need proper investigation. Alternatively, sublimation estimates can be improved by comparing model simulations with observed snow water equivalent and snow cover extent from satellite observations and requires further investigation. Sublimation estimates are difficult to validate in high altitude regions due to data limitations, and therefore more field measurements are required in the future.

Glaciers

In this thesis, glaciers are distinguished by clean ice and debris covered surfaces. Separate melt factors are used to calculate melt from different glacier surface types (chapter 3,4 and 5). The thesis presents static (chapter 4 and 5) and dynamic glacier melt (chapter 3) approaches to simulate the melt from the glacier surface. The static approach uses a static glacier boundary which does not differentiate between glacier melt, snow melt and rainfall-runoff from glaciers, but defines all runoff from glacier areas as glacier melt. On the other hand, the dynamic approach uses a mass conserving ice-redistribution scheme which distributes the ice from the accumulation zone to the ablation zone allowing glaciers to shrink and also provide a distinction between the melt components over the glacier surface. Although the presented approach is a step forward and bought new insight there are few points that require major improvement in future. One limitation of such dynamic implementation is that it cannot simulate glacier surges. Use of such dynamic approaches over these regions could introduce additional uncertainties in glacier simulation and water availability under climate change scenarios. Implementation or use of ice flow schemes provides a better alternative to understand glacier dynamics (Wijngaard et al., 2019). The authors coupled a glacier mass balance model with a dynamical ice flow model and applied it to understand the effects of natural and anthropogenic climate change on the changing glacier dynamics

(from the end of the Little Ice Age (1850) to 2016). For the dynamic ice flow model, the authors used spatially distributed formulation of the shallow ice approximation (SIA).

Models based on a spatially distributed SIA approximation are easy to apply (low computational time and complexity) and do not require a priori knowledge on the number and orientation of flowlines on glaciers. The models based on these approximations are able to simulate the evolution of glaciers by incorporating the natural feedback mechanism between the mass balance and glacier dynamics (Wijngaard et al., 2019). However, these models are sensitive to the fast growing and steep sloped glaciers, as they do not account for higher order physics such as longitudinal and lateral stress gradients (Adhikari and Marshall, 2013; Le Meur et al., 2004; Wijngaard et al., 2019). Despite its simplicity, the efficiency of the SIA approximation makes it suitable for potential use in catchment and regional scale cryospheric-hydrological models and requires further investigation. Other key aspects such as avalanches (Dunning et al., 2015; Faillettaz et al., 2015; Gilany and Iqbal, 2019; Liu et al., 2021), crevasses (Colgan et al., 2016), ice cliffs (Brun et al., 2018; Buri et al., 2021), supraglacial ponds (King et al., 2019; Röhl, 2008; Watson et al., 2016) and debris-covered glacier thickness (Herreid and Pellicciotti, 2020; Rounce et al., 2018) and its response on the melt rates (Brun, 2018; Reznichenko et al., 2010) are missing in this thesis. Including these aspects might contribute to improve melt simulation by glacio-hydrological models and needs further investigation.

Permafrost

Permafrost process was not considered for the modeling exercise in this thesis. Understanding hydrologic changes and permafrost-carbon feedback mechanisms in response to permafrost degradation and climate change is critical for ecosystems (Lawrence et al., 2015; Schuur et al., 2015; Walvoord and Kurylyk, 2016). Hydrological modeling in permafrost environments presents challenges due to data availability, subsurface characterization, process understanding and integrated modeling approaches (Walvoord and Kurylyk, 2016). Inclusion of a simple heat transfer equation into physically based hydrological models could significantly improve the permafrost melt calculation (Hayashi et al., 2007). The analytical solution of the Stefan soil freeze-thaw equation could be a potential easier approach to represent permafrost processes in cryospheric-hydrological models (Hayashi et al., 2007; Kurylyk et al., 2016). The only limitation of this method is that it requires the surface temperature, which is often not available at high altitude regions. Many modifications to this simple implementation have been proposed in the past and need further exploration.

6.6.1.2 Other hydrological processes

Among other key hydrological processes such as evaporation, condensation, precipitation, interception, infiltration, percolation, transpiration, runoff, and storage. I will highlight key issues and methods on improving the evaporation and routing processes in hydrological models.

Evaporation

The modified Hargreaves method (Hargreaves and Samani, 1985) is used in this thesis (Chapter 3, 4 and 5) to estimate potential evaporation. Since the method is based on a simple temperature-based approach, the uncertainty in evaporation estimates (and thus water balance) are high, in particular for cloudy and windy days (Allen et al., 1998). More complex methods such as the energy based Penman-Monteith (Allen et al., 1998) or the radiation based Priestley-Taylor method (Priestley and Taylor, 1972) could provide a potential alternative, however at higher data and computational expense, to the simple approach used in thesis. With improvement in remote sensing techniques, the understanding of evaporation can be improved and needs further investigation (Kalma et al., 2008).

Flow routing

Chapter 3 of this thesis uses a modified version of the accuflux routing function (where the delay is accounted for via a calibration parameter i.e., 'kx') implemented within the PCRaster modelling framework, which accumulates the total flow upstream following the topological linkages (Deursen, 1995; Karssenberg et al., 2010; Wesselung et al., 1996). This approach is only suitable for rivers where the travel time along the longest river stretch is shorter than the model timestep but not suitable when the timestep of the model approaches the average travel time through the cell. To this end, a more complex routing scheme, i.e., a kinematic wave approximation of the Saint-Venant equation is used in chapter 4 and 5 for routing (Sutanudjaja et al., 2018). The method uses calibration of Manning's n coefficient for the main channel and flood plains. This method provides a more realistic representation of flood wave propagation and also allows to model the floodplain inundation. The choice of routing scheme has a considerable influence on the timing of simulated river discharge and its peak values (Hattermann et al., 2017; Zaherpour et al., 2018; Zhao et al., 2017). A more complex dynamic wave formulation, which calculates flows through the channel network as a function of water level slope, channel profile and channel roughness characteristics, is implemented in newer releases of PCRaster and should be explored in the future.

6.6.2 Improvement of atmospheric modeling and increase in efforts related to measurement of ground data

Precipitation, a key source of water for the land surface water budget, is the most important meteorological variable for an accurate water balance calculation (Fekete et al., 2004). For accurate streamflow predictions it is important to have reliable precipitation data (Bárdossy and Das, 2008; Beven, 2012; Immerzeel et al., 2015b; Moulin et al., 2009). Remotely sensed products, in recent decades, have proven to be cost-effective and reliable tools to understand precipitation patterns and trends at various spatial and temporal scales (Gehne et al., 2016). Even though the spatial patterns match, there is no consensus on the magnitude of precipitation in HMA among remotely sensed products (Ashouri et al., 2015; Beck et al., 2017; Funk et al., 2015; Huffman et al., 2007; Joyce et al., 2004; Yatagai et al., 2012). The direct use of remotely sensed products to derive climatological and hydrological trends requires correction which is often hampered by the mismatch in resolution and insufficient geo-statistical interpolation accuracy of sparse and low quality station data (Andermann et al., 2011; Cheema and Bastiaanssen, 2012; Gebregiorgis and Hossain, 2015; Gehne et al., 2016; Guo et al., 2015). Therefore, limited number of weather stations in high altitude regions should be increased to get more insight on meteorological characteristics. Long-term collaborative efforts and research is required to understand the climate of high altitude regions (Locci et al., 2014; Matthews et al., 2020; Salerno et al., 2015).

A gridded reanalysis product, which assimilates information from multiple sources; airborne balloons, scatterometers radiosonde, dropsonde, aircraft measurements, satellites, and ground-based radar-gauge composite, could provide an alternative to the sparse and inconsistent point scale observations to find spatial patterns of change especially at higher altitudes (Alexander et al., 2006; Dee et al., 2011; Hersbach et al., 2020). Improvements in spatial patterns and magnitude of precipitation can potentially be achieved by the Global Precipitation Measurement Mission Core Observatory products (Li et al., 2021). High resolution atmospheric modelling could also help in improving the quality and accuracy spatial patterns and magnitude of precipitation in high altitude regions (Bonekamp et al., 2019; Collier and Immerzeel, 2015; Kormann et al., 2016; Pritchard et al., 2019; Wang et al., 2021).

Despite advances in numerical weather prediction (NWP) models in recent decades, predictions of small-scale processes such as precipitation, severe storm, hurricanes, and thunderstorms still need improvement. Machine learning (ML), an approach based on learning from data, could be used to develop complex relationships between diverse geophysical domains (i.e., atmosphere, ocean, biosphere and hydrosphere) at multiple spatial and temporal scales (Boukabara et al., 2019). Scarcity of the data in mountainous regions, such as HMA, could be an issue for training ML models (Chantry et al., 2021; Najafabadi et al., 2015). Nevertheless, ML and other artificial intelligence techniques could be a

potential new realm to explore as these methods have shown promising capabilities for NWP and needs further exploration (Arcomano et al., 2020; Brenowitz and Bretherton, 2018; Chevallier et al., 2000; Krasnopolsky et al., 2010).

6.6.3 Integrated modeling approach

Even though the spatio-temporal scales of hazards vary considerably, their compound impacts are commonly felt at smaller space and time scales. These small-scale events are mainly driven by large-scale and planetary systems such as thermodynamic changes, radiation balance and circulation patterns. Therefore, robust modeling approaches are required that can represent the processes and their interaction at a range of space and time scale. More research is required for coupling of key atmospheric, cryospheric, hydrological and oceanic processes as discussed in section 6.6.1 and 6.6.2 in the future. Most studies, depending on the objective, focus on either one or a limited number of disciplines (Bilskie et al., 2014; Bonekamp et al., 2020; Collier et al., 2013; Fersch et al., 2019; Wagner et al., 2016). A spatio-temporal stochastic weather generator coupled with a chain of cryosphere, hydrological, hydraulic and ocean model could be a potential way forward for the risk assessment (Ailliot et al., 2015; Bakhtyar et al., 2020; Falter et al., 2015; te Linde et al., 2010; Merz et al., 2018; de Moel et al., 2015). Future research will benefit from fully integrated modeling approaches (Clark et al., 2015b; Shukla et al., 2010).

In this thesis, I only focus on the hazard component of the risk framework. However, exposure and vulnerability aspects are equally important for flood risk assessment (Klijn et al., 2015; Koks et al., 2015; de Moel et al., 2015). The spatio-temporal interdependencies and interactions between the risk chain components, i.e., hazard, exposure and vulnerability, should be considered in flood risk assessment (Duha Metin et al., 2018; Merz et al., 2014; Vorogushyn et al., 2018).

Compound events are not the exception, but rather the rule in extreme events, and should be treated as such. Return period analysis of such events requires either a very long time series or large model ensembles (van den Hurk et al., 2015; Poschlod et al., 2020). I mainly focused on model ensembles generated from global climate models and used them in multiple physically based impact models to understand impacts at different spatio-temporal scales. Often these physically based impact models are complex and require a lot of computational resource. Use of statistical models and approaches in combination with physical modeling could help to simplify the problem. A wide variety of statistical modelling methods are available to deal with many aspects of compound events. For instance, statistical methods provide considerable accuracy in downscaling of drivers or impacts without the computation effort required for dynamical methods. However, a long sample of observed data is required for the calibration of a statistical model. Stochastic weather generator approaches which are able to represent the dynamic spatio-temporal weather characteristics could be useful in such cases (Diederen and Liu, 2020). Statistical models could be used in lieu with physical models to validate the results (Bevacqua et al., 2017, 2019). Additionally, the uncertainty propagation in statistical models is easier to estimate compared to physically based approaches. I think physically based modeling together with statistical models could help to improve the understanding of the system and needs further exploration.

6.6.4 Climate change and compound events

Compound climate and weather-related risk analysis should focus on high impact event characterization rather than extreme hazard events. Compound risk analysis needs a shift in paradigm from the classical ‘top-down approach’ to a ‘bottom-up approach’. The traditional top-down approach requires the generation of climate scenarios from global climate models, downscaling and bias correcting these scenarios to the regional or local scale using regional climate models and finally translation of this information into quantities of interest through impact models (Hazeleger et al., 2015). The top-down approach results in a large uncertainty as it inherits uncertainty from each step involved (Wilby and Dessai, 2010). Further, representation of the multivariate nature of compound events including its physical mechanism in climate models is not clear as most studies focus on assessing the skill of a

climate model using a single variable (Derbyshire, 2017; Maraun et al., 2017). Impact-related metrics affected by multiple drivers are needed to validate the future climate projections that are to be used for compound event analysis (Maraun et al., 2017). The bottom-up approach on the other hand starts from the identification of a high impact event and thus helps to identify the underlying drivers and/or hazards that lead to large impacts. The bottom-up approach works backwards and provides useful insights to the likelihood of possible combinations (and sequence) of drivers which is important in determining the outcome (Culley et al., 2016; Zscheischler et al., 2018). This approach effectively studies multiple hazards and associated physical mechanisms both in separation and simultaneously.

The storyline (narratives or tales) approach could be a potential way to excel compound event research forward in future (Hazeleger et al., 2015; Moezzi et al., 2017; Shepherd, 2016, 2019; Shepherd et al., 2018). There are large uncertainties related to the future evolution of circulation patterns which are associated either to internal variability of a system or model errors (Fischer and Knutti, 2013; Pfahl et al., 2017; Shepherd, 2014; Trenberth et al., 2015). The climate related uncertainties are higher and difficult to estimate at regional and local scale (Shepherd, 2014). The global climate models overlook the essential small-scale processes which are important for high impact events (Sillmann et al., 2021). For instance, hourly summertime precipitation extremes can only be simulated by high resolution (< 4 km) regional climate models that explicitly represent deep convection which is missing in conventional coarse resolution regional models (Kendon et al., 2017). This suggest that scientific approaches are required to construct useful information from global to regional and local scale. The storyline approach could bridge this gap by investigating an observed single event from the past and assessing how the same event would look like for a plausible future. For instance, rather than quantifying the probability of a recurring flood event it would be interesting to know how much worse the flooding is if it were to happen in warmer conditions in future (Trenberth et al., 2015). This approach requires simulation of one or a few events from the past, therefore allowing a higher resolution, detailed modeling which is not possible in traditional climate impact analysis (Hazeleger et al., 2015). This approach could be useful to understand compound floods in a warmer climate in the future which has not been investigated in detail yet. The storyline approach provides a physically consistent unfolding of past events, or of plausible future events and pathways with an emphasis on plausibility rather than probability (Hazeleger et al., 2015). The development of storylines, or narratives, of climate change provides an informative way to characterise and communicate future climate projections to stakeholders and policy makers (van den Hurk et al., 2014; Shepherd et al., 2018). The storyline approach has been used by several studies to investigate impact of regional climate change on seasonal precipitation and wind extremes (Zappa, 2019), impact of rain-on-snow events on floods in the Swiss Alps (Shepherd et al., 2018), mid latitude circulation and precipitation relationship (Mindlin et al., 2020), La Niña and drought-heatwave relationships (Hoerling et al., 2013), anthropogenic warming and drought components (Rupp et al., 2015), environmental responses to extreme weather events (Lloyd and Shepherd, 2020), role of high resolution modeling for flood events (Schaller et al., 2020) and role of climate change in extreme events (Van Garderen et al., 2021). High resolution event-based storyline approaches provide additional insights which are hidden in other approaches and allow for a detailed mapping of consequences (Schaller et al., 2020).

The storyline approach is therefore an ideal method to quantify not only the impacts of climate change, but also to assess effectiveness of adaptation measures where the human element becomes part of the analysis rather than a confounding factor (Shepherd, 2019). This approach should not be used alone but complemented by several scenario-based analyses. A credibility assessment of model (or chain of models), in representing all the relevant physical processes, spatio-temporal scales and interactions is a prerequisite for the storyline approach. Since there is no notion of probability in the storyline approach, full stakeholder engagement is required to better connect with decision-makers, and to incorporate aspects of vulnerability and exposure in the risk assessment (Sillmann et al., 2019). The approach only addresses the potential change in likelihood of the dynamical situation leading to the event (Shepherd, 2016). These limitations need further exploration in future.

Appendix

Appendix A

This appendix contains tables and figures that are not part of the chapter 2 but relate to the results section.

Table A1: Average temperature (°C) for the reference time period (1979–2018) selected for the analysis. The number inside the parenthesis represents the trend (°C yr^{-1}) and the bold number represents the significance of trend at p<0.05 level.

BASIN	*Annual*	*DJF*	*MAM*	*JJAS*	*ON*
Brahmaputra	1.7 (**0.029**)	-7.3 (**0.054**)	1.0 (**0.022**)	9.7 (**0.020**)	-0.2 (0.027)
Ganges	6.8 (**0.029**)	-1.6 (**0.038**)	6.5 (**0.031**)	13.9 (**0.019**)	5.4 (**0.03**)
Irrawaddy	12.9 (**0.018**)	6.3 (**0.022**)	13.0 (0.010)	18.0 (**0.021**)	12.3 (0.014)
Mekong	0.8 (**0.034**)	-9.3 (**0.063**)	0.4 (0.024)	10.1 (**0.03**)	-2.3 (0.027)
Salween	-2.1 (**0.035**)	-12.7 (**0.052**)	-2.9 (**0.023**)	8.0 (**0.030**)	-5.4 (0.022)
Yangtze	1.9 (**0.033**)	-7.8 (**0.042**)	1.9 (**0.021**)	10.4 (**0.037**)	-0.8 (0.024)
Yellow	0.5 (**0.042**)	-10.9 (**0.025**)	0.9 (**0.046**)	10.3 (**0.053**)	-2.8 (**0.037**)
Amu Darya	0.8 (**0.029**)	-10.9 (0.011)	0.4 (**0.042**)	11.3 (**0.038**)	-2.2 (0.026)
Lake Balkash	1.2 (**0.022**)	-11.3 (-0.019)	2.0 (**0.055**)	11.6 (**0.027**)	-2.1 (0.017)
Helmand	9.8 (**0.053**)	-3.7 (**0.063**)	9.1 (**0.073**)	21.2 (**0.043**)	8.2 (**0.027**)
Indus	0.6 (**0.036**)	-10.7 (**0.034**)	-0.4 (**0.046**)	11.1 (**0.033**)	-1.9 (**0.052**)
Syr Darya	2.5 (**0.026**)	-9.7 (-0.005)	2.9 (**0.058**)	12.8 (**0.028**)	-0.9 (0.016)
Alaguy	6.8 (**0.027**)	-9.1 (-0.014)	8.7 (**0.054**)	19.7 (**0.039**)	1.9 (0.03)
Pai-t'a Ho	0.6 (**0.049**)	-12.3 (0.029)	1.2 (**0.073**)	11.4 (**0.056**)	-3.1 (**0.034**)
Jo-Shui	1.3 (**0.046**)	-12.1 (0.024)	2.0 (**0.068**)	12.6 (**0.054**)	-2.9 (**0.035**)
Junggar	3.0 (**0.020**)	-12.7 (-0.030)	4.3 (**0.059**)	15.8 (**0.035**)	-1.6 (0.021)
Plateau of Tibet Interior	-3.2 (**0.033**)	-13.3 (**0.053**)	-3.6 (**0.024**)	6.2 (**0.018**)	-6.5 (0.036)
Tarim Interior East	-2.4 (**0.039**)	-14.0 (**0.030**)	-2.2 (**0.045**)	8.0 (**0.046**)	-6.4 (**0.026**)
Tarim Interior West	-0.9 (**0.034**)	-13.3 (0.001)	-0.3 (**0.052**)	9.6 (**0.037**)	-4.7 (**0.037**)

Appendix A

Table A2: Average HWDI (days) for the reference time period (1979–2018) selected for the analysis. The number inside the parenthesis represents the trend (days yr^{-2}) and the bold number represents the significance of trend at p<0.05 level.

BASIN	*Annual*	*DJF*	*MAM*	*JJAS*	*ON*
Brahmaputra	4.4 (**0.142**)	2.7 (**0.054**)	0.7 (**0.004**)	0.1 (0.000)	0.7 (**0.006**)
Ganges	3.4 (**0.057**)	2.0 (**0.018**)	0.7 (0.000)	0.2 (0.000)	0.3 (**0.000**)
Irrawaddy	0.6 (0.000)	0.4 (**0.000**)	0.1 (0.000)	0.0 (0.000)	0.0 (0.000)
Mekong	8.0 (0.117)	3.3 (**0.046**)	1.3 (0.007)	0.4 (0.000)	2.7 (0.000)
Salween	6.9 (0.104)	2.9 (**0.062**)	1.2 (0.007)	0.4 (0.000)	2.2 (0.000)
Yangtze	5.4 (**0.165**)	2.4 (**0.048**)	1.1 (**0.028**)	0.5 (**0.007**)	1.0 (0.008)
Yellow	5.8 (**0.240**)	2.2 (**0.075**)	1.1 (**0.031**)	1.5 (**0.051**)	0.8 (0.000)
Amu Darya	7.2 (**0.194**)	2.7 (0.018)	1.9 (**0.078**)	0.4 (**0.001**)	1.9 (0.008)
Lake Balkash	5.4 (**0.108**)	1.4 (**-0.018**)	1.5 (**0.021**)	0.5 (0.000)	1.7 (0.004)
Helmand	12 (**0.439**)	7.0 (**0.207**)	4.2 (**0.018**)	0.0 (0.000)	0.3 (0.000)
Indus	6.2 (**0.223**)	2.3 (0.024)	1.6 (**0.028**)	0.6 (0.004)	1.4 (**0.034**)
Syr Darya	5.6 (**0.119**)	2.0 (0.014)	1.6 (**0.035**)	0.2 (0.000)	1.6 (0.000)
Alaguy	6.5 (0.103)	1.1 (0.000)	2.9 (**0.020**)	0.6 (0.000)	1.5 (0.000)
Pai-t'a Ho	6.8 (**0.235**)	2.2 (0.000)	2.3 (0.000)	1.2 (0.000)	0.8 (0.000)
Jo-Shui	5.9 (**0.197**)	2.0 (0.016)	2.2 (**0.031**)	0.7 (**0.000**)	0.8 (0.000)
Junggar	9.2 (0.095)	2.4 (-0.017)	3.1 (**0.054**)	0.9 (0.004)	2.1 (0.000)
Plateau of Tibet Interior	4.1 (**0.129**)	1.7 (**0.006**)	0.8 (0.002)	0.9 (0.000)	0.4 (**0.001**)
Tarim Interior East	3.1 (**0.133**)	1 .0(**0.014**)	0.8 (**0.028**)	0.8 (**0.004**)	0.3 (0.000)
Tarim Interior West	5.0 (**0.142**)	1.4 (0.002)	1.8 (**0.043**)	0.4 (**0.007**)	0.9 (0.009)

Table A3: Average precipitation (mm) for the reference time period (1979–2018) selected for the analysis. The number inside the parenthesis represents the trend (mm yr^{-1}) and the bold number represents the significance of trend at $p<0.05$ level.

BASIN	*Annual*	*DJF*	*MAM*	*JJAS*	*ON*
Brahmaputra	1978 (-2.245)	171 (**-0.891**)	460 (-0.410)	1189 (-1.471)	158 (-0.031)
Ganges	1755 (**5.018**)	167 (-0.523)	252 (-0.196)	1249 (**5.495**)	87 (-0.087)
Irrawaddy	3593 (**-24.725**)	279 (**-2.85**)	768 (-3.015)	2236 (**-13.746**)	310 (**-3.858**)
Mekong	1035 (-1.368)	65 (**-0.334**)	180 (0.242)	690 (-0.881)	99 (-0.324)
Salween	1096 (-2.306)	85 (**-0.610**)	220 (-0.181)	686 (-1.421)	106 (-0.181)
Yangtze	1108 (-0.134)	66 (-0.114)	215 (0.255)	710 (-0.119)	116 (-0.239)
Yellow	740 (-0.064)	35 (-0.012)	148 (0.153)	482 (-0.307)	75 (0.105)
Amu Darya	678 (-1.288)	186 (-0.045)	265 (-0.747)	139 (-0.521)	87 (-0.025)
Lake Balkash	877 (-0.279)	88 (0.146)	236 (-0.372)	444 (-0.116)	110 (0.236)
Helmand	367 (-2.111)	174 (-1.470)	153 (-1.556)	14 (-0.038)	27 (0.483)
Indus	837 (-1.984)	198 (-0.056)	242 (**-2.13**)	335 (0.439)	62 (-0.179)
Syr Darya	941 (1.101)	152 (0.670)	305 (-0.662)	356 (0.109)	127 (0.232)
Alaguy	218 (-0.468)	13 (0.042)	52 (0.113)	135 (-0.49)	19 (-0.116)
Pai-t'a Ho	633 (-1.071)	28 (-0.092)	123 (-0.234)	428 (-0.921)	55 (0.016)
Jo-Shui	395 (0.573)	19 (-0.034)	77 (0.073)	274 (0.660)	26 (0.020)
Junggar	387 (-0.183)	25 (0.054)	98 (0.014)	225 (-0.214)	39 (-0.002)
Plateau of Tibet Interior	444 (**3.565**)	15 (-0.072)	57 (0.281)	353 (**3.196**)	19 (0.002)
Tarim Interior East	305 (**1.625**)	17 (0.004)	63 (0.015)	209 (**1.447**)	17 (**0.121**)
Tarim Interior West	371 (0.143)	27 (0.106)	89 (-0.181)	229 (0.469)	26 (0.055)

Appendix A

Table A4: Average R10 (days) for the reference time period (1979–2018) selected for the analysis. The number inside the parenthesis represents the trend (days yr^{-2}) and the bold number represents the significance of trend at $p<0.05$ level.

BASIN	*Annual*	*DJF*	*MAM*	*JJAS*	*ON*
Brahmaputra	55 (0.002)	4.5 (**-0.028**)	12.8 (0)	34 (0.038)	3.8 (0.001)
Ganges	51.2 (**0.146**)	4.6 (-0.017)	6.5 (-0.021)	38.6 (**0.176**)	1.6 (-0.006)
Irrawaddy	112.3 (**-0.591**)	9.1 (**-0.113**)	25.6 (-0.102)	68.9 (**-0.25**)	8.7 (**-0.091**)
Mekong	27.3 (**-0.1**)	0.9 (-0.005)	3.3 (0.01)	21.4 (-0.086)	1.8 (-0.011)
Salween	27.8 (**-0.144**)	1.3 (**-0.014**)	4.8 (-0.013)	19.9 (**-0.097**)	1.9 (-0.009)
Yangtze	29.7 (-0.01)	0.5 (-0.003)	4.6 (0.025)	22.3 (-0.029)	2.3 (-0.01)
Yellow	17.4 (-0.006)	0 (0)	2.5 (0.02)	13.8 (-0.014)	1.1 (-0.005)
Amu Darya	17 (-0.042)	4.8 (0.004)	7.8 (-0.022)	2.4 (-0.02)	2.1 (-0.004)
Balkash	22.3 (-0.015)	0.8 (0.001)	6 (-0.009)	13 (-0.006)	2.5 (0.004)
Helmand	10.1 (**-0.09**)	5.1 (-0.053)	4.2 (-0.064)	0.3 (0)	0.5 (0.006)
Indus	20.7 (**-0.094**)	5.4 (-0.009)	6.9 (**-0.073**)	7.1 (-0.005)	1.4 (-0.01)
Syr Darya	25.8 (0.044)	3.5 (0.026)	9.1 (-0.006)	9.5 (-0.004)	3.7 (0.007)
Alaguy	3.3 (-0.001)	0 (0)	0.6 (0.005)	2.5 (-0.008)	0.2 (-0.002)
Pai-t'a Ho	13.9 (-0.037)	0 (0)	1.6 (-0.003)	11.8 (-0.026)	0.5 (0)
Jo-Shui	7.7 (**0.054**)	0 (0)	0.8 (0.004)	6.8 (**0.05**)	0.1 (0.001)
Junggar	8.4 (-0.003)	0.1 (0.002)	1.9 (0.007)	5.9 (-0.005)	0.5 (0)
Plateau of Tibet Interior	5.5 (**0.063**)	0 (0)	0.2 (0.004)	5.3 (**0.056**)	0.1 (0)
Tarim Interior East	3.4 (**0.04**)	0 (**0**)	0.3 (0)	3 (**0.038**)	0 (0)
Tarim Interior West	4.9 (0)	0.1 (0.001)	1 (-0.005)	3.6 (0.01)	0.2 (0)

Table A5: Average RX5 (mm) for the reference time period (1979–2018) selected for the analysis. The number inside the parenthesis represents the trend (mm yr^{-1}) and the bold number represents the significance of trend at p<0.05 level.

BASIN	*Annual*	*DJF*	*MAM*	*JJAS*	*ON*
Brahmaputra	148.6 (-0.409)	35.6 (0.012)	79.5 (0.014)	142.5 (-0.294)	53.9 (-0.138)
Ganges	182.5 (0.441)	50.8 (-0.214)	56.6 (-0.106)	178.7 (0.487)	36.2 (-0.035)
Irrawaddy	284.3 (**-1.808**)	72.2 (-0.045)	156.6 (-0.121)	274 (**-1.595**)	116.8 (-0.934)
Mekong	76 (**-0.184**)	17.7 (0.021)	40.2 (0.176)	72.7 (-0.147)	35.6 (-0.061)
Salween	78.8 (**-0.322**)	20.7 (-0.004)	45.3 (0.065)	75.2 (-0.209)	36.2 (-0.044)
Yangtze	77.7 (-0.02)	14.6 (-0.001)	41.5 (**0.153**)	76.8 (-0.008)	33 (-0.034)
Yellow	58.5 (0.064)	8.6 (0.01)	31.6 (0.09)	58 (0.068)	24.7 (-0.009)
Amu Darya	55.5 (0.083)	39.5 (0.053)	49 (0.059)	26.2 (-0.07)	29 (-0.047)
Balkash	61 (-0.095)	19.7 (0.045)	45.2 (-0.091)	56.9 (-0.092)	31.3 (0.142)
Helmand	60.9 (0.008)	49.5 (0.164)	45.5 (**-0.645**)	9.3 (-0.006)	14.4 (**0.26**)
Indus	87.9 (-0.047)	53.7 (0.184)	57.5 (**-0.44**)	67.1 (0.006)	25.5 (-0.111)
Syr Darya	66.8 (-0.026)	35.1 (0.178)	54.8 (-0.14)	49.4 (-0.056)	39.1 (0.154)
Alaguy	25.5 (-0.025)	4.6 (0.016)	13.8 (0.034)	23.8 (-0.051)	8.2 (-0.057)
Pai-t'a Ho	56.2 (0.014)	6.9 (-0.03)	25.9 (-0.016)	55.9 (0.056)	18.2 (0.05)
Jo-Shui	41.6 (0.095)	5.3 (**-0.028**)	18.9 (-0.011)	40.9 (0.107)	10 (-0.005)
Junggar	38 (0.016)	7.3 (0.026)	22.8 (0)	36.2 (0.019)	13.8 (-0.008)
Plateau of Tibet Interior	43.4 (**0.193**)	4.3 (-0.004)	13.8 (0.075)	43.4 (**0.193**)	7.6 (-0.013)
Tarim Interior East	30 (**0.186**)	4.1 (0.004)	14.7 (-0.006)	29.7 (**0.184**)	6.3 (0.034)
Tarim Interior West	36.2 (0.006)	7.8 (0.036)	22.1 (-0.063)	34 (0.036)	10.6 (0.019)

Table A6: Average R95P (mm) for the time period (1979–2018) selected for the analysis. The number inside the parenthesis represent the trend (mm yr^{-1}) and the bold number represent significance of trend at p<0.05 level.

BASIN	*Annual*	*DJF*	*MAM*	*JJAS*	*ON*
Brahmaputra	415.1 (0.062)	6.8 (-0.323)	73.7 (**-2.505**)	314.2 (-0.163)	20.3 (**-0.163**)
Ganges	448.1 (-0.026)	32.8 (-0.152)	24.3 (3.064)	377 (0.025)	13.9 (**0.025**)
Irrawaddy	793.2 (-0.051)	15.8 (-0.302)	111.1 (-11.539)	606.3 (-1.012)	60 (-1.012)
Mekong	176.8 (-0.01)	5.2 (**0.085**)	22.8 (-0.736)	134.4 (-0.134)	14.4 (-0.134)
Salween	192.9 (-0.026)	5.8 (-0.047)	31.4 (-1.48)	139.9 (-0.118)	15.8 (-0.118)
Yangtze	200.7 (0.002)	1 (0.185)	23.8 (**-0.355**)	166.8 (-0.032)	9 (**-0.032**)
Yellow	131.2 (0)	0 (0.133)	13.7 (-0.269)	113.6 (0.003)	3.9 (0.003)
Lake Balkash	150.5 (0.004)	2.9 (**-0.015**)	39.7 (-0.279)	94.5 (0.081)	13.4 (0.081)
Amu Darya	118.3 (-0.003)	28.3 (-0.346)	61.9 (**-0.118**)	14.2 (-0.064)	13.8 (**-0.064**)
Helmand	74 (-0.127)	39.4 (-0.739)	29.6 (**0**)	2.5 (0)	2.5 (**0**)
Indus	189.4 (0.274)	46.9 (**-1.209**)	61.7 (0.285)	71.5 (-0.104)	9.4 (-0.104)
Syr Darya	165.8 (0.257)	17.3 (-0.197)	65.6 (-0.152)	58.2 (0.129)	24.7 (**0.129**)
Alaguy	35.7 (0)	0.2 (0.066)	6.3 (-0.103)	27.4 (-0.016)	1.9 (-0.016)
Pai-t'a Ho	116.8 (**0**)	0 (-0.019)	8 (0.048)	106.9 (0)	1.9 (0)
Jo-Shui	68.9 (0)	0 (0.061)	5.1 (0.439)	63.2 (0)	0.5 (0)
Junggar	68.8 (0.003)	0.3 (0.029)	14.1 (-0.037)	51.1 (-0.032)	3.3 (-0.032)
Plateau of Tibet Interior	65.7 (0)	0.1 (0.032)	2.1 (0.741)	62.9 (-0.001)	0.7 (-0.001)
Tarim Interior East	45.4 (0)	0 (0.008)	3.7 (0.564)	41.5 (0)	0.2 (0)
Tarim Interior West	60 (0.007)	0.7 (-0.058)	12.6 (**0.143**)	44.5 (-0.009)	2.2 (**-0.009**)

Table A7: Average CDD (days) for the time period (1979–2018) selected for the analysis. The number inside the parenthesis represents the trend (days yr^{-2}) and the bold number represents the significance of trend at p<0.05 level.

BASIN	*Annual*	*DJF*	*MAM*	*JJAS*	*ON*
Brahmaputra	31 (0.084)	24.6 (0.014)	12.6 (-0.014)	4.8 (-0.03)	18.7 (0.034)
Ganges	33.5 (0.031)	22.7 (0.032)	14.8 (0.017)	6 (-0.027)	22.6 (-0.002)
Irrawaddy	21.9 (**0.146**)	19.1 (**0.14**)	8.7 (0.009)	1.8 (0.01)	12.8 (0.109)
Mekong	27.9 (**0.105**)	25 (**0.11**)	12.1 (0.014)	5.1 (0.011)	15.7 (0.021)
Salween	26 (0.096)	22.8 (0.089)	11.4 (-0.022)	5.2 (-0.005)	14.6 (0.028)
Yangtze	28 (0.038)	25 (0.053)	11.5 (-0.014)	4.9 (0.014)	15.1 (-0.001)
Yellow	30.3 (-0.047)	26.6 (0.027)	13 (**0.077**)	7.1 (**0.041**)	17.1 (**-0.11**)
Amu Darya	48.5 (0.254)	13.8 (-0.024)	11.3 (0.01)	41.4 (0.132)	17.7 (-0.029)
Balkash	18.9 (-0.045)	16.3 (-0.025)	9.9 (0.044)	9.7 (-0.021)	11.2 (0.005)
Helmand	135.4 (0.546)	17.9 (**0.208**)	23.5 (-0.008)	98 (0.271)	35.3 (-0.176)
Indus	39 (-0.003)	18.4 (-0.002)	15.7 (**0.083**)	19.5 (**-0.077**)	26.5 (-0.037)
Syr Darya	22.5 (-0.088)	15.1 (-0.069)	8.9 (0.03)	14.7 (-0.035)	12.3 (0.011)
Alaguy	66.1 (0.279)	50.3 (-0.059)	33 (0.032)	33 (0.079)	30.6 (0.158)
Pai-t'a Ho	32.1 (-0.068)	28.4 (0.065)	13.7 (0.079)	8 (**0.046**)	17.9 (-0.111)
Jo-Shui	48.8 (0.094)	39 (-0.004)	23.5 (0.091)	16.5 (0.036)	27.6 (-0.072)
Junggar	49.4 (-0.024)	40.5 (-0.052)	25 (0.021)	22.3 (0.007)	23.7 (0.033)
Plateau of Tibet Interior	68 (-0.049)	53.9 (0.057)	29.9 (0.042)	12.7 (-0.104)	36.2 (-0.075)
Tarim Interior East	67.2 (-0.071)	50.2 (-0.111)	28.2 (0.114)	19.5 (-0.03)	35.7 (**-0.122**)
Tarim Interior West	55.9 (0.013)	39.7 (-0.15)	24.5 (0.054)	20.2 (0.071)	30.9 (-0.083)

Appendix A

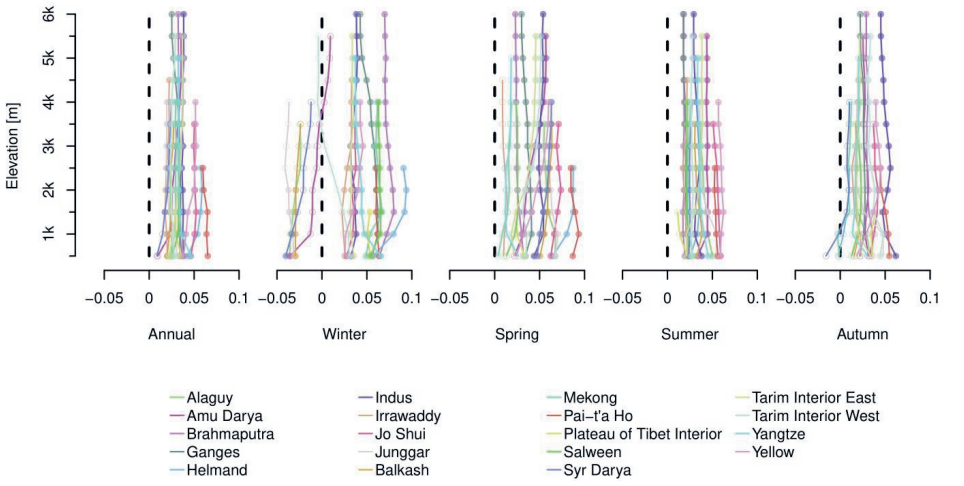

Figure A1: The elevation-dependent mean trends for the basin in HMA. The trends were calculated for 500 meters bins. The filled circles represent the statistical significance at $p<0.05$ and vice versa.

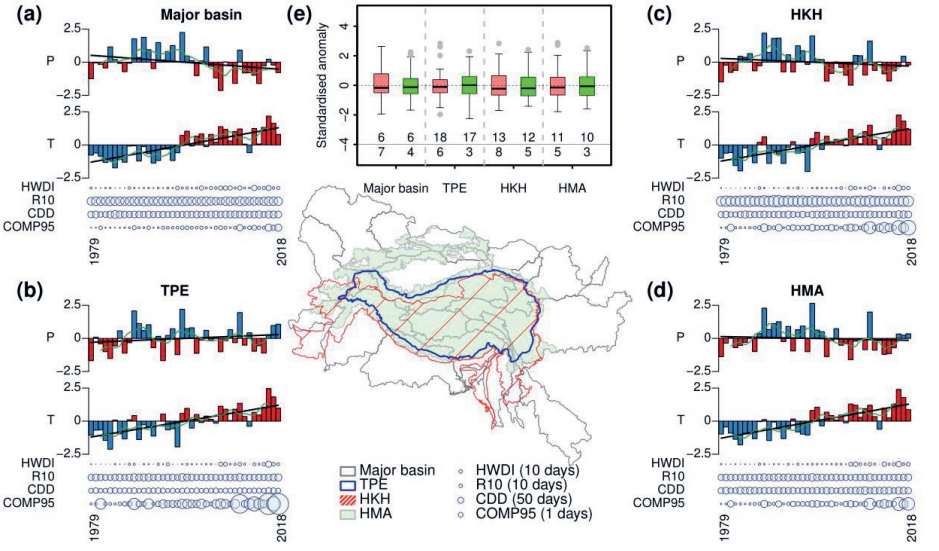

Figure A2: Area aggregated trend in precipitation and temperature and the annual value of extreme indices for different regions as shown in the central base map (a–d). The first two rows in each plot represent the standardised precipitation and temperature anomalies. The blue (red) color represents a positive (negative) anomaly for precipitation or temperature. The X-axis represents the years 1979–2018. The black line represents the linear trend and the green line represents the moving 5-year average. The bubbles represent the annual value of each extreme indices with different linear scaling as specified in the legend. Panel (e) represents the box plots for R95P (red) and RX5 (green) standardised anomalies for the years 1979–2018. The number below the box plot represents the percentage of pixels with positive (upper row) and negative trend (lower row) for R95P and RX5.

Appendix B

This appendix contains a detailed description of the basin delineation (Text B1), first order second moment uncertainty analysis method (Text B2), tables and figures that are not part of the chapter 3 but relate to the results section.

Text B1. Upstream basin delineation

The upstream basin in this study was delineated in a way that included all the areas above 2000 m asl. The HydroSHEDS digital elevation model (DEM, 5x5 km) was used to calculate the elevation mask (Lehner et al., 2008b). The same DEM was also used to delineate the river and flow accumulation netoworks using the PCRaster tool (Karssenberg et al., 2010). The flow accumulation map overlaid with an elevation mask was used to manually select the outlet points on the stream originating from the upstream areas. While selecting the outlet points, the locations of major dams at the transition from upstream to downstream in the GRanD dams database were also used to define outlet locations of the upstream domain (Lehner et al., 2011). The rationale behind this was to minimize the effect on the hydrological regime due to the dams and reservoirs. Most of the dams were in the lower flat plains in the regions, however, there were few exceptions, especially in BRA and YEL, where there were few dams located in the upstream part. For these two basins, the outlets were selected downstream of dams to include most of the area, if not all, above 2000 meters. We neglect the changes in hydrological regime due to the dams in these basins as the location of the dams were further upstream than the outlet points selected. The resulting outlets were then used to delineate the upstream basin boundaries.

Text B2. First order second moment uncertainty analysis

To find the uncertainty estimates quantitatively, a first-order second moment (FOSM) uncertainty analysis of model inputs and parameters as shown in eq B1 was performed (Immerzeel et al., 2010; Wong, 1985).

$$\sigma_F^2 = \sum_{i=1}^{n} \left[\frac{dF\ (x_i \ldots . x_n)}{dx_i}\right]^2 \sigma_{x_i}^2 \qquad \text{(B1)}$$

where, x_i is a model parameter and ($\sigma_{x_i}^2$) is the parameter variance.

The degree day factor for snow (DDFS), degree day factor for clean ice (DDFCI), precipitation (P), and temperature (T) were included in this analysis. The errors in the parameters DDFCI and DDFS were assumed to be normally distributed. The 5th and 95th percentile of the distribution was assumed to be 3 and 7 mm °C^{-1} day^{-1} for DDFCI and 2 and 7 mm °C^{-1} day^{-1} for DDFS. These ranges were estimated based on the values reported by previous studies in the region (Lutz et al., 2014; Wijngaard et al., 2017). For precipitation, a monthly standard deviation of 15%, calculated from the mean monthly ERA5 climatology (1979–2018), was assumed. The assumption of 15% standard deviation was based on values reported by several regional and global studies (Beck et al., 2019; Cucchi et al., 2020; Fallah et al., 2020; Jiang et al., 2020). For temperature, a monthly standard deviation of 1°C is assumed. The hydrological model run for the reference period (1985–2014) was re-simulated with a 5% increase in DDFCI, DDFS, and P; and 0.1°C increase for T as compared to the calibrated model parameters in the runs of the uncertainty analysis (mention number of runs). The total variance due to change in parameters for the total runoff is computed and shown in Figure 3.7 of chapter 3.

Table B1: Calibrated model parameters

Parameter	Description	Units	Calibrated value													
			AMU	BRA	GAN	HEL	IND	IRR	BAL	MEK	TP	SAL	SYR	TIE	TIW	YAN	YEL
DDFs	Degree day factor for snow	mm °C^{-1} day-1	4.5	4.5	4.5	4.5	4.5	4.5	4.5	4.5	4.5	4.5	4.5	4.5	4.5	4.5	4.5
Tcrit	Critical temperature	°C	0	0	0	0	0	0	0	0	0	0	0	0	0	0	0
SnowSC	Water storage capacity of snow pack	mm mm^{-1}	0.5	0.5	0.5	0.5	0.5	0.5	0.5	0.5	0.5	0.5	0.5	0.5	0.5	0.5	0.5
Sfact	Sublimation factor	-	1	0.9	1	1	1	0	0	1	0.3	1	1	0.5	1	1	1
DDFci*	Degree day factor for debris free glaciers	mm °C^{-1} day-1	4.17	4.25	3.57	-	4.26	4.03	4.08	3.92	3.51	3.07	3.45	4.26	5.19	4.11	3
DDFdc*	Degree day factor for debris covered glaciers	mm °C^{-1} day-1	0.83	0.85	0.71	-	0.85	0.81	0.82	0.78	0.7	0.61	0.69	0.85	1.04	0.82	0.6
TlapCor*	Vertical lapse rate correction factor	°C m^{-1}	0.000	-0.001	-0.001	-	-0.001	-0.001	-0.002	-0.002	-0.002	-0.004	-0.001	-0.001	0.000	-0.002	0.000
Soilfactor	Soil multiplication factor	-	1	0.7	1.3	1	0.7	1	1	1.3	0.7	1	1	1	0.7	0.7	0.7
Rootdepth	Depth of top root layer zone	mm	500	100	50	500	50	50	500	50	100	50	500	50	50	50	50
αGW	Baseflow recession coefficient	-	0.933	0.933	0.933	0.933	0.933	0.933	0.933	0.933	0.933	0.933	0.933	0.933	0.933	0.933	0.933
δGW	Groundwater recharge delay time	days	150	1	150	150	1	1	150	1	1	1	1	75	1	75	75
Kc_mul	Crop coefficient multiplication factor	-	0.7	1.3	1.3	0.7	0.7	1.3	0.7	0.7	1.3	1.3	1.3	0.7	0.7	0.7	0.7
Kx	Routing recession coefficient	-	0.945	0.945	0.945	0.945	0.945	0.945	0.945	0.945	0.945	0.945	0.945	0.945	0.945	0.945	0.945

*Parameters with * are calibrated spatially and presented as basin aggregates in this table*

Table B2: Comparison of the runoff contributors from this study to other studies. The numbers in parentheses are the percentage contribution compared to total runoff for time period 1979–2018.

Basin	location	reference	Period	Contribution reported (%)			
				Glacier melt	Snow melt	Rain runoff	Base flow
Indus	Dainyor bridge	Mukhopadhyay and Khan, (2014)	1969-2010	74 (86.1)		26 (13.9)	
Indus	Dainyor bridge	Lutz et al., (2014)	1998-2007	80.6 (37.4)	9.6 (48.7)	1.3 (8.5)	8.5 (5.4)
Indus	Dainyor bridge	Wijngaard et al., (2017)	1998-2010	17.8 (37.4)	69 (48.7)	1.0 (8.5)	12.2 (5.4)
Indus	Dainyor bridge	Shrestha et al., (2015)	2002-2004	33.3 (37.4)	49.3 (48.7)	17.4 (13.9)	
Ganges	Devghat	Wijngaard et al., (2017)	1998-2011	3.4 (4.1)	12.4 (9.0)	63.4 (65.9)	20.8 (21.0)
Brahmaputra	Wangdirapids	Wijngaard et al., (2017)	1998-2012	4.9 (4.5)	28.1 (19.4)	56.2 (48.0)	10.8 (28.1)

Table B3: Hydro-meteorological characteristic of the basins used for the reference ERA-5 period (1985-2014). P, ET and Sub represent the precipitation, evapotranspiration and sublimation.

	P (mm)	Snow (%)	P (monsoon) (%)	P (winter) (%)	Flow (mm)	Flow (monsoon) (%)	Flow (winter) (%)	Base flow (%)	Snow melt (%)	Glacier flow (%)	Rain flow (%)	ET (%)	Sub (%)	Monsoon (snow flow %)	Monsoon (glacier flow %)
AMU	676	45.1	20.9	21.2	407	40.3	6.9	15.8	74.4	4.4	5.4	30.3	8.9	69.8	10.5
BRA	2018	8.8	60.0	9.8	1575	66.4	6.9	22.8	13.2	1.8	62.1	19.3	2.5	7.7	2.5
GAN	1763	9.5	71.2	7.3	1293	73.8	9.6	22.0	10.3	3.1	64.7	23.2	2.9	6.4	3.9
HEL	360	30.1	4.0	18.5	195	6.3	5.2	17.4	77.5	0.0	5.2	43.7	2.2	2.7	0.0
IND	832	34.6	40.3	13.0	577	60.1	5.3	11.4	39.7	5.1	43.9	19.7	10.0	35.2	8.3
IRR	3638	2.4	61.9	10.2	3223	67.3	8.3	16.7	5.1	0.0	78.2	11.4	0.0	2.2	0.0
BAL	856	23.7	51.0	16.1	543	40.0	16.9	42.3	46.3	2.2	9.3	35.6	0.0	35.6	5.3
MEK	1066	8.8	66.2	11.0	528	75.7	8.3	37.2	7.4	0.3	55.1	43.8	6.7	1.0	0.3
TP	451	12.0	79.6	5.4	117	88.7	2.7	49.6	15.3	2.3	32.8	65.1	9.0	5.8	2.6
SAL	1091	15.2	62.7	11.3	627	71.5	7.1	28.3	14.7	1.4	55.7	32.7	10.1	5.2	1.8
SYR	942	28.7	38.3	18.9	456	30.3	7.9	20.2	72.9	1.3	5.6	49.1	2.1	55.9	4.2
TIE	305	24.2	67.9	7.3	126	72.3	11.2	29.0	20.2	1.1	49.7	40.5	17.7	11.7	1.5
TIW	373	31.4	61.3	9.3	166	73.5	3.1	21.4	28.4	5.8	44.4	35.0	17.3	15.1	7.5
YAN	1127	7.4	63.8	12.4	849	65.2	15.3	23.3	5.5	0.2	71.0	20.1	4.6	0.7	0.3
YEL	751	11.0	64.6	11.5	468	64.9	16.1	26.5	9.6	0.1	63.9	31.2	6.5	1.4	0.1

149

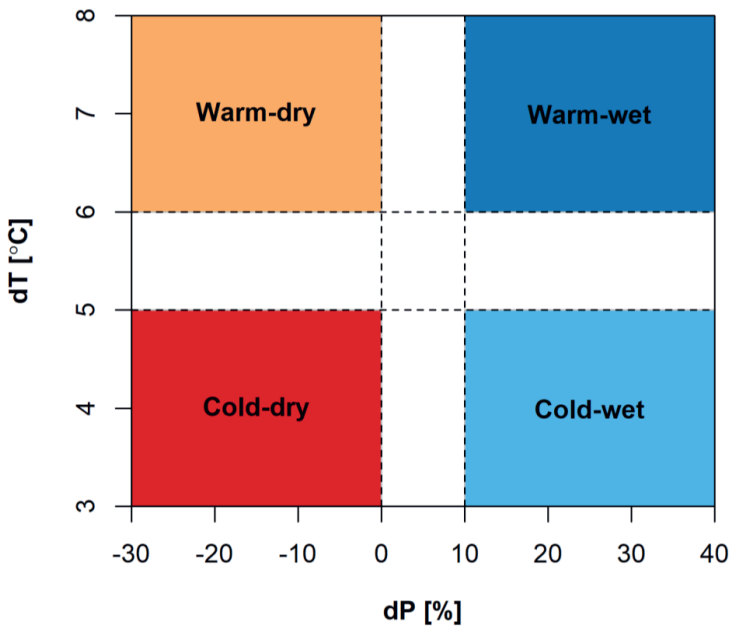

Figure B1: Climate runs categorized into four groups of 12 combination; warm-wet (dT from 6°C to 8°C, dP from 10% to 40%), cold-wet (dT from 3°C to 5°C, dP from 10% to 40%), warm-dry (dT from 6°C to 8°C, dP from -30% to 0%) and cold-dry (dT from 3°C to 5°C, dP from -30% to 0%) used chapter 3.

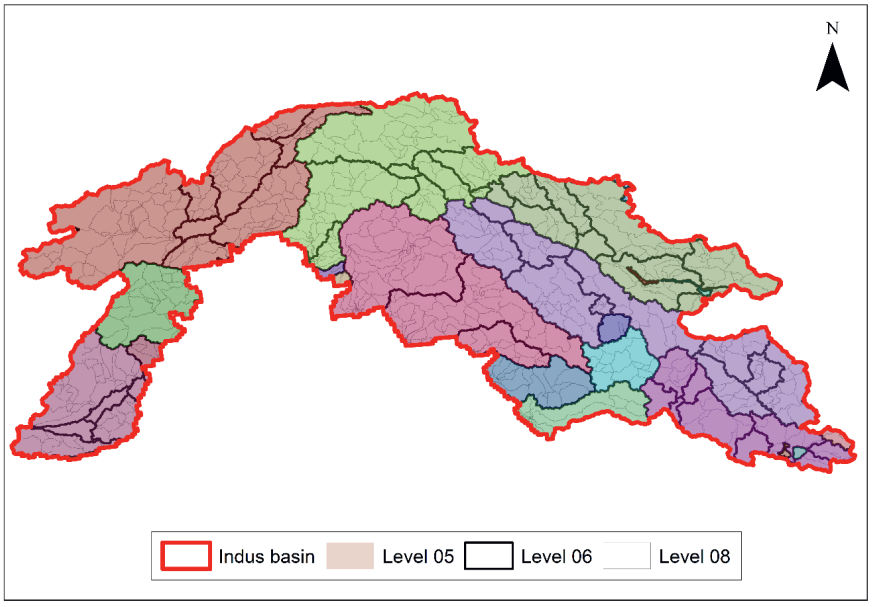

Figure B2: Basin boundaries and HYDRO BASIN aggregation level (05,06 and 08) used in chapter 3. The aggregation level 05 (colored polygons) is coarser than aggregation level 08 (light grey polygons).

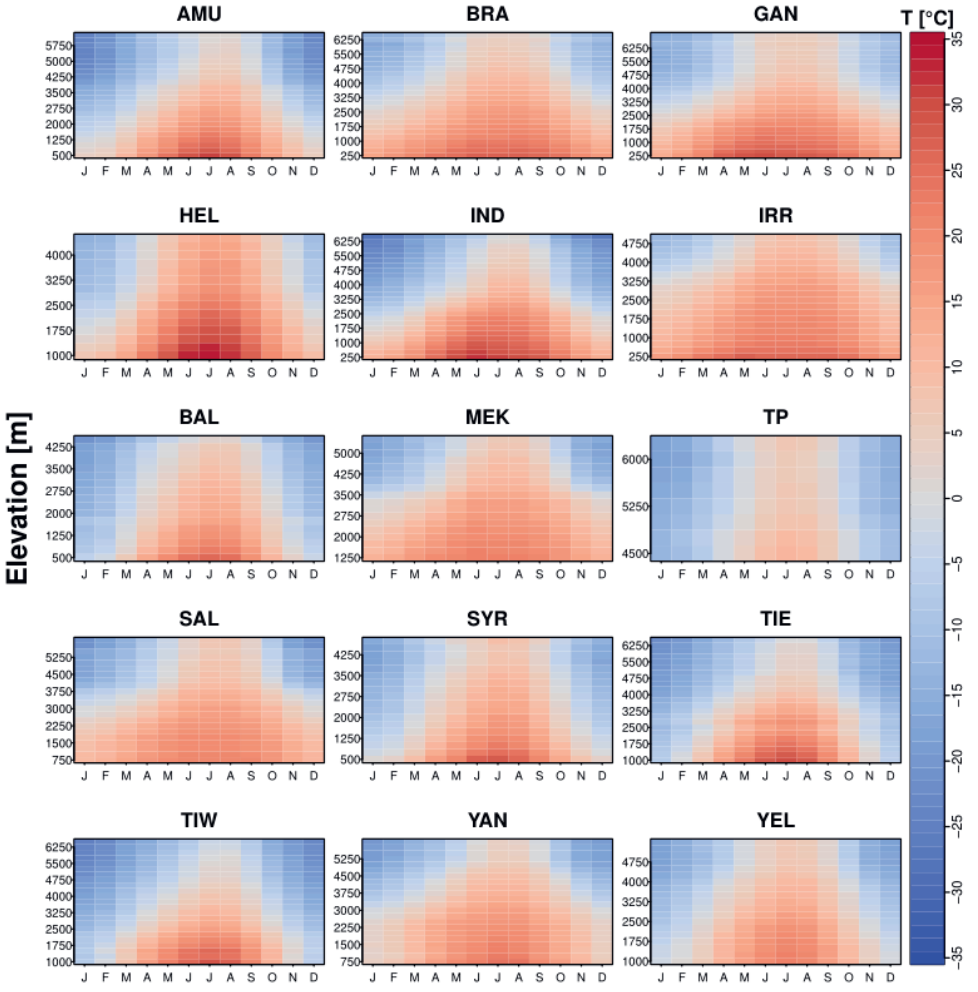

Figure B3: Average monthly temperature climatology per elevation band (250 meters) for full ERA-5 period (1979-2018) in the upper catchments. X and Y-axis represent the months and elevation band.

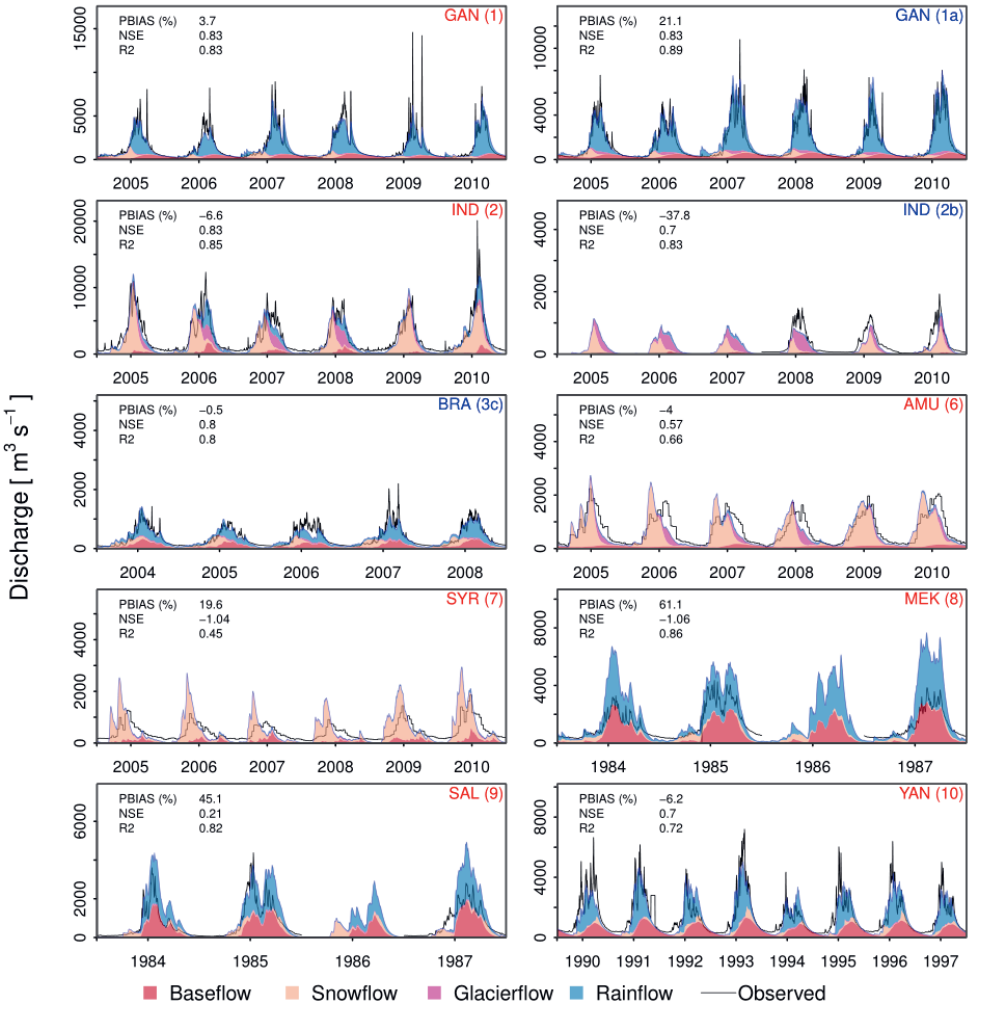

Figure B4: Observed and simulated discharge with the distinction of flow components at validation locations shown in Figure 3.1 and Table 3.1 for the validation period. Each panel shows values for model performance indicators; Nash-Sutcliffe efficiency criterion (NSE), percent bias (PBIAS), and coefficient of determination (R2) at the top left corner.

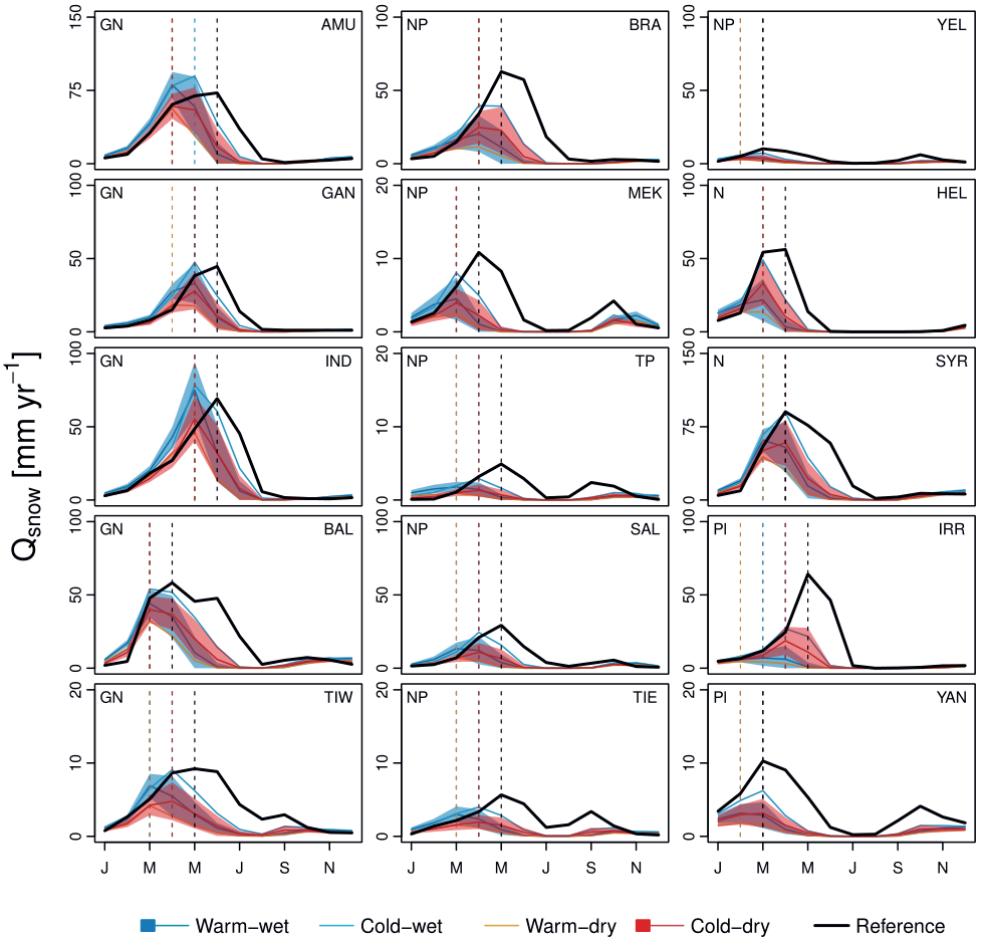

Figure B5: Changes in the mean annual cycles of snow runoff by the end of the century (2071–2100) for the four hydrological regimes. The colored lines represent the mean of four groups of future scenarios, consisting of twelve dT/dP combinations each; warm-wet (6°C to 8°C, 10% to 40%), cold-wet (3°C to 5°C, 10% to 40%) , warm-dry (6°C to 8°C, -30% to 0%) and cold-dry (3°C to 5°C, -30% to 0%). The color shadings represent ±2 standard deviation for a group of scenarios (only shown for warm-wet and cold-dry). The black solid lines represent the reference (1985–2014) mean annual cycle of snow runoff. The vertical dashed lines represent the peak flow months for each group of scenarios. The text on the top-left and top-right gives the hydrological regime and basin name, respectively.

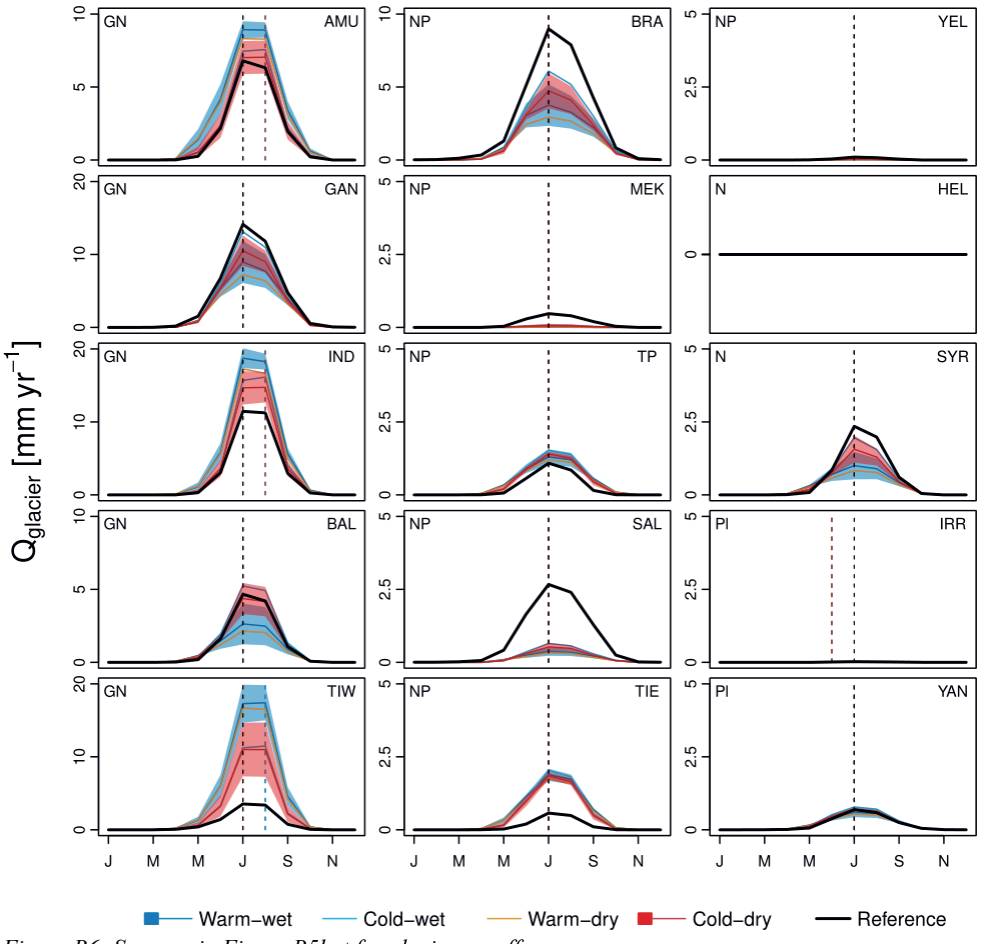

Figure B6: Same as in Figure B5but for glacier runoff.

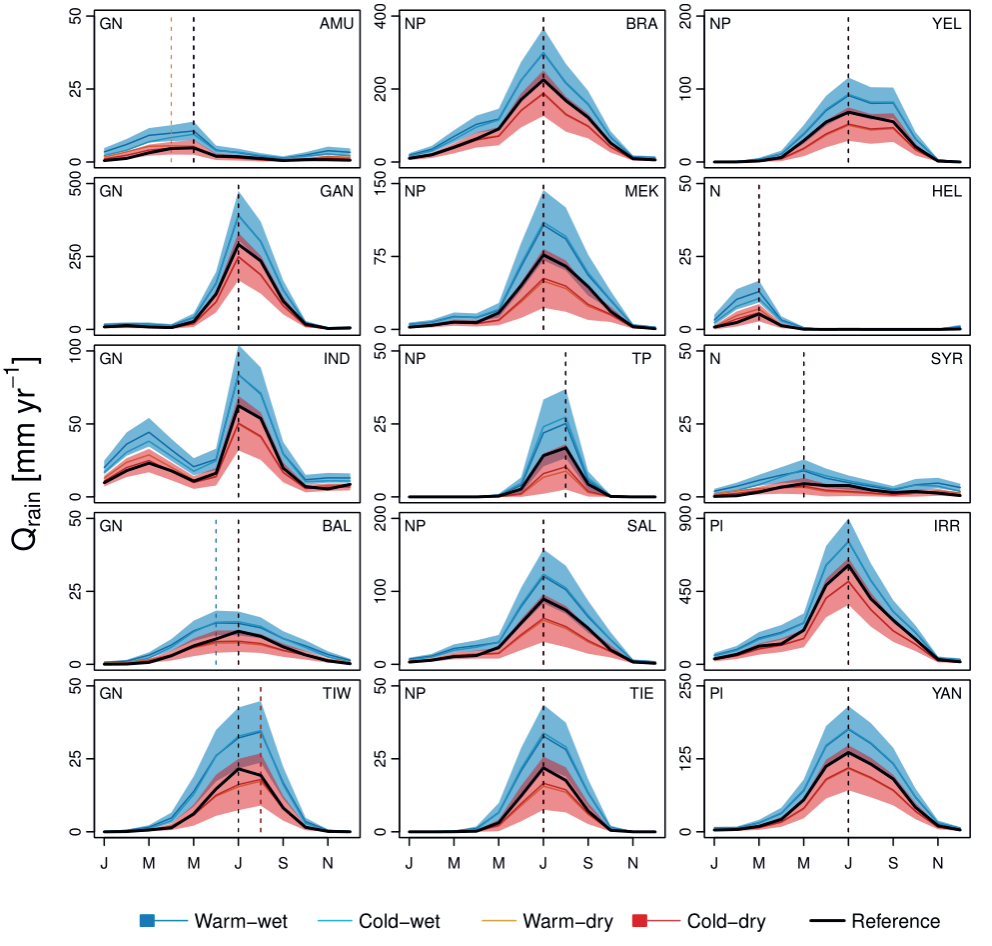

Figure B7: Same as in Figure B5but for rainfall runoff.

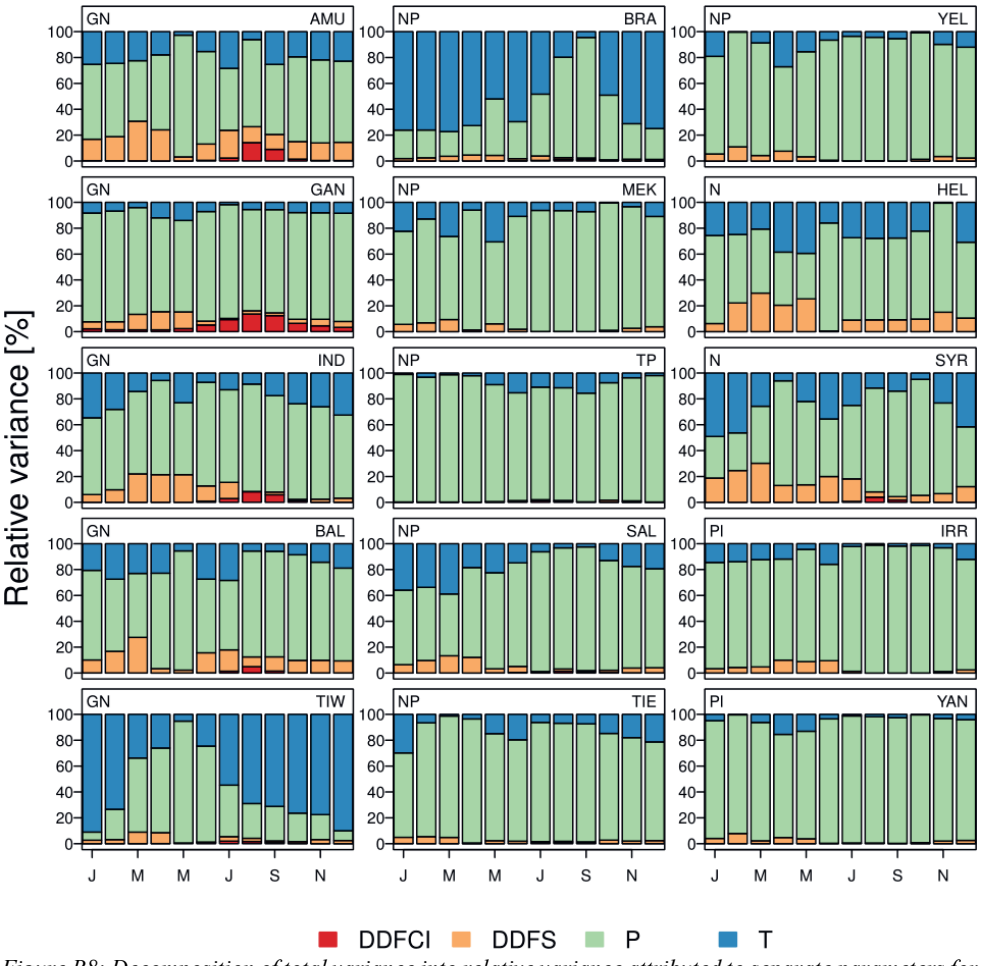

Figure B8: Decomposition of total variance into relative variance attributed to separate parameters for the reference run (1985–2014). The vertical bar represents the months. The color represents the parameter, degree day factor for snow, DDFS; degree day factor for clean ice, DDFCI; precipitation P; and temperature, T.

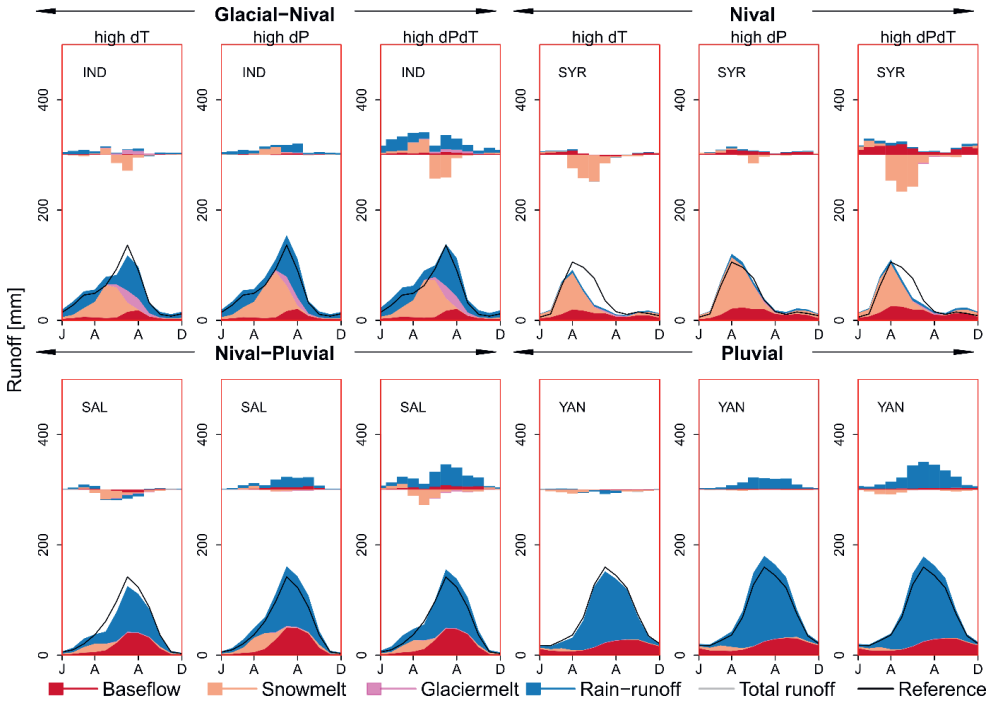

Figure B9: Hydrological response to climate change at seasonal timescales for the mid-century period (2036-2065) for one illustrative basin from each hydrological regime i.e., Glacial-Nival (IND), Nival-Pluvial (SAL), Nival (SYR), and Pluvial (YAN). Changes in the flow regime are assessed for three different future scenarios i.e., high dT, high dP, and high dPdT. The bars represent changes per-flow component relative to the reference period (1985–2014). The black solid lines in seasonal plots represent the reference mean annual cycle of total runoff.

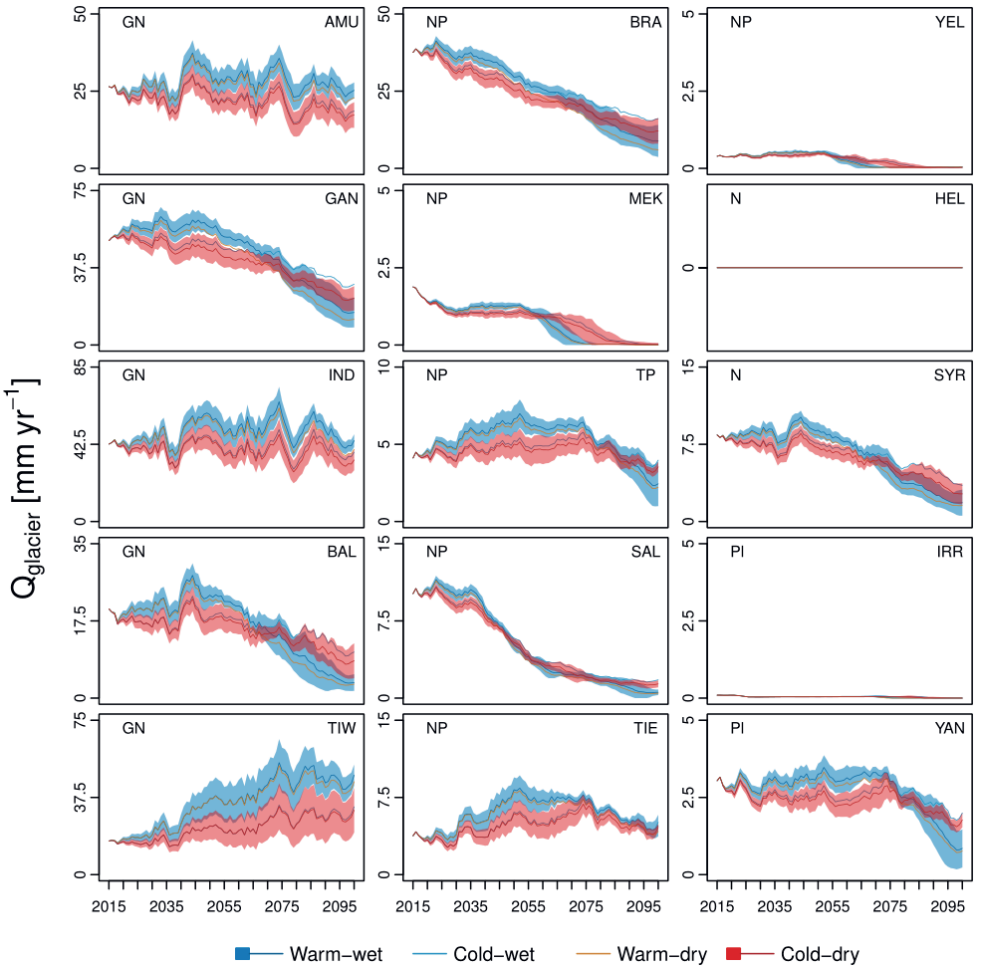

Figure B10: Time evolution of the glacier melt runoff (running mean 5 years) starting in 2015. The colored lines represent the mean of four groups of future scenarios, consisting of twelve dT/dP combinations each; warm-wet (6°C to 8°C, 10% to 40%), cold-wet (3°C to 5°C, 10% to 40%) , warm-dry (6°C to 8°C, -30% to 0%) and cold-dry (3°C to 5°C, -30% to 0%). The color shadings represent ±2 standard deviation for a group of scenarios (only shown for warm-wet and cold-dry). The text on the top-left and top-right gives the hydrological regime and basin name, respectively.

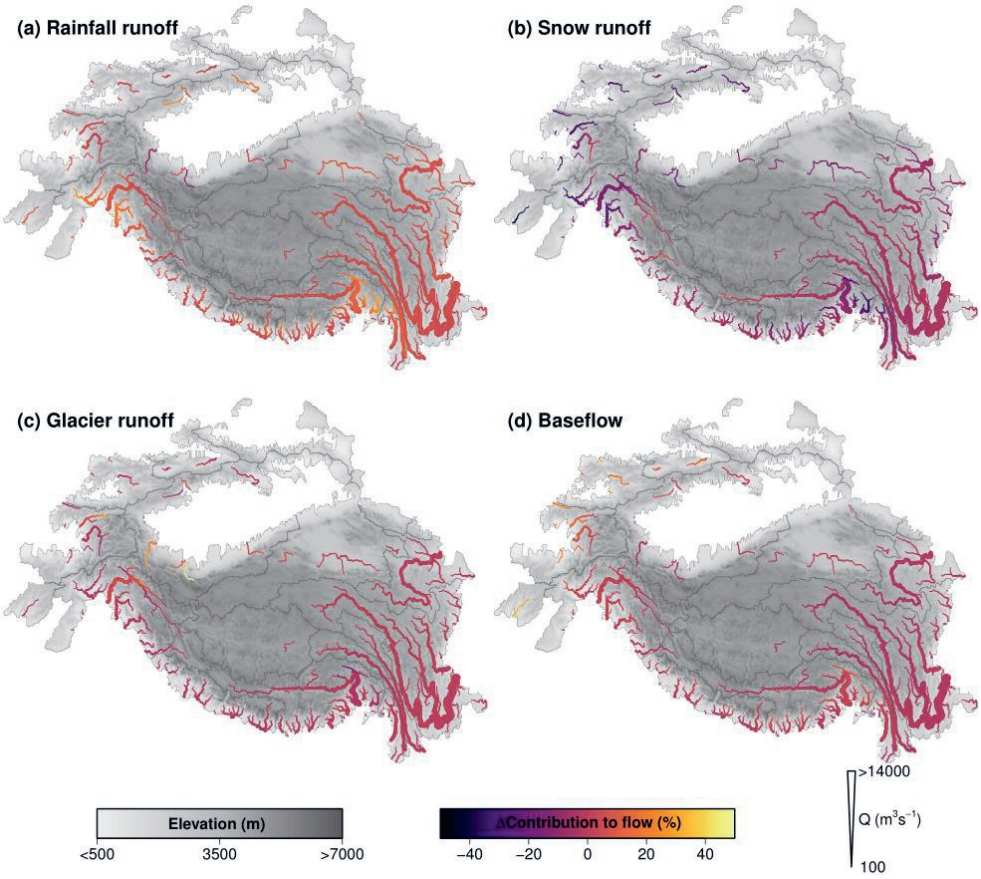

Figure B11: Change in flow components [%] for the end of century (2071–2100) compared with the reference period (1985–2014) for warm-wet (6°C to 8°C, 10% to 40%) scenario. The thickness of the line represents the magnitude of flow; color indicates the relative change in contribution to the total annual flow.

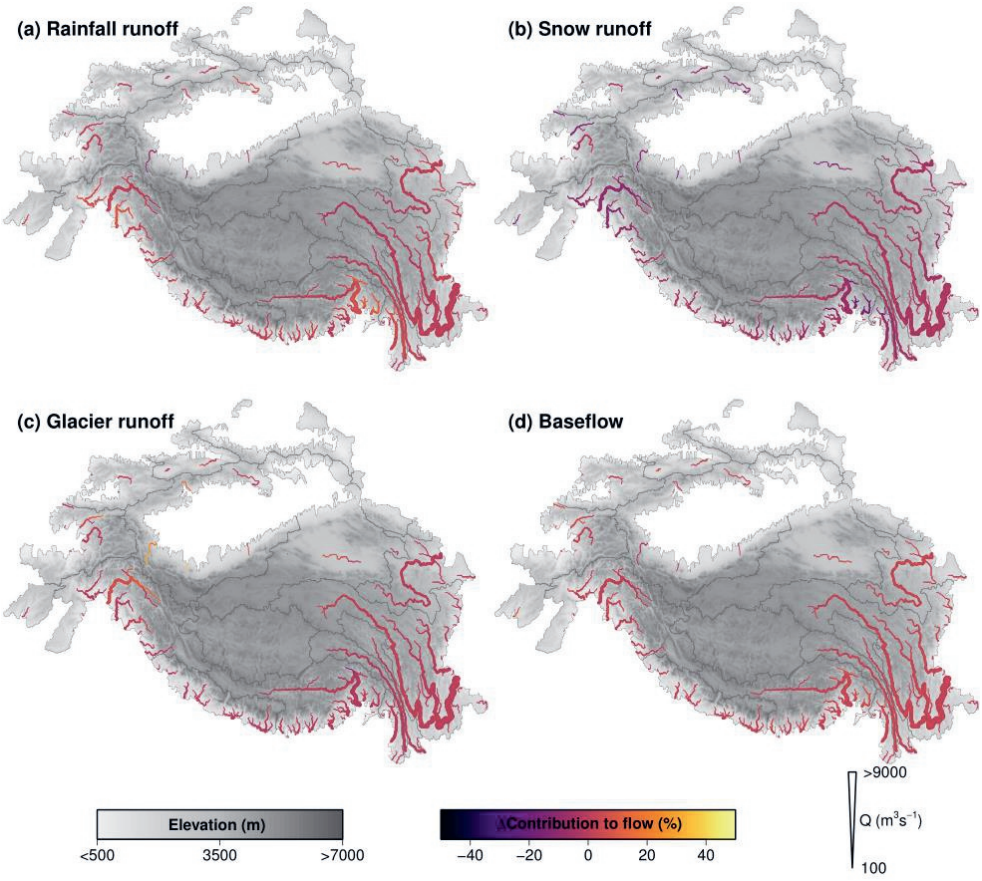

Figure B12: Change in flow components [%] for the end of century (2071–2100) compared with the reference period (1985–2014) for cold-dry (3°C to 5°C, -30% to 0%) scenario. The thickness of the line represents the magnitude of flow; color indicates the relative change in contribution to the total annual flow.

Appendix C

This appendix contains figures that are not part of the chapter 4 but relate to the results section.

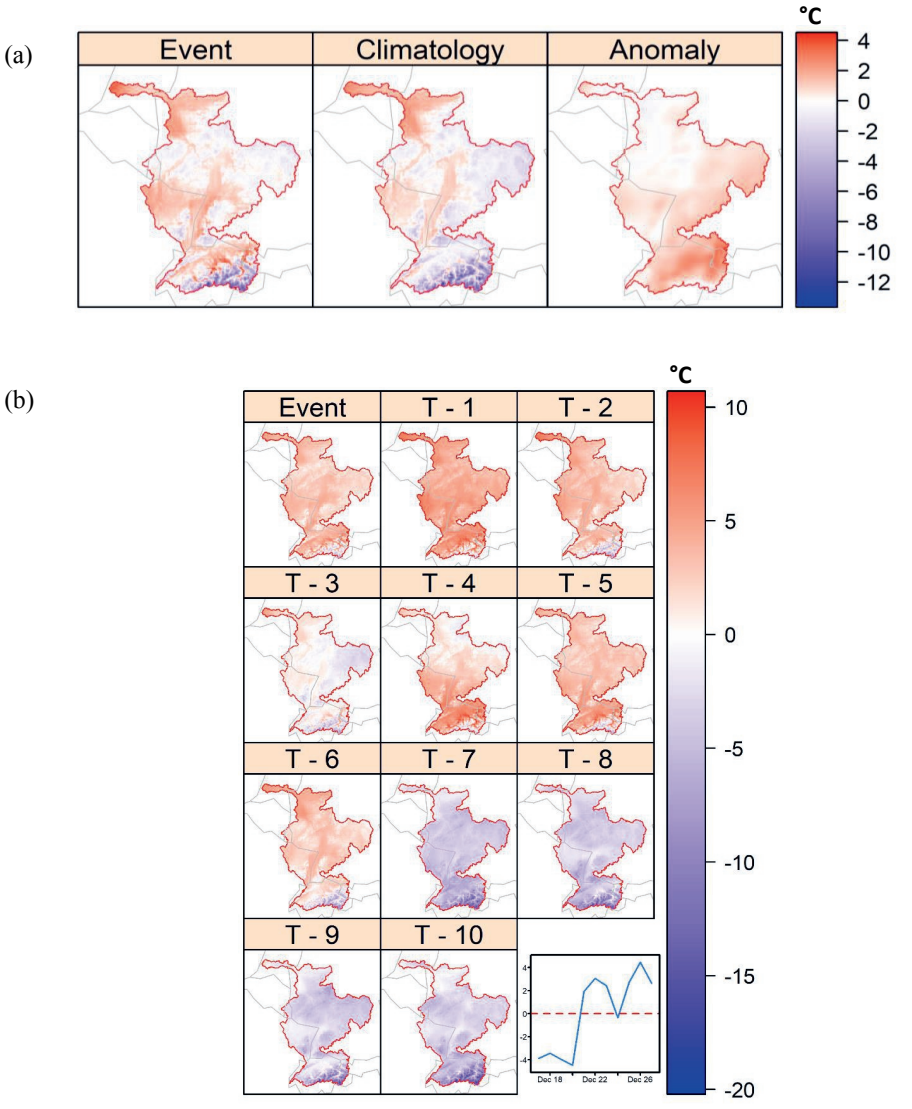

Figure C1: (a) Average temperature over the past 10 days prior to event, climatological mean and its anomaly event for the original run. (b) Temperature distribution of 10 days prior to the extreme discharge. The lower right panel shows the timeseries of the basin average value (solid blue line). The horizontal dashed red line denotes the 0° C.

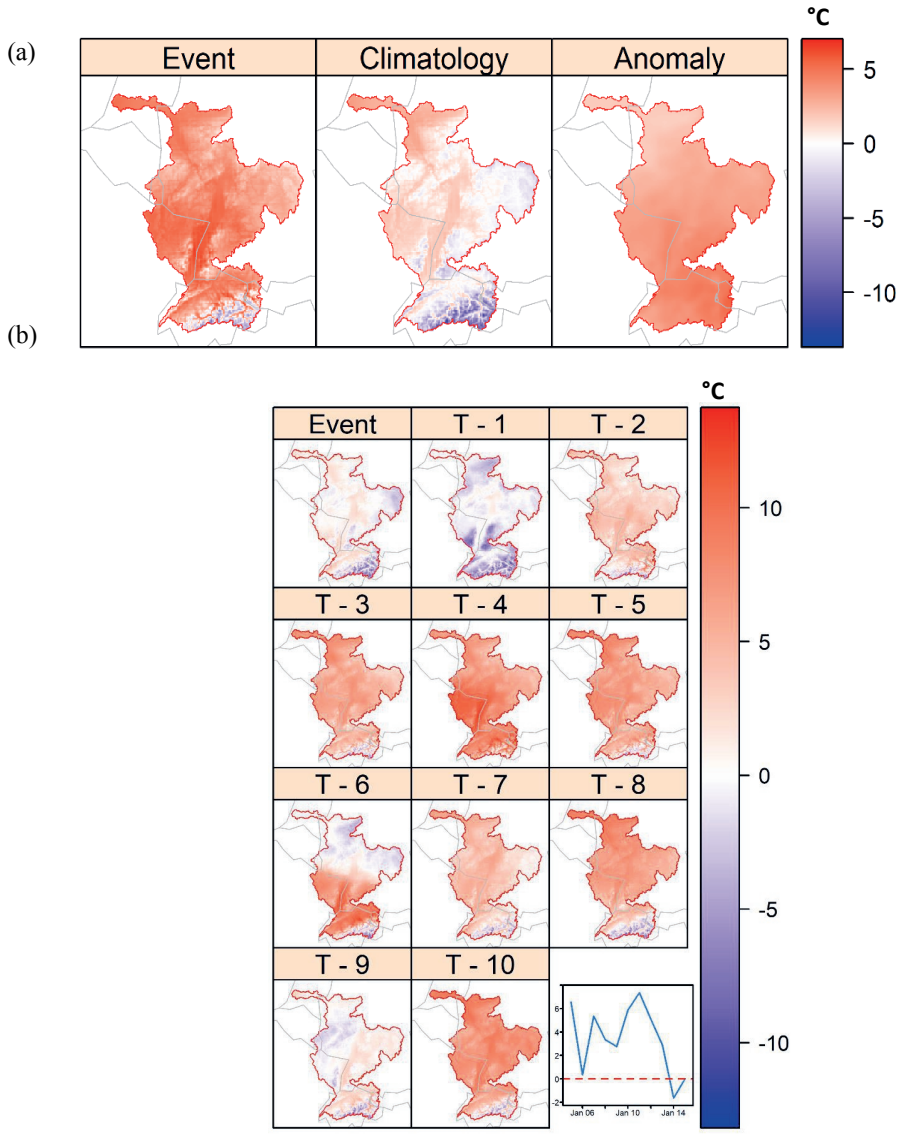

Figure C2: (a) Average temperature over the past 10 days prior to event, climatological mean and its anomaly event for shuffled block one day run. (b) Temperature distribution of 10 days prior to the extreme discharge. The lower right panel shows the timeseries of the basin average value (solid blue line). The horizontal dashed red line denotes the 0° C.

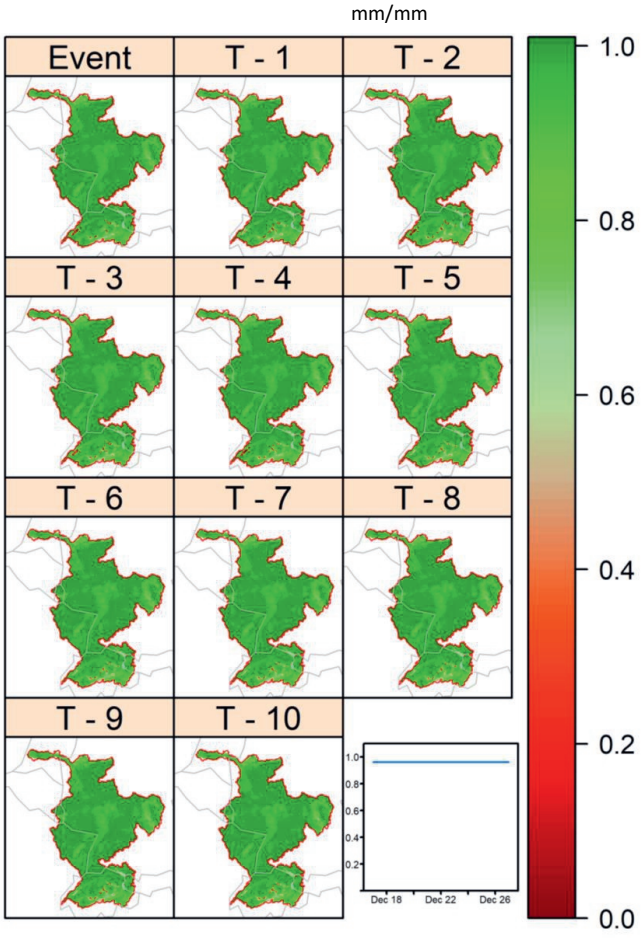

Figure C3: Soil moisture distribution of 10 days prior to the extreme discharge event for the original run. The lower right panel shows the timeseries of the basin average value (solid blue line).

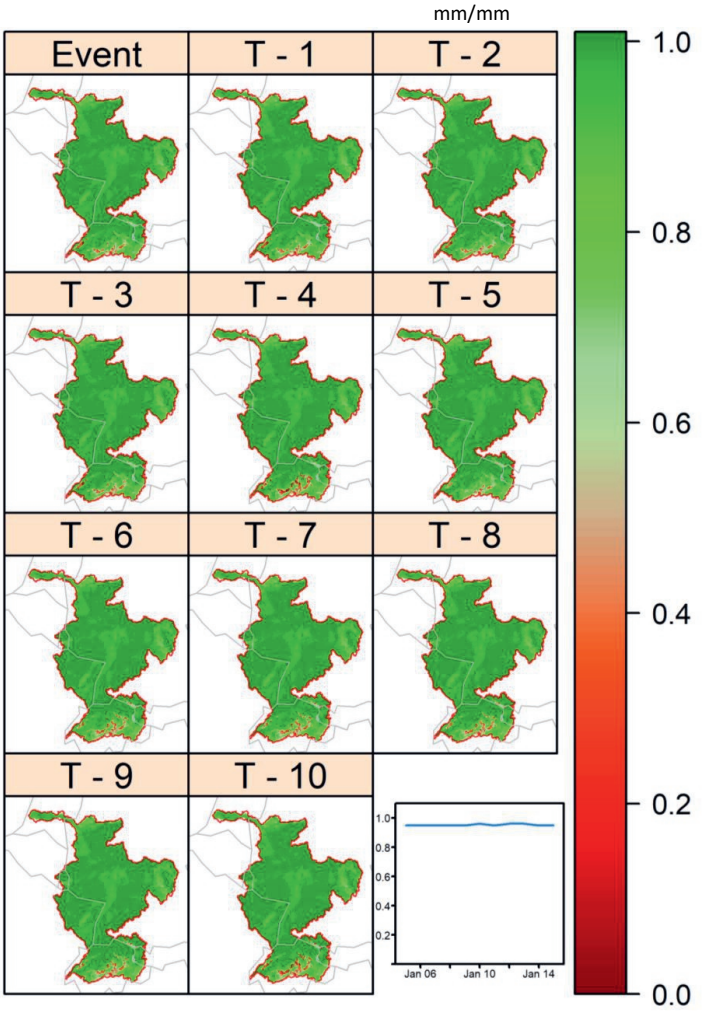

Figure C4: Soil moisture distribution of 10 days prior to the extreme discharge event for the shuffled one-day block run. The lower right panel shows the timeseries of the basin average value (solid blue line).

Appendix D

This appendix contains figures that are not part of the chapter 5 but relate to the results section.

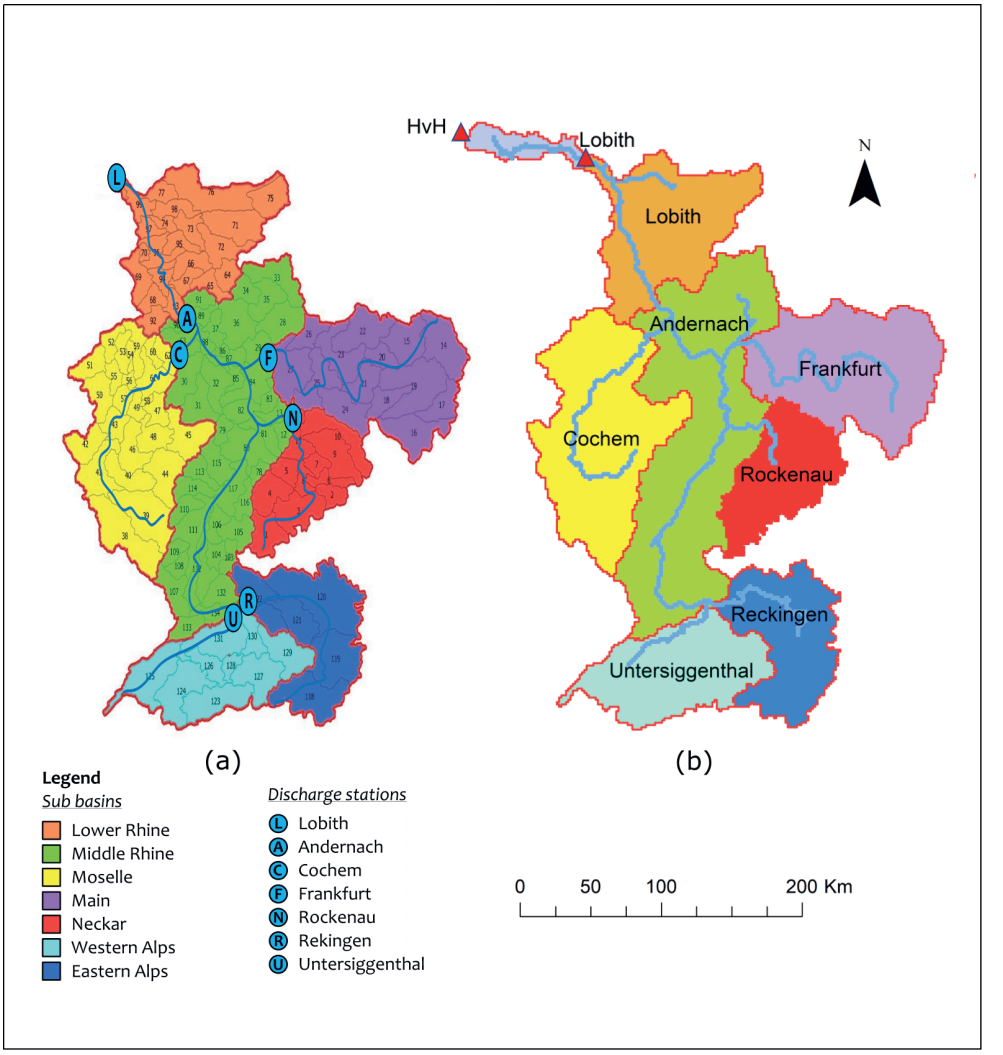

Figure D1: Sub-basin discretization for HBV model (left, Huiskes 2016) and SPHY (right). HBV model used 134 sub basins to calibrate the model whereas, SPHY model was calibrated at 7 sub basins. The major sub-basin in the model is delineated at the same location.

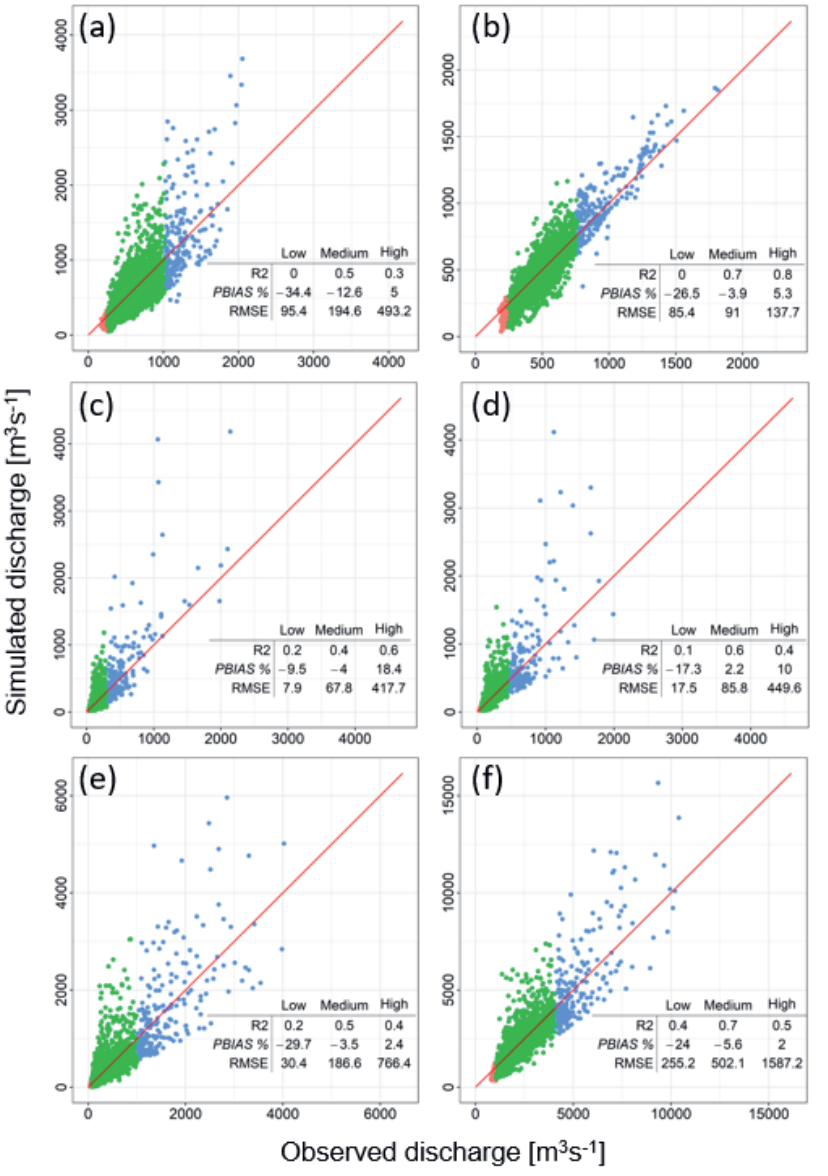

Figure D2: Observed versus modeled daily streamflow at (a) Untersiggenthal (b) Reckingen (c) Rockenau, (d) Frankfurt (e) Cochem and (f) Andernach for SPHY model. Colours indicate three ranges based on observed percentiles: "low" (<5%, red), "med" (5–95%, green) and "high" (>95%, blue). The solid red line represents the 1:1 slope. The tables on the figure represent the performance statistics coefficient of determination (R^2), percent bias (PBIAS, %) and root mean square error (RMSE, m^3s^{-1}) for three ranges of quantiles.

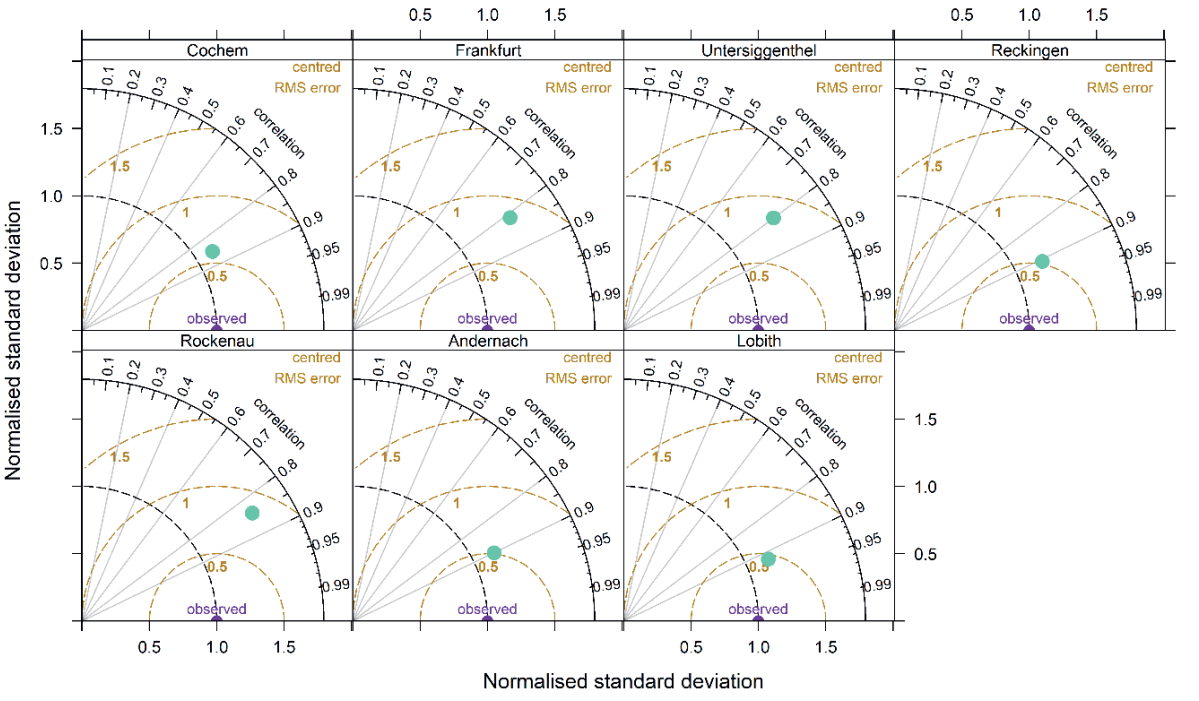

Figure D3: Taylor diagram at different locations for SPHY model. The axis represents the normalized standard deviation (sd). The purple triangle represents the observed and the green dot represents the simulated discharge respectively. These statistics compared here are correlation coefficient (R), sd and root-mean-square error. The plot is made using "TaylorDiagram" function from "open air" R package (Carslaw and Ropkins, 2012).

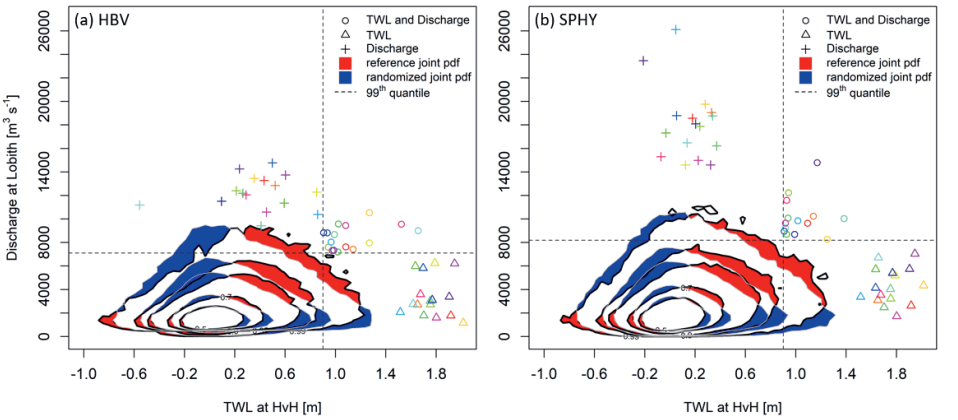

Figure D4: Joint probability density for total water level at HvH and discharge at Lobith (6-day lagged) for winter six months period (left-(a) HBV and right-(b) SPHY). The contours show different quantiles of the joint distribution (50th, 70th, 90th, 95th and 99th). Shading is used to contrast density estimates from direct model output and randomized (shuffled) data, where correlations have been artificially removed. Red/blue shading indicates regions where model data is more/less populated than the shuffled data. The thin dashed lines show the 99% quantiles of each variable in the respective dataset. The colored points correspond to the highest TWL (Δ), discharge (+) and compound events (o) for individual ensemble members.

Equation for the NSE index calculation.

$$NSE = 1 - \frac{\sum_{t=1}^{T}(Q_m^t - Q_o^t)^2}{\sum_{t=1}^{T}(Q_o^t - \bar{Q}_o)^2} \quad \text{(D)}$$

Where;
$\bar{Q}_o$ is the mean of observed discharges.
Q_m is modeled discharges at timestep t.
Q_o is observed discharges at timestep t.

Bibliography

Aas, K., Czado, C., Frigessi, A. and Bakken, H.: Pair-copula constructions of multiple dependence, Insur. Math. Econ., 44(2), 182–198, doi:10.1016/j.insmatheco.2007.02.001, 2009.

Adam, L., Eisner, S., Reinecke, R., Riedel, C., Döll, P., Song, Q., Müller Schmied, H., Fink, G., Zhang, J., Portmann, F. T., Oki, T., Flörke, M. and Kim, H.: Variations of global and continental water balance components as impacted by climate forcing uncertainty and human water use, Hydrol. Earth Syst. Sci., 20(7), 2877–2898, doi:10.5194/hess-20-2877-2016, 2016.

Adhikari, S. and Marshall, S. J.: Influence of high-order mechanics on simulation of glacier response to climate change: Insights from Haig Glacier, Canadian Rocky Mountains, Cryosphere, 7(5), 1527–1541, doi:10.5194/tc-7-1527-2013, 2013.

AghaKouchak, A., Cheng, L., Mazdiyasni, O. and Farahmand, A.: Global warming and changes in risk of concurrent climate extremes: Insights from the 2014 California drought, Geophys. Res. Lett., 41(24), 8847–8852, doi:10.1002/2014GL062308, 2014.

Aich, V., Akhundzadah, N., Knuerr, A., Khoshbeen, A., Hattermann, F., Paeth, H., Scanlon, A. and Paton, E.: Climate change in Afghanistan deduced from reanalysis and coordinated regional climate downscaling experiment (CORDEX)—South Asia simulations, Climate, 5(2), 38, 2017.

Ailliot, P., Allard, D., Monbet, V. and Naveau, P.: Stochastic weather generators: an overview of weather type models, J. la Société Française Stat., 156(1), 101–113, 2015.

Aizen, V. B., Aizen, E. M., Melack, J. M. and Dozier, J.: Climatic and hydrologic changes in the Tien Shan, central Asia, J. Clim., 10(6), 1393–1404, doi:10.1175/1520-0442(1997)010<1393:CAHCIT>2.0.CO;2, 1997.

Alexander, L. V., Zhang, X., Peterson, T. C., Caesar, J., Gleason, B., Klein Tank, A. M. G., Haylock, M., Collins, D., Trewin, B., Rahimzadeh, F., Tagipour, A., Rupa Kumar, K., Revadekar, J., Griffiths, G., Vincent, L., Stephenson, D. B., Burn, J., Aguilar, E., Brunet, M., Taylor, M., New, M., Zhai, P., Rusticucci, M. and Vazquez-Aguirre, J. L.: Global observed changes in daily climate extremes of temperature and precipitation, J. Geophys. Res., 111(D5), D05109, doi:10.1029/2005JD006290, 2006.

Alfieri, L., Bisselink, B., Dottori, F., Naumann, G., de Roo, A., Salamon, P., Wyser, K. and Feyen, L.: Global projections of river flood risk in a warmer world, Earth's Futur., 5(2), 171–182, doi:10.1002/2016EF000485, 2017.

Allen, C. D., Breshears, D. D. and McDowell, N. G.: On underestimation of global vulnerability to tree mortality and forest die-off from hotter drought in the Anthropocene, Ecosphere, 6(8), 1–55, doi:10.1890/ES15-00203.1, 2015.

Allen, R. G., Pereira, L. S., Raes, D. and Smith, M.: Crop Evapotranspiration: Guidelines for Computing Crop Water Requirements, Irrig. Drain. Pap. No. 56, FAO, Rome, Italy, doi:10.4000/trema.1752, 1998.

Almazroui, M., Saeed, S., Saeed, F., Islam, M. N. and Ismail, M.: Projections of Precipitation and Temperature over the South Asian Countries in CMIP6, Earth Syst. Environ., (Lal 2013), doi:10.1007/s41748-020-00157-7, 2020.

Amato, R., Steptoe, H., Buonomo, E. and Jones, R.: High-resolution history: Downscaling china's climate from the 20crv2c reanalysis, J. Appl. Meteorol. Climatol., 58(10), 2141–2157, doi:10.1175/JAMC-D-19-0083.1, 2019.

Amenu, G. G., Kumar, P. and Liang, X.-Z.: Interannual Variability of Deep-Layer Hydrologic Memory and Mechanisms of Its Influence on Surface Energy Fluxes, J. Clim., 18(23), 5024–5045, doi:10.1175/JCLI3590.1, 2005.

Ammon, C. J., Ji, C., Thio, H. K., Robinson, D., Ni, S., Hjorleifsdottir, V., Kanamori, H., Lay, T., Das, S., Helmberger, D., Ichinose, G., Polet, J. and Wald, D.: Rupture process of the 2004 Sumatra-Andaman earthquake, Science (80-.)., 308(5725), 1133–1139, doi:10.1126/science.1112260, 2005.

An, W., Hou, S., Hu, Y. and Wu, S.: Delayed warming hiatus over the Tibetan plateau, Earth Sp. Sci., 4(3), 128–137, doi:10.1002/2016EA000179, 2017.

Andermann, C., Bonnet, S. and Gloaguen, R.: Evaluation of precipitation data sets along the Himalayan front, Geochemistry, Geophys. Geosystems, 12(7), doi:10.1029/2011GC003513, 2011.

Anderson, W. B., Seager, R., Baethgen, W., Cane, M. and You, L.: Synchronous crop failures and climate-forced production variability, Sci. Adv., 5(7), eaaw1976, doi:10.1126/sciadv.aaw1976, 2019.

Anon: The Impact of Meteorological and Hydrological Memory on Compound Peak Flows in the Rhine River Basin, , 1–19, doi:10.3390/atmos10040171, 2019.

Archfield, S. A., Hirsch, R. M., Viglione, A. and Blöschl, G.: Fragmented patterns of flood change across the United States, Geophys. Res. Lett., 43(19), 10,232-10,239, doi:10.1002/2016GL070590, 2016.

Arcomano, T., Szunyogh, I., Pathak, J., Wikner, A., Hunt, B. R. and Ott, E.: A Machine Learning-Based Global Atmospheric Forecast Model, Geophys. Res. Lett., 47(9), e2020GL087776, doi:10.1029/2020GL087776, 2020.

Armstrong, R. L., Rittger, K., Brodzik, M. J., Racoviteanu, A., Barrett, A. P., Khalsa, S. S., Raup, B., Hill, A. F., Khan, A. L., Wilson, A. M., Kayastha, R. B., Fetterer, F., Armstrong, B., Armstrong, R. L., Barrett, A. P. and Hill, A. F.: Runoff from glacier ice and seasonal snow in High Asia : separating melt water sources in river flow, ,

1249–1261, 2019.
Arnold, J. G., Srinivasan, R., Muttiah, R. S. and Williams, J. R.: LARGE AREA HYDROLOGIC MODELING AND ASSESSMENT PART I: MODEL DEVELOPMENT, J. Am. Water Resour. Assoc., 34(1), 73–89, doi:10.1111/j.1752-1688.1998.tb05961.x, 1998.
Ashouri, H., Hsu, K. L., Sorooshian, S., Braithwaite, D. K., Knapp, K. R., Cecil, L. D., Nelson, B. R. and Prat, O. P.: PERSIANN-CDR: Daily precipitation climate data record from multisatellite observations for hydrological and climate studies, Bull. Am. Meteorol. Soc., 96(1), 69–83, doi:10.1175/BAMS-D-13-00068.1, 2015.
Bakhtyar, R., Maitaria, K., Velissariou, P., Trimble, B., Mashriqui, H., Moghimi, S., Abdolali, A., Van der Westhuysen, A. J., Ma, Z., Clark, E. P. and Flowers, T.: A New 1D/2D Coupled Modeling Approach for a Riverine-Estuarine System Under Storm Events: Application to Delaware River Basin, J. Geophys. Res. Ocean., 125(9), e2019JC015822, doi:10.1029/2019JC015822, 2020.
Baldwin, J. W., Dessy, J. B., Vecchi, G. A. and Oppenheimer, M.: Temporally Compound Heat Wave Events and Global Warming: An Emerging Hazard, Earth's Futur., 7(4), 411–427, doi:10.1029/2018EF000989, 2019.
Ballesteros-Cánovas, J. A., Trappmann, D., Madrigal-González, J., Eckert, N. and Stoffel, M.: Climate warming enhances snow avalanche risk in the Western Himalayas, Proc. Natl. Acad. Sci. U. S. A., 115(13), 3410–3415, doi:10.1073/pnas.1716913115, 2018.
Bao, Y. and You, Q.: How do westerly jet streams regulate the winter snow depth over the Tibetan Plateau ? North Atlantic oscillation South Tibetan Plateau jet, Clim. Dyn., 53(1), 353–370, doi:10.1007/s00382-018-4589-1, 2019.
Bárdossy, A.: Calibration of hydrological model parameters for ungauged catchments, Hydrol. Earth Syst. Sci., 11(2), 703–710, doi:10.5194/hess-11-703-2007, 2007.
Bárdossy, A. and Das, T.: Influence of rainfall observation network on model calibration and application, Hydrol. Earth Syst. Sci., 12(1), 77–89, doi:10.5194/hess-12-77-2008, 2008.
Barnard, P. L., Erikson, L. H., Foxgrover, A. C., Hart, J. A. F., Limber, P., O'Neill, A. C., van Ormondt, M., Vitousek, S., Wood, N., Hayden, M. K. and Jones, J. M.: Dynamic flood modeling essential to assess the coastal impacts of climate change, Sci. Rep., 9(1), 1–13, doi:10.1038/s41598-019-40742-z, 2019.
Barnett, T. P., Adam, J. C. and Lettenmaier, D. P.: Potential impacts of a warming climate on water availability in snow-dominated regions, Nature, 438(7066), 303–309, doi:10.1038/nature04141, 2005.
Barton, Y., Giannakaki, P., von Waldow, H., Chevalier, C., Pfahl, S. and Martius, O.: Clustering of regional-scale extreme precipitation events in southern Switzerland, Mon. Weather Rev., 144(1), 347–369, doi:10.1175/MWR-D-15-0205.1, 2016.
Bastola, S. and Murphy, C.: Sensitivity of the performance of a conceptual rainfall-runoff model to the temporal sampling of calibration data, Hydrol. Res., 44(3), 484–494, doi:10.2166/nh.2012.061, 2013.
Bates, P. D., Neal, J., Sampson, C., Smith, A. and Trigg, M.: Progress Toward Hyperresolution Models of Global Flood Hazard, in Risk Modeling for Hazards and Disasters, pp. 211–232, Elsevier., 2018.
BBC: India heatwave: Delhi temperature hits 47C as north India reels - BBC News, [online] Available from: https://www.bbc.com/news/world-asia-india-52816493 (Accessed 9 September 2020), 2020.
Beck, H. E., Van Dijk, A. I. J. M., Levizzani, V., Schellekens, J., Miralles, D. G., Martens, B. and De Roo, A.: MSWEP: 3-hourly 0.25° global gridded precipitation (1979-2015) by merging gauge, satellite, and reanalysis data, Hydrol. Earth Syst. Sci., 21(1), 589–615, doi:10.5194/hess-21-589-2017, 2017.
Beck, H. E., Pan, M., Roy, T., Weedon, G. P., Pappenberger, F., Van Dijk, A. I. J. M., Huffman, G. J., Adler, R. F. and Wood, E. F.: Daily evaluation of 26 precipitation datasets using Stage-IV gauge-radar data for the CONUS, Hydrol. Earth Syst. Sci., 23(1), 207–224, doi:10.5194/hess-23-207-2019, 2019.
Beck, H. E., Wood, E. F., McVicar, T. R., Zambrano-Bigiarini, M., Alvarez-Garreton, C., Baez-Villanueva, O. M., Sheffield, J. and Karger, D. N.: Bias correction of global high-resolution precipitation climatologies using streamflow observations from 9372 catchments, J. Clim., 33(4), 1299–1315, doi:10.1175/JCLI-D-19-0332.1, 2020.
Bedford, T., Daneshkhah, A. and Wilson, K. J.: Approximate Uncertainty Modeling in Risk Analysis with Vine Copulas, Risk Anal., 36(4), 792–815, doi:10.1111/risa.12471, 2016.
Beersma, J.: Extreme hydro-meteorological events and their probabilities, Wagenngen University: Wageningen, The Netherlands. [online] Available from: http://www.knmi.nl/publications/fulltexts/thesis_beersma_21823.pdf, 2007.
Beersma, J. J., Kwadijk, J. C. J. and Lammersen, R.: Effects of climate change on the Rhine discharges, Exploring high end climate change scenarios for flood protection of the Netherlands: An international scientific assessment, Deltares: Delft, The Netherlands., 2008.
Bender, J., Wahl, T., Müller, A. and Jensen, J.: A multivariate design framework for river confluences, Hydrol. Sci. J., 61(3), 471–482, doi:10.1080/02626667.2015.1052816, 2016.
Beniston, M., Farinotti, D., Stoffel, M., Andreassen, L. M., Coppola, E., Eckert, N., Fantini, A., Giacona, F., Hauck, C., Huss, M., Huwald, H., Lehning, M., López-Moreno, J. I., Magnusson, J., Marty, C., Morán-Tejéda, E., Morin, S., Naaim, M., Provenzale, A., Rabatel, A., Six, D., Stötter, J., Strasser, U., Terzago, S. and Vincent, C.: The European mountain cryosphere: A review of its current state, trends, and future challenges, Cryosphere, 12(2),

doi:10.5194/tc-12-759-2018, 2018.
Berghuijs, W. R., Woods, R. A., Hutton, C. J. and Sivapalan, M.: Dominant flood generating mechanisms across the United States, Geophys. Res. Lett., 43(9), doi:10.1002/2016GL068070, 2016.
Berghuijs, W. R., Harrigan, S., Molnar, P., Slater, L. J. and Kirchner, J. W.: The Relative Importance of Different Flood-Generating Mechanisms Across Europe, Water Resour. Res., 55(6), 4582–4593, doi:10.1029/2019WR024841, 2019.
Bergström, S.: Development and application of a conceptual runoff model for Scandinavian catchments, Bull. Ser. A, 52(NO 7), 134, 1976.
Bergström, S.: The HBV model - its structure and applications, Swedish Meteorol. Hydrol. Inst. Reports Hydrol., doi:10.3368/le.88.4.685, 1992.
Bevacqua, E., Maraun, D., Hobæk Haff, I., Widmann, M. and Vrac, M.: Multivariate statistical modelling of compound events via pair-copula constructions: Analysis of floods in Ravenna (Italy), Hydrol. Earth Syst. Sci., doi:10.5194/hess-21-2701-2017, 2017.
Bevacqua, E., Maraun, D., Vousdoukas, M. I., Voukouvalas, E., Vrac, M., Mentaschi, L. and Widmann, M.: Higher probability of compound flooding from precipitation and storm surge in Europe under anthropogenic climate change, Sci. Adv., 5(9), eaaw5531, doi:10.1126/sciadv.aaw5531, 2019.
Bevacqua, E., Vousdoukas, M. I., Zappa, G., Hodges, K., Shepherd, T. G., Maraun, D., Mentaschi, L. and Feyen, L.: More meteorological events that drive compound coastal flooding are projected under climate change, Commun. Earth Environ., 1(1), doi:10.1038/s43247-020-00044-z, 2020.
Beven, K.: How far can we go in distributed hydrological modelling?, Hydrol. Earth Syst. Sci., 5(1), 1–12, doi:10.5194/hess-5-1-2001, 2001.
Beven, K.: Robert E. Horton's perceptual model of infiltration processes, Hydrol. Process., 18(17), 3447–3460, doi:10.1002/hyp.5740, 2004.
Beven, K.: Rainfall-Runoff Modelling: The Primer., 2012.
Biancamaria, S., Bates, P. D., Boone, A. and Mognard, N. M.: Large-scale coupled hydrologic and hydraulic modelling of the Ob river in Siberia, J. Hydrol., 379(1–2), 136–150, doi:10.1016/j.jhydrol.2009.09.054, 2009.
Biemans, H., Siderius, C., Lutz, A. F., Ahmad, B., Hassan, T., Bloh, W. Von, Wijngaard, R. R., Wester, P., Shrestha, A. B. and Immerzeel, W. W.: Importance of snow and glacier meltwater for agriculture on the Indo-Gangetic Plain, Nat. Sustain., 2(July), doi:10.1038/s41893-019-0305-3, 2019.
Bierkens, M. F. P. and van den Hurk, B. J. J. M.: Groundwater convergence as a possible mechanism for multi-year persistence in rainfall, Geophys. Res. Lett., 34(2), 1–5, doi:10.1029/2006GL028396, 2007.
Bierkens, M. F. P., Finke, P. and Willigen, P.: Upscaling and Downscaling Methods for Environmental Research, Dordr. etc., Kluwer, 2000. Dev. Plant Soil Sci. 88, 190 pp, 88, 2001.
Bierkens, M. F. P., Bell, V. A., Burek, P., Chaney, N., Condon, L. E., David, C. H., De Roo, A., Döll, P., Drost, N., Famiglietti, J. S., Flörke, M., Keune, J., Kollet, S., Maxwell, R. M., Reager, J. T., Samaniego, L., Sudicky, E., Sutanudjaja, E. H. and Wood, E. F.: Hyper-resolution global hydrological modelling: what is next? " Everywhere and locally relevant ", Hydrol. Process., doi:10.1002/hyp.10391, 2015.
Bilskie, M. V. and Hagen, S. C.: Defining Flood Zone Transitions in Low-Gradient Coastal Regions, Geophys. Res. Lett., 45(6), 2761–2770, doi:10.1002/2018GL077524, 2018.
Bilskie, M. V., Hagen, S. C., Medeiros, S. C. and Passeri, D. L.: Dynamics of sea level rise and coastal flooding on a changing landscape, Geophys. Res. Lett., 41(3), 927–934, doi:10.1002/2013GL058759, 2014.
Birkmann, J., Buckle, P., Jaeger, J., Pelling, M., Setiadi, N., Garschagen, M., Fernando, N. and Kropp, J.: Extreme events and disasters: A window of opportunity for change? Analysis of organizational, institutional and political changes, formal and informal responses after mega-disasters, Nat. Hazards, 55(3), 637–655, doi:10.1007/s11069-008-9319-2, 2010.
Bisht, D. S., Chatterjee, C., Raghuwanshi, N. S. and Sridhar, V.: Spatio-temporal trends of rainfall across Indian river basins, Theor. Appl. Climatol., 132(1–2), 419–436, doi:10.1007/s00704-017-2095-8, 2018.
Biskaborn, B. K., Smith, S. L., Noetzli, J., Matthes, H., Vieira, G., Streletskiy, D. A., Schoeneich, P., Romanovsky, V. E., Lewkowicz, A. G., Abramov, A., Allard, M., Boike, J., Cable, W. L., Christiansen, H. H., Delaloye, R., Diekmann, B., Drozdov, D., Etzelmüller, B., Grosse, G., Guglielmin, M., Ingeman-Nielsen, T., Isaksen, K., Ishikawa, M., Johansson, M., Johannsson, H., Joo, A., Kaverin, D., Kholodov, A., Konstantinov, P., Kröger, T., Lambiel, C., Lanckman, J. P., Luo, D., Malkova, G., Meiklejohn, I., Moskalenko, N., Oliva, M., Phillips, M., Ramos, M., Sannel, A. B. K., Sergeev, D., Seybold, C., Skryabin, P., Vasiliev, A., Wu, Q., Yoshikawa, K., Zheleznyak, M. and Lantuit, H.: Permafrost is warming at a global scale, Nat. Commun., 10(1), 1–11, doi:10.1038/s41467-018-08240-4, 2019.
Black, R., Arnell, N. W., Adger, W. N., Thomas, D. and Geddes, A.: Migration, immobility and displacement outcomes following extreme events, Environ. Sci. Policy, 27, S32–S43, doi:10.1016/j.envsci.2012.09.001, 2013.
Blender, R. and Fraedrich, K.: Long-term memory of the hydrological cycle and river runoffs in China in a high-resolution climate model, Int. J. Climatol., 26(12), 1547–1565, doi:10.1002/joc.1325, 2006.
Blöschl, G. and Sivapalan, M.: Scale issues in hydrological modelling: A review, Hydrol. Process., 9(3–4), 251–

290, doi:10.1002/hyp.3360090305, 1995.
Blöschl, G. and Zehe, E.: On hydrological predictability, Hydrol. Process., 19(19), 3923–3929, doi:10.1002/hyp.6075, 2005.
Blöschl, G., Hall, J., Parajka, J., Perdigão, R. A. P., Merz, B., Arheimer, B., Aronica, G. T., Bilibashi, A., Bonacci, O., Borga, M., Ivan, Č., Castellarin, A. and Chirico, G. B.: European floods, Science (80-.)., 357(6351), 588–590, doi:10.1126/science.aan2506, 2017.
Blöschl, G., Kiss, A., Viglione, A., Barriendos, M., Böhm, O., Brázdil, R., Coeur, D., Demarée, G., Llasat, M. C., Macdonald, N., Retsö, D., Roald, L., Schmocker-Fackel, P., Amorim, I., Bělínová, M., Benito, G., Bertolin, C., Camuffo, D., Cornel, D., Doktor, R., Elleder, L., Enzi, S., Garcia, J. C., Glaser, R., Hall, J., Haslinger, K., Hofstätter, M., Komma, J., Limanówka, D., Lun, D., Panin, A., Parajka, J., Petrić, H., Rodrigo, F. S., Rohr, C., Schönbein, J., Schulte, L., Silva, L. P., Toonen, W. H. J., Valent, P., Waser, J. and Wetter, O.: Current European flood-rich period exceptional compared with past 500 years, Nature, 583(7817), 560–566, doi:10.1038/s41586-020-2478-3, 2020.
Boer, F. D.: HiHydroSoil : A high resolution soil map of hydraulic properties (Version 1.2), Rep. Futur. 134, 31(January), 1–32, 2016.
Boers, N., Goswami, B., Rheinwalt, A., Bookhagen, B., Hoskins, B. and Kurths, J.: Complex networks reveal global pattern of extreme-rainfall teleconnections, Nature, 566(7744), 373–377, doi:10.1038/s41586-018-0872-x, 2019.
Bojariu, R. and Gimeno, L.: The role of snow cover fluctuations in multiannual NAO persistence, Geophys. Res. Lett., 30(4), 1–4, doi:10.1029/2002GL015651, 2003.
Bolch, T., Kulkarni, A., Kääb, A., Huggel, C., Paul, F., Cogley, J. G., Frey, H., Kargel, J. S., Fujita, K., Scheel, M., Bajracharya, S. and Stoffel, M.: The state and fate of himalayan glaciers, Science (80-.)., 336(6079), 310–314, doi:10.1126/science.1215828, 2012.
Bonan, G. B. and Stillwell-soller, L. M.: Soil water and the persistence of floods and droughts in the Mississippi River Basin, Water Resour. Res., 34(10), 2693–2701, 1998.
Bonekamp, P. N. J., de Kok, R. J., Collier, E. and Immerzeel, W. W.: Contrasting meteorological drivers of the glacier mass balance between the Karakoram and central Himalaya, Front. Earth Sci., 7(June), 1–14, doi:10.3389/feart.2019.00107, 2019.
Bonekamp, P. N. J., Wanders, N., Wiel, K., Lutz, A. F. and Immerzeel, W. W.: Using large ensemble modelling to derive future changes in mountain specific climate indicators in a 2 °C and 3 °C warmer world in High Mountain Asia, Int. J. Climatol., doi:10.1002/joc.6742, 2020.
Bookhagen, B. and Burbank, D. W.: Topography, relief, and TRMM-derived rainfall variations along the Himalaya, Geophys. Res. Lett., 33(8), 1–5, doi:10.1029/2006GL026037, 2006.
Bookhagen, B. and Burbank, D. W.: Toward a complete Himalayan hydrological budget: Spatiotemporal distribution of snowmelt and rainfall and their impact on river discharge, J. Geophys. Res. Earth Surf., 115(3), 1–25, doi:10.1029/2009JF001426, 2010.
Boukabara, S.-A., Krasnopolsky, V., Stewart, J., Penny, S., Hoffman, R. and Maddy, E.: Artificial Intelligence May Be Key to Better Weather Forecasts, Eos (Washington. DC)., 100(August 2020), doi:10.1029/2019eo129967, 2019.
Bowling, L. C., Pomeroy, J. W. and Lettenmaier, D. P.: Parameterization of Blowing-Snow Sublimation in a Macroscale Hydrology Model, J. Hydrometeorol., doi:10.1175/1525-7541(2004)005<0745:POBSIA>2.0.CO;2, 2004.
Braithwaite, R. J.: Temperature and precipitation climate at the equilibrium-line altitude of glaciers expressed by the degree-day factor for melting snow, J. Glaciol., 54(186), 437–444, doi:10.3189/002214308785836968, 2008.
Braithwaite, R. J. and Zhang, Y.: Sensitivity of mass balance of five Swiss glaciers to temperature changes assessed by tuning a degree-day model, J. Glaciol., doi:10.3189/172756500781833511, 2000.
Brenowitz, N. D. and Bretherton, C. S.: Prognostic Validation of a Neural Network Unified Physics Parameterization, Geophys. Res. Lett., 45(12), 6289–6298, doi:10.1029/2018GL078510, 2018.
Brienen, S., Rust, H. W., Sauter, T., Themeßl, M., Venema, V. K. C., Chun, K. P., Maraun, D., Wetterhall, F., Ireson, A. M., Chandler, R. E., Kendon, E. J., Widmann, M., Goodess, C. M., Jones, R. G., Onof, C., Vrac, M. and Thiele-Eich, I.: Precipitation Downscaling Under Climate Change : Recent Developments To Bridge the Gap Between Dynamical Models and the End User, Rev. Geophys., 48(2009), 1–34, doi:10.1029/2009RG000314.1.INTRODUCTION, 2010.
Brigode, P., Oudin, L. and Perrin, C.: Hydrological model parameter instability: A source of additional uncertainty in estimating the hydrological impacts of climate change?, J. Hydrol., 476, 410–425, doi:10.1016/j.jhydrol.2012.11.012, 2013.
van den Brink, H. W., Können, G. P., Opsteegh, J. D., van Oldenborgh, G. J. and Burgers, G.: Estimating return periods of extreme events from ECMWF seasonal forecast ensembles, Int. J. Climatol., 25(10), 1345–1354, doi:10.1002/joc.1155, 2005.
Brun, F.: Impact of the debris cover on High Mountain Asia glacier mass balances : a multi-scale approach,

Université Grenoble Alpes., 2018.
Brun, F., Berthier, E., Wagnon, P., Kääb, A. and Treichler, D.: A spatially resolved estimate of High Mountain Asia glacier mass balances from 2000 to 2016, Nat. Geosci., 10, 668 [online] Available from: https://doi.org/10.1038/ngeo2999, 2017.
Brun, F., Wagnon, P., Berthier, E., Shea, J. M., Immerzeel, W. W., Kraaijenbrink, P. D. A., Vincent, C., Reverchon, C., Shrestha, D. and Arnaud, Y.: Ice cliff contribution to the tongue-wide ablation of Changri Nup Glacier, Nepal, central Himalaya, Cryosphere, doi:10.5194/tc-12-3439-2018, 2018.
Brunner, M. I., Seibert, J. and Favre, A.-C.: Bivariate return periods and their importance for flood peak and volume estimation, Wiley Interdiscip. Rev. Water, 3(6), 819–833, doi:10.1002/wat2.1173, 2016.
Bunde, A., Eichner, J. F., Kantelhardt, J. W. and Havlin, S.: Long-term memory: A natural mechanism for the clustering of extreme events and anomalous residual times in climate records, Phys. Rev. Lett., 94(4), 1–4, doi:10.1103/PhysRevLett.94.048701, 2005.
Buri, P., Miles, E. S., Steiner, J. F., Ragettli, S. and Pellicciotti, F.: Supraglacial Ice Cliffs Can Substantially Increase the Mass Loss of Debris-Covered Glaciers, Geophys. Res. Lett., 48(6), doi:10.1029/2020gl092150, 2021.
Caesar, J., Alexander, L. V., Trewin, B., Tse-ring, K., Sorany, L., Vuniyayawa, V., Keosavang, N., Shimana, A., Htay, M. M., Karmacharya, J., Jayasinghearachchi, D. A., Sakkamart, J., Soares, E., Hung, L. T., Thuong, L. T., Hue, C. T., Dung, N. T. T., Hung, P. V., Cuong, H. D., Cuong, N. M. and Sirabaha, S.: Changes in temperature and precipitation extremes over the Indo-Pacific region from 1971 to 2005, Int. J. Climatol., 31(6), 791–801, doi:10.1002/joc.2118, 2011.
Cai, W., Wang, G., Dewitte, B., Wu, L., Santoso, A., Takahashi, K., Yang, Y., Carréric, A. and McPhaden, M. J.: Increased variability of eastern Pacific El Niño under greenhouse warming, Nature, 564(7735), 201, 2018.
Cannon, F., Carvalho, L. M. V., Jones, C. and Norris, J.: Winter westerly disturbance dynamics and precipitation in the western Himalaya and Karakoram: a wave-tracking approach, Theor. Appl. Climatol., 125(1–2), 27–44, doi:10.1007/s00704-015-1489-8, 2016.
Cao, B., Gruber, S., Zheng, D. and Li, X.: The ERA5-Land Soil-Temperature Bias in Permafrost Regions, , (April), 1–22, 2020.
Cao, L., Zhao, P., Yan, Z., Jones, P., Zhu, Y., Yu, Y. and Tang, G.: Instrumental temperature series in eastern and central China back to the nineteenth century, J. Geophys. Res. Atmos., 118(15), 8197–8207, doi:10.1002/jgrd.50615, 2013.
Cao, L., Yan, Z., Zhao, P., Zhu, Y., Yu, Y., Tang, G. and Jones, P.: Climatic warming in China during 1901-2015 based on an extended dataset of instrumental temperature records, Environ. Res. Lett., 12(6), doi:10.1088/1748-9326/aa68e8, 2017.
Carenzo, M., Pellicciotti, F., Rimkus, S. and Burlando, P.: Assessing the transferability and robustness of an enhanced temperature-index glacier-melt model, J. Glaciol., 55(190), 258–274, doi:10.3189/002214309788608804, 2009.
Carslaw, D. and Ropkins, K.: openair - An R package for air quality data analysis, Environ. Model. Softw., 27–28, 52–61, doi:10.1016/j.envsoft.2011.09.008, 2012.
Castellarin, A., Kohnová, S., Gaál, L., Fleig, A., Salinas, J. L., Toumazis, A., Kjeldsen, T. and Macdonald, N.: Review of applied-statistical methods for flood-frequency analysis in Europe, Rev. Applied-statistical Methods Flood-frequency Anal. Eur., 2012.
CAWater: CAWater Info :: Portal of Knowledge for Water and Environmental Issues in Central Asia, [online] Available from: http://www.cawater-info.net/index_e.htm (Accessed 15 July 2020), 2020.
Cazorzi, F. and Dalla Fontana, G.: Snowmelt modelling by combining air temperature and a distributed radiation index, J. Hydrol., 181(1–4), 169–187, doi:10.1016/0022-1694(95)02913-3, 1996.
Chandler, R. E.: On the use of generalized linear models for interpreting climate variability, Environmetrics, 16(7), 699–715, doi:10.1002/env.731, 2005.
Chanson, H.: Hydraulics of Open Channel Flow - 2nd Edition. [online] Available from: https://www.elsevier.com/books/hydraulics-of-open-channel-flow/chanson/978-0-7506-5978-9 (Accessed 19 April 2021), 2004.
Chantry, M., Christensen, H., Dueben, P. and Palmer, T.: Opportunities and challenges for machine learning in weather and climate modelling: Hard, medium and soft AI, Philos. Trans. R. Soc. A Math. Phys. Eng. Sci., 379(2194), doi:10.1098/rsta.2020.0083, 2021.
Chaudhry, M. H.: Open-channel flow, Springer Science \& Business Media., 2007.
Che, Y., Zhang, M., Li, Z., Wei, Y., Nan, Z., Li, H., Wang, S. and Su, B.: Energy balance model of mass balance and its sensitivity to meteorological variability on Urumqi River Glacier No.1 in the Chinese Tien Shan, Sci. Rep., 9(1), 1–13, doi:10.1038/s41598-019-50398-4, 2019.
Chebana, F. and Ouarda, T. B. M. J.: Index flood-based multivariate regional frequency analysis, Water Resour. Res., 45(10), 1–15, doi:10.1029/2008WR007490, 2009.
Cheema, M. J. M. and Bastiaanssen, W. G. M.: Local calibration of remotely sensed rainfall from the TRMM satellite for different periods and spatial scales in the Indus Basin, Int. J. Remote Sens., 33(8), 2603–2627,

doi:10.1080/01431161.2011.617397, 2012.
Chen, F., Huang, W., Jin, L., Chen, J. and Wang, J.: Spatiotemporal precipitation variations in the arid Central Asia in the context of global warming, Sci. China Earth Sci., 54(12), 1812–1821, 2011.
Chen, L. and Guo, S.: Copulas and Its Application in Hydrology and Water Resources. [online] Available from: http://link.springer.com/10.1007/978-981-13-0574-0, 2019.
Chen, Y., Takeuchi, K., Xu, C., Chen, Y. and Xu, Z.: Regional climate change and its effects on river runoff in the Tarim Basin, China, Hydrol. Process., 20(10), 2207–2216, doi:10.1002/hyp.6200, 2006.
Chevallier, F., Morcrette, J.-J., Chéruy, F. and Scott, N. A.: Use of a neural-network-based long-wave radiative-transfer scheme in the ECMWF atmospheric model, Q. J. R. Meteorol. Soc., 126(563), 761–776, doi:10.1002/qj.49712656318, 2000.
Choi, G., Collins, D., Ren, G., Trewin, B., Baldi, M., Fukuda, Y., Afzaal, M., Pianmana, T., Gomboluudev, P., Huong, P. T. T., Lias, N., Kwon, W. T., Boo, K. O., Cha, Y. M. and Zhou, Y.: Changes in means and extreme events of temperature and precipitation in the Asia-Pacific Network region, 1955-2007, Int. J. Climatol., 29(13), 1906–1925, doi:10.1002/joc.1979, 2009.
Te Chow, V.: Applied hydrology, Tata McGraw-Hill Education., 2010.
Christensen, J. H., Boberg, F., Christensen, O. B. and Lucas-Picher, P.: On the need for bias correction of regional climate change projections of temperature and precipitation, Geophys. Res. Lett., 35(20), doi:10.1029/2008GL035694, 2008.
Clark, M. P., Nijssen, B., Lundquist, J. D., Kavetski, D., Rupp, D. E., Woods, R. A., Freer, J. E., Gutmann, E. D., Wood, A. W., Gochis, D. J., Rasmussen, R. M., Tarboton, D. G., Mahat, V., Flerchinger, G. N. and Marks, D. G.: A unified approach for process-based hydrologic modeling: 2. Model implementation and case studies, Water Resour. Res., 51(4), 2515–2542, doi:10.1002/2015WR017200, 2015a.
Clark, M. P., Fan, Y., Lawrence, D. M., Adam, J. C., Bolster, D., Gochis, D. J., Hooper, R. P., Kumar, M., Leung, L. R., Mackay, D. S., Maxwell, R. M., Shen, C., Swenson, S. C. and Zeng, X.: Improving the representation of hydrologic processes in Earth System Models, Water Resour. Res., 51(8), 5929–5956, doi:10.1002/2015WR017096, 2015b.
Clark, M. P., Bierkens, M. F. P., Samaniego, L., Woods, R. A., Uijlenhoet, R., Bennett, K. E., Pauwels, V. R. N., Cai, X., Wood, A. W. and Peters-Lidard, C. D.: The evolution of process-based hydrologic models: Historical challenges and the collective quest for physical realism, Hydrol. Earth Syst. Sci., 21(7), 3427–3440, doi:10.5194/hess-21-3427-2017, 2017.
Coenders-Gerrits, A. M. J., Van Der Ent, R. J., Bogaard, T. A., Wang-Erlandsson, L., Hrachowitz, M. and Savenije, H. H. G.: Uncertainties in transpiration estimates, Nature, 506(7487), E1–E2, doi:10.1038/nature12925, 2014.
Coffel, E. D., Keith, B., Lesk, C., Horton, R. M., Bower, E., Lee, J. and Mankin, J. S.: Future Hot and Dry Years Worsen Nile Basin Water Scarcity Despite Projected Precipitation Increases, Earth's Futur., 7(8), 967–977, doi:10.1029/2019EF001247, 2019.
Cohen, J. and Fletcher, C.: Improved skill of northern hemisphere winter surface temperature predictions based on land-atmosphere fall anomalies, J. Clim., 20(16), 4118–4132, doi:10.1175/JCLI4241.1, 2007.
Cohen, J. and Rind, D.: The Effect of Snow Cover on the Climate, J. Clim., 4(7), 689–706, doi:10.1175/1520-0442(1991)004<0689:TEOSCO>2.0.CO;2, 1991.
Cohen, J., Screen, J. A., Furtado, J. C., Barlow, M., Whittleston, D., Coumou, D., Francis, J., Dethloff, K., Entekhabi, D., Overland, J. and Jones, J.: Recent Arctic amplification and extreme mid-latitude weather, Nat. Geosci., 7(9), 627–637, doi:10.1038/ngeo2234, 2014.
Cohen, J., Zhang, X., Francis, J., Jung, T., Kwok, R., Overland, J., Ballinger, T. J., Bhatt, U. S., Chen, H. W., Coumou, D., Feldstein, S., Gu, H., Handorf, D., Henderson, G., Ionita, M., Kretschmer, M., Laliberte, F., Lee, S., Linderholm, H. W., Maslowski, W., Peings, Y., Pfeiffer, K., Rigor, I., Semmler, T., Stroeve, J., Taylor, P. C., Vavrus, S., Vihma, T., Wang, S., Wendisch, M., Wu, Y. and Yoon, J.: Divergent consensuses on Arctic amplification influence on midlatitude severe winter weather., 2020.
Cohen, J. L., Furtado, J. C., Barlow, M. A., Alexeev, V. A. and Cherry, J. E.: Arctic warming, increasing snow cover and widespread boreal winter cooling, Environ. Res. Lett., 7(1), doi:10.1088/1748-9326/7/1/014007, 2012.
Coles, S.: An Introduction to Statistical Modeling of Extreme Values, Springer London, London., 2001.
Colgan, W., Rajaram, H., Abdalati, W., McCutchan, C., Mottram, R., Moussavi, M. S. and Grigsby, S.: Glacier crevasses: Observations, models, and mass balance implications, Rev. Geophys., doi:10.1002/2015RG000504, 2016.
Collier, E. and Immerzeel, W. W.: High-resolution modeling of atmospheric dynamics in the Nepalese Himalaya, J. Geophys. Res., 120(19), 9882–9896, doi:10.1002/2015JD023266, 2015.
Collier, E., Mölg, T., Maussion, F., Scherer, D., Mayer, C. and Bush, A. B. G.: High-resolution interactive modelling of the mountain glacier-atmosphere interface: An application over the Karakoram, Cryosphere, doi:10.5194/tc-7-779-2013, 2013.
Collins, M., Sutherland, M., Bouwer, L., Cheong, S.-M., Frölicher, T. L., Jacot Des Combes, H., Roxy, M. K.,

Losada, I., McInnes, K., Ratter, B., Rivera-Arriaga, E., Susanto, R. D., Swingedouw, D., Tibig, L., Bakker, P., Eakin, C. M., Emanuel, K., Grose, M., Hemer, M., Jackson, L., Kääb, A., Kajtar, J. B., Knutson, T., Laufkötter, C., Noy, I., Payne, M., Ranasinghe, R., Sgubin, G. and Timmermans, M.-L.: Extremes, Abrupt Changes and Managing Risks, IPCC Spec. Rep. Ocean Cryosph. a Chang. Clim., 589–655 [online] Available from: https://report.ipcc.ch/srocc/pdf/SROCC_FinalDraft_Chapter6.pdf, 2019.

Cong, Z., Zhao, J., Yang, D. and Ni, G.: Understanding the hydrological trends of river basins in China, J. Hydrol., 388(3–4), 350–356, doi:10.1016/j.jhydrol.2010.05.013, 2010.

Cook, M. A., King, C. W., Davidson, F. T. and Webber, M. E.: Assessing the impacts of droughts and heat waves at thermoelectric power plants in the United States using integrated regression, thermodynamic, and climate models, Energy Reports, 1, 193–203, doi:10.1016/j.egyr.2015.10.002, 2015.

Cook, S. J. and Quincey, D. J.: Estimating the volume of Alpine glacial lakes, Earth Surf. Dyn. Discuss., 3(3), 909–940, doi:10.5194/esurfd-3-909-2015, 2015.

Cucchi, M., Weedon, G., Amici, A., Bellouin, N., Lange, S., Schmied, H. M., Hersbach, H. and Buontempo, C.: WFDE5: bias adjusted ERA5 reanalysis data for impact studies, Earth Syst. Sci. Data Discuss., (April), 1–32, doi:10.5194/essd-2020-28, 2020.

Culley, S., Noble, S., Yates, A., Timbs, M., Westra, S., Maier, H. R., Giuliani, M. and Castelletti, A.: A bottom-up approach to identifying the maximum operational adaptive capacity of water resource systems to a changing climate, Water Resour. Res., 52(9), 6751–6768, doi:10.1002/2015WR018253, 2016.

Cunge, J. A.: On the subject of a flood propagation computation method (musklngum method), J. Hydraul. Res., 7(2), 205–230, doi:10.1080/00221686909500264, 1969.

Cuo, L., Zhang, Y., Wang, Q., Zhang, L., Zhou, B., Hao, Z. and Su, F.: Climate change on the northern Tibetan Plateau during 1957-2009: Spatial patterns and possible mechanisms, J. Clim., 26(1), 85–109, doi:10.1175/JCLI-D-11-00738.1, 2013.

D'Ippoliti, D., Michelozzi, P., Marino, C., De'Donato, F., Menne, B., Katsouyanni, K., Kirchmayer, U., Analitis, A., Medina-Ramón, M., Paldy, A., Atkinson, R., Kovats, S., Bisanti, L., Schneider, A., Lefranc, A., Iñiguez, C. and Perucci, C. A.: The impact of heat waves on mortality in 9 European cities: Results from the EuroHEAT project, Environ. Heal. A Glob. Access Sci. Source, 9(1), 1–9, doi:10.1186/1476-069X-9-37, 2010.

Dai, A.: Increasing drought under global warming in observations and models, Nat. Clim. Chang., 3(1), 52–58, doi:10.1038/nclimate1633, 2013.

Daneshkhah, A., Remesan, R., Chatrabgoun, O. and Holman, I. P.: Probabilistic modeling of flood characterizations with parametric and minimum information pair-copula model, J. Hydrol., 540, 469–487, doi:10.1016/j.jhydrol.2016.06.044, 2016.

Dash, S. K. and Mamgain, A.: Changes in the frequency of different categories of temperature extremes in India, J. Appl. Meteorol. Climatol., 50(9), 1842–1858, doi:10.1175/2011JAMC2687.1, 2011.

Dash, S. K., Jenamani, R. K., Kalsi, S. R. and Panda, S. K.: Some evidence of climate change in twentieth-century India, Clim. Change, 85(3–4), 299–321, doi:10.1007/s10584-007-9305-9, 2007.

Davison, A. C., Padoan, S. A. and Ribatet, M.: Statistical Modeling of Spatial Extremes, Stat. Sci., 27(2), 161–186, doi:10.1214/11-STS376, 2012.

Dee, D. P., Uppala, S. M., Simmons, A. J., Berrisford, P., Poli, P., Kobayashi, S., Andrae, U., Balmaseda, M. A., Balsamo, G., Bauer, P., Bechtold, P., Beljaars, A. C. M., van de Berg, L., Bidlot, J., Bormann, N., Delsol, C., Dragani, R., Fuentes, M., Geer, A. J., Haimberger, L., Healy, S. B., Hersbach, H., Hólm, E. V., Isaksen, L., Kållberg, P., Köhler, M., Matricardi, M., Mcnally, A. P., Monge-Sanz, B. M., Morcrette, J. J., Park, B. K., Peubey, C., de Rosnay, P., Tavolato, C., Thépaut, J. N. and Vitart, F.: The ERA-Interim reanalysis: Configuration and performance of the data assimilation system, Q. J. R. Meteorol. Soc., 137(656), 553–597, doi:10.1002/qj.828, 2011.

Delworth, T. L. and Manabe, S.: The Influence of Potential Evaporation on the Variabilities of Simulated Soil Wetness and Climate, J. Clim., 1(5), 523–547, doi:10.1175/1520-0442(1988)001<0523:TIOPEO>2.0.CO;2, 1988.

Deng, H. and Chen, Y.: Influences of recent climate change and human activities on water storage variations in Central Asia, J. Hydrol., 544, 46–57, 2017.

Derbyshire, J.: The siren call of probability: Dangers associated with using probability for consideration of the future, Futures, 88, 43–54, doi:10.1016/j.futures.2017.03.011, 2017.

Deschenes, O.: Temperature, human health, and adaptation: A review of the empirical literature, Energy Econ., 46, 606–619, doi:10.1016/j.eneco.2013.10.013, 2014.

Deser, C., Knutti, R., Solomon, S. and Phillips, A. S.: Communication of the role of natural variability in future North American climate, Nat. Clim. Chang., 2(11), 775–779, doi:10.1038/nclimate1562, 2012.

Deursen, W. P. A.: Geographic Information Systems and Dynamic Models, Netherlands Geogr. Stud., 190, 1995.

Diederen, D. and Liu, Y.: Dynamic spatio-temporal generation of large-scale synthetic gridded precipitation: with improved spatial coherence of extremes, Stoch. Environ. Res. Risk Assess., 34(9), 1369–1383, doi:10.1007/s00477-019-01724-9, 2020.

Dimri, A. P., Bookhagen, B., Stoffel, M. and Yasunari, T.: Himalayan weather and climate and their impact on

the environment., 2019.
Dirmeyer, P. A., Schlosser, C. A. and Brubaker, K. L.: Precipitation, Recycling, and Land Memory: An Integrated Analysis, J. Hydrometeorol., 10(1), 278–288, doi:10.1175/2008JHM1016.1, 2009.
Disse, M. and Engel, H.: Flood events in the Rhine basin: genesis, influences and mitigation, Nat. Hazards, 23(2–3), 271–290, 2001.
Do, H. X., Westra, S. and Leonard, M.: A global-scale investigation of trends in annual maximum streamflow, J. Hydrol., 552, 28–43, doi:10.1016/j.jhydrol.2017.06.015, 2017.
Dobinski, W.: Permafrost, Earth-Science Rev., 108(3–4), 158–169, doi:10.1016/j.earscirev.2011.06.007, 2011.
Domeneghetti, A., Castellarin, A. and Brath, A.: Assessing rating-curve uncertainty and its effects on hydraulic model calibration, Hydrol. Earth Syst. Sci., 16(4), 1191–1202, 2012.
Donat, M. G., Sillmann, J., Wild, S., Alexander, L. V., Lippmann, T. and Zwiers, F. W.: Consistency of temperature and precipitation extremes across various global gridded in situ and reanalysis datasets, J. Clim., 27(13), 5019–5035, doi:10.1175/JCLI-D-13-00405.1, 2014.
Doocy, S., Daniels, A., Murray, S. and Kirsch, T. D.: The Human Impact: a Historical Review of Events and Systematic Literature Review, PLOS Curr. Disasters, 1(October 2012), 1–32, doi:10.1371/currents.dis.f4deb457904936b07c09daa98ee8171a, 2013.
Dottori, F., Szewczyk, W., Ciscar, J. C., Zhao, F., Alfieri, L., Hirabayashi, Y., Bianchi, A., Mongelli, I., Frieler, K., Betts, R. A. and Feyen, L.: Increased human and economic losses from river flooding with anthropogenic warming, Nat. Clim. Chang., 8(9), 781–786, doi:10.1038/s41558-018-0257-z, 2018.
Duan, A. and Xiao, Z.: Does the climate warming hiatus exist over the Tibetan Plateau?, Sci. Rep., 5, 1–9, doi:10.1038/srep13711, 2015.
Duan, Y., Ma, Z. and Yang, Q.: Characteristics of consecutive dry days variations in China, Theor. Appl. Climatol., 130(1–2), 701–709, doi:10.1007/s00704-016-1984-6, 2017.
Duha Metin, A., Viet Dung, N., Schröter, K., Guse, B., Apel, H., Kreibich, H., Vorogushyn, S. and Merz, B.: How do changes along the risk chain affect flood risk?, Nat. Hazards Earth Syst. Sci., 18(11), 3089–3108, doi:10.5194/nhess-18-3089-2018, 2018.
Dunn, R. J. H., Alexander, L. V., Donat, M. G., Zhang, X., Bador, M., Herold, N., Lippmann, T., Allan, R., Aguilar, E., Barry, A. A., Brunet, M., Caesar, J., Chagnaud, G., Cheng, V., Cinco, T., Durre, I., Guzman, R., Htay, T. M., Wan Ibadullah, W. M., Bin Ibrahim, M. K. I., Khoshkam, M., Kruger, A., Kubota, H., Leng, T. W., Lim, G., Li-Sha, L., Marengo, J., Mbatha, S., McGree, S., Menne, M., Milagros Skansi, M., Ngwenya, S., Nkrumah, F., Oonariya, C., Pabon-Caicedo, J. D., Panthou, G., Pham, C., Rahimzadeh, F., Ramos, A., Salgado, E., Salinger, J., Sané, Y., Sopaheluwakan, A., Srivastava, A., Sun, Y., Timbal, B., Trachow, N., Trewin, B., Schrier, G., Vazquez-Aguirre, J., Vasquez, R., Villarroel, C., Vincent, L., Vischel, T., Vose, R. and Bin Hj Yussof, M. N.: Development of an Updated Global Land In Situ-Based Data Set of Temperature and Precipitation Extremes: HadEX3, J. Geophys. Res. Atmos., 125(16), 2019–032263, doi:10.1029/2019JD032263, 2020.
Dunne, T.: Field Studies of Hillslope Flow Processes, Hillslope Hydrol., 227–293, 1978.
Dunning, S. A., Rosser, N. J., McColl, S. T. and Reznichenko, N. V.: Rapid sequestration of rock avalanche deposits within glaciers, Nat. Commun., 6, 1–7, doi:10.1038/ncomms8964, 2015.
Durante, F. and Salvadori, G.: On the construction of multivariate extreme value models via copulas, Environmetrics, 21(2), 143–161, doi:10.1002/env.988, 2010.
Ehret, U., Zehe, E., Wulfmeyer, V., Warrach-Sagi, K. and Liebert, J.: HESS Opinions "should we apply bias correction to global and regional climate model data?," Hydrol. Earth Syst. Sci., 16(9), 3391–3404, doi:10.5194/hess-16-3391-2012, 2012.
Elliott, J., Deryng, D., Müller, C., Frieler, K., Konzmann, M., Gerten, D., Glotter, M., Flörke, M., Wada, Y., Best, N., Eisner, S., Fekete, B. M., Folberth, C., Foster, I., Gosling, S. N., Haddeland, I., Khabarov, N., Ludwig, F., Masaki, Y., Olin, S., Rosenzweig, C., Ruane, A. C., Satoh, Y., Schmid, E., Stacke, T., Tang, Q. and Wisser, D.: Constraints and potentials of future irrigation water availability on agricultural production under climate change, Proc. Natl. Acad. Sci. U. S. A., 111(9), 3239–3244, doi:10.1073/pnas.1222474110, 2014.
Embrechts, P., Klüppelberg, C. and Mikosch, T.: Modelling extremal events: for insurance and finance, Springer Science & Business Media., 2013.
EMDAT: (No Title), [online] Available from: https://public.emdat.be/ (Accessed 9 September 2020), 2020.
Emerton, R. E., Stephens, E. M., Pappenberger, F., Pagano, T. C., Weerts, A. H., Wood, A. W., Salamon, P., Brown, J. D., Hjerdt, N., Donnelly, C., Baugh, C. A. and Cloke, H. L.: Continental and global scale flood forecasting systems, Wiley Interdiscip. Rev. Water, 3(3), 391–418, doi:10.1002/wat2.1137, 2016.
Emery, W. and Camps, A.: Introduction to satellite remote sensing: Atmosphere, ocean, cryosphere and land applications, Elsevier., 2017.
Engel, H.: The flood events of 1993/1994 and 1995 in the Rhine River basin, in Destructive Water: Water-caused natural disasters, their abatement and control, IAHS Publication no 239, edited by F. H. M. Leavesly, G. H., Lins, H. F., Nobilis, F., Parker, R. S., Schneider, V. R., and Van de Ven, pp. 21–32, IAHS Press, Wallingford, UK., 1997.

Engel, M. D. and H.: Flood events in the rhine basin: genesis, influences and mitigation, Nat. Hazards, 23(2–3), 271–290, doi:10.1023/A, 2001.
Entin, J. K., Robock, A., Vinnikov, K. Y., Hollinger, S. E., Liu, S. and Namkhai, A.: Temporal and spatial scales of observed soil moisture variations in the extratropics, J. Geophys. Res., 105(D9), 11865–11877, 2000.
Eregno, F. E., Xu, C. Y. and Kitterød, N. O.: Modeling hydrological impacts of climate change in different climatic zones, Int. J. Clim. Chang. Strateg. Manag., doi:10.1108/IJCCSM-04-2012-0024, 2013.
Essery, R., Morin, S., Lejeune, Y. and B Ménard, C.: A comparison of 1701 snow models using observations from an alpine site, Adv. Water Resour., 55, 131–148, doi:10.1016/j.advwatres.2012.07.013, 2013.
Eyring, V., Bony, S., Meehl, G. A., Senior, C. A., Stevens, B., Stouffer, R. J. and Taylor, K. E.: Overview of the Coupled Model Intercomparison Project Phase 6 (CMIP6) experimental design and organization, Geosci. Model Dev., 9(5), 1937–1958, doi:10.5194/gmd-9-1937-2016, 2016.
Faillettaz, J., Funk, M. and Vincent, C.: Avalanching glacier instabilities: Review on processes and early warning perspectives, Rev. Geophys., 53(2), 203–224, doi:10.1002/2014RG000466, 2015.
Fallah, A., Sungmin, O. and Orth, R.: Climate-dependent propagation of precipitation uncertainty into the water cycle, Hydrol. Earth Syst. Sci., 24(7), 3725–3735, doi:10.5194/hess-24-3725-2020, 2020.
Falter, D., Schröter, K., Dung, N. V., Vorogushyn, S., Kreibich, H., Hundecha, Y., Apel, H. and Merz, B.: Spatially coherent flood risk assessment based on long-term continuous simulation with a coupled model chain, J. Hydrol., 524(June 2016), 182–193, doi:10.1016/j.jhydrol.2015.02.021, 2015.
Fan, H. and He, D.: Temperature and precipitation variability and its effects on streamflow in the upstream regions of the Lancang-Mekong and Nu-Salween Rivers, J. Hydrometeorol., 16(5), 2248–2263, doi:10.1175/JHM-D-14-0238.1, 2015.
Farinotti, D., Huss, M., Fürst, J. J., Landmann, J., Machguth, H., Maussion, F. and Pandit, A.: A consensus estimate for the ice thickness distribution of all glaciers on Earth, Nat. Geosci., 12(3), 168–173, doi:10.1038/s41561-019-0300-3, 2019.
Farr, T. G., Rosen, P. A., Caro, E., Crippen, R., Duren, R., Hensley, S., Kobrick, M., Paller, M., Rodriguez, E., Roth, L., Seal, D., Shaffer, S., Shimada, J., Umland, J., Werner, M., Oskin, M., Burbank, D. and Alsdorf, D.: The Shuttle Radar Topography Mission, Rev. Geophys., 45(2), doi:10.1029/2005RG000183, 2007.
Fatichi, S., Vivoni, E. R., Ogden, F. L., Ivanov, V. Y., Mirus, B., Gochis, D., Downer, C. W., Camporese, M., Davison, J. H., Ebel, B., Jones, N., Kim, J., Mascaro, G., Niswonger, R., Restrepo, P., Rigon, R., Shen, C., Sulis, M. and Tarboton, D.: An overview of current applications, challenges, and future trends in distributed process-based models in hydrology, J. Hydrol., 537(March), 45–60, doi:10.1016/j.jhydrol.2016.03.026, 2016.
Favre, A.-C., El Adlouni, S., Perreault, L., Thiémonge, N. and Bobée, B.: Multivariate hydrological frequency analysis using copulas, Water Resour. Res., 40(1), 1–12, doi:10.1029/2003WR002456, 2004.
Fekete, B. M., Vörösmarty, C. J., Roads, J. O. and Willmott, C. J.: Uncertainties in precipitation and their impacts on runoff estimates, J. Clim., 17(2), 294–304, doi:10.1175/1520-0442(2004)017<0294:UIPATI>2.0.CO;2, 2004.
Feng, S., Wu, X., Hao, Z., Hao, Y., Zhang, X. and Hao, F.: A database for characteristics and variations of global compound dry and hot events, Weather Clim. Extrem., 30, 100299, doi:10.1016/j.wace.2020.100299, 2020.
Fersch, B., Senatore, A., Adler, B., Arnault, J., Mauder, M., Schneider, K., Völksch, I. and Kunstmann, H.: High-resolution fully-coupled atmospheric–hydrological modeling: a cross-compartment regional water and energy cycle evaluation, Hydrol. Earth Syst. Sci. Discuss., 2019(October), 1–37, doi:10.5194/hess-2019-478, 2019.
Fink, A. H., Brücher, T., Ermert, V., Krüger, A. and Pinto, J. G.: The European storm Kyrill in January 2007: Synoptic evolution, meteorological impacts and some considerations with respect to climate change, Nat. Hazards Earth Syst. Sci., 9(2), 405–423, doi:10.5194/nhess-9-405-2009, 2009.
Fischer, E. M. and Knutti, R.: Robust projections of combined humidity and temperature extremes, Nat. Clim. Chang., 3(2), 126–130, doi:10.1038/nclimate1682, 2013.
Forkel, M., Thonicke, K., Beer, C., Cramer, W., Bartalev, S. and Schmullius, C.: Extreme fire events are related to previous-year surface moisture conditions in permafrost-underlain larch forests of Siberia, Environ. Res. Lett., 7(4), doi:10.1088/1748-9326/7/4/044021, 2012.
Fowler, H. J. and Archer, D. R.: Conflicting signals of climatic change in the upper Indus Basin, J. Clim., 19(17), 4276–4293, doi:10.1175/JCLI3860.1, 2006.
Franz, D., Portmann, F. T., Döll, P., Eisner, S., Flörke, M., Wattenbach, M. and Müller Schmied, H.: Sensitivity of simulated global-scale freshwater fluxes and storages to input data, hydrological model structure, human water use and calibration, Hydrol. Earth Syst. Sci., 18(9), 3511–3538, doi:10.5194/hess-18-3511-2014, 2014.
Frauenfeld, O. W., Zhang, T. and Serreze, M. C.: Climate change and variability using European Centre for Medium-Range Weather Forecasts reanalysis (ERA-40) temperatures on the Tibetan Plateau, J. Geophys. Res. D Atmos., 110(2), 1–9, doi:10.1029/2004JD005230, 2005.
Frich, P., Alexander, L. V., Della-Marta, P., Gleason, B., Haylock, M., Tank Klein, A. M. G. and Peterson, T.: Observed coherent changes in climatic extremes during the second half of the twentieth century, Clim. Res., 19(3), 193–212, doi:10.3354/cr019193, 2002.
Fu, P. and Rich, P. M.: Design and Implementation of the Solar Analyst: an ArcView Extension for Modeling

Solar Radiation at Landscape Scales, 19th Annu. ESRI User Conf., (February), 1–24, 1999.
Funk, C., Peterson, P., Landsfeld, M., Pedreros, D., Verdin, J., Shukla, S., Husak, G., Rowland, J., Harrison, L., Hoell, A. and Michaelsen, J.: The climate hazards infrared precipitation with stations - A new environmental record for monitoring extremes, Sci. Data, 2, 1–21, doi:10.1038/sdata.2015.66, 2015.
Gaál, L., Szolgay, J., Kohnová, S., Parajka, J., Merz, R., Viglione, A. and Blöschl, G.: Flood timescales: Understanding the interplay of climate and catchment processes through comparative hydrology, Water Resour. Res., 48(4), 1–21, doi:10.1029/2011WR011509, 2012.
Gabbi, J., Carenzo, M., Pellicciotti, F., Bauder, A. and Funk, M.: A comparison of empirical and physically based glacier surface melt models for long-term simulations of glacier response, J. Glaciol., doi:10.3189/2014JoG14J011, 2014.
Ganguli, P., Paprotny, D., Hasan, M., Güntner, A. and Merz, B.: Projected Changes in Compound Flood Hazard From Riverine and Coastal Floods in Northwestern Europe, Earth's Futur., 8(11), doi:10.1029/2020EF001752, 2020.
Gao, H., Wang, J., Yang, Y., Pan, X., Ding, Y. and Duan, Z.: Permafrost Hydrology of the Qinghai-Tibet Plateau: A Review of Processes and Modeling, Front. Earth Sci., 8, 535, doi:10.3389/feart.2020.576838, 2021.
Gao, Y., Chen, F., Lettenmaier, D. P., Xu, J., Xiao, L. and Li, X.: Does elevation-dependent warming hold true above 5000 m elevation? Lessons from the Tibetan Plateau, npj Clim. Atmos. Sci., 1(1), 19, 2018.
Gardelle, J., Berthier, E., Arnaud, Y. and Kääb, A.: Region-wide glacier mass balances over the Pamir-Karakoram-Himalaya during 1999–2011, Cryosphere, 7(4), 1263–1286, doi:10.5194/tc-7-1263-2013, 2013.
Van Garderen, L., Feser, F. and Shepherd, T. G.: A methodology for attributing the role of climate change in extreme events: A global spectrally nudged storyline, Nat. Hazards Earth Syst. Sci., 21(1), 171–186, doi:10.5194/nhess-21-171-2021, 2021.
Gariano, S. L. and Guzzetti, F.: Landslides in a changing climate, Earth-Science Rev., 162, 227–252, doi:10.1016/j.earscirev.2016.08.011, 2016.
Gebregiorgis, A. S. and Hossain, F.: How well can we estimate error variance of satellite precipitation data around the world?, Atmos. Res., 154, 39–59, doi:10.1016/j.atmosres.2014.11.005, 2015.
Geerse, C.: Correlatie tussen stormvloeden en afvoeren voor de benedenrivieren, Mate van correlatie en geschatte invloed op de Toetspeilen, Report PR2442.10, HKV Lijn in Water, May2013, In opdracht van Rijkswaterstaat Waterdienst., 2013.
Gehne, M., Hamill, T. M., Kiladis, G. N. and Trenberth, K. E.: Comparison of global precipitation estimates across a range of temporal and spatial scales, J. Clim., 29(21), 7773–7795, doi:10.1175/JCLI-D-15-0618.1, 2016.
Georgakakos, K. P., Seo, D. J., Gupta, H., Schaake, J. and Butts, M. B.: Towards the characterization of streamflow simulation uncertainty through multimodel ensembles, in Journal of Hydrology, vol. 298, pp. 222–241, Elsevier., 2004.
Gerritsen, H.: What happened in 1953? The Big Flood in the Netherlands in retrospect, Philos. Trans. R. Soc. A Math. Phys. Eng. Sci., 363(1831), 1271–1291, doi:10.1098/rsta.2005.1568, 2005.
Gerritsen, H., de Vries, H. and Philippart, M.: The Dutch Continental Shelf Model TT -, in Quantitative Skill Assessment for Coastal Ocean Models, pp. 425–467, American Geophysical Union : Washington, D. C., 2013.
Ghimire, U., Babel, M. S., Shrestha, S. and Srinivasan, G.: A multi-temporal analysis of streamflow using multiple CMIP5 GCMs in the Upper Ayerawaddy Basin, Myanmar, Clim. Change, 1–21, 2019.
Gilany, N. and Iqbal, J.: Simulation of Glacial Avalanche Hazards in Shyok Basin of Upper Indus, Sci. Rep., 9(1), 1–14, doi:10.1038/s41598-019-56523-7, 2019.
Gilbert, R. O.: Statistical methods for environmental pollution monitoring, John Wiley & Sons., 1987.
Gilleland, E. and Katz, R. W.: Analyzing Seasonal To Interannual Extreme Weather and, New York, (2005), P2.15 [online] Available from: http://www.assessment.ucar.edu/pdf/Gilleland2006revised.pdf, 2006.
Gilleland, E. and Nychka, D.: Statistical models for monitoring and regulating ground-level ozone, Environmetrics, 16(5), 535–546, doi:10.1002/env.720, 2005.
Gomes, M. I., Guillou, A., Gomes, M. I., Guillou, A., Value, E., Extremes, U. and Gomes, M. I.: Extreme Value Theory and Statistics of Univariate Extremes : A Review To cite this version : HAL Id : hal-01311707 Extreme Value Theory and Statistics of Univariate Extremes : A Review, 2016.
Goodall, J. L., Robinson, B. F. and Castronova, A. M.: Modeling water resource systems using a service-oriented computing paradigm, Environ. Model. Softw., 26(5), 573–582, doi:10.1016/j.envsoft.2010.11.013, 2011.
Goulden, M. L. and Bales, R. C.: California forest die-off linked to multi-year deep soil drying in 2012–2015 drought, Nat. Geosci., 12(8), 632–637, doi:10.1038/s41561-019-0388-5, 2019.
Grayson, R. B., Blöschl, G., Western, A. W. and McMahon, T. A.: Advances in the use of observed spatial patterns of catchment hydrological response, Adv. Water Resour., 25(8–12), 1313–1334, doi:10.1016/S0309-1708(02)00060-X, 2002.
GRDC: GRDC, [online] Available from: http://www.bafg.de/GRDC/EN/01_GRDC/grdc_node.html (Accessed 1 November 2016), 2016.
GRDC: BfG - The GRDC - Global Runoff Database, [online] Available from:

https://www.bafg.de/GRDC/EN/01_GRDC/13_dtbse/database_node.html (Accessed 11 September 2020), 2020.
Grimaldi, S., Schumann, G. J. P., Shokri, A., Walker, J. P. and Pauwels, V. R. N.: Challenges, Opportunities, and Pitfalls for Global Coupled Hydrologic-Hydraulic Modeling of Floods., 2019.
Groisman, P. Y. and Knight, R. W.: Prolonged dry episodes over the conterminous United States: New tendencies emerging during the last 40 years, J. Clim., 21(9), 1850–1862, doi:10.1175/2007JCLI2013.1, 2008.
Groot Zwaaftink, C. D., Löwe, H., Mott, R., Bavay, M. and Lehning, M.: Drifting snow sublimation: A high-resolution 3-D model with temperature and moisture feedbacks, J. Geophys. Res. Atmos., 116(16), 1–14, doi:10.1029/2011JD015754, 2011.
Groot Zwaaftink, C. D., Mott, R. and Lehning, M.: Seasonal simulation of drifting snow sublimation in Alpine terrain, Water Resour. Res., 49(3), 1581–1590, doi:10.1002/wrcr.20137, 2013.
Gu, H., Yu, Z., Yang, C. and Ju, Q.: Projected Changes in Hydrological Extremes in the Yangtze River Basin with an Ensemble of Regional Climate Simulations, Water, 10(9), 1279, 2018.
Guisado-Pintado, E. and Jackson, D. W. T.: Multi-scale variability of storm Ophelia 2017: The importance of synchronised environmental variables in coastal impact, Sci. Total Environ., 630, 287–301, doi:10.1016/j.scitotenv.2018.02.188, 2018.
Günther, D., Marke, T., Essery, R. and Strasser, U.: Uncertainties in Snowpack Simulations—Assessing the Impact of Model Structure, Parameter Choice, and Forcing Data Error on Point-Scale Energy Balance Snow Model Performance, Water Resour. Res., 55(4), 2779–2800, doi:10.1029/2018WR023403, 2019.
Güntner, A., Stuck, J., Werth, S., Döll, P., Verzano, K. and Merz, B.: A global analysis of temporal and spatial variations in continental water storage, Water Resour. Res., 43(5), 1–19, doi:10.1029/2006WR005247, 2007.
Guo, D. and Wang, H.: The significant climate warming in the northern Tibetan Plateau and its possible causes, Int. J. Climatol., 32(12), 1775–1781, doi:10.1002/joc.2388, 2012.
Guo, H., Chen, S., Bao, A., Hu, J., Gebregiorgis, A. S., Xue, X. and Zhang, X.: Inter-comparison of high-resolution satellite precipitation products over Central Asia, Remote Sens., 7(6), 7181–7211, doi:10.3390/rs70607181, 2015.
Haigh, I. D., Wadey, M. P., Wahl, T., Ozsoy, O., Nicholls, R. J., Brown, J. M., Horsburgh, K. and Gouldby, B.: Spatial and temporal analysis of extreme sea level and storm surge events around the coastline of the UK, Sci. Data, 3(1), 1–14, doi:10.1038/sdata.2016.107, 2016.
Hall, D. K. and Riggs, G. A.: MODIS/Terra Snow Cover Monthly L3 Global 0.05Deg CMG Dataset Version 6, https://nsidc.org/data/MOD10CM, 2015.
Hall, J., Arheimer, B., Borga, M., Brázdil, R., Claps, P., Kiss, A., Kjeldsen, T. R., Kriaučuniene, J., Kundzewicz, Z. W., Lang, M., Llasat, M. C., Macdonald, N., McIntyre, N., Mediero, L., Merz, B., Merz, R., Molnar, P., Montanari, A., Neuhold, C., Parajka, J., Perdigão, R. A. P., Plavcová, L., Rogger, M., Salinas, J. L., Sauquet, E., Schär, C., Szolgay, J., Viglione, A. and Blöschl, G.: Understanding flood regime changes in Europe: A state-of-the-art assessment, Hydrol. Earth Syst. Sci., 18(7), 2735–2772, doi:10.5194/hess-18-2735-2014, 2014.
Hao, Z., Singh, V. P. and Hao, F.: Compound extremes in hydroclimatology: A review, Water (Switzerland), 10(6), 16–21, doi:10.3390/w10060718, 2018.
Hao, Z., Hao, F., Singh, V. P. and Zhang, X.: Statistical prediction of the severity of compound dry-hot events based on El Niño-Southern Oscillation, J. Hydrol., 572, 243–250, doi:10.1016/j.jhydrol.2019.03.001, 2019.
Hargreaves, G. and Samani, Z.: Reference Crop Evapotranspiration from Temperature, Appl. Eng. Agric., 1(2), 96–99, doi:10.13031/2013.26773, 1985.
Harrigan, S. and Berghuijs, W.: The Mystery of Evaporation, Streams Thought (Young Hydrol. Soc., (July), 1–5, 2016.
Hattermann, F. F., Krysanova, V. and Gosling, S. N.: Cross - scale intercomparison of climate change impacts simulated by regional and global hydrological models in eleven large river basins, Clim. Change, 561–576, doi:10.1007/s10584-016-1829-4, 2017.
Hawcroft, M. K., Shaffrey, L. C., Hodges, K. I. and Dacre, H. F.: How much Northern Hemisphere precipitation is associated with extratropical cyclones?, Geophys. Res. Lett., 39(24), 1–7, doi:10.1029/2012GL053866, 2012.
Hayashi, M., Goeller, N., Quinton, W. L. and Wright, N.: A simple heat-conduction method for simulating the frost-table depth in hydrological models, Hydrol. Process., 21(19), 2610–2622, doi:10.1002/hyp.6792, 2007.
Haylock, M. R., Hofstra, N., Klein Tank, A. M. G., Klok, E. J., Jones, P. D. and New, M.: A European daily high-resolution gridded data set of surface temperature and precipitation for 1950-2006, J. Geophys. Res. Atmos., 113(20), doi:10.1029/2008JD010201, 2008.
Hazeleger, W., Wang, X., Severijns, C., Ştefănescu, S., Bintanja, R., Sterl, A., Wyser, K., Semmler, T., Yang, S., van den Hurk, B., van Noije, T., van der Linden, E. and van der Wiel, K.: EC-Earth V2.2: Description and validation of a new seamless earth system prediction model, Clim. Dyn., 39(11), 2611–2629, doi:10.1007/s00382-011-1228-5, 2012.
Hazeleger, W., van den Hurk, B. J. J. M., Min, E., van Oldenborgh, G. J., Petersen, A. C., Stainforth, D. A., Vasileiadou, E. and Smith, L. A.: Tales of future weather, Nat. Clim. Chang., 5(2), 107–113, doi:10.1038/nclimate2450, 2015.
He, Y. and Wang, K.: Contrast patterns and trends of lapse rates calculated from near-surface air and land surface

temperatures in China from 1961 to 2014, Sci. Bull., 65(14), 1217–1224, doi:10.1016/j.scib.2020.04.001, 2020.
Hegnauer, M., Beersma, J. J., van den Boogaard, H. F. P., Buishand, T. A. and Passchier, R. H.: Generator of Rainfall and Discharge Extremes (GRADE) for the Rhine and Meuse basins. Final report of GRADE 2.0, Deltares: Delft, The Netherlands., 2014.
Hegnauer, M., Kwadijk, J. and Klijn, F.: The plausibility of extreme high discharges in the river Rhine, Deltares: Delft, The Netherlands., 2015.
Heinke, J., Gudmundsson, L., Voss, F., Koirala, S., Clark, D. B., Hagemann, S., Hanasaki, N., Gerten, D., Tallaksen, L. M., Stahl, K., Bertrand, N. and Dumont, E.: Comparing Large-Scale Hydrological Model Simulations to Observed Runoff Percentiles in Europe, J. Hydrometeorol., 13(2), 604–620, doi:10.1175/jhm-d-11-083.1, 2011.
Hendry, A., Haigh, I. D., Nicholls, R. J., Winter, H., Neal, R., Wahl, T., Joly-Lauge, A. and Darby, S. E.: Assessing the characteristics and drivers of compound flooding events around the UK coast, Hydrol. Earth Syst. Sci., 23(7), 3117–3139, doi:10.5194/hess-23-3117-2019, 2019.
Herreid, S. and Pellicciotti, F.: The state of rock debris covering Earth's glaciers, Nat. Geosci., 13(9), 621–627, doi:10.1038/s41561-020-0615-0, 2020.
Hersbach, H., Bell, B., Berrisford, P., Hirahara, S., Horányi, A., Muñoz-Sabater, J., Nicolas, J., Peubey, C., Radu, R., Schepers, D., Simmons, A., Soci, C., Abdalla, S., Abellan, X., Balsamo, G., Bechtold, P., Biavati, G., Bidlot, J., Bonavita, M., De Chiara, G., Dahlgren, P., Dee, D., Diamantakis, M., Dragani, R., Flemming, J., Forbes, R., Fuentes, M., Geer, A., Haimberger, L., Healy, S., Hogan, R. J., Hólm, E., Janisková, M., Keeley, S., Laloyaux, P., Lopez, P., Lupu, C., Radnoti, G., de Rosnay, P., Rozum, I., Vamborg, F., Villaume, S. and Thépaut, J. N.: The ERA5 global reanalysis, Q. J. R. Meteorol. Soc., 146(730), 1999–2049, doi:10.1002/qj.3803, 2020.
Heynen, M., Miles, E., Ragettli, S., Buri, P., Immerzeel, W. W. and Pellicciotti, F.: Air temperature variability in a high-elevation Himalayan catchment, Ann. Glaciol., doi:10.3189/2016AoG71A076, 2016.
Hillier, J. K. and Dixon, R. S.: Seasonal impact-based mapping of compound hazards, Environ. Res. Lett., 15(11), doi:10.1088/1748-9326/abbc3d, 2020.
Hirabayashi, Y., Kanae, S., Emori, S., Oki, T. and Kimoto, M.: Global projections of changing risks of floods and droughts in a changing climate, Hydrol. Sci. J., 53(4), 754–772, doi:10.1623/hysj.53.4.754, 2008.
Hirabayashi, Y., Mahendran, R., Koirala, S., Konoshima, L., Yamazaki, D., Watanabe, S., Kim, H. and Kanae, S.: Global flood risk under climate change, Nat. Clim. Chang., 3(9), 816–821, doi:10.1038/nclimate1911, 2013.
Hock, R.: Temperature index melt modelling in mountain areas, J. Hydrol., 282(1–4), 104–115, doi:10.1016/S0022-1694(03)00257-9, 2003.
Hock, R.: Glacier melt: A review of processes and their modelling, Prog. Phys. Geogr., doi:10.1191/0309133305pp453ra, 2005.
Hock, R. and Holmgren, B.: A distributed surface energy-balance model for complex topography and its application to Storglaciären, Sweden, J. Glaciol., 51(172), 25–36, doi:10.3189/172756505781829566, 2005.
Hock, R., Hutchings, J. K. and Lehning, M.: Grand challenges in cryospheric sciences: Toward better predictability of glaciers, snow and sea ice, Front. Earth Sci., 5(August), 1–14, doi:10.3389/feart.2017.00064, 2017.
Hock, R., Rasul, G., Adler, C., Cáceres, B., Gruber, S., Hirabayashi, Y., Jackson, M., Kääb, A., Kang, S., Kutuzov, S., Milner, A., Molau, U., Morin, S., Orlove, B. and Steltzer, H. I.: Chapter 2: High Mountain Areas. IPCC Special Report on the Ocean and Cryosphere in a Changing Climate, IPCC Spec. Rep. Ocean Cryosph. a Chang. Clim., 131–202, 2019a.
Hock, R., Bliss, A., Marzeion, B. E. N., Giesen, R. H., Hirabayashi, Y., Huss, M., Radic, V. and Slangen, A. B. A.: GlacierMIP-A model intercomparison of global-scale glacier mass-balance models and projections, J. Glaciol., 65(251), 453–467, doi:10.1017/jog.2019.22, 2019b.
Hoerling, M., Kumar, A., Dole, R., Nielsen-Gammon, J. W., Eischeid, J., Perlwitz, J., Quan, X. W., zhang, T., pegion, P. and Chen, M.: Anatomy of an extreme event, J. Clim., 26(9), 2811–2832, doi:10.1175/JCLI-D-12-00270.1, 2013.
Højberg, A. and Refsgaard, J.: Model uncertainty - Parameter uncertainty versus conceptual models, Water Sci. Technol., 52, 177–186, doi:10.2166/wst.2005.0166, 2005.
Holländer, H. M., Bormann, H., Blume, T., Buytaert, W., Chirico, G. B., Exbrayat, J. F., Gustafsson, D., Hölzel, H., Krauße, T., Kraft, P., Stoll, S., Blöschl, G. and Flühler, H.: Impact of modellers' decisions on hydrological a priori predictions, Hydrol. Earth Syst. Sci., 18(6), 2065–2085, doi:10.5194/hess-18-2065-2014, 2014.
Hood, E., Williams, M. and Cline, D.: Sublimation from a seasonal snowpack at a continental, mid-latitude alpine site, Hydrol. Process., 13(12–13), 1781–1797, doi:10.1002/(SICI)1099-1085(199909)13:12/13<1781::AID-HYP860>3.0.CO;2-C, 1999.
Hrachowitz, M. and Clark, M. P.: HESS Opinions: The complementary merits of competing modelling philosophies in hydrology, Hydrol. Earth Syst. Sci., doi:10.5194/hess-21-3953-2017, 2017.
Hu, Z., Zhang, C., Hu, Q. and Tian, H.: Temperature changes in central Asia from 1979 to 2011 based on multiple datasets, J. Clim., 27(3), 1143–1167, doi:10.1175/JCLI-D-13-00064.1, 2014.
Huffman, G. J., Bolvin, D. T., Nelkin, E. J., Wolff, D. B., Adler, R. F., Gu, G., Hong, Y., Bowman, K. P. and

Stocker, E. F.: The TRMM Multisatellite Precipitation Analysis (TMPA): Quasi-Global, Multiyear, Combined-Sensor Precipitation Estimates at Fine Scales, J. Hydrometeorol., doi:10.1175/JHM560.1, 2007.
Huggel, C., Clague, J. J. and Korup, O.: Is climate change responsible for changing landslide activity in high mountains?, Earth Surf. Process. Landforms, 37(1), 77–91, doi:10.1002/esp.2223, 2012.
Huggel, C., Carey, M., Clague, J. J. and Kääb, A.: The high-mountain cryosphere: Environmental changes and human risks, Cambridge University Press., 2015.
Hughes, T. P., Kerry, J. T., Connolly, S. R., Baird, A. H., Eakin, C. M., Heron, S. F., Hoey, A. S., Hoogenboom, M. O., Jacobson, M., Liu, G., Pratchett, M. S., Skirving, W. and Torda, G.: Ecological memory modifies the cumulative impact of recurrent climate extremes, Nat. Clim. Chang., 9(1), 40–43, doi:10.1038/s41558-018-0351-2, 2019.
Huintjes, E., Sauter, T., Schroter, B., Maussion, F., Yang, W., Kropaček, J., Buchroithner, M., Scherer, D., Kang, S. and Schneider, C.: Evaluation of a Coupled Snow and Energy Balance Model for Zhadang Glacier, Tibetan Plateau, Using Glaciological Measurements and Time-Lapse Photography, Arctic, Antarct. Alp. Res., 47(3), 573–590, doi:10.1657/AAAR0014-073, 2015.
Huiskes, I.: Using Ensemble Streamflow Predictions for extreme discharge purposes in the river Rhine, University of Twente. [online] Available from: https://www.utwente.nl/en/et/wem/education/msc-thesis/2016/huiskes.pdf, 2016.
van den Hurk, B., Siegmund, P., Klein Tank, A., Attema, J., Bakker, A., Beersma, J., Bessembinder, J., Boers, R., Brandsma, T., Brink, H. Van Den, Drijfhout, S., Eskes, H., Haarsma, R., Hazeleger, W., Jilderda, R., Katsman, C., Lenderink, G., Loriaux, J., Meijgaard, E. Van, Noije, T. Van, Oldenborgh, G. J. Van, Selten, F., Siebesma, P., Sterl, A., Vries, H. De, van Weele, M., de Winter, R. and van Zadelhoff, G.: KNMI'14: Climate Change scenarios for the 21st Century – A Netherlands perspective, Sci. Rep. WR2014-01, (May), 115 [online] Available from: www.climatescenarios.nl, 2014.
van den Hurk, B., van Meijgaard, E., de Valk, P., van Heeringen, K.-J. and Gooijer, J.: Analysis of a compounding surge and precipitation event in the Netherlands, Environ. Res. Lett., 10(3), 035001, doi:10.1088/1748-9326/10/3/035001, 2015.
Hurst, H. E.: Long-term storage capacity of reservoirs, Trans. Amer. Soc. Civ. Eng., 116, 770–808, 1951.
Huss, M. and Hock, R.: Global-scale hydrological response to future glacier mass loss, Nat. Clim. Chang., 1, doi:10.1038/s41558-017-0049-x, 2018.
Huss, M., Funk, M. and Ohmura, A.: Strong Alpine glacier melt in the 1940s due to enhanced solar radiation, Geophys. Res. Lett., 36(23), 1–5, doi:10.1029/2009GL040789, 2009.
Ikeuchi, H., Hirabayashi, Y., Yamazaki, D., Kiguchi, M., Koirala, S., Nagano, T., Kotera, A. and Kanae, S.: Modeling complex flow dynamics of fluvial floods exacerbated by sea level rise in the Ganges–Brahmaputra–Meghna Delta, Environ. Res. Lett., 10(12), doi:10.1088/1748-9326/10/12/124011, 2015.
Im, E.-S., Pal, J. S. and Eltahir, E. A. B.: Deadly heat waves projected in the densely populated agricultural regions of South Asia, Sci. Adv., 3(8), e1603322, 2017.
Immerzeel, W.: Historical trends and future predictions of climate variability in the Brahmaputra basin, Int. J. Climatol. A J. R. Meteorol. Soc., 28(2), 243–254, 2008.
Immerzeel, W. W.: Climate change will effect the asian water tower, Science (80-.)., 1382, doi:10.1126/science.1183188, 2010.
Immerzeel, W. W. and Bierkens, M. F. P.: Asia's water balance, Nat. Geosci., 5(12), 841–842, doi:10.1038/ngeo1643, 2012.
Immerzeel, W. W., van Beek, L. P. H. and Bierkens, M. F. P.: Climate change will affect the Asian water towers., Science, 328(5984), 1382–5, doi:10.1126/science.1183188, 2010.
Immerzeel, W. W., van Beek, L. P. H., Konz, M., Shrestha, A. B. and Bierkens, M. F. P.: Hydrological response to climate change in a glacierized catchment in the Himalayas, Clim. Change, 110(3–4), 721–736, doi:10.1007/s10584-011-0143-4, 2012.
Immerzeel, W. W., Pellicciotti, F. and Bierkens, M. F. P.: Rising river flows throughout the twenty-first century in two Himalayan glacierized watersheds, Nat. Geosci., 6(9), 742–745, doi:10.1038/ngeo1896, 2013.
Immerzeel, W. W., Wanders, N., Lutz, A. F., Shea, J. M. and Bierkens, M. F. P.: Reconciling high-altitude precipitation in the upper Indus basin, , 4673–4687, doi:10.5194/hess-19-4673-2015, 2015a.
Immerzeel, W. W., Wanders, N., Lutz, A. F., Shea, J. M. and Bierkens, M. F. P.: Reconciling high altitude precipitation with glacier mass balances and runoff, Hydrol. Earth Syst. Sci., 12, 4755–4784, doi:10.5194/hessd-12-4755-2015, 2015b.
Immerzeel, W. W., Lutz, A. F., Andrade, M., Bahl, A., Biemans, H., Bolch, T., Hyde, S., Brumby, S., Davies, B. J., Elmore, A. C., Emmer, A., Feng, M., Fernández, A., Haritashya, U., Kargel, J. S., Koppes, M., Kraaijenbrink, P. D. A., Kulkarni, A. V., Mayewski, P. A., Nepal, S., Pacheco, P., Painter, T. H., Pellicciotti, F., Rajaram, H., Rupper, S., Sinisalo, A., Shrestha, A. B., Viviroli, D., Wada, Y., Xiao, C., Yao, T. and Baillie, J. E. M.: Importance and vulnerability of the world's water towers, Nature, 577(7790), 364–369, doi:10.1038/s41586-019-1822-y, 2020.

Ivancic, T. J. and Shaw, S. B.: Examining why trends in very heavy precipitation should not be mistaken for trends in very high river discharge, Clim. Change, 133(4), 681–693, doi:10.1007/s10584-015-1476-1, 2015.
Jacobeit, J., Wanner, H., Luterbacher, J., Beck, C., Philipp, A. and Sturm, K.: Atmospheric circulation variability in the North-Atlantic-European area since the mid-seventeenth century, Clim. Dyn., 20(4), 341–352, doi:10.1007/s00382-002-0278-0, 2003.
Jacobs, L., Maes, J., Mertens, K., Sekajugo, J., Thiery, W., Lipzig, N., Poesen, J., Kervyn, M. and Dewitte, O.: Reconstruction of a flash flood event through a multi-hazard approach: focus on the Rwenzori Mountains, Uganda, Nat. Hazards, 84, doi:10.1007/s11069-016-2458-y, 2016.
Ji, P. and Yuan, X.: Underestimation of the Warming Trend over the Tibetan Plateau during 1998–2013 by Global Land Data Assimilation Systems and Atmospheric Reanalyses, J. Meteorol. Res., 34(1), 88–100, doi:10.1007/s13351-020-9100-3, 2020.
Jiang, Q., Li, W., Fan, Z., He, X., Sun, W., Chen, S., Wen, J., Gao, J. and Wang, J.: Evaluation of the ERA5 reanalysis precipitation dataset over Chinese Mainland, J. Hydrol., 125660, doi:10.1016/j.jhydrol.2020.125660, 2020.
Jin, X.-Y., Jin, H.-J., Iwahana, G., Marchenko, S. S., Luo, D.-L., Li, X.-Y. and Liang, S.-H.: Impacts of climate-induced permafrost degradation on vegetation: A review, Adv. Clim. Chang. Res., doi:10.1016/j.accre.2020.07.002, 2020.
Joe, H.: Multivariate Models and Multivariate Dependence Concepts, Taylor & Francis. [online] Available from: https://books.google.nl/books?id=iJbRZL2QzMAC, 1997.
de Jong, C.: Challenges for mountain hydrology in the third millennium, Front. Environ. Sci., 3, 38, doi:10.3389/fenvs.2015.00038, 2015.
Joyce, R. J., Janowiak, J. E., Arkin, P. A. and Xie, P.: CMORPH: A method that produces global precipitation estimates from passive microwave and infrared data at high spatial and temporal resolution, J. Hydrometeorol., 5(3), 487–503, doi:10.1175/1525-7541(2004)005<0487:CAMTPG>2.0.CO;2, 2004.
Junghans, N., Cullmann, J. and Huss, M.: Evaluating the effect of snow and ice melt in an Alpine headwater catchment and further downstream in the River Rhine, Hydrol. Sci. J., 56(6), 981–993, doi:10.1080/02626667.2011.595372, 2011.
Kääb, A., Berthier, E., Nuth, C., Gardelle, J. and Arnaud, Y.: Contrasting patterns of early twenty-first-century glacier mass change in the Himalayas, Nature, 488(7412), 495–498, doi:10.1038/nature11324, 2012.
Kalma, J. D., McVicar, T. R. and McCabe, M. F.: Estimating land surface evaporation: A review of methods using remotely sensed surface temperature data, Surv. Geophys., 29(4–5), 421–469, doi:10.1007/s10712-008-9037-z, 2008.
Kampf, S. K. and Burges, S. J.: A framework for classifying and comparing distributed hillslope and catchment hydrologic models, Water Resour. Res., 43(5), 2007.
Kang, S., Xu, Y., You, Q., Flügel, W. A., Pepin, N. and Yao, T.: Review of climate and cryospheric change in the Tibetan Plateau, Environ. Res. Lett., 5(1), doi:10.1088/1748-9326/5/1/015101, 2010.
Kargel, J. S., Leonard, G. J., Shugar, D. H., Haritashya, U. K., Bevington, A., Fielding, E. J., Fujita, K., Geertsema, M., Miles, E. S., Steiner, J., Anderson, E., Bajracharya, S., Bawden, G. W., Breashears, D. F., Byers, A., Collins, B., Dhital, M. R., Donnellan, A., Evans, T. L., Geai, M. L., Glasscoe, M. T., Green, D., Gurung, D. R., Heijenk, R., Hilborn, A., Hudnut, K., Huyck, C., Immerzeel, W. W., Jiang, L., Jibson, R., Kääb, A., Khanal, N. R., Kirschbaum, D., Kraaijenbrink, P. D. A., Lamsal, D., Liu, S., Lv, M., McKinney, D., Nahirnick, N. K., Nan, Z., Ojha, S., Olsenholler, J., Painter, T. H., Pleasants, M., Pratima, K. C., Yuan, Q. I., Raup, B. H., Regmi, D., Rounce, D. R., Sakai, A., Shangguan, D., Shea, J. M., Shrestha, A. B., Shukla, A., Stumm, D., Van Der Kooij, M., Voss, K., Wang, X., Weihs, B., Wolfe, D., Wu, L., Yao, X., Yoder, M. R. and Young, N.: Geomorphic and geologic controls of geohazards induced by Nepal's 2015 Gorkha earthquake, Science (80-.)., 351(6269), doi:10.1126/science.aac8353, 2016.
Karssenberg, D., Schmitz, O., Salamon, P., Jong], K. [de and Bierkens, M. F. P.: A software framework for construction of process-based stochastic spatio-temporal models and data assimilation, Environ. Model. Softw., 25(4), 489–502, doi:https://doi.org/10.1016/j.envsoft.2009.10.004, 2010.
Kaser, G., Grosshauser, M. and Marzeion, B.: Contribution potential of glaciers to water availability in different climate regimes, Proc. Natl. Acad. Sci., 107(47), 20223–20227, doi:10.1073/pnas.1008162107, 2010.
Kates, R. W., Colten, C. E., Laska, S. and Leatherman, S. P.: Reconstruction of New Orleans after Hurricane Katrina: A research perspective, Proc. Natl. Acad. Sci. U. S. A., 103(40), 14653–14660, doi:10.1073/pnas.0605726103, 2006.
Kattel, D. B., Yao, T., Yang, W. and Tian, L.: Comparison of temperature lapse rates from the northern to the southern slopes of the Himalayas, , 4443(February), 4431–4443, doi:10.1002/joc.4297, 2015.
Katz, R.: Statistics of Extremes in Climatology and Hydrology, Adv. Water Resour., 25, 1287–1304, 2002.
Katz, R. W. and Brown, B. G.: Extreme events in a changing climate: variability is more important than averages, Clim. Change, 21(3), 289–302, 1992.
Kendon, E. J., Ban, N., Roberts, N. M., Fowler, H. J., Roberts, M. J., Chan, S. C., Evans, J. P., Fosser, G. and

Wilkinson, J. M.: Do convection-permitting regional climate models improve projections of future precipitation change?, Bull. Am. Meteorol. Soc., 98(1), 79–93, doi:10.1175/BAMS-D-15-0004.1, 2017.
Kew, S. F., Selten, F. M., Lenderink, G. and Hazeleger, W.: Robust assessment of future changes in extreme precipitation over the Rhine basin using a GCM, Hydrol. Earth Syst. Sci., 15(4), 1157–1166, doi:10.5194/hess-15-1157-2011, 2011.
Kew, S. F., Selten, F. M., Lenderink, G. and Hazeleger, W.: The simultaneous occurrence of surge and discharge extremes for the Rhine delta, Nat. Hazards Earth Syst. Sci., 13(8), 2017–2029, doi:10.5194/nhess-13-2017-2013, 2013.
Khanal, S., Ridder, N., Vries, H. De, Terink, W. and Hurk, B. Van Den: Storm Surge and Extreme River Discharge : A Compound Event Analysis Using Ensemble Impact Modeling, Front. Earth Sci., 7(September), 1–15, doi:10.3389/feart.2019.00224, 2019.
Khandu, Awange, J. L., Kuhn, M., Anyah, R. and Forootan, E.: Changes and variability of precipitation and temperature in the Ganges–Brahmaputra–Meghna River Basin based on global high-resolution reanalyses, Int. J. Climatol., 37(4), 2141–2159, doi:10.1002/joc.4842, 2017.
Khattak, M. S., Babel, M. S. and Sharif, M.: Hydro-meteorological trends in the upper Indus River basin in Pakistan, Clim. Res., 46(2), 103–119, doi:10.3354/cr00957, 2011.
Kiang, J. E., Gazoorian, C., McMillan, H., Coxon, G., Le Coz, J., Westerberg, I. K., Belleville, A., Sevrez, D., Sikorska, A. E., Petersen-Øverleir, A. and others: A comparison of methods for streamflow uncertainty estimation, Water Resour. Res., 54(10), 7149–7176, 2018.
King, O., Bhattacharya, A., Bhambri, R. and Bolch, T.: Glacial lakes exacerbate Himalayan glacier mass loss, Sci. Rep., 9(1), 1–9, doi:10.1038/s41598-019-53733-x, 2019.
Kirches, G., Brockmann, C., Boettcher, M., Peters, M., Bontemps, S., Lamarche, C., Schlerf, M., Santoro, M. and Defourny, P.: Land cover cci-product user guide-version 2, ESA Public Doc. CCI-LC-PUG, (2.4), 2014.
Kirschbaum, D., Kapnick, S. B., Stanley, T. and Pascale, S.: Changes in Extreme Precipitation and Landslides Over High Mountain Asia, Geophys. Res. Lett., 47(4), 1–9, doi:10.1029/2019GL085347, 2020.
Kjellstrom, T., Briggs, D., Freyberg, C., Lemke, B., Otto, M. and Hyatt, O.: Heat, Human Performance, and Occupational Health: A Key Issue for the Assessment of Global Climate Change Impacts, Annu. Rev. Public Health, 37(1), 97–112, doi:10.1146/annurev-publhealth-032315-021740, 2016.
Klein, B., Pahlow, M., Hundecha, Y. and Schumann, A.: Probability Analysis of Hydrological Loads for the Design of Flood Control Systems Using Copulas, J. Hydrol. Eng., 15(5), 360–369, doi:10.1061/(asce)he.1943-5584.0000204, 2010.
Kleinn, J., Frei, C., Gurtz, J., Lüthi, D., Vidale, P. L. and Schär, C.: Hydrologic simulations in the Rhine basin driven by a regional climate model, J. Geophys. Res. D Atmos., 110(4), 1–18, doi:10.1029/2004JD005143, 2005.
Klemeš, V.: The modelling of mountain hydrology: the ultimate challenge, in Hydrology of Mountainous Areas (Proceedings of the Strbské Pleso Workshop, Czechoslovakia, June 1988). IAHS Publ. no. 190., 1990.
Klerk, W. J., Winsemius, H. C., van Verseveld, W. J., Bakker, A. M. R. and Diermanse, F. L. M.: The co-incidence of storm surges and extreme discharges within the Rhine–Meuse Delta, Environ. Res. Lett., 10(3), 035005, doi:10.1088/1748-9326/10/3/035005, 2015.
Klijn, F., Kreibich, H., de Moel, H. and Penning-Rowsell, E.: Adaptive flood risk management planning based on a comprehensive flood risk conceptualisation, Mitig. Adapt. Strateg. Glob. Chang., 20(6), 845–864, doi:10.1007/s11027-015-9638-z, 2015.
Knowles, J. F., Blanken, P. D., Williams, M. W. and Chowanski, K. M.: Energy and surface moisture seasonally limit evaporation and sublimation from snow-free alpine tundra, Agric. For. Meteorol., 157, 106–115, doi:10.1016/j.agrformet.2012.01.017, 2012.
Koch, J., Cornelissen, T., Fang, Z., Bogena, H., Diekkrüger, B., Kollet, S. and Stisen, S.: Inter-comparison of three distributed hydrological models with respect to seasonal variability of soil moisture patterns at a small forested catchment, J. Hydrol., 533, 234–249, doi:10.1016/j.jhydrol.2015.12.002, 2016.
Kokkonen, T., Koivusalo, H., Jakeman, A. and Norton, J.: Construction of a degree–day snow model in the light of the ten iterative steps in model development, Proc. iEMSs Third Bienn. Meet. "Summit Environ. Model. Software" (July 2006), (Step 2), 12, 2006.
Koks, E. E., Jongman, B., Husby, T. G. and Botzen, W. J. W.: Combining hazard, exposure and social vulnerability to provide lessons for flood risk management, Environ. Sci. Policy, 47, 42–52, doi:10.1016/j.envsci.2014.10.013, 2015.
Koks, E. E., Rozenberg, J., Zorn, C., Tariverdi, M., Vousdoukas, M., Fraser, S. A., Hall, J. W. and Hallegatte, S.: A global multi-hazard risk analysis of road and railway infrastructure assets, Nat. Commun., 10(1), 1–11, doi:10.1038/s41467-019-10442-3, 2019.
Kormann, C., Bronstert, A., Francke, T., Recknagel, T. and Graeff, T.: Model-Based Attribution of High-Resolution Streamflow Trends in Two Alpine Basins of Western Austria, Hydrology, doi:10.3390/hydrology3010007, 2016.
Kornhuber, K., Osprey, S., Coumou, D., Petri, S., Petoukhov, V., Rahmstorf, S. and Gray, L.: Extreme weather

events in early summer 2018 connected by a recurrent hemispheric wave-7 pattern, Environ. Res. Lett., 14(5), 054002, doi:10.1088/1748-9326/ab13bf, 2019.
Kornhuber, K., Coumou, D., Vogel, E., Lesk, C., Donges, J. F., Lehmann, J. and Horton, R. M.: Amplified Rossby waves enhance risk of concurrent heatwaves in major breadbasket regions, Nat. Clim. Chang., 10(1), 48–53, doi:10.1038/s41558-019-0637-z, 2020.
Kosaka, Y. and Xie, S.-P.: Recent global-warming hiatus tied to equatorial Pacific surface cooling, Nature, 501(7467), 403, 2013.
Koster, R. D. and Suarez, M. J.: Soil Moisture Memory in Climate Models, J. Hydrometeorol., 2(6), 558–570, doi:10.1175/1525-7541(2001)002<0558:SMMICM>2.0.CO;2, 2001.
Koutsoyiannis, D.: The Hurst phenomenon and fractional Gaussian noise made easy The Hurst phenomenon and fractional Gaussian noise made easy, Hydrol. Sci. J., 47(4), 573–595, doi:10.1080/02626660209492961, 2002.
Koutsoyiannis, D.: Hydrologic Persistence and The Hurst Phenomenon, pp. 210–221., 2005a.
Koutsoyiannis, D.: Uncertainty, entropy, scaling and hydrological stochastic 2. Time dependence of hydrological processes and time scaling, Hydrol. Sci. J., 50(June), 405–426, 2005b.
Kraaijenbrink, P. D. A., Bierkens, M. F. P., Lutz, A. F. and Immerzeel, W. W.: Impact of a global temperature rise of 1.5 degrees Celsius on Asia's glaciers, Nature, 549, 257 [online] Available from: https://doi.org/10.1038/nature23878, 2017.
Kramer, N., Beckers, J. and Weerts, A.: Generator of Rainfall and Discharge Extremes (GRADE) - Part D & E, Deltares report Q4424, Deltares, Delft., 2008.
Krasnopolsky, V. M., Fox-Rabinovitz, M. S., Hou, Y. T., Lord, S. J. and Belochitski, A. A.: Accurate and fast neural network emulations of model radiation for the NCEP coupled climate forecast system: Climate simulations and seasonal predictions, Mon. Weather Rev., 138(5), 1822–1842, doi:10.1175/2009MWR3149.1, 2010.
Krishnan, R., Shrestha, A. B., Ren, G., Rajbhandari, R., Saeed, S., Sanjay, J., Syed, M. A., Vellore, R., Xu, Y., You, Q. and others: Unravelling climate change in the Hindu Kush Himalaya: rapid warming in the mountains and increasing extremes, in The Hindu Kush Himalaya Assessment, pp. 57–97, Springer., 2019.
Kron, W.: Flood risk = hazard • values • vulnerability, Water Int., 30(1), 58–68, doi:10.1080/02508060508691837, 2005.
Krysanova, V., Donnelly, C., Gelfan, A., Gerten, D., Arheimer, B., Hattermann, F. and Kundzewicz, Z. W.: How the performance of hydrological models relates to credibility of projections under climate change, Hydrol. Sci. J., 63(5), 696–720, doi:10.1080/02626667.2018.1446214, 2018.
Kundzewicz, Z. W., Kanae, S., Seneviratne, S. I., Handmer, J., Nicholls, N., Peduzzi, P., Mechler, R., Bouwer, L. M., Arnell, N., Mach, K., Muir-Wood, R., Brakenridge, G. R., Kron, W., Benito, G., Honda, Y., Takahashi, K. and Sherstyukov, B.: Flood risk and climate change: global and regional perspectives, Hydrol. Sci. J., 59(1), 1–28, doi:10.1080/02626667.2013.857411, 2014.
Kurowicka, D. and Cooke, R. M.: Uncertainty analysis with high dimensional dependence modelling, John Wiley \& Sons., 2006.
Kurylyk, B. L., Hayashi, M., Quinton, W. L., McKenzie, J. M. and Voss, C. I.: Influence of vertical and lateral heat transfer on permafrost thaw, peatland landscape transition, and groundwater flow, Water Resour. Res., 52(2), 1286–1305, doi:10.1002/2015WR018057, 2016.
Kwadijk, J. and Deursen, W. Van: Development and testing of a GIS based water balance model for the Rhine drainage basin, Utrecht University: Utrecht, The Netherlands,. [online] Available from: Internationale Komission f.ur die Hydrologie des Rheinge-bietes/Commission Internationale de l'Hydrologie du Bassin duRhin, 1999.
Lafrenière, M. J. and Lamoureux, S. F.: Effects of changing permafrost conditions on hydrological processes and fluvial fluxes, Earth-Science Rev., 191, 212–223, doi:10.1016/j.earscirev.2019.02.018, 2019.
Laganier, O., Ayral, P. A., Salze, D. and Sauvagnargues, S.: A coupling of hydrologic and hydraulic models appropriate for the fast floods of the Gardon River basin (France), Nat. Hazards Earth Syst. Sci., 14(11), 2899–2920, doi:10.5194/nhess-14-2899-2014, 2014.
Van Lanen, H. A. J., Wanders, N., Tallaksen, L. M. and Van Loon, A. F.: Hydrological drought across the world: Impact of climate and physical catchment structure, Hydrol. Earth Syst. Sci., 17(5), 1715–1732, doi:10.5194/hess-17-1715-2013, 2013.
Lau, W. K. M. and Kim, K.-M.: The 2010 Pakistan Flood and Russian Heat Wave: Teleconnection of Hydrometeorological Extremes, J. Hydrometeorol., doi:10.1175/JHM-D-11-016.1, 2012.
Lau, W. K. M. and Kim, K. M.: Impact of snow darkening by deposition of light-absorbing aerosols on snow cover in the Himalayas-Tibetan Plateau and influence on the Asian summer monsoon: A possible mechanism for the blanford hypothesis, Atmosphere (Basel)., doi:10.3390/atmos9110438, 2018.
Lawrence, D. M., Koven, C. D., Swenson, S. C., Riley, W. J. and Slater, A. G.: Permafrost thaw and resulting soil moisture changes regulate projected high-latitude CO2 and CH4 emissions, Environ. Res. Lett., 10(9), doi:10.1088/1748-9326/10/9/094011, 2015.
Ledford, A. W. and Tawn, J. A.: Statistics for near independence in multivariate extreme values, Biometrika, 83(1), 169–187, doi:10.1093/biomet/83.1.169, 1996.

Ledford, A. W. and Tawn, J. A.: Modelling Dependence Within Joint Tail Regions, J. R. Stat. Soc., 59(2), 475–499 [online] Available from: https://www.jstor.org/stable/2346058, 1997.
Ledford, A. W. and Tawn, J. A.: Diagnostics for Dependence within Time Series Extremes, J. R. Stat. Soc., 65(2), 521–543 [online] Available from: https://www.jstor.org/stable/3647519, 2003.
Lehner, B. and Grill, G.: Global river hydrography and network routing: Baseline data and new approaches to study the world's large river systems, Hydrol. Process., 27(15), 2171–2186, doi:10.1002/hyp.9740, 2013.
Lehner, B., Verdin, K. and Jarvis, A.: HydroSHEDS, , 1–27, 2008a.
Lehner, B., Verdin, K. and Jarvis, A.: New global hydrography derived from spaceborne elevation data, Eos (Washington. DC)., 89(10), 93–94, doi:10.1029/2008EO100001, 2008b.
Lehner, B., Reidy Liermann, C., Revenga, C., Vorosmarty, C., Fekete, B., Crouzet, P., Doll, P., Endejan, M., Frenken, K., Magome, J., Nilsson, C., Robertson, J. C., Rodel, R., Sindorf, N. and Wisser, D.: Global Reservoir and Dam Database, Version 1 (GRanDv1): Dams, Revision 01, [online] Available from: https://doi.org/10.7927/H4N877QK, 2011.
Leonard, M., Westra, S., Phatak, A., Lambert, M., van den Hurk, B., Mcinnes, K., Risbey, J., Schuster, S., Jakob, D. and Stafford-Smith, M.: A compound event framework for understanding extreme impacts, Wiley Interdiscip. Rev. Clim. Chang., 5(1), 113–128, doi:10.1002/wcc.252, 2014.
Lettenmaier, D. P., Wallis, J. R. and Wood, E. F.: Effect of regional heterogeneity on flood frequency estimation, Water Resour. Res., 23(2), 313–323, doi:10.1029/WR023i002p00313, 1987.
Li, G., Yu, Z., Wang, W., Ju, Q. and Chen, X.: Analysis of the spatial Distribution of precipitation and topography with GPM data in the Tibetan Plateau, Atmos. Res., 247(January), 105259, doi:10.1016/j.atmosres.2020.105259, 2021.
Li, L., Yang, S., Wang, Z., Zhu, X. and Tang, H.: Evidence of warming and wetting climate over the Qinghai-Tibet plateau, Arctic, Antarct. Alp. Res., 42(4), 449–457, doi:10.1657/1938-4246-42.4.449, 2010.
Li, L., Gochis, D. J., Sobolowski, S. and Mesquita, M. D. S.: Evaluating the present annual water budget of a Himalayan headwater river basin using a high-resolution atmosphere-hydrology model, J. Geophys. Res. Atmos., 122(9), 4786–4807, doi:10.1002/2016JD026279, 2017.
Li, N., Liu, X., Xie, W., Wu, J. and Zhang, P.: The Return Period Analysis of Natural Disasters with Statistical Modeling of Bivariate Joint Probability Distribution, Risk Anal., 33(1), 134–145, doi:10.1111/j.1539-6924.2012.01838.x, 2013.
Li, W., Guo, W., Qiu, B., Xue, Y., Hsu, P. C. and Wei, J.: Influence of Tibetan Plateau snow cover on East Asian atmospheric circulation at medium-range time scales, Nat. Commun., doi:10.1038/s41467-018-06762-5, 2018.
Li, Z., Guo, X., Yang, Y., Hong, Y., Wang, Z. and You, L.: Heatwave Trends and the Population Exposure Over China in the 21st Century as Well as Under 1.5° C and 2.0° C Global Warmer Future Scenarios, Sustainability, 11(12), 3318, 2019.
Lian, Y., Chan, I. C., Singh, J., Demissie, M., Knapp, V. and Xie, H.: Coupling of hydrologic and hydraulic models for the Illinois River Basin, J. Hydrol., 344(3–4), 210–222, doi:10.1016/j.jhydrol.2007.08.004, 2007.
Liberato, M. L. R.: The 19 January 2013 windstorm over the North Atlantic: Large-scale dynamics and impacts on Iberia, Weather Clim. Extrem., 5(1), 16–28, doi:10.1016/j.wace.2014.06.002, 2014.
Lin, N., Emanuel, K. A., Smith, J. A. and Vanmarcke, E.: Risk assessment of hurricane storm surge for New York City, J. Geophys. Res. Atmos., 115(18), 1–11, doi:10.1029/2009JD013630, 2010.
te Linde, A. H., Aerts, J. C. J. H., Bakker, A. M. R. and Kwadijk, J. C. J.: Simulating low-probability peak discharges for the Rhine basin using resampled climate modeling data, Water Resour. Res., 46(3), 1–19, doi:10.1029/2009WR007707, 2010.
Lindenschmidt, K.-E., Drastig, K. and Baborowski, M.: Structural Uncertainty in a River Water Quality Modelling System, Ecol. Modell., 204, 289–300, doi:10.1016/j.ecolmodel.2007.01.004, 2007.
Lindström, G., Johansson, B., Persson, M., Gardelin, M. and Bergström, S.: Development and test of the distributed HBV-96 hydrological model, J. Hydrol., 201(1–4), 272–288, doi:10.1016/S0022-1694(97)00041-3, 1997.
Litt, M., Shea, J., Wagnon, P., Steiner, J., Koch, I., Stigter, E. and Immerzeel, W.: Glacier ablation and temperature indexed melt models in the Nepalese Himalaya, Sci. Rep., 9(1), 5264, doi:10.1038/s41598-019-41657-5, 2019.
Littlewood, I. G. and Croke, B. F. W.: Data time-step dependency of conceptual rainfall-streamflow model parameters: An empirical study with implications for regionalisation, Hydrol. Sci. J., 53(4), 685–695, doi:10.1623/hysj.53.4.685, 2008.
Liu, D., Wang, G., Mei, R., Yu, Z. and Yu, M.: Impact of initial soil moisture anomalies on climate mean and extremes over Asia, J. Geophys. Res., 119(2), 529–545, doi:10.1002/2013JD020890, 2014a.
Liu, J., Wu, Y. and Gao, X.: Increase in occurrence of large glacier-related landslides in the high mountains of Asia, Sci. Rep., 11(1), 1–12, doi:10.1038/s41598-021-81212-9, 2021.
Liu, J. J., Cheng, Z. L. and Su, P. C.: The relationship between air temperature fluctuation and Glacial Lake Outburst Floods in Tibet, China, Quat. Int., 321, 78–87, doi:10.1016/j.quaint.2013.11.023, 2014b.
Liu, X. and Chen, B.: Climatic warming in the Tibetan Plateau during recent decades, Int. J. Climatol., 20(14),

1729–1742, doi:10.1002/1097-0088(20001130)20:14<1729::AID-JOC556>3.0.CO;2-Y, 2000.
Liu, X., Cheng, Z., Yan, L., Yin, Z.-Y. and others: Elevation dependency of recent and future minimum surface air temperature trends in the Tibetan Plateau and its surroundings, Glob. Planet. Change, 68(3), 164, 2009.
Liu, Y. and Gupta, H. V.: Uncertainty in hydrologic modeling: Toward an integrated data assimilation framework, Water Resour. Res., 43(7), 1–18, doi:10.1029/2006WR005756, 2007.
Lloyd, E. A. and Shepherd, T. G.: Environmental catastrophes, climate change, and attribution, Ann. N. Y. Acad. Sci., 1469(1), 105–124, doi:10.1111/nyas.14308, 2020.
Lo, M. H. and Famiglietti, J. S.: Effect of water table dynamics on land surface hydrologic memory, J. Geophys. Res. Atmos., 115(22), 1–12, doi:10.1029/2010JD014191, 2010.
Locci, F., Melis, M. T., Dessì, F., Stocchi, P., Akinde, M. O., Bønes, V., Bonasoni, P. and Vuillermoz, E.: Implementation of a web GIS service platform for high mountain climate research: the SHARE GeoNetwork project , Geosci. Data J., 1(2), 140–157, doi:10.1002/gdj3.14, 2014.
Loftis, J. D., Wang, H. V., DeYoung, R. J. and Ball, W. B.: Using Lidar Elevation Data to Develop a Topobathymetric Digital Elevation Model for Sub-Grid Inundation Modeling at Langley Research Center, J. Coast. Res., 76(sp1), 134–148, doi:10.2112/SI76-012, 2016.
Lorenz, E. N.: The predictability of a flow which possesses many scales of motion, Tellus, 21(3), 289–307, doi:10.3402/tellusa.v21i3.10086, 1969.
Lutz, A. F., Immerzeel, W. W., Shrestha, A. B. and Bierkens, M. F. P.: Consistent increase in High Asia's runoff due to increasing glacier melt and precipitation, Nat. Clim. Chang., 4(7), 587–592, doi:10.1038/nclimate2237, 2014.
Lutz, A. F., Immerzeel, W. W., Kraaijenbrink, P. D. A., Shrestha, A. B. and Bierkens, M. F. P.: Climate Change Impacts on the Upper Indus Hydrology : Sources , Shifts and Extremes, , (November), doi:10.1371/journal.pone.0165630, 2016.
Lutz, A. F., ter Maat, H. W., Wijngaard, R. R., Biemans, H., Syed, A., Shrestha, A. B., Wester, P. and Immerzeel, W. W.: South Asian river basins in a 1.5 °C warmer world, Reg. Environ. Chang., 19(3), 833–847, doi:10.1007/s10113-018-1433-4, 2019.
Lv, Z. and Pomeroy, J. W.: Assimilating snow observations to snow interception process simulations, Hydrol. Process., 34(10), 2229–2246, doi:10.1002/hyp.13720, 2020.
MacDonald, M. K., Pomeroy, J. W. and Pietroniro, A.: On the importance of sublimation to an alpine snow mass balance in the Canadian Rocky Mountains, Hydrol. Earth Syst. Sci., 14(7), 1401–1415, doi:10.5194/hess-14-1401-2010, 2010.
Madhura, R. K., Krishnan, R., Revadekar, J. V., Mujumdar, M. and Goswami, B. N.: Changes in western disturbances over the Western Himalayas in a warming environment, Clim. Dyn., 44(3–4), 1157–1168, doi:10.1007/s00382-014-2166-9, 2014.
Mann, H. B.: Nonparametric Tests Against Trend, Econometrica, 13(3), 245–259 [online] Available from: http://www.jstor.org/stable/1907187, 1945.
Manning, C., Widmann, M., Bevacqua, E., Van Loon, A. F., Maraun, D. and Vrac, M.: Soil moisture drought in Europe: A compound event of precipitation and potential evapotranspiration on multiple time scales, J. Hydrometeorol., 19(8), 1255–1271, doi:10.1175/JHM-D-18-0017.1, 2018.
Maraun, D. and Widmann, M.: Statistical Downscaling and Bias Correction for Climate Research, Cambridge University Press., 2018.
Maraun, D., Shepherd, T. G., Widmann, M., Zappa, G., Walton, D., Gutiérrez, J. M., Hagemann, S., Richter, I., Soares, P. M. M., Hall, A. and Mearns, L. O.: Towards process-informed bias correction of climate change simulations, in Nature Climate Change, vol. 7, pp. 764–773, Nature Publishing Group., 2017.
Marsh, C. B., Pomeroy, J. W., Spiteri, R. J. and Wheater, H. S.: A Finite Volume Blowing Snow Model for Use With Variable Resolution Meshes, Water Resour. Res., 56(2), e2019WR025307, doi:10.1029/2019WR025307, 2020.
Marshak, S.: Earth: Portrait of a Planet, 3rd ed., W. W. Norton & Company, Inc., 2008.
Martinec, J. and Rango, A.: Parameter values for snowmelt runoff modelling, J. Hydrol., doi:10.1016/0022-1694(86)90123-X, 1986.
Martius, O., Pfahl, S. and Chevalier, C.: A global quantification of compound precipitation and wind extremes, Geophys. Res. Lett., 43(14), 7709–7717, doi:10.1002/2016GL070017, 2016.
Marzeion, B., Hock, R., Anderson, B., Bliss, A., Champollion, N., Fujita, K., Huss, M., Immerzeel, W. W., Kraaijenbrink, P., Malles, J. H., Maussion, F., Radić, V., Rounce, D. R., Sakai, A., Shannon, S., van de Wal, R. and Zekollari, H.: Partitioning the Uncertainty of Ensemble Projections of Global Glacier Mass Change, Earth's Futur., 8(7), 1–25, doi:10.1029/2019EF001470, 2020.
Masina, M., Lamberti, A. and Archetti, R.: Coastal flooding: A copula based approach for estimating the joint probability of water levels and waves, Coast. Eng., 97, 37–52, doi:10.1016/j.coastaleng.2014.12.010, 2015.
Matthews, T., Wilby, R. L. and Murphy, C.: An emerging tropical cyclone–deadly heat compound hazard, Nat. Clim. Chang., 9(8), 602–606, doi:10.1038/s41558-019-0525-6, 2019.

Matthews, T., Perry, L. B., Koch, I., Aryal, D., Khadka, A., Shrestha, D., Abernathy, K., Elmore, A. C., Seimon, A., Tait, A., Elvin, S., Tuladhar, S., Baidya, S. K., Potocki, M., Birkel, S. D., Kang, S., Sherpa, T. C., Gajurel, A. and Mayewski, P. A.: Going to extremes: Installing the world's highest weather stations on mount everest, Bull. Am. Meteorol. Soc., 101(2020), E1870–E1890, doi:10.1175/BAMS-D-19-0198.1, 2020.

Maurer, J. M., Schaefer, J. M., Rupper, S. and Corley, A.: Acceleration of ice loss across the Himalayas over the past 40 years, Sci. Adv., 5(6), doi:10.1126/sciadv.aav7266, 2019a.

Maurer, J. M., Schaefer, J. M., Rupper, S. and Corley, A.: Acceleration of ice loss across the Himalayas over the past 40 years, 2019b.

Maussion, F., Scherer, D., Mölg, T., Collier, E., Curio, J. and Finkelnburg, R.: Precipitation seasonality and variability over the Tibetan Plateau as resolved by the high Asia reanalysis, J. Clim., 27(5), 1910–1927, doi:10.1175/JCLI-D-13-00282.1, 2014.

Mcgrath, G. S., Hinz, C., Sivapalan, M., Mcgrath, G. S., Hinz, C. and Temporal, M. S.: Temporal dynamics of hydrological threshold events To cite this version : Temporal dynamics of hydrological threshold events, , 11(2), 923–938, 2007.

McMillan, H. K., Westerberg, I. K. and Krueger, T.: Hydrological data uncertainty and its implications, Wiley Interdiscip. Rev. Water, 5(6), e1319, 2018.

McNamara, J. P., Kane, D. L. and Hinzman, L. D.: An analysis of streamflow hydrology in the Kuparuk River Basin, Arctic Alaska: A nested watershed approach, J. Hydrol., 206(1–2), 39–57, doi:10.1016/S0022-1694(98)00083-3, 1998.

McPhillips, L. E., Chang, H., Chester, M. V., Depietri, Y., Friedman, E., Grimm, N. B., Kominoski, J. S., McPhearson, T., Méndez-Lázaro, P., Rosi, E. J. and Shafiei Shiva, J.: Defining Extreme Events: A Cross-Disciplinary Review, Earth's Futur., 6(3), 441–455, doi:10.1002/2017EF000686, 2018.

Mei, Y., Anagnostou, E. N., Nikolopoulos, E. I. and Borga, M.: Error analysis of satellite precipitation products in mountainous basins, J. Hydrometeorol., 15(5), 1778–1793, doi:10.1175/JHM-D-13-0194.1, 2014.

van Meijgaard, E., Ulft, L. H. Van, Bosveld, F. C., Lenderink, G. and Siebesma, a P.: The KNMI regional atmospheric climate model RACMO version 2.1, Utrecht, Netherlands., 2008.

van Meijgaard, E., van Ulft, L. H., Lenderink, G., de Roode, S. R. and Timmermans, R. M. A.: Refinement and application of a regional atmospheric model for climate scenario calculations of Western Europe., 2012.

Mendoza, P. A., Clark, M. P., Mizukami, N., Newman, A. J., Barlage, M., Gutmann, E. D., Rasmussen, R. M., Rajagopalan, B., Brekke, L. D. and Arnold, J. R.: Effects of hydrologic model choice and calibration on the portrayal of climate change impacts, J. Hydrometeorol., 16(2), 762–780, doi:10.1175/JHM-D-14-0104.1, 2015.

Merz, B., Aerts, J., Arnbjerg-Nielsen, K., Baldi, M., Becker, A., Bichet, A., Blöschl, G., Bouwer, L. M., Brauer, A., Cioffi, F., Delgado, J. M., Gocht, M., Guzzetti, F., Harrigan, S., Hirschboeck, K., Kilsby, C., Kron, W., Kwon, H. H., Lall, U., Merz, R., Nissen, K., Salvatti, P., Swierczynski, T., Ulbrich, U., Viglione, A., Ward, P. J., Weiler, M., Wilhelm, B. and Nied, M.: Floods and climate: Emerging perspectives for flood risk assessment and management, Nat. Hazards Earth Syst. Sci., 14(7), 1921–1942, doi:10.5194/nhess-14-1921-2014, 2014.

Merz, B., Apel, H., Nguyen, D., Falter, D., Guse, B., Hundecha, Y., Kreibich, H., Schröter, K. and Vorogushyn, S.: From Precipitation to Damage, pp. 169–183, American Geophysical Union (AGU)., 2018.

Merz, R. and Blöschl, G.: A process typology of regional floods, Water Resour. Res., 39(12), 1–20, doi:10.1029/2002WR001952, 2003.

Merz, R. and Blöschl, G.: Regionalisation of catchment model parameters, J. Hydrol., 287(1–4), 95–123, doi:10.1016/j.jhydrol.2003.09.028, 2004.

Merz, R. and Blöschl, G.: Flood frequency hydrology: 1. Temporal, spatial, and causal expansion of information, Water Resour. Res., 44(8), 1–17, doi:10.1029/2007WR006744, 2008.

Le Meur, E., Gagliardini, O., Zwinger, T. and Ruokolainen, J.: Glacier flow modelling: A comparison of the Shallow Ice Approximation and the full-Stokes solution, Comptes Rendus Phys., 5(7), 709–722, doi:10.1016/j.crhy.2004.10.001, 2004.

De Michele, C., Salvadori, G., Canossi, M., Petaccia, A. and Rosso, R.: Bivariate Statistical Approach to Check Adequacy of Dam Spillway, J. Hydrol. Eng., 10(1), 50–57, doi:10.1061/(ASCE)1084-0699(2005)10:1(50), 2005.

Middelkoop, H., Daamen, K., Gellens, D., Grabs, W., Kwadijk, J. C. J., Lang, H., Parmet, B. W. A. H., Schädler, B., Schulla, J. and Wilke, K.: Impact of Climate Change on Hydrological Regimes and Water Resources Management in the Rhine Basin, Clim. Change, 49(1), 105–128, doi:10.1023/A:1010784727448, 2001.

Miller, A. J. D., Immerzeel, W. W. and Rees, G.: Climate Change Impacts on Glacier Hydrology and River Discharge in the Hindu Kush – Himalayas Climate Change Impacts on Glacier Hydrology and River Discharge in the Hindu Kush – Himalayas, , 32(4), 461–467, 2012.

Milly, P. C. D., Wetherald, R. T., Dunne, K. A. and Delworth, T. L.: Increasing risk of great floods in a changing climate, Nature, 415(6871), 514–517, doi:10.1038/415514a, 2002.

Mindlin, J., Shepherd, T. G., Vera, C. S., Osman, M., Zappa, G., Lee, R. W. and Hodges, K. I.: Storyline description of Southern Hemisphere midlatitude circulation and precipitation response to greenhouse gas forcing, Clim. Dyn., 54(9–10), 4399–4421, doi:10.1007/s00382-020-05234-1, 2020.

Minville, M., Velázquez, J. A., Gauvin St-Denis, B., Muerth, M. J., Schmid, J., Chaumont, D., Ludwig, R., Caya, D., Turcotte, R. and Ricard, S.: On the need for bias correction in regional climate scenarios to assess climate change impacts on river runoff, Hydrol. Earth Syst. Sci., 17(3), 1189–1204, doi:10.5194/hess-17-1189-2013, 2013.
Mishra, A. K. and Singh, V. P.: A review of drought concepts, J. Hydrol., 391(1–2), 202–216, doi:10.1016/j.jhydrol.2010.07.012, 2010.
Mishra, V., Shah, R., Azhar, S., Shah, H., Modi, P. and Kumar, R.: Reconstruction of droughts in India using multiple land-surface models (1951-2015), Hydrol. Earth Syst. Sci., 22(4), 2269–2284, doi:10.5194/hess-22-2269-2018, 2018.
de Moel, H., Jongman, B., Kreibich, H., Merz, B., Penning-Rowsell, E. and Ward, P. J.: Flood risk assessments at different spatial scales, Mitig. Adapt. Strateg. Glob. Chang., 20(6), doi:10.1007/s11027-015-9654-z, 2015.
Moezzi, M., Janda, K. B. and Rotmann, S.: Using stories, narratives, and storytelling in energy and climate change research, Energy Res. Soc. Sci., 31, 1–10, doi:10.1016/j.erss.2017.06.034, 2017.
Moftakhari, H. R., Salvadori, G., AghaKouchak, A., Sanders, B. F. and Matthew, R. A.: Compounding effects of sea level rise and fluvial flooding, Proc. Natl. Acad. Sci., 114(37), 9785–9790, doi:10.1073/pnas.1620325114, 2017.
Moges, E., Demissie, Y., Larsen, L. and Yassin, F.: Review: Sources of hydrological model uncertainties and advances in their analysis, Water (Switzerland), 13(1), 1–23, doi:10.3390/w13010028, 2021.
Montanari, A., Rosso, R. and Taqqu, M. S.: Fractionally dilferenced ARIMA models applied to hydrologic time series: Identification, estimation, and simulation, Water Resour. Res., 33(5), 1035–1044, 1997.
Montesi, J., Elder, K., Schmidt, R. A. and Davis, R. E.: Sublimation of intercepted snow within a subalpine forest canopy at two elevations, J. Hydrometeorol., 5(5), 763–773, doi:10.1175/1525-7541(2004)005<0763:SOISWA>2.0.CO;2, 2004.
Moore, F. C., Baldos, U., Hertel, T. and Diaz, D.: New science of climate change impacts on agriculture implies higher social cost of carbon, Nat. Commun., 8(1), 1–9, doi:10.1038/s41467-017-01792-x, 2017.
Moriasi, D. N., Arnold, J. G., Liew, M. W. Van, Bingner, R. L., Harmel, R. D. and Veith, T. L.: Model Evaluation Guidelines for Systematic Quantification of Accuracy in Watershed Simulations, , 50(3), 885–900, 2007.
Mott, R., Vionnet, V. and Grünewald, T.: The Seasonal Snow Cover Dynamics: Review on Wind-Driven Coupling Processes, Front. Earth Sci., 6, doi:10.3389/feart.2018.00197, 2018.
Moulin, L., Gaume, E. and Obled, C.: Uncertainties on mean areal precipitation: Assessment and impact on streamflow simulations, Hydrol. Earth Syst. Sci., 13(2), 99–114, doi:10.5194/hess-13-99-2009, 2009.
Mudelsee, M., Borngen, M., Tetzlaff, G. and Grunewald, U.: No Upward Trends İn The Occurrence Of Extreme Floods İn Central Europe, Nature, 425(September), 166*169, 2003.
Mukhopadhyay, B. and Khan, A.: A quantitative assessment of the genetic sources of the hydrologic flow regimes in Upper Indus Basin and its significance in a changing climate, J. Hydrol., 509, 549–572, doi:10.1016/j.jhydrol.2013.11.059, 2014.
Na, Y., Fu, Q. and Kodama, C.: Precipitation Probability and Its Future Changes From a Global Cloud-Resolving Model and CMIP6 Simulations, J. Geophys. Res. Atmos., 125(5), 1–23, doi:10.1029/2019JD031926, 2020.
Najafabadi, M. M., Villanustre, F., Khoshgoftaar, T. M., Seliya, N., Wald, R. and Muharemagic, E.: Deep learning applications and challenges in big data analytics, J. Big Data, 2(1), 1–21, doi:10.1186/s40537-014-0007-7, 2015.
Nash, J. E. and Sutcliffe, J. V: River Flow Forecasting Through Conceptual Models Part I-a Discussion of Principles*, J. Hydrol., 10, 282–290, doi:10.1016/0022-1694(70)90255-6, 1970.
Nelson, G. C., Valin, H., Sands, R. D., Havlík, P., Ahammad, H., Deryng, D., Elliott, J., Fujimori, S., Hasegawa, T., Heyhoe, E., Kyle, P., Von Lampe, M., Lotze-Campen, H., Mason D'Croz, D., Van Meijl, H., Van Der Mensbrugghe, D., Müller, C., Popp, A., Robertson, R., Robinson, S., Schmid, E., Schmitz, C., Tabeau, A. and Willenbockel, D.: Climate change effects on agriculture: Economic responses to biophysical shocks, Proc. Natl. Acad. Sci. U. S. A., 111(9), 3274–3279, doi:10.1073/pnas.1222465110, 2014.
Nelson, J. A., Pérez-Priego, O., Zhou, S., Poyatos, R., Zhang, Y., Blanken, P. D., Gimeno, T. E., Wohlfahrt, G., Desai, A. R., Gioli, B., Limousin, J. M., Bonal, D., Paul-Limoges, E., Scott, R. L., Varlagin, A., Fuchs, K., Montagnani, L., Wolf, S., Delpierre, N., Berveiller, D., Gharun, M., Belelli Marchesini, L., Gianelle, D., Šigut, L., Mammarella, I., Siebicke, L., Andrew Black, T., Knohl, A., Hörtnagl, L., Magliulo, V., Besnard, S., Weber, U., Carvalhais, N., Migliavacca, M., Reichstein, M. and Jung, M.: Ecosystem transpiration and evaporation: Insights from three water flux partitioning methods across FLUXNET sites, Glob. Chang. Biol., 26(12), 6916–6930, doi:10.1111/gcb.15314, 2020.
Nepal, S.: Impacts of climate change on the hydrological regime of the Koshi river basin in the Himalayan region, J. Hydro-environment Res., 10, 76–89, doi:10.1016/j.jher.2015.12.001, 2016.
Nepal, S., Flügel, W.-A., Krause, P., Fink, M. and Fischer, C.: Assessment of Spatial Transferability of Process-Based Hydrological Model Parameters in Two Neighboring Catchments in the Himalayan Region, Hydrol. Process., doi:10.1002/hyp.11199, 2017.
Nicholson, S. E.: Land Surface Processes and Land Use Change Land, Rev. Geophys. 38, 1 / Febr. 2000, 38(1999), 117–139, doi:10.1029/1999RG900014, 2000.

Nied, M., Pardowitz, T., Nissen, K., Ulbrich, U., Hundecha, Y. and Merz, B.: On the relationship between hydro-meteorological patterns and flood types, J. Hydrol., 519(PD), 3249–3262, doi:10.1016/j.jhydrol.2014.09.089, 2014.
Nigrelli, G., Fratianni, S., Zampollo, A., Turconi, L. and Chiarle, M.: The altitudinal temperature lapse rates applied to high elevation rockfalls studies in the Western European Alps, Theor. Appl. Climatol., doi:10.1007/s00704-017-2066-0, 2018.
Ning, L., Zhan, C., Luo, Y., Wang, Y. and Liu, L.: A review of fully coupled atmosphere-hydrology simulations, J. Geogr. Sci., 29(3), 465–479, doi:10.1007/s11442-019-1610-5, 2019.
NOAA: Climate at a Glance | National Centers for Environmental Information (NCEI), [online] Available from: https://www.ncdc.noaa.gov/cag/global/time-series (Accessed 7 October 2020), 2020.
Nobre, C., Brasseur, G. P., Shapiro, M. A., Lahsen, M., Brunet, G., Busalacchi, A. J., Hibbard, K., Seitzinger, S., Noone, K. and Ometto, J. P.: Addressing the complexity of the Earth system, Bull. Am. Meteorol. Soc., 91(10), 1389–1396, doi:10.1175/2010BAMS3012.1, 2010.
North, G. R.: Theory of Energy-Balance Climate Models, J. Atmos. Sci., 32(11), 2033–2043, doi:10.1175/1520-0469(1975)032<2033:TOEBCM>2.0.CO;2, 1975.
O'Gorman, P. A.: Precipitation Extremes Under Climate Change, Curr. Clim. Chang. Reports, 1(2), 49–59, doi:10.1007/s40641-015-0009-3, 2015.
Ochoa-Rodriguez, S., Wang, L. P., Gires, A., Pina, R. D., Reinoso-Rondinel, R., Bruni, G., Ichiba, A., Gaitan, S., Cristiano, E., Van Assel, J., Kroll, S., Murlà-Tuyls, D., Tisserand, B., Schertzer, D., Tchiguirinskaia, I., Onof, C., Willems, P. and Ten Veldhuis, M. C.: Impact of spatial and temporal resolution of rainfall inputs on urban hydrodynamic modelling outputs: A multi-catchment investigation, J. Hydrol., 531, 389–407, doi:10.1016/j.jhydrol.2015.05.035, 2015.
Ohmura, A., Bauder, A., Müller, H. and Kappenberger, G.: Long-term change of mass balance and the role of radiation, Ann. Glaciol., 46(October 2007), 367–374, doi:10.3189/172756407782871297, 2007.
Olbert, A. I. and Hartnett, M.: Storms and surges in Irish coastal waters, Ocean Model., 34(1–2), 50–62, doi:10.1016/j.ocemod.2010.04.004, 2010.
Olbert, A. I., Comer, J., Nash, S. and Hartnett, M.: High-resolution multi-scale modelling of coastal flooding due to tides, storm surges and rivers inflows. A Cork City example, Coast. Eng., 121(December 2016), 278–296, doi:10.1016/j.coastaleng.2016.12.006, 2017.
Orlowsky, B. and Seneviratne, S. I.: Global changes in extreme events: Regional and seasonal dimension, Clim. Change, 110(3–4), 669–696, doi:10.1007/s10584-011-0122-9, 2012.
Orsolini, Y., Wegmann, M., Dutra, E., Liu, B., Balsamo, G., Yang, K., Rosnay, P. De, Zhu, C., Wang, W., Senan, R. and Arduini, G.: Evaluation of snow depth and snow cover over the Tibetan Plateau in global reanalyses using in situ and satellite remote sensing observations, , 2221–2239, 2019.
Orth, R. and Seneviratne, S. I.: Analysis of soil moisture memory from observations in Europe, J. Geophys. Res. Atmos., 117(15), 1–19, doi:10.1029/2011JD017366, 2012.
Orth, R., Staudinger, M., Seneviratne, S. I., Seibert, J. and Zappa, M.: Does model performance improve with complexity? A case study with three hydrological models, J. Hydrol., 523, 147–159, doi:10.1016/j.jhydrol.2015.01.044, 2015.
Östrem, G.: Ice Melting under a Thin Layer of Moraine, and the Existence of Ice Cores in Moraine Ridges, Geogr. Ann., 41(4), 228–230 [online] Available from: http://www.jstor.org/stable/4626805, 1959.
Ostrowski, M., Bach, M., Desimone, S. and Gamerith, V.: Analysis of the time-step dependency of parameters in conceptual hydrological models, 2010.
Oudin, L., Michel, C. and Anctil, F.: Which potential evapotranspiration input for a lumped rainfall-runoff model? Part 1 - Can rainfall-runoff models effectively handle detailed potential evapotranspiration inputs?, J. Hydrol., 303(1–4), 275–289, doi:10.1016/j.jhydrol.2004.08.025, 2005.
Palazzi, E., Von Hardenberg, J. and Provenzale, A.: Precipitation in the hindu-kush karakoram himalaya: Observations and future scenarios, J. Geophys. Res. Atmos., 118(1), 85–100, doi:10.1029/2012JD018697, 2013.
Palazzi, E., Von Hardenberg, J., Terzago, S. and Provenzale, A.: Precipitation in the Karakoram-Himalaya: a CMIP5 view, Clim. Dyn., 45(1–2), 21–45, doi:10.1007/s00382-014-2341-z, 2015.
Papacharalampous, G., Koutsoyiannis, D. and Montanari, A.: Quantification of predictive uncertainty in hydrological modelling by harnessing the wisdom of the crowd: Methodology development and investigationusingtoymodels, Adv. Water Resour., 136(103470), 1–63, 2019.
Pappenberger, F., Beven, K. J., Hunter, N. M., Bates, P. D., Gouweleeuw, B. T., Thielen, J. and de Roo, A. P. J.: Cascading model uncertainty from medium range weather forecasts (10 days) through a rainfall-runoff model to flood inundation predictions within the European Flood Forecasting System (EFFS), Hydrol. Earth Syst. Sci., 9(4), 381–393, doi:10.5194/hess-9-381-2005, 2005.
Pasquier, U., He, Y., Hooton, S., Goulden, M. and Hiscock, K. M.: An integrated 1D–2D hydraulic modelling approach to assess the sensitivity of a coastal region to compound flooding hazard under climate change, Nat. Hazards, 98(3), 915–937, doi:10.1007/s11069-018-3462-1, 2019.

Patil, S. and Stieglitz, M.: Modelling daily streamflow at ungauged catchments: What information is necessary?, Hydrol. Process., 28(3), 1159–1169, doi:10.1002/hyp.9660, 2014.
Paul, F. and Kotlarski, S.: Forcing a distributed glacier mass balance model with the regional climate model REMO. Part II: Downscaling strategy and results for two swiss glaciers, J. Clim., 23(6), 1607–1620, doi:10.1175/2009JCLI3345.1, 2010.
Pecl, G. T., Araújo, M. B., Bell, J. D., Blanchard, J., Bonebrake, T. C., Chen, I. C., Clark, T. D., Colwell, R. K., Danielsen, F., Evengård, B., Falconi, L., Ferrier, S., Frusher, S., Garcia, R. A., Griffis, R. B., Hobday, A. J., Janion-Scheepers, C., Jarzyna, M. A., Jennings, S., Lenoir, J., Linnetved, H. I., Martin, V. Y., McCormack, P. C., McDonald, J., Mitchell, N. J., Mustonen, T., Pandolfi, J. M., Pettorelli, N., Popova, E., Robinson, S. A., Scheffers, B. R., Shaw, J. D., Sorte, C. J. B., Strugnell, J. M., Sunday, J. M., Tuanmu, M. N., Vergés, A., Villanueva, C., Wernberg, T., Wapstra, E. and Williams, S. E.: Biodiversity redistribution under climate change: Impacts on ecosystems and human well-being, Science (80-.)., 355(6332), doi:10.1126/science.aai9214, 2017.
Pelletier, J. D. and Turcotte, D. L.: Long-range persistence in climatological and hydrological time series: Analysis, modeling and application to drought hazard assessment, J. Hydrol., 203(1–4), 198–208, doi:10.1016/S0022-1694(97)00102-9, 1997.
Pellicciotti, F., Brock, B., Strasser, U., Burlando, P., Funk, M. and Corripio, J.: An enhanced temperature-index glacier melt model including the shortwave radiation balance: Development and testing for Haut Glacier d'Arolla, Switzerland, J. Glaciol., doi:10.3189/172756505781829124, 2005.
Pellicciotti, F., Buergi, C., Immerzeel, W. W., Konz, M. and Shrestha, A. B.: Challenges and uncertainties in hydrological modeling of remote hindu KushKarakoramHimalayan (HKH) Basins: Suggestions for calibration strategies, Mt. Res. Dev., 32(1), 39–50, doi:10.1659/MRD-JOURNAL-D-11-00092.1, 2012.
Peng, D., Zhou, T., Zhang, L. and Zou, L.: Detecting human influence on the temperature changes in Central Asia, Clim. Dyn., 1–16, 2019.
Pepin, N., Bradley, R. S., Diaz, H. F., Baraër, M., Caceres, E. B., Forsythe, N., Fowler, H., Greenwood, G., Hashmi, M. Z., Liu, X. D. and Others: Elevation-dependent warming in mountain regions of the world, Nat. Clim. Chang., 5(5), 424–430, doi:10.1038/nclimate2563, 2015.
Perkins-Kirkpatrick, S. E. and Lewis, S. C.: Increasing trends in regional heatwaves, Nat. Commun., 11(1), 1–8, doi:10.1038/s41467-020-16970-7, 2020.
Peters-Lidard, C. D., Clark, M., Samaniego, L., Verhoest, N. E. C., Van Emmerik, T., Uijlenhoet, R., Achieng, K., Franz, T. E. and Woods, R.: Scaling, similarity, and the fourth paradigm for hydrology, Hydrol. Earth Syst. Sci., 21(7), 3701–3713, doi:10.5194/hess-21-3701-2017, 2017.
Pfahl, S., O'Gorman, P. A. and Fischer, E. M.: Understanding the regional pattern of projected future changes in extreme precipitation, Nat. Clim. Chang., 7(6), 423–427, doi:10.1038/nclimate3287, 2017.
Photiadou, C. S., Weerts, A. H. and M. Van Den Hurk, B. J. J.: Evaluation of two precipitation data sets for the Rhine River using streamflow simulations, Hydrol. Earth Syst. Sci., 15(11), 3355–3366, doi:10.5194/hess-15-3355-2011, 2011.
Pinter, N., Van der Ploeg, R. R., Schweigert, P. and Hoefer, G.: Flood magnification on the River Rhine, Hydrol. Process., 20(1), 147–164, doi:10.1002/hyp.5908, 2006.
Pomeroy, J. W. and Gray, D. M.: Snowcover Accumulation, Relocation and Management, National Hydrology Research Institute. [online] Available from: https://books.google.nl/books?id=dS21PhlMcn8C, 1995.
Poschlod, B., Zscheischler, J., Sillmann, J., Wood, R. R. and Ludwig, R.: Climate change effects on hydrometeorological compound events over southern Norway, Weather Clim. Extrem., 28, 100253, doi:10.1016/j.wace.2020.100253, 2020.
Poulin, A., Huard, D., Favre, A.-C. and Pugin, S.: Importance of Tail Dependence in Bivariate Frequency Analysis, J. Hydrol. Eng., 12(4), 394–403, doi:10.1061/(ASCE)1084-0699(2007)12:4(394), 2007.
Priestley, C. H. B. and Taylor, R. J.: On the Assessment of Surface Heat Flux and Evaporation Using Large-Scale Parameters, Mon. Weather Rev., doi:10.1175/1520-0493(1972)100<0081:OTAOSH>2.3.CO;2, 1972.
Pritchard, D. M. W., Forsythe, N., Fowler, H. J., O'Donnell, G. M. and Li, X. F.: Evaluation of upper indus near-surface climate representation by WRF in the High Asia Refined Analysis, J. Hydrometeorol., 20(3), 467–487, doi:10.1175/JHM-D-18-0030.1, 2019.
Prudhomme, C. and Genevier, M.: Can atmospheric circulation be linked to flooding in Europe?, Hydrol. Process., 25(7), 1180–1190, doi:10.1002/hyp.7879, 2011.
Prudhomme, C., Giuntoli, I., Robinson, E. L., Clark, D. B., Arnell, N. W., Dankers, R., Fekete, B. M., Franssen, W., Gerten, D., Gosling, S. N., Hagemann, S., Hannah, D. M., Kim, H., Masaki, Y., Satoh, Y., Stacke, T., Wada, Y. and Wisser, D.: Hydrological droughts in the 21st century, hotspots and uncertainties from a global multimodel ensemble experiment, Proc. Natl. Acad. Sci. U. S. A., 111(9), 3262–3267, doi:10.1073/pnas.1222473110, 2014.
Puma, M. J. and Cook, B. I.: Effects of irrigation on global climate during the 20th century, J. Geophys. Res. Atmos., 115(16), 1–15, doi:10.1029/2010JD014122, 2010.
Qin, J., Yang, K., Liang, S. and Guo, X.: The altitudinal dependence of recent rapid warming over the Tibetan Plateau, Clim. Change, 97(1), 321–327, doi:10.1007/s10584-009-9733-9, 2009.

Qin, Y., Abatzoglou, J. T., Siebert, S., Huning, L. S., AghaKouchak, A., Mankin, J. S., Hong, C., Tong, D., Davis, S. J. and Mueller, N. D.: Agricultural risks from changing snowmelt, Nat. Clim. Chang., 10(5), 459–465, doi:10.1038/s41558-020-0746-8, 2020.
Quinton, W. L. and Baltzer, J. L.: The active-layer hydrology of a peat plateau with thawing permafrost (Scotty Creek, Canada), Hydrogeol. J., 21(1), 201–220, doi:10.1007/s10040-012-0935-2, 2013.
Qutbudin, I., Shiru, M. S., Sharafati, A., Ahmed, K., Al-Ansari, N., Yaseen, Z. M., Shahid, S. and Wang, X.: Seasonal Drought Pattern Changes Due to Climate Variability: Case Study in Afghanistan, Water, 11(5), 1096, 2019.
Ragettli, S. and Pellicciotti, F.: Calibration of a physically based, spatially distributed hydrological model in a glacierized basin: On the use of knowledge from glaciometeorological processes to constrain model parameters, Water Resour. Res., doi:10.1029/2011WR010559, 2012.
Ragettli, S., Immerzeel, W. W. and Pellicciotti, F.: Contrasting climate change impact on river flows from high-altitude catchments in the Himalayan and Andes Mountains, , 113(33), doi:10.1073/pnas.1606526113, 2016.
Rajagopalan, B. and Lall, U.: A k-nearest-neighbor Simulator for Daily Precipitation and Other Variables, Water Resour. Res., 35(10), 3089–3101, doi:10.1029/1999WR900028, 1999.
Ramanathan, V. and Carmichael, G.: Global and regional climate changes due to black carbon, Nat. Geosci., 1(4), 221–227, doi:10.1038/ngeo156, 2008.
Rango, A. and Martinec, J.: Revisiting the Degree-Day Method for Snowmelt Computations, JAWRA J. Am. Water Resour. Assoc., 31(4), 657–669, doi:10.1111/j.1752-1688.1995.tb03392.x, 1995.
Raveh-Rubin, S. and Wernli, H.: Large-scale wind and precipitation extremes in the Mediterranean: a climatological analysis for 1979-2012, Q. J. R. Meteorol. Soc., 141(691), 2404–2417, doi:10.1002/qj.2531, 2015.
Raymond, C., Matthews, T. and Horton, R. M.: The emergence of heat and humidity too severe for human tolerance, Sci. Adv., 6(19), doi:10.1126/sciadv.aaw1838, 2020.
Reba, M. L., Pomeroy, J., Marks, D. and Link, T. E.: Estimating surface sublimation losses from snowpacks in a mountain catchment using eddy covariance and turbulent transfer calculations, Hydrol. Process., 26(24), 3699–3711, doi:10.1002/hyp.8372, 2012.
Reed, S., Koren, V., Smith, M., Zhang, Z., Moreda, F. and Seo, D. J.: Overall distributed model intercomparison project results, J. Hydrol., 298(1–4), 27–60, doi:10.1016/j.jhydrol.2004.03.031, 2004.
Rees, H. G. and Collins, D. N.: Regional differences in response of flow in glacier-fed Himalayan rivers to climatic warming, in Hydrological Processes, vol. 20, pp. 2157–2169, John Wiley & Sons, Ltd., 2006.
Refsgaard, J. C. and Knudsen, J.: Operational validation and intercomparison of different types of hydrological models, Water Resour. Res., 32(7), 2189–2202, doi:10.1029/96WR00896, 1996.
Refsgaard, J. C., Christensen, S., Sonnenborg, T. O., Seifert, D., Højberg, A. L. and Troldborg, L.: Review of strategies for handling geological uncertainty in groundwater flow and transport modeling, Adv. Water Resour., 36, 36–50, doi:https://doi.org/10.1016/j.advwatres.2011.04.006, 2012.
Reid, T. D. and Brock, B. W.: An energy-balance model for debris-covered glaciers including heat conduction through the debris layer, J. Glaciol., 56(199), 903–916, doi:10.3189/002214310794457218, 2010.
Ren, L., Ren, L., Zhou, T., Zhou, T., Zhou, T. and Zhang, W.: Attribution of the record-breaking heat event over Northeast Asia in summer 2018: The role of circulation, Environ. Res. Lett., 15(5), doi:10.1088/1748-9326/ab8032, 2020.
Ren, Y.-Y., Ren, G.-Y., Sun, X.-B., Shrestha, A. B., You, Q.-L., Zhan, Y.-J., Rajbhandari, R., Zhang, P.-F. and Wen, K.-M.: Observed changes in surface air temperature and precipitation in the Hindu Kush Himalayan region over the last 100-plus years, Adv. Clim. Chang. Res., 8(3), 148–156, 2017.
Renard, B., Kavetski, D., Kuczera, G., Thyer, M. and Franks, S. W.: Understanding predictive uncertainty in hydrologic modeling: The challenge of identifying input and structural errors, Water Resour. Res., 46(5), 1–22, doi:10.1029/2009WR008328, 2010.
Renard, B., Kochanek, K., Lang, M., Garavaglia, F., Paquet, E., Neppel, L., Najib, K., Carreau, J., Arnaud, P., Aubert, Y., Borchi, F., Soubeyroux, J. M., Jourdain, S., Veysseire, J. M., Sauquet, E., Cipriani, T. and Auffray, A.: Data-based comparison of frequency analysis methods: A general framework, Water Resour. Res., 49(2), 825–843, doi:10.1002/wrcr.20087, 2013.
Resnick, S. I.: Heavy-tail phenomena: probabilistic and statistical modeling, Springer Science & Business Media., 2007.
Reznichenko, N., Davies, T., Shulmeister, J. and McSaveney, M.: Effects of debris on ice-surface melting rates: An experimental study, J. Glaciol., 56(197), 384–394, doi:10.3189/002214310792447725, 2010.
RGI Consortium: GLIMS: Global Land Ice Measurements from Space, A Dataset Glob. Glacier Outlines Version 6.0 Tech. Report, Glob. L. Ice Meas. from Space, Color. USA., 1, doi:https://doi.org/10.7265/N5-RGI-60, 2017.
Ridder, N., Vries, H. De, Drijfhout, S., Brink, H. Van Den, Meijgaard, E. Van and Vries, H. De: Extreme storm surge modelling in the North Sea The role of the sea state , forcing frequency and spatial forcing resolution, , (i), 255–272, doi:10.1007/s10236-018-1133-0, 2018a.
Ridder, N., Vries, H. De and Drijfhout, S.: The role of atmospheric rivers in compound events consisting of heavy

precipitation and high storm surges along the Dutch coast, , 3311–3326, 2018b.
Robine, J. M., Cheung, S. L. K., Le Roy, S., Van Oyen, H., Griffiths, C., Michel, J. P. and Herrmann, F. R.: Death toll exceeded 70,000 in Europe during the summer of 2003, Comptes Rendus - Biol., 331(2), 171–178, doi:10.1016/j.crvi.2007.12.001, 2008.
Rodell, M., Beaudoing, H. K., L'Ecuyer, T. S., Olson, W. S., Famiglietti, J. S., Houser, P. R., Adler, R., Bosilovich, M. G., Clayson, C. A., Chambers, D., Clark, E., Fetzer, E. J., Gao, X., Gu, G., Hilburn, K., Huffman, G. J., Lettenmaier, D. P., Liu, W. T., Robertson, F. R., Schlosser, C. A., Sheffield, J. and Wood, E. F.: The observed state of the water cycle in the early twenty-first century, J. Clim., 28(21), 8289–8318, doi:10.1175/JCLI-D-14-00555.1, 2015.
Rohini, P., Rajeevan, M. and Srivastava, A. K.: On the Variability and Increasing Trends of Heat Waves over India, Sci. Rep., 6, 1–9, doi:10.1038/srep26153, 2016.
Röhl, K.: Characteristics and evolution of supraglacial ponds on debris-covered Tasman Glacier, New Zealand, J. Glaciol., 54(188), 867–880, doi:10.3189/002214308787779861, 2008.
Rojas, R., Feyen, L. and Dassargues, A.: Conceptual model uncertainty in groundwater modeling: Combining generalized likelihood uncertainty estimation and Bayesian model averaging, Water Resour. Res., 44(12), 1–16, doi:10.1029/2008WR006908, 2008.
Rosenzweig, C., Elliott, J., Deryng, D., Ruane, A. C., Müller, C., Arneth, A., Boote, K. J., Folberth, C., Glotter, M., Khabarov, N., Neumann, K., Piontek, F., Pugh, T. A. M., Schmid, E., Stehfest, E., Yang, H. and Jones, J. W.: Assessing agricultural risks of climate change in the 21st century in a global gridded crop model intercomparison, Proc. Natl. Acad. Sci. U. S. A., 111(9), 3268–3273, doi:10.1073/pnas.1222463110, 2014.
Rössler, O., Froidevaux, P., Boerst, U., Rickli, R., Martius, O. and Weingartner, R.: Retrospective analysis of a nonforecasted rain-on-snow flood in the Alps-A matter of model limitations or unpredictable nature?, Hydrol. Earth Syst. Sci. Discuss., 10, 12861–12904, doi:10.5194/hessd-10-12861-2013, 2013.
Rounce, D. R., King, O., McCarthy, M., Shean, D. E. and Salerno, F.: Quantifying Debris Thickness of Debris-Covered Glaciers in the Everest Region of Nepal Through Inversion of a Subdebris Melt Model, J. Geophys. Res. Earth Surf., 123(5), 1094–1115, doi:10.1029/2017JF004395, 2018.
Roy, N. Sen and Kaur, S.: Climatology of monsoon rains of Myanmar (Burma), Int. J. Climatol., 20(8), 913–928, 2000.
Ruffault, J., Curt, T., Martin-Stpaul, N. K., Moron, V. and Trigo, R. M.: Extreme wildfire events are linked to global-change-type droughts in the northern Mediterranean, Nat. Hazards Earth Syst. Sci., 18(3), 847–856, doi:10.5194/nhess-18-847-2018, 2018.
de Ruiter, M. C., Couasnon, A., van den Homberg, M. J. C., Daniell, J. E., Gill, J. C. and Ward, P. J.: Why We Can No Longer Ignore Consecutive Disasters, Earth's Futur., 8(3), doi:10.1029/2019EF001425, 2020.
Rupp, D. E., Li, S., Massey, N., Sparrow, S. N., Mote, P. W. and Allen, M.: Anthropogenic influence on the changing likelihood of an exceptionally warm summer in Texas, 2011, Geophys. Res. Lett., 42(7), 2392–2400, doi:10.1002/2014GL062683, 2015.
Saha, A. and Ghosh, S.: Can the weakening of Indian Monsoon be attributed to anthropogenic aerosols?, Environ. Res. Commun., 1(6), 061006, doi:10.1088/2515-7620/ab2c65, 2019.
Saha, A., Ghosh, S., Sahana, A. S. and Rao, E. P.: Failure of CMIP5 climate models in simulating post-1950 decreasing trend of Indian monsoon, Geophys. Res. Lett., 41(20), 7323–7330, doi:10.1002/2014GL061573, 2014.
Sakai, A. and Fujita, K.: Contrasting glacier responses to recent climate change in high-mountain Asia, Sci. Rep., 7(1), 1–8, doi:10.1038/s41598-017-14256-5, 2017.
Salama, M. S., van der Velde, R., Zhong, L., Ma, Y., Ofwono, M. and Su, Z.: Decadal variations of land surface temperature anomalies observed over the Tibetan Plateau by the Special Sensor Microwave Imager (SSM/I) from 1987 to 2008, Clim. Change, 114(3–4), 769–781, doi:10.1007/s10584-012-0427-3, 2012.
Salerno, F., Guyennon, N., Thakuri, S., Viviano, G., Romano, E., Vuillermoz, E., Cristofanelli, P., Stocchi, P., Agrillo, G., Ma, Y. and Tartari, G.: Weak precipitation, warm winters and springs impact glaciers of south slopes of Mt. Everest (central Himalaya) in the last 2 decades (1994-2013), Cryosphere, 9(3), 1229–1247, doi:10.5194/tc-9-1229-2015, 2015.
Saloranta, T., Thapa, A., Kirkham, J. D., Koch, I., Melvold, K., Stigter, E., Litt, M. and Møen, K.: A Model Setup for Mapping Snow Conditions in High-Mountain Himalaya, Front. Earth Sci., 7, doi:10.3389/feart.2019.00129, 2019.
Salvadori, G., De Michele, C., Kottegoda, N. T. and Rosso, R.: Extremes in nature: an approach using copulas, Springer Science & Business Media., 2007.
Salvadori, G., Durante, F., De Michele, C., Bernardi, M. and Petrella, L.: A multivariate copula-based framework for dealing with hazard scenarios and failure probabilities, Water Resour. Res., 52(5), 3701–3721, doi:10.1002/2015WR017225, 2016.
Santiago-Collazo, F. L., Bilskie, M. V. and Hagen, S. C.: A comprehensive review of compound inundation models in low-gradient coastal watersheds, Environ. Model. Softw., 119(June), 166–181, doi:10.1016/j.envsoft.2019.06.002, 2019.

Savenije, H. H. G.: The importance of interception and why we should delete the term evapotranspiration from our vocabulary, Hydrol. Process., 18(8), 1507–1511, doi:10.1002/hyp.5563, 2004.
Schaller, N., Sillmann, J., Müller, M., Haarsma, R., Hazeleger, W., Hegdahl, T. J., Kelder, T., van den Oord, G., Weerts, A. and Whan, K.: The role of spatial and temporal model resolution in a flood event storyline approach in western Norway, Weather Clim. Extrem., 29, 100259, doi:10.1016/j.wace.2020.100259, 2020.
Schanze, J.: Flood risk management - A basic framework, in Flood Risk Management: Hazards, Vulnerability and Mitigation Measures, vol. 67, pp. 1–20., 2006.
Scherler, D., Bookhagen, B. and Strecker, M. R.: Spatially variable response of Himalayan glaciers to climate change affected by debris cover, Nat. Geosci., 4(3), 156–159, doi:10.1038/ngeo1068, 2011.
Schewe, J., Heinke, J., Gerten, D., Haddeland, I., Arnell, N. W., Clark, D. B., Dankers, R., Eisner, S., Fekete, B. M., Colón-González, F. J., Gosling, S. N., Kim, H., Liu, X., Masaki, Y., Portmann, F. T., Satoh, Y., Stacke, T., Tang, Q., Wada, Y., Wisser, D., Albrecht, T., Frieler, K., Piontek, F., Warszawski, L. and Kabat, P.: Multimodel assessment of water scarcity under climate change, Proc. Natl. Acad. Sci. U. S. A., 111(9), 3245–3250, doi:10.1073/pnas.1222460110, 2014.
Schewe, J., Gosling, S. N., Reyer, C., Zhao, F., Ciais, P., Elliott, J., Francois, L., Huber, V., Lotze, H. K., Seneviratne, S. I., van Vliet, M. T. H., Vautard, R., Wada, Y., Breuer, L., Büchner, M., Carozza, D. A., Chang, J., Coll, M., Deryng, D., de Wit, A., Eddy, T. D., Folberth, C., Frieler, K., Friend, A. D., Gerten, D., Gudmundsson, L., Hanasaki, N., Ito, A., Khabarov, N., Kim, H., Lawrence, P., Morfopoulos, C., Müller, C., Müller Schmied, H., Orth, R., Ostberg, S., Pokhrel, Y., Pugh, T. A. M., Sakurai, G., Satoh, Y., Schmid, E., Stacke, T., Steenbeek, J., Steinkamp, J., Tang, Q., Tian, H., Tittensor, D. P., Volkholz, J., Wang, X. and Warszawski, L.: State-of-the-art global models underestimate impacts from climate extremes, Nat. Commun., 10(1), 1–14, doi:10.1038/s41467-019-08745-6, 2019.
Schiemann, R., Lüthi, D. and Schär, C.: Seasonality and interannual variability of the westerley jet in the Tibetan Plateau region, J. Clim., 22(11), 2940–2957, doi:10.1175/2008JCLI2625.1, 2009.
Schulla, J.: Model Description WaSiM, Zürich, Switzerland., 2017.
Schumacher, D. L., Keune, J., van Heerwaarden, C. C., Vilà-Guerau de Arellano, J., Teuling, A. J. and Miralles, D. G.: Amplification of mega-heatwaves through heat torrents fuelled by upwind drought, Nat. Geosci., 12(9), 712–717, doi:10.1038/s41561-019-0431-6, 2019.
Schumann, G. J. P., Stampoulis, D., Smith, A. M., Sampson, C. C., Andreadis, K. M., Neal, J. C. and Bates, P. D.: Rethinking flood hazard at the global scale, Geophys. Res. Lett., 43(19), 10,249-10,256, doi:10.1002/2016GL070260, 2016.
Schuur, E. A. G., McGuire, A. D., Schädel, C., Grosse, G., Harden, J. W., Hayes, D. J., Hugelius, G., Koven, C. D., Kuhry, P., Lawrence, D. M., Natali, S. M., Olefeldt, D., Romanovsky, V. E., Schaefer, K., Turetsky, M. R., Treat, C. C. and Vonk, J. E.: Climate change and the permafrost carbon feedback, Nature, 520(7546), 171–179, doi:10.1038/nature14338, 2015.
Scott, R., Entekhabi, D., Koster, R. and Suarez, M.: Timescales of land surface evapotranspiration response, J. Clim., 10(4), 559–566, doi:10.1175/1520-0442(1997)010<0559:TOLSER>2.0.CO;2, 1997.
Sen, P. K.: Estimates of the Regression Coefficient Based on Kendall's Tau, J. Am. Stat. Assoc., 63(324), 1379–1389, doi:10.1080/01621459.1968.10480934, 1968.
Seneviratne, S., Nicholls, N., Easterling, D., Goodess, C., Kanae, S., Kossin, J., Luo, Y., Marengo, J., McInnes, K., Rahimi, M., Reichstein, M., Sorteberg, A., Vera, C. and Zhang, X.: Changes in climate extremes and their impacts on the natural physical environment, Manag. Risk Extrem. Events Disasters to Adv. Clim. Chang. Adapt., 109–230, 2012.
Seneviratne, S. I. and Koster, R. D.: A Revised Framework for Analyzing Soil Moisture Memory in Climate Data: Derivation and Interpretation, J. Hydrometeorol., 13(1), 404–412, doi:10.1175/JHM-D-11-044.1, 2012.
Serinaldi, F.: An uncertain journey around the tails of multivariate hydrological distributions, Water Resour. Res., 49(10), 6527–6547, doi:10.1002/wrcr.20531, 2013.
Serinaldi, F., Bárdossy, A. and Kilsby, C. G.: Upper tail dependence in rainfall extremes: would we know it if we saw it?, Stoch. Environ. Res. Risk Assess., 29(4), 1211–1233, doi:10.1007/s00477-014-0946-8, 2015.
Sexstone, G. A., Clow, D. W., Stannard, D. I. and Fassnacht, S. R.: Comparison of methods for quantifying surface sublimation over seasonally snow-covered terrain, Hydrol. Process., 30(19), 3373–3389, doi:10.1002/hyp.10864, 2016.
Sexstone, G. A., Clow, D. W., Fassnacht, S. R., Liston, G. E., Hiemstra, C. A., Knowles, J. F. and Penn, C. A.: Snow Sublimation in Mountain Environments and Its Sensitivity to Forest Disturbance and Climate Warming, Water Resour. Res., 54(2), 1191–1211, doi:10.1002/2017WR021172, 2018.
Seyfried, M. S., Grant, L. E., Marks, D., Winstral, A. and McNamara, J.: Simulated soil water storage effects on streamflow generation in a mountainous snowmelt environment, Idaho, USA, Hydrol. Process., 23(6), 858–873, doi:10.1002/hyp.7211, 2009.
Sharma, A., Wasko, C. and Lettenmaier, D. P.: If Precipitation Extremes Are Increasing, Why Aren't Floods?, Water Resour. Res., 54(11), 8545–8551, doi:10.1029/2018WR023749, 2018.

Shaun Harrigan: DRAFT - GloFAS-ERA5 operational global river discharge reanalysis, , (January), 1–23, 2020.
Shaw, T., Yang, W., Ayala, Á., Bravo, C., Zhao, C. and Pellicciotti, F.: Distributed summer air temperatures across mountain glaciers: climatic sensitivity and glacier size, Cryosph. Discuss., 1–29, doi:10.5194/tc-2020-198, 2020.
Shea, J. M. and Moore, R. D.: Prediction of spatially distributed regional-scale fields of air temperature and vapor pressure over mountain glaciers, J. Geophys. Res. Atmos., 115(23), 1–15, doi:10.1029/2010JD014351, 2010.
Shean, D. E., Bhushan, S., Montesano, P., Rounce, D. R., Arendt, A. and Osmanoglu, B.: A Systematic , Regional Assessment of High Mountain Asia Glacier Mass Balance, , 7(January), 1–19, doi:10.3389/feart.2019.00363, 2020.
Shepherd, T. G.: Atmospheric circulation as a source of uncertainty in climate change projections, Nat. Geosci., 7(10), 703–708, doi:10.1038/NGEO2253, 2014.
Shepherd, T. G.: A Common Framework for Approaches to Extreme Event Attribution, Curr. Clim. Chang. Reports, 2(1), 28–38, doi:10.1007/s40641-016-0033-y, 2016.
Shepherd, T. G.: Storyline approach to the construction of regional climate change information, Proc. R. Soc. A Math. Phys. Eng. Sci., 475(2225), doi:10.1098/rspa.2019.0013, 2019.
Shepherd, T. G., Boyd, E., Calel, R. A., Chapman, S. C., Dessai, S., Dima-West, I. M., Fowler, H. J., James, R., Maraun, D., Martius, O., Senior, C. A., Sobel, A. H., Stainforth, D. A., Tett, S. F. B., Trenberth, K. E., van den Hurk, B. J. J. M., Watkins, N. W., Wilby, R. L. and Zenghelis, D. A.: Storylines: an alternative approach to representing uncertainty in physical aspects of climate change, Clim. Change, 151(3–4), 555–571, doi:10.1007/s10584-018-2317-9, 2018.
Shi, J., Cui, L., Wen, K., Tian, Z., Wei, P. and Zhang, B.: Trends in the consecutive days of temperature and precipitation extremes in China during 1961--2015, Environ. Res., 161, 381–391, 2018.
Shiau, J. T.: Return period of bivariate distributed extreme hydrological events, Stoch. Environ. Res. Risk Assess., 17(1–2), 42–57, doi:10.1007/s00477-003-0125-9, 2003.
Shiau, J. T.: Fitting drought duration and severity with two-dimensional copulas, Water Resour. Manag., 20(5), 795–815, doi:10.1007/s11269-005-9008-9, 2006.
Shinoda, M.: Climate memory of snow mass as soil moisture over central Eurasia, J. Geophys. Res. Atmos., 106(D24), 33393–33403, doi:10.1029/2001JD000525, 2001.
Shrestha, A. B., Wake, C. P., Mayewski, P. A. and Dibb, J. E.: Maximum temperature trends in the Himalaya and its vicinity: An analysis based on temperature records from Nepal for the period 1971-94, J. Clim., 12(9), 2775–2786, doi:10.1175/1520-0442(1999)012<2775:MTTITH>2.0.CO;2, 1999.
Shrestha, A. B., Wake, C. P., Dibb, J. E. and Mayewski, P. A.: Precipitation fluctuations in the Nepal Himalaya and its vicinity and relationship with some large scale climatological parameters, Int. J. Climatol., 20(3), 317–327, doi:10.1002/(SICI)1097-0088(20000315)20:3<317::AID-JOC476>3.0.CO;2-G, 2000.
Shrestha, M., Koike, T., Hirabayashi, Y., Xue, Y., Wang, L., Rasul, G. and Ahmad, B.: Journal of Geophysical Research : Atmospheres, , 4889–4919, doi:10.1002/2014JD022666.Received, 2015.
Shukla, J., Palmer, T. N., Hagedorn, R., Hoskins, B., Kinter, J., Marotzke, J., Miller, M. and Slingo, J.: Toward a new generation of world climate research and computing facilities, Bull. Am. Meteorol. Soc., 91(10), 1407–1412, doi:10.1175/2010BAMS2900.1, 2010.
Sigdel, M. and Ma, Y.: Variability and trends in daily precipitation extremes on the northern and southern slopes of the central Himalaya, Theor. Appl. Climatol., 130(1–2), 571–581, 2017.
Sillmann, J. and Sippel, S.: Climate extremes and their implications for impact and risk assessment: A short introduction, in Climate Extremes and Their Implications for Impact and Risk Assessment, pp. 1–9, Elsevier., 2020.
Sillmann, J., Kharin, V. V., Zhang, X., Zwiers, F. W. and Bronaugh, D.: Climate extremes indices in the CMIP5 multimodel ensemble: Part 1. Model evaluation in the present climate, J. Geophys. Res. Atmos., 118(4), 1716–1733, doi:10.1002/jgrd.50203, 2013.
Sillmann, J., Shepherd, T., Hurk, B., Hazeleger, W., Martius, O. and Zscheischler, J.: Physical modeling supporting a storyline approach., 2019.
Sillmann, J., Shepherd, T. G., van den Hurk, B., Hazeleger, W., Martius, O., Slingo, J. and Zscheischler, J.: Event-Based Storylines to Address Climate Risk, Earth's Futur., 9(2), 1–6, doi:10.1029/2020EF001783, 2021.
Simmons, A. J., Willett, K. M., Jones, P. D., Thorne, P. W. and Dee, D. P.: Low-frequency variations in surface atmospheric humidity, temperature, and precipitation: Inferences from reanalyses and monthly gridded observational data sets, J. Geophys. Res. Atmos., 115(1), 1–21, doi:10.1029/2009JD012442, 2010.
Singh, D., Seager, R., Cook, B. I., Cane, M., Ting, M., Cook, E. and Davis, M.: Climate and the Global Famine of 1876-78, J. Clim., 31(23), 9445–9467, doi:10.1175/JCLI-D-18-0159.1, 2018.
Singh, P., Kumar, N. and Arora, M.: Degree-day factors for snow and ice for Dokriani Glacier, Garhwal Himalayas, J. Hydrol., 235(1–2), 1–11, doi:10.1016/S0022-1694(00)00249-3, 2000.
Singh, V. P.: Hydrologic modeling: progress and future directions, Geosci. Lett., 5(1), doi:10.1186/s40562-018-0113-z, 2018.
Singh, V. P. and Woolhiser, D. A.: Mathematical modeling of watershed hydrology, J. Hydrol. Eng., 7(4), 270–

292, 2002.
Sippel, S., Otto, F. E. L., Forkel, M., Allen, M. R., Guillod, B. P., Heimann, M., Reichstein, M., Seneviratne, S. I., Thonicke, K. and Mahecha, M. D.: A novel bias correction methodology for climate impact simulations, Earth Syst. Dyn., 7(1), 71–88, doi:10.5194/esd-7-71-2016, 2016.
Sippel, S., Forkel, M., Rammig, A., Thonicke, K., Flach, M., Heimann, M., Otto, F. E. L., Reichstein, M. and Mahecha, M. D.: Contrasting and interacting changes in simulated spring and summer carbon cycle extremes in European ecosystems, Environ. Res. Lett., 12(7), 75006, doi:10.1088/1748-9326/aa7398, 2017.
Sivapalan, M., Blöschl, G., Merz, R. and Gutknecht, D.: Linking flood frequency to long-term water balance: Incorporating effects of seasonality, Water Resour. Res., 41(6), 1–17, doi:10.1029/2004WR003439, 2005.
Sklar, M.: Fonctions de repartition an dimensions et leurs marges, Publ. inst. Stat. univ. Paris, 8, 229–231, 1959.
Smith, M. B., Koren, V. I., Zhang, Z., Reed, S. M., Pan, J. J. and Moreda, F.: Runoff response to spatial variability in precipitation: An analysis of observed data, in Journal of Hydrology, vol. 298, pp. 267–286, Elsevier., 2004a.
Smith, M. B., Seo, D. J., Koren, V. I., Reed, S. M., Zhang, Z., Duan, Q., Moreda, F. and Cong, S.: The distributed model intercomparison project (DMIP): Motivation and experiment design, J. Hydrol., 298(1–4), 4–26, doi:10.1016/j.jhydrol.2004.03.040, 2004b.
Smits, A., Tank, A. M. G. K. and Onnen, G. P. K.: TRENDS IN STORMINESS OVER THE NETHERLANDS , 1962 – 2002, , 1344, 1331–1344, doi:10.1002/joc.1195, 2005.
Song, C., Sheng, Y., Wang, J., Ke, L., Madson, A. and Nie, Y.: Heterogeneous glacial lake changes and links of lake expansions to the rapid thinning of adjacent glacier termini in the Himalayas, Geomorphology, 280(December 2018), 30–38, doi:10.1016/j.geomorph.2016.12.002, 2017.
Sorg, A., Huss, M., Rohrer, M. and Stoffel, M.: The days of plenty might soon be over in glacierized Central Asian catchments, Environ. Res. Lett., 9(10), doi:10.1088/1748-9326/9/10/104018, 2014.
Sorooshian, S., Hsu, K., Coppola, E., Tomassetti, B., Verdecchia, M. and Visconti, G.: Hydrological Modelling and the Water Cycle: Coupling the Atmospheric and Hydrological Models, Springer Berlin Heidelberg. [online] Available from: https://books.google.co.ke/books?id=rYTONAEACAAJ, 2008.
Stahl, K., Weiler, M., Kohn, I., Freudiger, D., Seibert, J., Vis, M. and Gerlinger, K.: The snow and glacier melt components of streamflow of the river Rhine and its tributaries considering the influence of climate change, , 146 [online] Available from: www.chr-khr.org/en/publications, 2016.
Stigter, E. E., Litt, M., Steiner, J. F. and Bonekamp, P. N. J.: The Importance of Snow Sublimation on a Himalayan Glacier, , 6(August), 1–16, doi:10.3389/feart.2018.00108, 2018.
Stocker, T. F., Qin, D., Plattner, G.-K., Tignor, M., Allen, S. K., Boschung, J., Nauels, A., Xia, Y., Bex, V., Midgley, P. M. and others: Climate change 2013: The physical science basis, Contrib. Work. Gr. I to fifth Assess. Rep. Intergov. panel Clim. Chang., 1535, 2013.
Strasser, U., Bernhardt, M., Weber, M., Liston, G. E. and Mauser, W.: Is snow sublimation important in the alpine water balance?, 2008.
Su, F., Duan, X., Chen, D., Hao, Z. and Cuo, L.: Evaluation of the global climate models in the CMIP5 over the Tibetan Plateau, J. Clim., 26(10), 3187–3208, doi:10.1175/JCLI-D-12-00321.1, 2013.
Sudheer, K. P., Lakshmi, G. and Chaubey, I.: Application of a pseudo simulator to evaluate the sensitivity of parameters in complex watershed models, Environ. Model. Softw., 26(2), 135–143, doi:10.1016/j.envsoft.2010.07.007, 2011.
Sulis, M., Meyerhoff, S. B., Paniconi, C., Maxwell, R. M., Putti, M. and Kollet, S. J.: A comparison of two physics-based numerical models for simulating surface water-groundwater interactions, Adv. Water Resour., 33(4), 456–467, doi:10.1016/j.advwatres.2010.01.010, 2010.
Sun, X., Thyer, M., Renard, B. and Lang, M.: A general regional frequency analysis framework for quantifying local-scale climate effects: A case study of ENSO effects on Southeast Queensland rainfall, J. Hydrol., 512, 53–68, doi:10.1016/j.jhydrol.2014.02.025, 2014.
Sutanto, S. J., Van Den Hurk, B., Dirmeyer, P. A., Seneviratne, S. I., Röckmann, T., Trenberth, K. E., Blyth, E. M., Wenninger, J. and Hoffmann, G.: HESS Opinions "a perspective on isotope versus non-isotope approaches to determine the contribution of transpiration to total evaporation," Hydrol. Earth Syst. Sci., 18(8), 2815–2827, doi:10.5194/hess-18-2815-2014, 2014.
Sutanudjaja, E. H., Van Beek, R., Wanders, N., Wada, Y., Bosmans, J. H. C., Drost, N., Van Der Ent, R. J., De Graaf, I. E. M., Hoch, J. M., De Jong, K., Karssenberg, D., López López, P., Peßenteiner, S., Schmitz, O., Straatsma, M. W., Vannametee, E., Wisser, D. and Bierkens, M. F. P.: PCR-GLOBWB 2: A 5 arcmin global hydrological and water resources model, Geosci. Model Dev., 11(6), 2429–2453, doi:10.5194/gmd-11-2429-2018, 2018.
Svensson, C. and Jones, D. A.: Dependence between sea surge, river flow and precipitation in south and west Britain, Hydrol. Earth Syst. Sci., 8(5), 973–992, doi:10.5194/hess-8-973-2004, 2004.
Syed, K. H., Goodrich, D. C., Myers, D. E. and Sorooshian, S.: Spatial characteristics of thunderstorm rainfall fields and their relation to runoff, J. Hydrol., 271(1–4), 1–21, doi:10.1016/S0022-1694(02)00311-6, 2003.
Tang, H. S., Chien, S. I. J., Temimi, M., Blain, C. A., Ke, Q., Zhao, L. and Kraatz, S.: Vulnerability of population

and transportation infrastructure at the east bank of Delaware Bay due to coastal flooding in sea-level rise conditions, Nat. Hazards, 69(1), 141–163, doi:10.1007/s11069-013-0691-1, 2013.
Tawn, J. A.: Modelling Multivariate Extreme Value Distributions, Biometrika, 77(2), 245–253 [online] Available from: https://www.jstor.org/stable/2336802, 1990.
Terink, W., Lutz, A. F., Simons, G. W. H., Immerzeel, W. W. and Droogers, P.: SPHY: Spatial Processes in Hydrology, Geosci. Model Dev. Discuss., 8(October), 1687–1748, doi:10.5194/gmdd-8-1687-2015, 2015.
Terink, W., Immerzeel, W. W., Lutz, A. F., Droogers, P., Khanal, S., Nepal, S. and Shrestha, A. B.: Hydrological and Climate Change Assessment for Hydropower development in the Tamakoshi River Basin, Nepal. FutureWater report 164, Wageningen, The Netherlands., 2017.
Thiery, W., Davin, E. L., Lawrence, D. M., Hirsch, A. L., Hauser, M. and Seneviratne, S. I.: Present-day irrigation mitigates heat extremes, J. Geophys. Res., 122(3), 1403–1422, doi:10.1002/2016JD025740, 2017.
Thywissen, K.: Components of risk: a comparative glossary., 2006.
Tilloy, A., Malamud, B. D., Winter, H. and Joly-Laugel, A.: A review of quantification methodologies for multi-hazard interrelationships, Earth-Science Rev., 196, 102881, doi:10.1016/j.earscirev.2019.102881, 2019.
Tobin, C., Schaefli, B., Nicótina, L., Simoni, S., Barrenetxea, G., Smith, R., Parlange, M. and Rinaldo, A.: Improving the degree-day method for sub-daily melt simulations with physically-based diurnal variations, Adv. Water Resour., 55, 149–164, doi:10.1016/j.advwatres.2012.08.008, 2013.
Tol, R. S. J. and Langen, A.: A concise history of dutch river floods, Clim. Change, 46(3), 357–369, doi:10.1023/A:1005655412478, 2000.
Tong, K., Su, F., Yang, D., Zhang, L. and Hao, Z.: Tibetan Plateau precipitation as depicted by gauge observations, reanalyses and satellite retrievals, Int. J. Climatol., 34(2), 265–285, doi:10.1002/joc.3682, 2014.
Torres, J. M., Bass, B., Irza, N., Fang, Z., Proft, J., Dawson, C., Kiani, M. and Bedient, P.: Characterizing the hydraulic interactions of hurricane storm surge and rainfall-runoff for the Houston-Galveston region, Coast. Eng., 106, 7–19, doi:10.1016/j.coastaleng.2015.09.004, 2015.
Towler, E., Rajagopalan, B., Gilleland, E., Summers, R. S., Yates, D. and Katz, R. W.: Modeling hydrologic and water quality extremes in a changing climate: A statistical approach based on extreme value theory, Water Resour. Res., 46(11), 1–11, doi:10.1029/2009WR008876, 2010.
Trenberth, K. E., Fasullo, J. T. and Shepherd, T. G.: Attribution of climate extreme events, Nat. Clim. Chang., 5(8), 725–730, doi:10.1038/nclimate2657, 2015.
Troin, M., Poulin, A., Baraer, M. and Brissette, F.: Comparing snow models under current and future climates: Uncertainties and implications for hydrological impact studies, J. Hydrol., 540, 588–602, doi:https://doi.org/10.1016/j.jhydrol.2016.06.055, 2016.
Udmale, P. D., Ichikawa, Y., Ning, S., Shrestha, S. and Pal, I.: A statistical approach towards defining national-scale meteorological droughts in India using crop data, Environ. Res. Lett., doi:10.1088/1748-9326/abacfa, 2020.
Uhe, P., Mitchell, D., Bates, P., Sampson, C., Smith, A. and ISLAM, A. K. M. S.: Enhanced flood risk with 1.5° C global warming in the Ganges-Brahmaputra-Meghna basin, Environ. Res. Lett., 2019.
Ulbrich, U., Leckebusch, G. C. and Pinto, J. G.: Extra-tropical cyclones in the present and future climate: A review, Theor. Appl. Climatol., 96(1–2), 117–131, doi:10.1007/s00704-008-0083-8, 2009.
Vanem, E.: Uncertainties in extreme value modelling of wave data in a climate change perspective, J. Ocean Eng. Mar. Energy, 1(4), 339–359, doi:10.1007/s40722-015-0025-3, 2015.
Vaze, J., Post, D. A., Chiew, F. H. S., Perraud, J. M., Viney, N. R. and Teng, J.: Climate non-stationarity – Validity of calibrated rainfall–runoff models for use in climate change studies, J. Hydrol., 394(3–4), 447–457, doi:http://dx.doi.org/10.1016/j.jhydrol.2010.09.018, 2010.
Vaze, J., Jordan, P., Beecham, R., Frost, A. and Summerell, G.: Guidelines for rainfall-runoff modelling: towards best practice model application, 2011.
Veh, G., Korup, O. and Walz, A.: Hazard from Himalayan glacier lake outburst floods, Proc. Natl. Acad. Sci. U. S. A., 117(2), 907–912, doi:10.1073/pnas.1914898117, 2020.
Villarini, G., Vecchi, G. A. and Smith, J. A.: Modeling the dependence of tropical storm counts in the north atlantic basin on climate indices, Mon. Weather Rev., 138(7), 2681–2705, doi:10.1175/2010MWR3315.1, 2010.
Vinnikov, K. Y., Robock, A., Speranskaya, N. A. and Schlosser, C. A.: Scales of temporal and spatial variability of mitlatitude soil moisture, J. Geophys. Res., 101(D3), 7163–7174, 1996.
Vionnet, V., Martin, E., Masson, V., Guyomarc'H, G., Naaim-Bouvet, F., Prokop, A., Durand, Y. and Lac, C.: Simulation of wind-induced snow transport and sublimation in alpine terrain using a fully coupled snowpack/atmosphere model, Cryosphere, 8(2), 395–415, doi:10.5194/tc-8-395-2014, 2014.
Viviroli, Daniel; Messerli, B.: Assessing the Hydrological Significance of the World's Mountains, Mt. Res. Dev., 23(4), 369–375, doi:10.1659/0276-4741(2003)023, 2003.
van Vliet, M. T. H., van Beek, L. P. H., Eisner, S., Flörke, M., Wada, Y. and Bierkens, M. F. P.: Multi-model assessment of global hydropower and cooling water discharge potential under climate change, Glob. Environ. Chang., 40, 156–170, doi:10.1016/j.gloenvcha.2016.07.007, 2016.
Volpi, E. and Fiori, A.: Hydraulic structures subject to bivariate hydrological loads: Return period, design, and

risk assessment, Water Resour. Res., 50(2), 885–897, doi:10.1002/2013WR014214, 2014.
Vorogushyn, S., Bates, P. D., de Bruijn, K., Castellarin, A., Kreibich, H., Priest, S., Schröter, K., Bagli, S., Blöschl, G., Domeneghetti, A., Gouldby, B., Klijn, F., Lammersen, R., Neal, J. C., Ridder, N., Terink, W., Viavattene, C., Viglione, A., Zanardo, S. and Merz, B.: Evolutionary leap in large-scale flood risk assessment needed, Wiley Interdiscip. Rev. Water, 5(2), e1266, doi:10.1002/wat2.1266, 2018.
Vousdoukas, M. I., Mentaschi, L., Voukouvalas, E., Verlaan, M., Jevrejeva, S., Jackson, L. P. and Feyen, L.: Global probabilistic projections of extreme sea levels show intensification of coastal flood hazard, Nat. Commun., 9(1), 1–12, doi:10.1038/s41467-018-04692-w, 2018.
Vries, H. De, Katsman, C. and Drijfhout, S.: Constructing scenarios of regional sea level change using global temperature pathways, Environ. Res. Lett., 9(11), doi:10.1088/1748-9326/9/11/115007, 2014.
Wagner, S., Fersch, B., Yuan, F., Yu, Z. and Kunstmann, H.: Fully coupled atmospheric-hydrological modeling at regional and long-term scales: Development, application, and analysis of WRF-HMS, Water Resour. Res., 52(4), 3187–3211, doi:10.1002/2015WR018185, 2016.
Wagner, W., C. Verhoest, N. E., Ludwig, R. and Tedesco, M.: Editorial Remote sensing in hydrological sciences, Hydrol. Earth Syst. Sci., 13(6), 813–817, doi:10.5194/hess-13-813-2009, 2009.
Wagnon, P., Vincent, C., Arnaud, Y., Berthier, E., Vuillermoz, E., Gruber, S., Ménégoz, M., Gilbert, A., Dumont, M., Shea, J. M., Stumm, D. and Pokhrel, B. K.: Seasonal and annual mass balances of Mera and Pokalde glaciers (Nepal Himalaya) since 2007, Cryosphere, 7(6), 1769–1786, doi:10.5194/tc-7-1769-2013, 2013.
Wahl, T., Jain, S., Bender, J., Meyers, S. D. and Luther, M. E.: Increasing risk of compound flooding from storm surge and rainfall for major US cities, Nat. Clim. Chang., 5(July), doi:10.1038/nclimate2736, 2015.
Wahl, T., Haigh, I. D., Nicholls, R. J., Arns, A., Dangendorf, S., Hinkel, J. and Slangen, A. B. A.: Understanding extreme sea levels for broad-scale coastal impact and adaptation analysis, Nat. Commun., 8, doi:10.1038/ncomms16075, 2017.
Walvoord, M. A. and Kurylyk, B. L.: Hydrologic Impacts of Thawing Permafrost-A Review, Vadose Zo. J., 15(6), vzj2016.01.0010, doi:10.2136/vzj2016.01.0010, 2016.
Wanders, N., Thober, S., Kumar, R., Pan, M., Sheffield, J., Samaniego, L. and Wood, E. F.: Development and evaluation of a Pan-European multi-model seasonal hydrological forecasting system, J. Hydrometeorol., 20(0), 99–115, doi:10.1175/JHM-D-18-0040.1, 2018.
Wang, S. S. -Y., Kim, H., Coumou, D., Yoon, J., Zhao, L. and Gillies, R. R.: Consecutive extreme flooding and heat wave in Japan: Are they becoming a norm?, Atmos. Sci. Lett., 20(10), e933, doi:10.1002/asl.933, 2019.
Wang, X., Tolksdorf, V., Otto, M. and Scherer, D.: WRF-based dynamical downscaling of ERA5 reanalysis data for High Mountain Asia: Towards a new version of the High Asia Refined analysis, Int. J. Climatol., (March), 1–20, doi:10.1002/joc.6686, 2020.
Wang, X., Tolksdorf, V., Otto, M. and Scherer, D.: WRF-based dynamical downscaling of <scp>ERA5</scp> reanalysis data for High Mountain Asia: Towards a new version of the High Asia Refined analysis, Int. J. Climatol., 41(1), 743–762, doi:10.1002/joc.6686, 2021.
Ward, P. J., Jongman, B., Salamon, P., Simpson, A., Bates, P., De Groeve, T., Muis, S., de Perez, E. C., Rudari, R., Trigg, M. A. and Winsemius, H. C.: Usefulness and limitations of global flood risk models, Nat. Clim. Chang., 5(8), 712–715, doi:10.1038/nclimate2742, 2015.
Ward, P. J., Jongman, B., Aerts, J. C. J. H., Bates, P. D., Botzen, W. J. W., Diaz Loaiza, A., Hallegatte, S., Kind, J. M., Kwadijk, J., Scussolini, P. and Winsemius, H. C.: A global framework for future costs and benefits of river-flood protection in urban areas, Nat. Clim. Chang., 7, 642 [online] Available from: https://doi.org/10.1038/nclimate3350, 2017.
Watson, C. S., Quincey, D. J., Carrivick, J. L. and Smith, M. W.: The dynamics of supraglacial water storage in the Everest region, central Himalaya, Glob. Planet. Change, 142, 14–27, doi:10.1016/j.gloplacha.2016.04.008, 2016.
Webster, P. J., Magaña, V. O., Palmer, T. N., Shukla, J., Tomas, R. A., Yanai, M. and Yasunari, T.: Monsoons: processes, predictability, and the prospects for prediction, J. Geophys. Res. Ocean., 103(C7), 14451–14510, doi:10.1029/97jc02719, 1998.
Wernli, H., Dirren, S., Liniger, M. A. and Zillig, M.: Dynamical aspects of the life cycle of the winter storm "Lothar" (24–26 December 1999), Q. J. R. Meteorol. Soc., 128(580), 405–429, doi:10.1256/003590002321042036, 2002.
Wesselung, C. G., Karssenberg, D.-J., Burrough, P. A. and Deursen, W. P. A.: Integrating dynamic environmental models in GIS: The development of a Dynamic Modelling language, Trans. GIS, 1(1), 40–48, doi:10.1111/j.1467-9671.1996.tb00032.x, 1996.
Whitmee, S., Haines, A., Beyrer, C., Boltz, F., Capon, A. G., De Souza Dias, B. F., Ezeh, A., Frumkin, H., Gong, P., Head, P., Horton, R., Mace, G. M., Marten, R., Myers, S. S., Nishtar, S., Osofsky, S. A., Pattanayak, S. K., Pongsiri, M. J., Romanelli, C., Soucat, A., Vega, J. and Yach, D.: Safeguarding human health in the Anthropocene epoch: Report of the Rockefeller Foundation-Lancet Commission on planetary health, Lancet, 386(10007), 1973–2028, doi:10.1016/S0140-6736(15)60901-1, 2015.

van der Wiel, K., Stoop, L. P., van Zuijlen, B. R. H., Blackport, R., van den Broek, M. A. and Selten, F. M.: Meteorological conditions leading to extreme low variable renewable energy production and extreme high energy shortfall, Renew. Sustain. Energy Rev., 111, 261–275, doi:10.1016/j.rser.2019.04.065, 2019.
Wijngaard, R. R., Lutz, A. F., Nepal, S., Khanal, S., Pradhananga, S., Shrestha, A. B. and Immerzeel, W. W.: Future changes in hydro-climatic extremes in the Upper Indus, Ganges, and Brahmaputra River basins, PLoS One, 12(12), e0190224, 2017.
Wijngaard, R. R., Steiner, J. F., Kraaijenbrink, P. D. A., Klug, C., Adhikari, S., Banerjee, A., Pellicciotti, F., van Beek, L. P. H., Bierkens, M. F. P., Lutz, A. F. and Immerzeel, W. W.: Modeling the response of the langtang glacier and the hintereisferner to a changing climate since the little ice age, Front. Earth Sci., 7(June), 1–24, doi:10.3389/feart.2019.00143, 2019.
Wilby, R. L.: Uncertainty in water resource model parameters used for climate change impact assessment, Hydrol. Process., 19(16), 3201–3219, doi:10.1002/hyp.5819, 2005.
Wilby, R. L. and Dessai, S.: Robust adaptation to climate change, Weather, 65(7), 180–185, doi:10.1002/wea.543, 2010.
Wiltshire, A. J., Ludwig, F., Chen, C., Clark, D. B., Voss, F., Hanasaki, N., Gosling, S. N., Haddeland, I., Hagemann, S., Heinke, J. and Folwell, S.: Climate change impact on available water resources obtained using multiple global climate and hydrology models, Earth Syst. Dyn., 4(1), 129–144, doi:10.5194/esd-4-129-2013, 2013.
Winsemius, H. C., Aerts, J. C. J. H., Van Beek, L. P. H., Bierkens, M. F. P., Bouwman, A., Jongman, B., Kwadijk, J. C. J., Ligtvoet, W., Lucas, P. L., Van Vuuren, D. P. and Ward, P. J.: Global drivers of future river flood risk, Nat. Clim. Chang., 6(4), 381–385, doi:10.1038/nclimate2893, 2016.
Winstral, A. and Marks, D.: Simulating wind fields and snow redistribution using terrain-based parameters to model snow accumulation and melt over a semi-arid mountain catchment, Hydrol. Process., 16(18), 3585–3603, doi:10.1002/hyp.1238, 2002.
Wong, F. S.: First-order, second-moment methods, Comput. Struct., 20(4), 779–791, doi:10.1016/0045-7949(85)90039-2, 1985.
Woo, M. K. and Winter, T. C.: The role of permafrost and seasonal frost in the hydrology of northern wetlands in North America, J. Hydrol., 141(1–4), 5–31, doi:10.1016/0022-1694(93)90043-9, 1993.
Wood, E. F., Roundy, J. K., Troy, T. J., van Beek, L. P. H., Bierkens, M. F. P., Blyth, E., de Roo, A., Döll, P., Ek, M., Famiglietti, J., Gochis, D., van de Giesen, N., Houser, P., Jaffé, P. R., Kollet, S., Lehner, B., Lettenmaier, D. P., Peters-Lidard, C., Sivapalan, M., Sheffield, J., Wade, A. and Whitehead, P.: Hyperresolution global land surface modeling: Meeting a grand challenge for monitoring Earth's terrestrial water, Water Resour. Res., 47(5), doi:10.1029/2010WR010090, 2011.
Wortmann, M., Bolch, T., Menz, C., Tong, J. and Krysanova, V.: Comparison and correction of high-mountain precipitation data based on glacio-hydrological modeling in the Tarim river headwaters (High Asia), J. Hydrometeorol., 19(5), 777–801, doi:10.1175/JHM-D-17-0106.1, 2018.
Wu, W. and Dickinson, R. E.: Time scales of layered soil moisture memory in the context of land-atmosphere interaction, J. Clim., 17(14), 2752–2764, doi:10.1175/1520-0442(2004)017<2752:TSOLSM>2.0.CO;2, 2004.
Wu, W., McInnes, K., O'Grady, J., Hoeke, R., Leonard, M. and Westra, S.: Mapping Dependence Between Extreme Rainfall and Storm Surge, J. Geophys. Res. Ocean., 123(4), 2461–2474, doi:10.1002/2017JC013472, 2018.
Xu, L. and Dirmeyer, P.: Snow-atmosphere coupling strength in a global atmospheric model, Geophys. Res. Lett., 38(13), doi:10.1029/2011GL048049, 2011.
Xu, M., Kang, S., Wu, H. and Yuan, X.: Detection of spatio-temporal variability of air temperature and precipitation based on long-term meteorological station observations over Tianshan Mountains, Central Asia, Atmos. Res., 203(December 2017), 141–163, doi:10.1016/j.atmosres.2017.12.007, 2018.
Xu, X., Li, J. and Tolson, B. A.: Progress in integrating remote sensing data and hydrologic modeling, Prog. Phys. Geogr., 38(4), 464–498, doi:10.1177/0309133314536583, 2014.
Xu, Y., Huang, G. and Fan, Y.: Multivariate flood risk analysis for Wei River, Stoch. Environ. Res. Risk Assess., 31(1), 225–242, doi:10.1007/s00477-015-1196-0, 2017.
Xu, Z., Liu, Z., Fu, G. and Chen, Y.: Trends of major hydroclimatic variables in the Tarim River basin during the past 50 years, J. Arid Environ., 74(2), 256–267, doi:10.1016/j.jaridenv.2009.08.014, 2010.
Yan, L. and Liu, X.: Has climatic warming over the Tibetan Plateau paused or continued in recent years, J. Earth Ocean Atmos. Sci, 1(1), 13–28, 2014.
Yan, Z. L., Bian, Q., Xu, Z., Zhao, L., Zhang, Y. F., Zheng, H., Shi, C., Zhang, S. and Xie, C.: Evaluation and intercomparison of multiple snow water equivalent products over the tibetan plateau, J. Hydrometeorol., 20(10), 2043–2055, doi:10.1175/JHM-D-19-0011.1, 2019.
Yang, K., Ye, B., Zhou, D., Wu, B., Foken, T., Qin, J. and Zhou, Z.: Response of hydrological cycle to recent climate changes in the Tibetan Plateau, Clim. Change, 109(3–4), 517–534, 2011.
Yang, K., Wu, H., Qin, J., Lin, C., Tang, W. and Chen, Y.: Recent climate changes over the Tibetan Plateau and

their impacts on energy and water cycle: A review, Glob. Planet. Change, 112, 79–91, doi:10.1016/j.gloplacha.2013.12.001, 2014.
Yang, M., Nelson, F. E., Shiklomanov, N. I., Guo, D. and Wan, G.: Permafrost degradation and its environmental effects on the Tibetan Plateau: A review of recent research, Earth-Science Rev., 103(1–2), 31–44, doi:10.1016/j.earscirev.2010.07.002, 2010.
Yao, T., Thompson, L. G., Mosbrugger, V., Zhang, F., Ma, Y., Luo, T., Xu, B., Yang, X., Joswiak, D. R., Wang, W., Joswiak, M. E., Devkota, L. P., Tayal, S., Jilani, R. and Fayziev, R.: Third Pole Environment (TPE), Environ. Dev., 3(1), 52–64, doi:10.1016/j.envdev.2012.04.002, 2012a.
Yao, T., Thompson, L. G., Mosbrugger, V., Zhang, F., Ma, Y., Luo, T., Xu, B., Yang, X., Joswiak, D. R., Wang, W., Joswiak, M. E., Devkota, L. P., Tayal, S., Jilani, R. and Fayziev, R.: Third Pole Environment (TPE), Environ. Dev., 3(1), 52–64, doi:10.1016/j.envdev.2012.04.002, 2012b.
Yatagai, A., Kamiguchi, K., Arakawa, O., Hamada, A., Yasutomi, N. and Kitoh, A.: APHRODITE constructing a long-term daily gridded precipitation dataset for Asia based on a dense network of rain gauges, Bull. Am. Meteorol. Soc., 93(9), 1401–1415, doi:10.1175/BAMS-D-11-00122.1, 2012.
You, Q.-L., Ren, G.-Y., Zhang, Y.-Q., Ren, Y.-Y., Sun, X.-B., Zhan, Y.-J., Shrestha, A. B. and Krishnan, R.: An overview of studies of observed climate change in the Hindu Kush Himalayan (HKH) region, Adv. Clim. Chang. Res., 8(3), 141–147, 2017.
You, Q., Kang, S., Aguilar, E. and Yan, Y.: Changes in daily climate extremes in the eastern and central Tibetan Plateau during 1961-2005, J. Geophys. Res. Atmos., 113(7), 1–17, doi:10.1029/2007JD009389, 2008.
You, Q., Min, J., Zhang, W., Pepin, N. and Kang, S.: Comparison of multiple datasets with gridded precipitation observations over the Tibetan Plateau, Clim. Dyn., 45(3–4), 791–806, doi:10.1007/s00382-014-2310-6, 2015a.
You, Q., Min, J., Lin, H., Pepin, N., Sillanpää, M. and Kang, S.: Observed climatology and trend in relative humidity in the central and eastern Tibetan Plateau, J. Geophys. Res. Atmos., 120(9), 3610–3621, doi:10.1002/2014JD023031, 2015b.
Yu, C., Huang, X., Chen, H., Huang, G., Ni, S., Wright, J. S., Hall, J., Ciais, P., Zhang, J., Xiao, Y., Sun, Z., Wang, X. and Yu, L.: Assessing the Impacts of Extreme Agricultural Droughts in China Under Climate and Socioeconomic Changes, Earth's Futur., 6(5), 689–703, doi:10.1002/2017EF000768, 2018.
Yue, S. and Rasmussen, P.: Bivariate frequency analysis: Discussion of some useful concepts in hydrological application, Hydrol. Process., 16(14), 2881–2898, doi:10.1002/hyp.1185, 2002.
Yue, S. and Wang, C. Y.: Applicability of prewhitening to eliminate the influence of serial correlation on the Mann-Kendall test, Water Resour. Res., 38(6), 1–4, 2002.
Yue, S., Pilon, P., Phinney, B. and Cavadias, G.: The influence of autocorrelation on the ability to detect trend in hydrological series, Hydrol. Process., 16(9), 1807–1829, doi:10.1002/hyp.1095, 2002.
Zaherpour, J., Masaki, Y., Hanasaki, N., Gosling, S. N., Mount, N., Hannes, M. and Ted, I. E.: Worldwide evaluation of mean and extreme runoff from six global-scale hydrological models that account for human impacts OPEN ACCESS Worldwide evaluation of mean and extreme runoff from six global-scale hydrological models that account for human impacts, Environ. Res. Lett., 13(6), 065015, 2018.
Zandler, H., Haag, I. and Samimi, C.: Evaluation needs and temporal performance differences of gridded precipitation products in peripheral mountain regions, Sci. Rep., 9(1), 1–15, doi:10.1038/s41598-019-51666-z, 2019.
Zappa, G.: Regional Climate Impacts of Future Changes in the Mid–Latitude Atmospheric Circulation: a Storyline View, Curr. Clim. Chang. Reports, 5(4), 358–371, doi:10.1007/s40641-019-00146-7, 2019.
Zehe, E. and Sivapalan, M.: Threshold behaviour in hydrological systems as (human) geo-ecosystems: Manifestations, controls, implications, Hydrol. Earth Syst. Sci., 13(7), 1273–1297, doi:10.5194/hess-13-1273-2009, 2009.
Zehe, E., Graeff, T., Morgner, M., Bauer, A. and Bronstert, A.: Plot and field scale soil moisture dynamics and subsurface wetness control on runoff generation in a headwater in the Ore Mountains, Hydrol. Earth Syst. Sci., 14(6), 873–889, doi:10.5194/hess-14-873-2010, 2010.
Zhan, Y. J., Ren, G. Y., Shrestha, A. B., Rajbhandari, R., Ren, Y. Y., Sanjay, J., Xu, Y., Sun, X. B., You, Q. L. and Wang, S.: Changes in extreme precipitation events over the Hindu Kush Himalayan region during 1961–2012, Adv. Clim. Chang. Res., 8(3), 166–175, doi:10.1016/j.accre.2017.08.002, 2017.
Zhang, C., Tang, Q., Chen, D., van der Ent, R. J., Liu, X., Li, W. and Haile, G. G.: Moisture source changes contributed to different precipitation changes over the northern and southern Tibetan Plateau, J. Hydrometeorol., 20(2), 217–229, 2019a.
Zhang, G., Yao, T., Xie, H., Wang, W. and Yang, W.: An inventory of glacial lakes in the Third Pole region and their changes in response to global warming, Glob. Planet. Change, 131, 148–157, doi:10.1016/j.gloplacha.2015.05.013, 2015.
Zhang, J., Chen, H. and Zhang, Q.: Extreme drought in the recent two decades in northern China resulting from Eurasian warming, Clim. Dyn., 52(5–6), 2885–2902, doi:10.1007/s00382-018-4312-2, 2019b.
Zhang, M., Chen, Y., Shen, Y. and Li, B.: Tracking climate change in Central Asia through temperature and

precipitation extremes, J. Geogr. Sci., 29(1), 3–28, 2019c.
Zhang, Q., Xiao, M., Singh, V. P. and Chen, X.: Copula-based risk evaluation of hydrological droughts in the East River basin, China, Stoch. Environ. Res. Risk Assess., 27(6), 1397–1406, doi:10.1007/s00477-012-0675-9, 2013.
Zhang, Q., Pan, Y., Wang, S., Xu, J. and Tang, J.: High-Resolution Regional Reanalysis in China: Evaluation of 1 Year Period Experiments, J. Geophys. Res. Atmos., 122(20), 10,801-10,819, doi:10.1002/2017JD027476, 2017.
Zhang, X., Alexander, L., Hegerl, G. C., Jones, P., Tank, A. K., Peterson, T. C., Trewin, B. and Zwiers, F. W.: Indices for monitoring changes in extremes based on daily temperature and precipitation data, Wiley Interdiscip. Rev. Clim. Chang., 2(6), 851–870, 2011.
Zhang, Y., Liu, S. and Ding, Y.: Observed degree-day factors and their spatial variation on glaciers in western China, Ann. Glaciol., 43(December 2013), 301–306, doi:10.3189/172756406781811952, 2006.
Zhao, F., Masaki, Y., Hanasaki, N., Biemans, H., Zaherpour, J., Gosling, S. N., Veldkamp, T. I. E., Frieler, K., Schewe, J., Ostberg, S. and Willner, S.: The critical role of the routing scheme in simulating peak river discharge in global hydrological models The critical role of the routing scheme in simulating peak river discharge in global hydrological models, Environ. Res. Lett., 12(7), 075003, 2017.
Zhao, L., Xia, J., Xu, C. yu, Wang, Z., Sobkowiak, L. and Long, C.: Evapotranspiration estimation methods in hydrological models, J. Geogr. Sci., 23(2), 359–369, doi:10.1007/s11442-013-1015-9, 2013.
Zhao, P., Yang, S. and Yu, R.: Long-Term Changes in Rainfall over Eastern China and Large-Scale Atmospheric Circulation Associated with Recent Global Warming, J. Clim., 23(6), 1544–1562, doi:10.1175/2009jcli2660.1, 2010.
Zheng, F., Westra, S. and Sisson, S. A.: Quantifying the dependence between extreme rainfall and storm surge in the coastal zone, J. Hydrol., 505, 172–187, doi:10.1016/j.jhydrol.2013.09.054, 2013.
Zhong, L., Su, Z., Ma, Y., Salama, M. S. and Sobrino, J. A.: Accelerated changes of environmental conditions on the Tibetan Plateau caused by climate change, J. Clim., 24(24), 6540–6550, doi:10.1175/JCLI-D-10-05000.1, 2011.
Zhong, L., Ma, Y., Xue, Y. and Piao, S.: Climate Change Trends and Impacts on Vegetation Greening over the Tibetan Plateau, J. Geophys. Res. Atmos., 124(14), 7540–7552, 2019.
Zhou, B., Wen, Q. H., Xu, Y., Song, L. and Zhang, X.: Projected changes in temperature and precipitation extremes in China by the CMIP5 multimodel ensembles, J. Clim., 27(17), 6591–6611, doi:10.1175/JCLI-D-13-00761.1, 2014.
Zhou, S., Zhang, Y., Williams, A. P. and Gentine, P.: Projected increases in intensity, frequency, and terrestrial carbon costs of compound drought and aridity events, Sci. Adv., 5(1), eaau5740, doi:10.1126/sciadv.aau5740, 2019.
Zscheischler, J. and Seneviratne, S. I.: Dependence of drivers affects risks associated with compound events, , (June), doi:10.1126/sciadv.1700263, 2017.
Zscheischler, J., Orth, R. and Seneviratne, S. I.: Bivariate return periods of temperature and precipitation explain a large fraction of European crop yields, Biogeosciences, 14(13), 3309–3320, doi:10.5194/bg-14-3309-2017, 2017.
Zscheischler, J., Westra, S., Van Den Hurk, B. J. J. M., Seneviratne, S. I., Ward, P. J., Pitman, A., Aghakouchak, A., Bresch, D. N., Leonard, M., Wahl, T. and Zhang, X.: Future climate risk from compound events, Nat. Clim. Chang., 8(6), 469–477, doi:10.1038/s41558-018-0156-3, 2018.
Zscheischler, J., Martius, O., Westra, S., Bevacqua, E., Raymond, C., Horton, R. M., van den Hurk, B., AghaKouchak, A., Jézéquel, A., Mahecha, M. D., Maraun, D., Ramos, A. M., Ridder, N. N., Thiery, W. and Vignotto, E.: A typology of compound weather and climate events, Nat. Rev. Earth Environ., (June), 1–15, doi:10.1038/s43017-020-0060-z, 2020.

Acknowledgements

First, I would like to thank Arthur, my daily supervisor, co-promoter at Utrecht University and colleague at FutureWater, for his immense support throughout this journey. Dear Arthur (dai), you have helped me greatly in improving my understanding, technical skills and scientific writing. You have always boosted my confidence regardless of my highs and lows. I have always got warmth of a brother and vibe of a friend from you. I enjoyed every bit of time spent together with you in office, travels, meetings, and trainings. I cannot thank you enough for your consistence support on the overall development of my skills and personality.

Second, I would like to thank my promotors, Bart and Walter. It was a privilege to have you both as my 'guru'. Dear Bart, I am always grateful to you for providing an opportunity to commence this Ph.D. under your guidance. Your high standards have motivated me to work hard over the years. Your critical thinking, suggestions and novel ideas have helped to bring this thesis to its current state. Thank you for providing me an opportunity to work at KNMI (Royal Netherlands Meteorological Institute). I highly regard your valuable time that was spent on my overall development despite your busy schedule. Dear Walter, I am unable to find words to express my feelings. I greatly admire your efficacy and approach of tackling an issue, regardless of its complexity. I would like to thank you for providing me an opportunity to work on the high mountain related projects. Most of the work that has ended up in this thesis would not have been possible without your support.

I would want to extend my sincere thanks to other supervisors, Nina and Hylke at KNMI, for their guidance and support. Dear Nina, I would like to thank you for your tremendous support during the initial days of my Ph.D. You were never bothered despite all my last hour crazy requests. Dear Hylke, I am very grateful for my time and experiences at KNMI. I have always enjoyed our brief chat about your crazy ultra-marathon hobby.

I want to express my most gratitude and appreciation to FutureWater. I am thankful to Peter Droogers for providing me a wonderful opportunity to work with FutureWater. I have always been intrigued by your practical viewpoint and efficiency. I would like to learn more from you in future. Thanks to Johannes, Gijs and Martijn for supporting me throughout this journey. Your support during the COVID-19 emergencies and other tough times are much appreciated. Special thanks to Corjan, Jonna and Reinier for helping me during the final phase of Ph.D. and thesis writeup. Tons of thank to all colleagues: Sergio, Jack, Vera, Amelia and Natalia.

I want to thank all the co-authors featured in this thesis. I would not have been able to finish this project successfully without their suggestions and guidance. Thanks to the reviewers and editorial team of my papers that helped me significantly improve the manuscripts.

Additionally, I would like to thank all my former colleagues at ICIMOD, Arun Shrestha, Aditi Mukherji, Santosh Nepal, Mandira Shrestha, Madhav Dhakal, and Pradeep Dangol. Particular thanks to Arun Shrestha for his encouragement to pursue a Ph.D. Dear Arun sir, this would not have been possible without your guidance and support.

I cherished the support of my friends and family. I want to thank Wilco for being a nice supervisor at work and a good friend after work hours. Thanks to Anton for all your mental support during these years. Thank you, Rene, for being a good friend and helping me around with everything. I have always enjoyed your company. Thanks to SKV6 Wageningen football team and special thanks to Frank, Evertjan and Paul for making me feel part of the community. In addition to people already mentioned, I want to mention few names Arun Pratihast, Puja Mishra, Shiksha Adhikari, Sudip Subedi, Kriti Shrestha, Bhaskar Shrestha and Khem Gyanwali for their continuous overall support.

Finally, I would like to thank my mum and dad, my sister Sarita who supported me over these years to achieve my goals. Last but not the least, I would also like to thank all other individuals who helped to facilitate this project by their contributions.

About the author

Sonu Khanal was born and raised in a remote village, Giddanda, situated on the banks of river Andhikhola and foothills of Himalayas (70 Km West of Pokhara city) in Nepal. Monsoon floods and landslides around his surroundings motivated him to pursue a career in water resources. He obtained his bachelor's degree in Civil Engineering with a minor in hydropower development from the Institute of Engineering (IOE), Pulchowk Campus, Nepal in 2011. He continued his master's in Water Resources Engineering with a specialization in hydropower design at IOE which included six months graduation internship at the International Centre for Integrated Mountain Development (ICIMOD), where he gathered a physical background and understanding of snow and glacier processes. During his master's thesis, he investigated the effect of climate change on snow and glaciers in the Marshyangdi basin, using Utah Energy Balance (UEB) Grid snowmelt model. After his graduation, Sonu continued working at ICIMOD as a Water resources researcher where he was involved in multiple projects related to hydrological modeling, flood forecasting and climate change impact assessment. He had also worked as a national water resources consultant for Practical Action Consulting (PAC), Nepal, a non-governmental institution, to establish an operational flood forecasting system. His work in community based early warning system at PAC is integrated at national level forecast system by Department of Hydrology and Meteorology, Nepal. He started as an external PhD candidate in October 2016 at Vrije University, Amsterdam, the Netherlands, to understand the processes related to compound flood drivers at multiple spatial and temporal scales. The first three years of his PhD was funded by Marie Skłodowska-Curie Actions Innovative Training Networks (MSCA-ITN) grant under the European Union's Horizon 2020 Research and Innovation. He spent those three years at FutureWater (FW), Wageningen, the Netherlands, which is a research and consultancy company that provides practical solution for water management. After expiration of research grant in September 2019, he continued working for FW. At FW, he was involved in national and international consulting and research work related to climate change impact and risk assessment for "Pan-Third Pole" region, training activities in China, Nepal and Mozambique, hydrological pre-feasibility assessment of hydropower plants in countries like Nepal, Georgia and Indonesia and many other water resources modeling projects.

List of peer-reviewed publications

First authored publication

Khanal, S., Tiwari, S., Lutz, A. F., Hurk, B. van den., Immerzeel, W. W; Historical climate trends over High Mountain Asia derived from ERA5 reanalysis data, Journal of applied meteorology and climatology (JAMC), 2021 (under review)

Khanal, S., Lutz, A. F., Kraaijenbrink, P. D. A., van den Hurk, B., Yao, T., & Immerzeel, W. W. (2021). Variable 21st century climate change response for rivers in High Mountain Asia at seasonal to decadal time scales. Water Resources Research, 57, e2020WR029266. https://doi.org/10.1029/2020WR029266

Khanal, S.; Lutz, A.F.; Immerzeel, W.W.; Vries, H.d.; Wanders, N.; Hurk, B.v.d. The Impact of Meteorological and Hydrological Memory on Compound Peak Flows in the Rhine River Basin. Atmosphere 2019, 10, 171. *https://doi.org/10.3390/atmos10040171*

Khanal S, Ridder N, de Vries H, Terink W and van den Hurk B (2019) Storm Surge and Extreme River Discharge: A Compound Event Analysis Using Ensemble Impact Modeling. Front. Earth Sci. 7:224. doi: 10.3389/feart.2019.00224

Co-authored publication

Blöschl, G., Bierkens, M. F. P., Chambel, A., Cudennec, C., Destouni, G., Fiori, A., Kirchner, J. W., McDonnell, J. J., Savenije, H. H. G., Sivapalan, M., Stumpp, C., Toth, E., Volpi, E., Carr, G., Lupton, C., Salinas, J., Széles, B., Viglione, A., Aksoy, H., ... Zhang, Y. (2019). Twenty-three unsolved problems in hydrology (UPH)–a community perspective. Hydrological Sciences Journal, 64(10), 1141-1158. https://doi.org/10.1080/02626667.2019.1620507

Wijngaard RR, Lutz AF, Nepal S, **Khanal S**, Pradhananga S, Shrestha AB, et al. (2017) Future changes in hydro-climatic extremes in the Upper Indus, Ganges, and Brahmaputra River basins. PLoS ONE 12(12): e0190224. https://doi.org/10.1371/journal.pone.0190224

Conference Abstracts

Manocsoc, M. L., Barendrecht, M., Bertola, M., Ciullo, A., Cumiskey, L., Curran, A., Tavares da Costa, R., Diederen, D., Farrag, M., Holz, F., **Khanal, S**., Metin, A. D., Sairam, N., Shustikova, I., Sosa, J., and Schröter, K.: A retrospective analysis of the Cumbria floods in 2009 and 2015 (UK), EGU General Assembly 2019, Vienna, Austria, 7 April–12 Apr 2019, EGU2019-12204, 2019

Khanal, S., Lutz, A. F., Immerzeel, W. W., Wanders, N., de Vries, H., & Hurk, B. V. D. (2018, December). Spatio-Temporal Scales of Compound Events in the Atmosphere-Catchment System. In AGU Fall Meeting Abstracts (Vol. 2018, pp. NH23A-06B).

Khanal, S., de Vries, H., Ridder, N., Terink, W., and van den Hurk, B.: Storm surge and extreme river discharge: a compound event analysis using ensemble impact modeling, EGU General Assembly 2018, Vienna, Austria, 8 April–13 Apr 2018, EGU2018-15227, 2018

Dugar, S., Smith, P., Parajuli, B., **Khanal, S**., Brown, S., Gautam, D., ... & Uprety, M. (2017, April). Enhancing community based early warning systems in Nepal with flood forecasting using local and global models. In EGU General Assembly Conference Abstracts (p. 8995).

Terink, W., Lutz, A. F., Immerzeel, W., Nepal, S., **Khanal, S**., & Shrestha, A. B. (2016, December). Improvement of the SPHY Model Glacier Module and its Application in the Tamakoshi River Basin, Nepal. In AGU Fall Meeting Abstracts (Vol. 2016, pp. H54A-05).

Khanal S, Ridder N, de Vries H, Terink W and van den Hurk B. (2017, September) Atmosphere-catchment nexus: An attribution to compound events pertaining to floods along the Dutch coast. In ICFM7 "Resilience to Global Changes - Anticipating the Unexpected" conference Abstracts (Vol. 2017, pp. Designing for uncertainty-260).

Financial support

The research presented in this thesis is financially funded by several research programmes and organisations. These organisation and funding agencies are listed below.

Marie Skłodowska-Curie Actions Innovative Training Networks (MSCA-ITN) grant under the European Union's Horizon 2020 Research and Innovation (project " System Risk" and agreement no. 676027).

Strategic Priority Research Program of the Chinese Academy of Sciences (Grant No. XDA20100300).

FutureWater, The Netherlands.